



NTNU – Trondheim
Norwegian University of
Science and Technology

Development of Induction Heating System in a Deposit Processing Subsea Cooler

Trym Brox Bjørvik

Master of Science in Mechanical Engineering

Submission date: June 2015

Supervisor: Martin Steinert, IPM

Co-supervisor: Fredrik Lund, EMPIG AS

Norwegian University of Science and Technology
Department of Engineering Design and Materials

THE NORWEGIAN UNIVERSITY
OF SCIENCE AND TECHNOLOGY
DEPARTMENT OF ENGINEERING DESIGN
AND MATERIALS

**MASTER THESIS SPRING 2015
FOR
STUD. TECHN. TRYM BROX BJØRVIK**

In collaboration with EMPIG AS / Inventas Trondheim AS

**Development of Induction Heating System in a Deposit Processing Subsea Cooler
Utvikling av induksjonsvarmesystem i en avleiringsprosesserende subsea-kjøler**

EMPIG AS develops flow assurance technologies for the oil- and gas industry, specifically for the removal of wax and hydrate deposits from pipelines through electromagnetic principles.

Cooling of petroleum streams causes precipitations that deposit on the pipe wall, and a main objective for EMPIG has always been the enabling of cold flow in transport pipelines, i.e. a petroleum flow that is in thermal equilibrium with the surrounding seawater. The core competency of the EMPIG system is to control the cooling process in a contained fashion such that the deposits are limited to a predetermined area and may be easily and continuously handled.

In the pre-master project, a new system concept was suggested comprising a far more compact embodiment of the EMPIG concept. This system approach incurred an extensive scope for the project work, requiring consideration of numerous different elements, thus limiting the time available for each. The master thesis continuation is to have a more specific focus, in which only selected elements from the pre-master project are addressed.

By the end of the pre-master project work, redundancy issues were considered the biggest threat and weakness of the new system concept, and consequent recommendations for the continued development state that some form of inherent redundancy should be achieved. The most uncertain element of the new system concept, and also arguably the most critical, is the suggested adaptation of the concept of pipe cleaning by induction heating previously explored by EMPIG. Building on the results from the pre-master project, the proper adaptation of this induction heating concept is considered the most natural subject for the master thesis continuation.

As such, the main goal of the master thesis is to ideate and explore alternative concepts for implementation of the induction cleaning solution on a bi-directional sled within the system concept suggested in the pre-master thesis.

In the course of the project work, the following will be completed:

1. Identify limiting factors for the implementation of the induction heating concept
2. Define a basic framework for the concept development

3. Ideate and explore different concepts for the implementation, and decide on the most promising one for continued development
4. Detailing of the chosen concept and possibly identification of realistic components
5. With the time and resources at hand; take the first step towards validation of selected design element(s)

Formal requirements:


Three weeks after start of the thesis work, an A3 sheet illustrating the work is to be handed in. A template for this presentation is available on the IPM's web site under the menu "Masteroppgave" (<http://www.ntnu.no/ipm/masteroppgave>). This sheet should be updated one week before the master's thesis is submitted.

Risk assessment of experimental activities shall always be performed. Experimental work defined in the problem description shall be planned and risk assessed up-front and within 3 weeks after receiving the problem text. Any specific experimental activities which are not properly covered by the general risk assessment shall be particularly assessed before performing the experimental work. Risk assessments should be signed by the supervisor and copies shall be included in the appendix of the thesis.

The thesis should include the signed problem text, and be written as a research report with summary both in English and Norwegian, conclusion, literature references, table of contents, etc. During preparation of the text, the candidate should make efforts to create a well arranged and well written report. To ease the evaluation of the thesis, it is important to cross-reference text, tables and figures. For evaluation of the work a thorough discussion of results is appreciated.

The thesis shall be submitted electronically via DAIM, NTNU's system for Digital Archiving and Submission of Master's theses.

The contact person is Martin Steinert/IPM and Fredrik Lund/EMPIG

for 
Torgeir Welo
Head of Division



Martin Steinert
Professor/Supervisor



Preface

This report documents my work with the master thesis in Product Development and Materials Engineering at the Department of Engineering Design and Materials in the spring of 2015, and concludes my education at the Norwegian University of Science and Technology for the degree of M.Sc. in Mechanical Engineering. The master thesis constitutes an intuitive continuation of the pre-master project carried out in the autumn of 2014, and was supervised by Martin Steinert and Fredrik Lund at the department and EMPIG respectively.

As I have come to know the field of product development, and that pertaining to startup businesses in particular, setbacks and general turbulence must be expected in the course of a project – and this has been no exception. Considerable effort was made pursuing paths eventually discontinued, and hence not documented herein. I am nevertheless satisfied with the pragmatic approach through which the assignment in the end was completed. All in all, my work with the master thesis was a challenge from which I have gained both experience and knowledge, and I believe the lessons learnt will prove significant in my continued endeavors, personally as well as professionally.

Contributors to my work with the thesis have been numerous and of great importance. So as to not forget anyone, I prefer for the many to whom I owe a thank you to remain unnamed. Still, I am greatly appreciative of the treatment I have received at Inventas throughout my time here, being provided critical resources and input, and welcomed into a hospitable and creative working environment.

Trym Brox Bjørvik, June 10th 2015, Trondheim

Abstract

Continuing the development subject to the pre-master project, the purpose of this master thesis was to properly address the implementation of an induction heating system into a compact embodiment of the EMPIG InFlow system, as described in the pre-master report, through conceptual development and preliminary feasibility assessments.

The principle of and technology related to electromagnetic induction heating was researched through literature and extensive dialogue with EFD Induction, a leading supplier of induction heating equipment and longtime cooperator of EMPIG, and a basic framework for current and future development was defined. The main limiting factors were identified as relating to the high frequency of the alternating current involved in the induction heating process, e.g. by complicating the transmission of electric power from the power supply to the induction coil. As thesis client, EMPIG was continuously involved, and had deciding authority, in the shaping of the project vision.

To realize the flow assurance functionality within the layered meandering pipe structure, a modular, mobile induction heater concept is proposed. The concept features a retrievable induction coil, carried by an all-electric actuated mechanism comprising sufficient degrees of freedom for the coil to traverse the entire pipeline unobstructed, except for the four vertical pipe bends which must be otherwise accommodated. Though no reasonable mechanism also able to traverse said vertical pipe bends has been identified thus far, a continuous scan heating work path across the respective horizontal layers of pipeline was enabled through an advantageous restructuring of pipes and supports.

The induction coil design featured in the concept proposed herein is not optimal with respect to heating efficiency, and will generate significant amounts of heat in operation. To minimize complexity, the opportunity of a passive cooling scheme for the coil was investigated through computational analyses of natural convection heat transfer from copper metal submerged in seawater. Though the credibility of said theoretical investigation has not been properly assessed, and it as such is insufficient for drawing a final conclusion, results were positive and substantiating for the belief that a passive cooling scheme is achievable.

Though introducing uncertainty to the concept in the form of additional moving parts, the proposed modular heater concept ensures redundancy through simultaneous application of multiple units, as well as fail-safe operation and possibly enables the secure in-field storage of both spare units and malfunctioning units awaiting intervention.

Sammendrag

Som videreføring av forprosjektet tar masteroppgaven for seg implementeringen av et induksjonsvarmesystem i en kompakt utførelse av EMPIG InFlow systemet, slik det ble beskrevet i forprosjektrapporten, gjennom konseptutvikling og overordnet vurdering av gjennomførbarhet.

Prinsipp og teknologi knyttet til elektromagnetisk induksjonsvarming ble studert ved litteratur og utfyllende dialog med EFD Induction, en ledende leverandør av induksjonsvarmeutstyr og langvarig samarbeidspartner for EMPIG, og et overordnet rammeverk for nåværende og fremtidig utvikling ble utledet. De viktigste begrensende faktorene ble funnet å være tilknyttet den høye frekvensen til vekselstrømmen som induksjonsprinsippet baserer seg på, eksempelvis ved å vanskeliggjøre overføringen av elektrisk kraft fra strømforsyningen til spolen. Som oppdragsgiver for avhandlingen var EMPIG nært involvert i utformingen av visjonen for prosjekt og produkt.

For å realisere flow assurance-funksjonaliteten i den lagdelte og horisontalt meanderformede rørstrukturen blir et mobilt og modulært induksjonsvarmekonsept foreslått, hvori en induksjonsspole med åpen utforming bæres av en helelektrisk aktuert mekanisme med tilstrekkelige frihetsgrader for at spolen skal kunne nå alle punkter i rørmatrisen, med unntak av de fire vertikale rørstykkene som følgelig må behandles på annet vis. Selv om ingen realistisk utformet mekanisme som også er i stand til å traversere nevnte vertikale rørstykker har blitt funnet så langt, ble en kontinuerlig arbeidsbane for spolen gjennom de horisontale rørlagene muliggjort gjennom en fordelaktig omstrukturering av rør og opplager.

Utformingen av induksjonsspolen slik den er antatt i konseptet er ikke optimal med hensyn til effektiviteten i oppvarmingen, og må forventes å generere betydelige mengder varme i drift. For å minimere kompleksiteten i konseptet ble muligheten for et passivt spolekjølingsopplegg undersøkt ved beregninger av varmeovergang gjennom fri konveksjon fra kobbermetall i sjøvann. Selv om troverdigheten av nevnte teoretiske undersøkelser ikke har blitt tilstrekkelig vurdert, og således ikke gir grunnlag for å trekke noen endelig konklusjon, betraktes resultatene som oppløftende og underbygger enn så lenge muligheten for at et slikt passivt kjøleopplegg er oppnåelig.

På tross av den økte usikkerheten som bevegelige deler typisk fører med seg, er redundans i konseptet ivarettatt gjennom samtidig bruk av flere identiske og modulære enheter, såvel som gjennom fail-safe operasjon og en mulig langtidslagring av reserveenheter, i tillegg til enheter med funksjonsfeil som avventer opphenting.

Table of Contents

PREFACE	V
ABSTRACT	VII
SAMMENDRAG	VIII
TABLE OF CONTENTS	IX
LIST OF FIGURES	XI
LIST OF TABLES	XIV
1. INTRODUCTION	1
2. THEORY AND BACKGROUND	2
2.1. Forming and deposition of wax and hydrates	2
2.1.1. Wax	3
2.1.2. Hydrates	3
2.1.3. Rate of deposition	4
2.2. EMPIG and cold flow	5
2.3. Pre-master	8
2.4. Electromagnetic induction and heating	10
2.4.1. Mechanisms for heat generation	10
2.4.2. Material properties	11
2.4.3. Electromagnetic effects	13
3. FRAMEWORK FOR DEVELOPMENT	17
3.1. Background and pre-master	17
3.1.1. Changed Premises	18
3.2. Induction Heating Technology	21
3.2.1. EFD Induction	21
3.2.2. Managing losses	22
3.2.3. High frequency operation	23
3.2.4. Efficiencies	25
3.3. General concerns	27
3.4. Potential hazards	29
3.5. All electric	29

4. PRELIMINARY CONCEPT EXPLORATION	30
4.1. Layout and motion	30
4.2. Primary sled	40
4.3. Coil interface	44
4.4. Realizing accessibility	50
5. INDUCTION COIL MARINIZATION	52
5.1. Electrical conductivity effects.....	54
5.2. Aluminum oxide coating	56
5.3. Thermal considerations	57
5.3.1. Solid coil profile	57
5.3.2. Thermal analyses of copper element.....	59
5.3.3. Thermal simulation of coil geometry	75
5.3.4. Conclusions.....	81
6. FURTHER CONCEPT DETAILING.....	83
6.1. Preliminary technology analysis	83
6.1.1. Inherent redundancy	83
6.1.2. BLDC and general considerations	83
6.1.3. Wittenstein Motion Control	84
6.1.4. Ultramotion	85
6.1.5. Tecnadyne.....	86
6.1.6. Linear solenoid actuation	86
6.1.7. Joints and bearings	87
6.2. Rigid single section arm	88
6.2.1. Reach and kinematics.....	88
6.2.2. Structure and materials	89
6.3. Coil carrying assembly.....	92
6.4. Cable management and system	97
6.5. Operation	101
6.5.1. Redundancy and safe operation	102
7. SUMMARY AND CONCLUSIONS.....	104
8. RECOMMENDATIONS FOR FURTHER WORK	106
9. REFERENCES	
10. APPENDIX	

List of Figures

Figure 2-1: Generic pipeline cross section (Rosvold, 2008).....	2
Figure 2-2: Wax build-up in pipeline (Aske, 2011).....	3
Figure 2-3: Characteristic gas hydrate structure (Maslin et al., 2010).....	4
Figure 2-4: EMPIG system overview (EMPIG AS, 2012)	5
Figure 2-5: SINTEF Saturn cold flow system overview (Larsen & Lund, n.d.).....	6
Figure 2-6: Inventas rendering of EMPIG InFlow concept vision (Kjerschow, 2014).....	7
Figure 2-7: EMPIG system concept proposed in the pre-master report (Bjørvik, 2014).....	8
Figure 2-8: Adaptation of the SINTEF Saturn recirculation loop (Bjørvik, 2014).....	9
Figure 2-9: Hysteresis loss (Haimbaugh, 2001).....	11
Figure 2-10: Redistribution of electric current in parallel conductors (Rudnev et al., 2002) ..	14
Figure 2-11: Current distribution in inductor-workpiece pair (Rudnev et al., 2002).....	14
Figure 2-12: Current distribution in non-symmetrical inductor-workpiece pair (Rudnev et al., 2002).....	15
Figure 2-13: Electromagnetic ring effect (Rudnev et al., 2002)	15
Figure 2-14: Magnetic field lines surrounding (PPLATO, 1996).....	16
Figure 3-1: Generic subsea processing scheme (Lindland, 2014)	19
Figure 3-2: Temperature profile for passive cooling of a bare pipeline (Larsen, 2011a)	20
Figure 3-3: General Induction Heating Setup	21
Figure 3-4: Typical variation of alternative electric current and the associated magnetic field strength (Semiatin, 1988)	22
Figure 3-5: Examples of different litz wire configurations (SYNFLEX, 2013)	24
Figure 3-6: Retrievable coil design used in testing by Kjerschow (2014)	27
Figure 3-7: Vertical component retrieval from Gullfaks wet gas compressor (Statoil, 2012). 28	
Figure 4-1: In-plane translational DOFs across general pipe layout.....	30
Figure 4-2: Cartesian motion in Ultimaker 3d-printer (Makerwise, 2013).....	31
Figure 4-3: Pipe bend arrangement, (a) and (b) showing front and back respectively. Also indicated in (a) by the bridged pipes is the SINTEF Saturn recirculation loop	32
Figure 4-4: Pipe supports as proposed in the pre-master report (Bjørvik, 2014).....	32
Figure 4-5: Core unit showing annotated compartmentalized operational space, sections divided by vertically planar pipe support racks	33
Figure 4-6: Sketch indicating DOFs for flexible multidirectional concept.....	34
Figure 4-7: Exploratory sketches of multidirectional arm concept.....	35

Figure 4-8: Multidirectional concept.....	36
Figure 4-9: Single sided work path along horizontally meandering pipeline. Crosshatching indicates inaccessible zone opposite the work path, allocated for pipe support structures.....	37
Figure 4-10: Pool handrail mounting bracket (M-TC Sport, 2013)	38
Figure 4-11: Generic pipe support structure with horizontal mounting brackets	38
Figure 4-12: Rendering of proposed pipe support structure, the layout of which accommodating a continuous work path for the induction heating apparatus	39
Figure 4-13: Rendering of primary sled suspended on linear rails above the pipe matrix	40
Figure 4-14: Side view of proposed primary sled structure	41
Figure 4-15: Example of typical roller pinions engaged on toothed linear racks (DirectIndustry, 2013).....	42
Figure 4-16: EFD Induction twin coil design.....	44
Figure 4-17: Illustration of relative dimensions in a 'twin coil' embodiment, showing both an open and closed (active) configuration	45
Figure 4-18: Adaptation of the retrievable 'horseshoe' coil design	46
Figure 4-19: Visualization of work path through 180° pipe bends in horizontal plane for retrievable coil, showing outside path and inside path on the left and right respectively.....	47
Figure 4-20: Retrievable coil traversing vertical pipe bend engaged from the side.....	48
Figure 4-21: Modified retrievable coil design, showing increased radii.....	49
Figure 4-22: Mineral insulated band heaters by Watlow (2015)	49
Figure 4-23: Early concept sketches	50
Figure 4-24: Rigid single section arm	51
Figure 5-1: Relative velocities at which impingement attack may occur in copper alloys in seawater (Powell & Webster, 2012).....	53
Figure 5-2: Screen capture from video of underwater induction heating demonstration at the facilities of EFD Induction in Skien.....	54
Figure 5-3: Dielectric breakdown of air from a charged Tesla-coil (Tresman, 2005)	55
Figure 5-4: Wristwatch featuring aluminum oxide crystal, metal housing showing visible wear from daily use, whereas the alumina is 'crystal clear'	56
Figure 5-5: Solid copper coil embodiment.....	58
Figure 5-6: Assumed areas through which the bulk of the current will be traveling, and consequently where the heating will concentrate. Area is measured to 0.022875 m^2	59
Figure 5-7: Temperature time plot given element side length 20 mm and thickness 6 mm	65

Figure 5-8: Temperature time plot given element side length 20 mm and thickness 4 mm	66
Figure 5-9: Temperature time plot from Solidworks Flow Simulation	67
Figure 5-10: Cut plot showing temperature distribution through the thickness of the copper element	67
Figure 5-11: Temperature time plot for 4 mm element thickness.....	68
Figure 5-12: Temperature time plot of corresponding conjugate heat transfer simulation.....	70
Figure 5-13: Elemental temperature distribution from conjugate heat simulation	71
Figure 5-14: Temperature time plot from Solidworks Flow Simulation, top surface heat loading	72
Figure 5-15: Surface temperature plots	72
Figure 5-16: Cut-plot showing resulting temperature distribution in the copper plate for the case of top surface heat loading	73
Figure 5-17: Convection currents in vicinity of copper element	74
Figure 5-18: Surface heat load on solid copper coil for Solidworks Flow Simulation	75
Figure 5-19: Temperature time plot for transient analysis of solid coil.....	76
Figure 5-20: Surface temperature plot at steady state conditions	76
Figure 5-21: Solid coil embodiment comprising cooling fins for increased convective cooling	77
Figure 5-22: Temperature time plot for transient analysis of ribbed coil	78
Figure 5-23: Surface temperature plot of ribbed coil at steady state	78
Figure 5-24: Flow trajectories illustrating convective currents around two of the cooling fins	79
Figure 5-25: Cut plot of flow velocities in vicinity of the coil structure	80
Figure 5-26: Cut plot of typical internal temperature distribution in a cross section of the ribbed coil.....	80
Figure 5-27: Phase diagram for seawater, showing the significant increase in boiling point at depths	82
Figure 6-1: Wittenstein Motion Control SSEAC subsea electric actuator: Dual Channel (Perry, 2015).....	84
Figure 6-2: Ultramotion U2 linear actuator (appendix I).....	85
Figure 6-3: Hydracon Subsea solenoid linear actuator (“Solenoid Actuators,” 2014)	86
Figure 6-4: Subsea manipulator arm (“ARM 7E,” 2015)	88

Figure 6-5: Kinematic scheme of actuated rigid arm. The blue circle with radius a traces the path of the retracted actuator, whereas the length b is the stroke of the actuator. The position of the arm frame mounting point traces the angle α	89
Figure 6-6: Visualization of rigid arm embodiment.....	90
Figure 6-7: Syntactic buoyancy foam elements	91
Figure 6-8: Coil assembly DOFs.....	92
Figure 6-9: Hinged mounting of Tecnadyne Model 20WD	93
Figure 6-10: Coil and rotary actuator comprising copper shielding	94
Figure 6-11: Transformer support and coil shielding.....	95
Figure 6-12: Combined pipe snap-connector and mechanical cleaning and guides	96
Figure 6-13: Industrial robot cable management (“Adjustable Retraction System,” 2013, “Robotic Cable Management Made Easy,” 2013; thomasnet.com, 2012).....	97
Figure 6-14: Two heater units suspended underneath subordinate sleds traversing the primary sled	98
Figure 6-15: Heater unit engaged on a pipe in the lowermost region. The upright and tilted transformer orientation directs the cable safely away from the surrounding structure	99
Figure 6-16: Front view of heater units; arrows indicate the transversal DOF of the subordinate sleds	100
Figure 6-17: Separate retrieval of modular heater units.....	102

List of tables

Table 3-1: Typical coupling efficiencies (Zinn & Semiatin, 1988)	26
Table 5-1: Input parameters of MATLAB function <i>Natural_convection.m</i>	63
Table 5-2: Input parameters of MATLAB function <i>Grashof.m</i>	63
Table 5-3: Input values for computational model	64
Table 5-4: Input values for computational model	65
Table 5-5: Input parameters for conjugate heat transfer computational model	70

1. Introduction

Upon leaving the reservoir, crude oil is typically hot and under high pressures. When cooled by the surroundings, paraffin dissolved in the stream will start to precipitate, and similar to condensation of water vapor on cold surfaces, this sticky substance will in turn deposit on the walls of the pipeline. This process slowly builds a narrowing of the cross section and ultimately a complete blockage if left untreated. Flow assurance is the field of mitigating these issues, and this is the core competency of EMPIG AS. Typical countermeasures involve costly combinations of insulation and/or heating of the pipeline to avoid the cooling altogether, as well as regular abrasive mechanical cleaning (“pigging”) and the use of environmentally harmful chemicals to inhibit the formation of unwanted precipitates.

EMPIG approaches the field of flow assurance by instead allowing for the flow in the pipelines to be cooled to ambient temperatures, though in a contained fashion such that deposition is limited to the same pre-designated area in which mitigation efforts then can be concentrated. If the stream reaches thermal equilibrium with the surroundings, it is considered inert downstream of the cooling zone.

An EMPIG patented flow assurance concept uses induction heating to melt off solid wax and hydrate deposits from the inner walls of pipelines. Proof of concept was achieved through the work of Kjerschow (2013, 2014), and this report will discuss the conceptual development of an induction heating system implementation in a system structure as described in the pre-master report (Bjørvik, 2014).

The aim of this project through master and pre-master has been to increase the maturity level of the EMPIG system, so as to bring it closer to the market. The concept as presented in the pre-master project saw the system take a far more compact embodiment, and the intuitive subject for the master thesis continuation was the proper implementation of the induction heating solution within a similar embodiment, as the adaptation proposed in the pre-master report suffered from complexity and lack of redundancy.

A framework for the present and future development is outlined with emphasis on the induction heating technology, and concept exploration and detailing follows.

2. Theory and Background

The central theoretical foundation and background for the thesis is presented in this chapter through selected topics, including outlined main results from the pre-master project. Particular emphasis is put on the principles of heating by electromagnetic induction, for reference in both current and future theses.

2.1. Formation and deposition of wax and hydrates

The term “fouling” commonly refers to the general deposition of unwanted substances on subsea equipment. Depending on type and location, this may pose different threats to the safe and efficient operation of the system in question. Of particular importance is fouling that occurs inside petroleum handling equipment requiring an uninterrupted flow, such as the inner walls of pipelines.

Uncontrolled fouling could ultimately result in a complete blockage of the pipe, and will in any case obstruct flow through a narrowing of the cross section, as illustrated in figure 2-1. As the flow is also affected by surface characteristics such as roughness, the deposits, effectively covering the original inner surface, may increase back-pressure in streams and cause throughput reductions (Gate Inc., 2013).

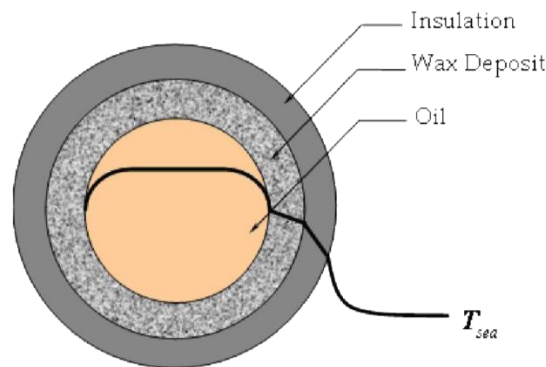


Figure 2-1: Generic pipeline cross section showing a typical temperature profile and wax deposit layer (Rosvold, 2008)

Wax and hydrates are the most common substances responsible for said fouling issues, and are as such the main focus of the EMPIG flow assurance technology. Characteristics and forming mechanisms are briefly presented in the following.

2.1.1. Wax

Crude oil is a complex hydrocarbon mixture that varies from field to field, and one of the main constituents in crude oil and most gas condensates is alkane, or paraffin (Lundberg, 2014). Long chains of paraffin as well as naphthenic hydrocarbons are the typical constituents of waxes present in petroleum streams. These exhibit high heat capacity, but low thermal conductivity, and have melting points ranging from 46°C to 68°C (Gate Inc., 2013).

Initially, the crude oil has a sufficiently high temperature to allow for these organic constituents to be dissolved in and carried by the liquid stream. However, due to the low ambient temperatures in the surrounding seawater, the stream will experience rapid cooling if not protected. It is the resulting temperature drop that causes precipitation and deposition of the solid wax.



Figure 2-2: Wax build-up in pipeline (Aske, 2011)

The fact that the wax precipitation is mainly governed by fluid temperature makes it very predictable. The temperature at which solid wax crystals start to form in the stream is referred to as the wax appearance temperature (WAT), and is typically below 40°C (Guðmundsson, 2010). As the wax crystallizes and solidifies it agglomerates and tends to further adhere to any cold surface providing a heat sink, such as the pipe walls.

2.1.2. Hydrates

Hydrates are crystalline compounds formed through a special combination of water and natural gas molecules of low molecular weight (Sloan, 1998). Their characteristic structure is illustrated in figure 2-3, showing how water molecules form a cage around the gas molecules.

The gas molecules are referred to as “guest molecules”, and they stabilize the compound structure through hydrogen bonds with the water molecules (Maslin et al., 2010). Once formed, the gas hydrates pose similar flow assurance challenges as hydrocarbon waxes.

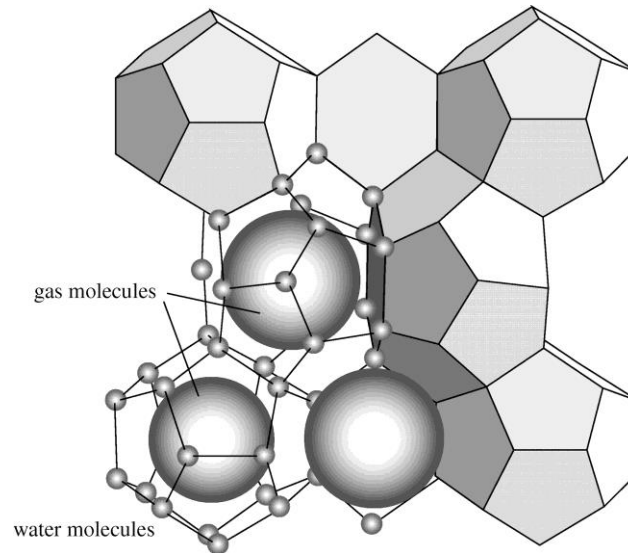


Figure 2-3: Characteristic gas hydrate structure comprising gas molecules encaged through hydrogen bonds by water molecules (Maslin et al., 2010)

The forming mechanisms for gas hydrates are far less deterministic in nature than for wax precipitation. While requiring a comparable temperature range, hydrate formation must also be accommodated by stream composition and high pressures. Typical hydrate forming gas molecules are methane, ethane and CO₂, and the correct amount of both water and such gas molecules must be present to allow for hydrate formation (Carroll, 2014).

The hydrate formation is also affected by different flow characteristics. Increased turbulence and mixing of the fluid flow is said to facilitate hydrate formation, and as for phase transitions in general, nucleation sites such as wall imperfections and other particles in the stream are also beneficial (Carroll, 2014). In fact, without advantageous nucleation sites, the hydrates may exhibit significant metastability. I.e., the hydrate forming process may not begin at all, despite other parameters indicating the system to be well within the hydrate stability region (Larsen, 2011a).

2.1.3. Rate of deposition

This thesis assumes the same wax deposition rates as Kjerschow (2014), in turn based on research and studies by Statoil and by Lund (1998) at Tulsa University. The Statoil study

charts the wax deposition layer thickness versus distance from the well, temperature and time, and suggests for the maximum expected wax layer thickness after 24 hours to be in the area of 0.5 mm (Frøseth, 2013, as cited in Kjerschow, 2014). The experiments presented by Lund were considered to be particularly relevant to the EMPIG case due to test parameters related to pipeline dimensions, temperature and loop runtime, and these indicated the corresponding wax thickness layer to be approximately 1.2 mm (Lund, 1998, as cited in Kjerschow, 2014).

2.2. EMPIG and cold flow

EMPIG AS holds several flow assurance technologies, all of which address the removal of wax and hydrate deposits from pipelines. Unique to the EMPIG concepts, however, is the close integration with a subsea cooling scheme. As mentioned in the introduction, the idea is to allow for the petroleum stream to cool rapidly, causing heavy deposition, but confined to a predetermined pipe section subject to continuous non-disruptive cleaning efforts. This ideally renders the stream inert with respect to fouling for any subsequent processing or long distance transport. Figure 2-4 shows a system overview:

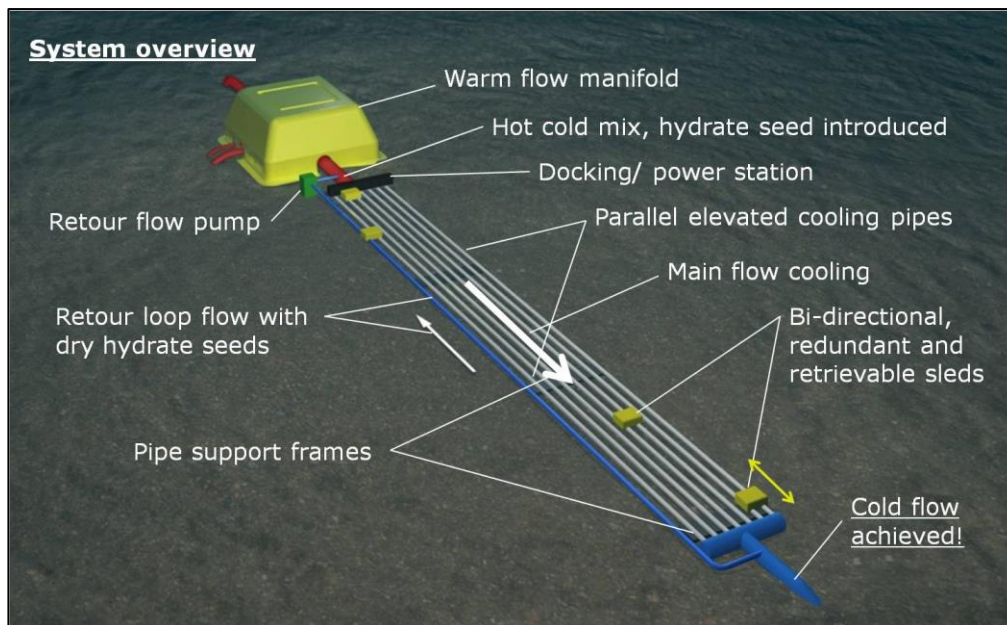


Figure 2-4: EMPIG system overview (EMPIG AS, 2012)

The idea of suspending inert solid precipitates in a flow in thermal equilibrium with the surroundings is referred to as “cold flow”, and this has been integral to the EMPIG vision from the outset.

The concept of cold flow itself was first explored by SINTEF in the early 1990s, following the discovery that a hydrate slurry at ambient temperatures could be safely transported without deposition (Larsen & Lund, n.d.). The seemingly unpredictable behavior of natural gas hydrates with respect to formation and deposition was the main focus of the SINTEF research, and their preferred ‘cold flow system’ embodiment addresses this through a pump driven flow loop that brings back a portion of the completely cooled stream and introduces it into the start of the cooling section, as illustrated in figure 2-5. The fully formed dry hydrate particles from the cold end thus provide excellent nucleation points to forcibly initiate the hydrate forming process amidst the stream, and the rapid particle growth is said to induce volumetric stresses that effectively break up the particles, limiting their size (Valencia, Ashrafiyan, & Krogstad, 2013).

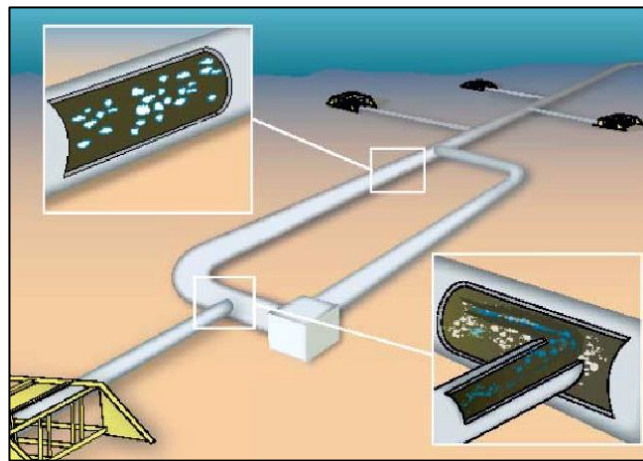


Figure 2-5: SINTEF Saturn cold flow system overview (Larsen & Lund, n.d.)

Seeing as fouling issues had not been considered by SINTEF for the cooling loop, and early EMPIG concepts were likely to give correspondingly inconsistent performance with respect to hydrates, a cooperation was considered advantageous for both parties (Larsen, 2011b). Proceeding EMPIG system embodiments generally assume an implementation of said back feed loop, as also indicated in figure 2-4.

The EMPIG Inductive Flow System (InFlow) offers a non-intrusive solution for the deposit removal in which the pipeline itself is heated by electromagnetic induction. Due to the low thermal conductivity of the wax, the heated pipe section will in turn melt only a thin layer of the deposits closest to the wall, causing the deposit body as a whole to separate from the pipe wall and be torn off in flakes by the turbulent stream. Once removed, the solid flakes are unable to deposit again. A whitepaper for the InFlow system is provided in appendix A.

The InFlow concept has long been considered the most promising, as it relies solely on an electromagnetic principle and does not require any moving parts to enter the pipe. Martin Kjerschow (2013, 2014) performed the proof of concept, and the development subject to this thesis builds upon the previous work to a large degree.



Figure 2-6: Inventas rendering of EMPIG InFlow concept vision (Kjerschow, 2014)

Essential to the EMPIG system in general is the fact that the flow assurance technology is to be carried on a bi-directional sled, linearly traversing the pipe structure, as shown in figure 2-6, though little detailing of this has been done previously.

2.3. Pre-master

The pre-master project addressed the EMPIG concept through a system approach, and brought about a complete restructuring of the originally lengthy layout. Featuring an industry customary subsea template, the updated system concept fits the entire cooling stretch into a modular unit through five layers of horizontally meandering pipeline. Figure 2-7 shows an overview of the system structure as proposed in the pre-master report.

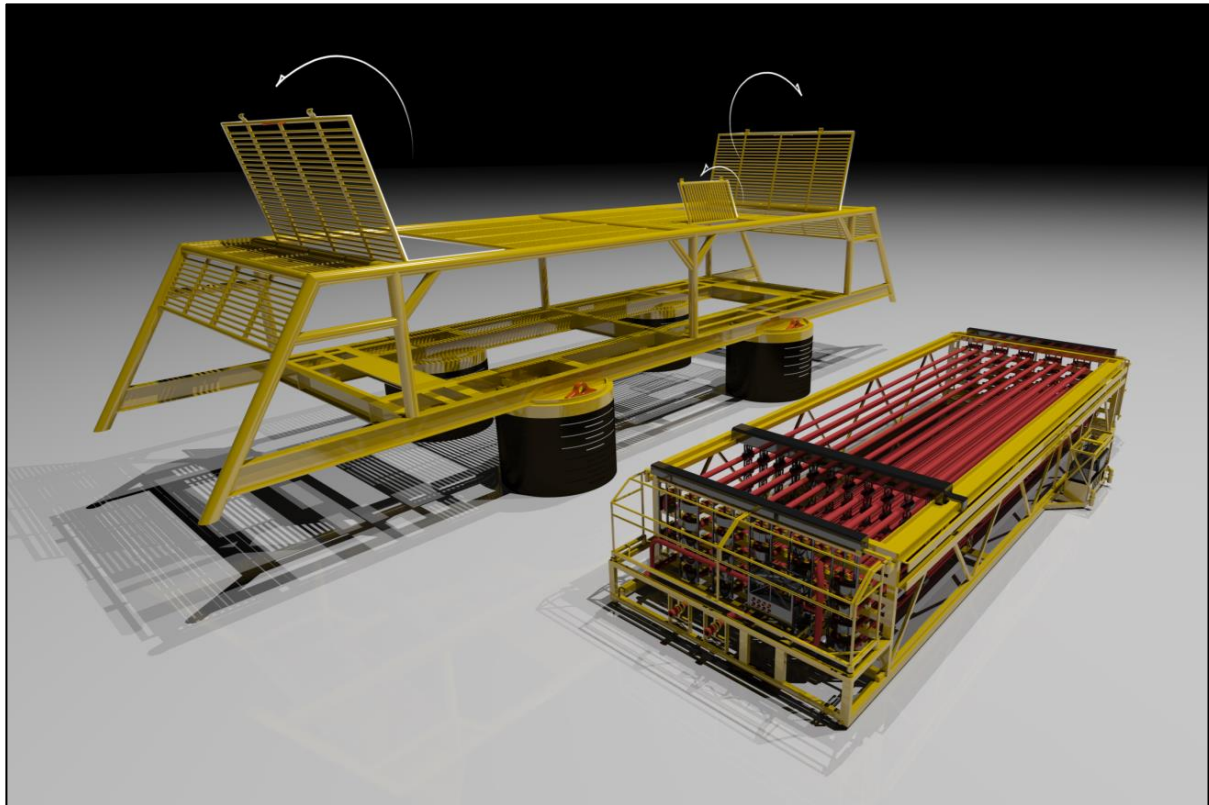


Figure 2-7: Illustration of the compact EMPIG system concept proposed in the pre-master report showing the core unit and subsea template separately (Bjørvik, 2014)

As depicted in figure 2-7, the proposed system concept comprises a ‘core unit’ to support the modular and vertically retrievable main functional components, which in turn is supported and shielded within the subsea template structure. As commonly seen in similar structures, hatches accommodating the vertical retrieval of components subject to maintenance are also indicated atop the template structure.

While keeping in line with selected main features of existing patent claims such as retrievability and modularity, the updated system concept still posed new challenges for the assumed technological foundation. As indicated on the core unit in figure 2-7, an envisioned

adaptation of the bi-directional sled introduced a rigid though vastly complex structure carrying numerous induction coils and transformers protruding into the pipe matrix. For the pipe bends connecting the linear pipeline segments, separate and similar heater modules would have to be implemented. Due to the resulting complexity of the mechanism and lack of scrutiny during the limited course of the pre-master project, the indicated adaptation of the induction heating solution was mainly to be considered a placeholder.

Figure 2-8 shows an adaptation of the recirculation loop from the SINTEF Saturn cold flow system. Due to the restructuring of the pipe layout, the implementation in the updated EMPIG system became a simple matter of bridging two neighboring pipes, as opposed to having a dedicated feedback pipe of equal length as the whole cooling section.



Figure 2-8: Adaptation of the SINTEF Saturn recirculation loop. Arrows indicate flow pattern, showing how a portion of the fully cooled stream is drawn through a multiphase pump (green) and injected into the start of the cooling section (Bjørsvik, 2014)

For the sake of coherence and continuity, selected elements of the system concept proposed in the pre-master report are revisited as appropriate.

2.4. Electromagnetic induction and heating

Integral to this thesis and resulting concept is the principle of electromagnetic induction. The basic theory is provided in the following.

The phenomenon itself was discovered in 1831 by the English physicist Michael Faraday when experimenting with two coils of wire wrapped around a common iron core. He found that a change of current in the first coil would “induce” an opposite momentary current in the second without any physical connection between the two. He concluded that an electric current can be produced in the presence of a changing magnetic field (Rudnev, Loveless, Cook, & Black, 2002).

This electromagnetic coupling effect became the basis for transformer technology, enabling easy change of voltage level for different circuits, and the application of electromagnetic induction for heating purposes in fact makes use of the same principle in that the “single turn” work piece to be heated may be considered the transformer secondary winding, in which so called eddy currents, or Foucault currents, are induced.

2.4.1. Mechanisms for heat generation

As with the practical use of all electromagnetic phenomena, induction heating equipment operates with losses, and these are dispersed as heat. The same heat generating mechanisms are present both in transformers and in induction heating equipment, but whereas these effects are normally sought minimized, they are encouraged and optimized for the latter.

2.4.1.1. Joule heating

The primary mechanism for heat generation in the workpiece is Joule heating, also called ohmic heating or resistive heating, due to the resistivity of the conductor. The eddy currents will be induced in any electrically conductive material exposed to a changing magnetic field, which also means that any conductor may be heated by electromagnetic induction. The amount of heat released in the conductor from Joule heating Q is proportional to the current squared such that

$$Q \propto I^2 \cdot R \cdot t \quad \text{Equation 1}$$

where R is the resistance of the conductor and t is the time in which the current I is flowing.

2.4.1.2. Hysteresis loss

When an external magnetic field is applied to a ferromagnetic material, the atomic dipoles will align themselves in the same direction, effectively magnetizing it. This means that when the external field is removed, there will still be a remaining flux density in the material, given by its remnance, B_r . When the external magnetic field is alternating, ferromagnetic materials will therefore experience an additional heating effect through what is called hysteresis loss, as energy is dissipated due to this continuous reversal of the magnetic domains (Clarke, 2008a). This “magnetic friction” means that ferromagnetic materials will heat more efficiently using electromagnetic induction, and this is illustrated below:

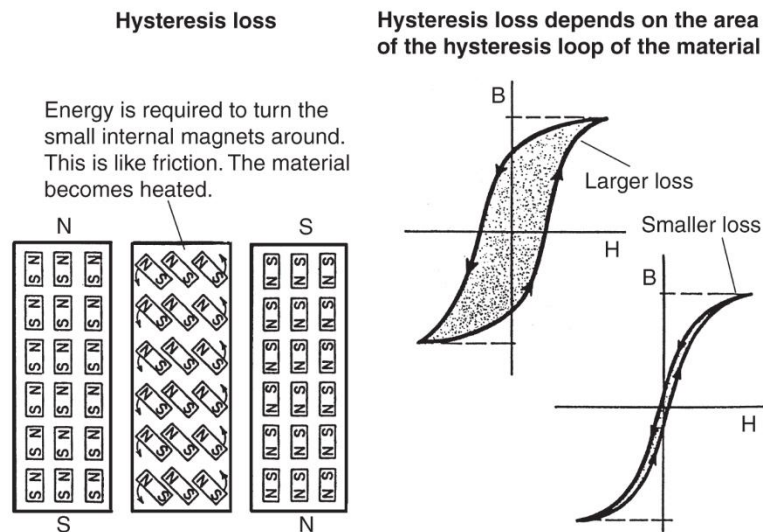


Figure 2-9: Hysteresis loss. N and S is north and south respectively, B is flux density in the material and H is the corresponding magnetic intensity (Haimbaugh, 2001).

2.4.2. Material properties

Several different properties are governing for a materials response when heated by electromagnetic induction. The performance of induction heaters are in fact mainly determined by the electromagnetic properties of the workpiece material (Rudnev et al., 2002), the most important of which are presented in the following.

2.4.2.1. Resistivity

The electrical resistivity of a material quantifies how strongly it will oppose an electric

current flowing through it and is denoted by ρ . The resistivity is the intrinsic material property, whereas the resistance R is derived from the resistivity and geometry. For a conductor of uniform cross section this may e.g. be approximated as

$$R = \rho \frac{l}{A} \quad \text{Equation 2}$$

where l is the conductor length and A is the cross-sectional area. The electrical resistivity of the workpiece is an important factor for the efficiency of the induction heating, as heat will build up more quickly in materials which strongly resist the flow of current. Steel is a material with high electrical resistivity, whereas copper, brass and aluminum are not. For most metals, the resistivity also rises with temperature.

2.4.2.2. Magnetic permeability

The magnetic permeability of a material, denoted μ , describes its ability to conduct a magnetic flux. Referring to 2.4.1.2, it can be seen as the relative increase or decrease in the resultant internal magnetic field of a material compared to the magnetic field that it is exposed to (“Magnetic Permeability,” 2015). Iron and other ferromagnetic materials have high magnetic permeabilities, whereas the permeabilities of plastics, wood, non-ferrous metals typically are much lower, often close to that of a vacuum. Analogous to electrical conductivity, the magnetic permeability is defined as the ratio of flux density B to magnetic field strength H (Clarke, 2008b),

$$\mu = \frac{B}{H} \quad \text{Equation 3}$$

In practice, the related parameter called relative magnetic permeability μ_r is commonly used. It describes the ‘magnetic conductivity’ in relation to a vacuum, i.e. compared to the magnetic permeability of empty space, defined as a constant $\mu_0 = 4\pi \cdot 10^{-7} \frac{H}{m}$ (NIST, 2011), such that

$$\frac{B}{H} = \mu_r \mu_0 \quad \text{Equation 4}$$

The magnetic permeability depends on many other material properties such as structure and chemical composition, but also to a large degree on temperature. E.g. for a typical ferrite, a temperature increase from 20°C to 80°C could inflict a magnetic permeability reduction of

25% (Clarke, 2008b).

As it affects so many of the associated phenomena, the magnetic permeability is an important factor in induction heating system design.

2.4.3. *Electromagnetic effects*

The current distribution in a conductor carrying an alternating current is not uniform. Rather, it is governed by a series of electromagnetic effects as described in the following.

2.4.3.1. Skin effect

The current density in a conductor carrying an alternating current has a disposition to concentrate in a layer closest to the outer surface of the conductor. This is referred to as the skin effect, and is present for both the induction coil and the workpiece. The skin depth is defined as the depth into the material at which the current density has fallen to $\frac{1}{e}$ (~0,37) relative to its value at the surface, and is often well approximated as

$$\delta = \sqrt{\frac{2\rho}{2\pi f \mu_r \mu_0}} \quad \text{Equation 5}$$

where f is the frequency of the alternating current, μ_r is the relative magnetic permeability of the conductor, and μ_0 is the permeability of free space.

As can be seen, the skin depth is inversely proportional to the square root of the frequency and will become very small for high frequencies. Since less of the conductor cross section is being utilized for transporting the current, the skin effect will cause the apparent resistance of the conductor to increase, and must be taken into account in high frequency applications.

2.4.3.2. Proximity effect

Another electromagnetic effect significantly affecting the current distribution in a conductor is the proximity effect. Any current carrying electrical conductor will create its own magnetic field, and this will in turn interact with other fields nearby. When there are several conductors present, their interactions with respect to current and power density distributions are described by the proximity effect.

Specifically, when two parallel conductors carry an electric current in the same direction, the current densities will redistribute such that the current is concentrated on opposite sides of both conductors, i.e. facing outwards. Similarly, for opposing currents, the redistribution sees the currents concentrate on conductor regions facing each other (Rudnev et al., 2002). This is illustrated in figure 2-10.

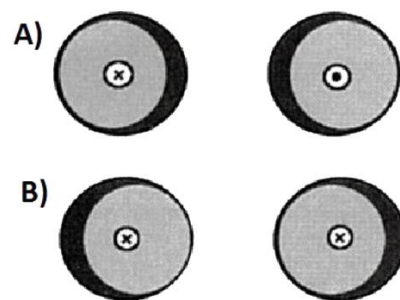


Figure 2-10: Redistribution of electric current in parallel conductors due to proximity effect.

A) Currents in opposite directions; B) Currents in same direction (Rudnev et al., 2002)

For the case of an induction heating system, the effect is further illustrated in figure 2-11. In fact, it is applicable for the inductor-workpiece coupling similar to the transformer analogy in 2.4 in that the induction coil and workpiece pair literally are two conductors in close proximity. Seeing as the eddy currents generated in the workpiece necessarily will have opposite directions relative to the coil current, the respective currents will thus concentrate in the regions facing each other.

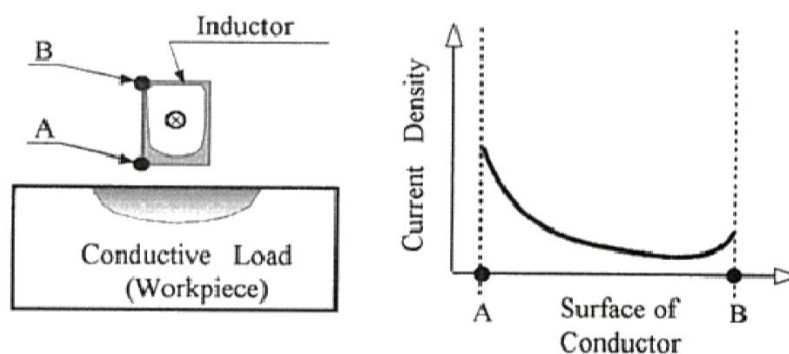


Figure 2-11: Redistribution of electric current in inductor-workpiece pair (Rudnev et al., 2002)

Further, the shape of the current distributions in the workpiece and inductor is largely

dependent on the distance between them. A large separation distance will incur a larger cross sectional area through which the eddy currents generated in the workpiece will travel, and thus a wider heating pattern, while a closer separation incurs higher current densities and a deep and narrow heating pattern. This is illustrated in figure 2-12.

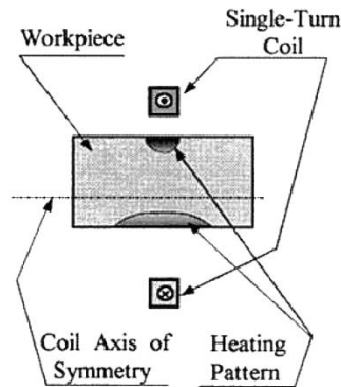


Figure 2-12: Current distribution in non-symmetrical inductor-workpiece pair (Rudnev et al., 2002)

2.4.3.3. Ring effect

It is well known that an electric current will tend to take the ‘path of least resistance’, and oftentimes this also means the shortest path. Similar to the proximity effect, the electromagnetic ring effect is relevant for circular or “ring” shaped conductor segments, where the magnetic flux lines will concentrate inside the ring, and the highest current density will be located at the inward facing surfaces (Rudnev et al., 2002) as illustrated below:

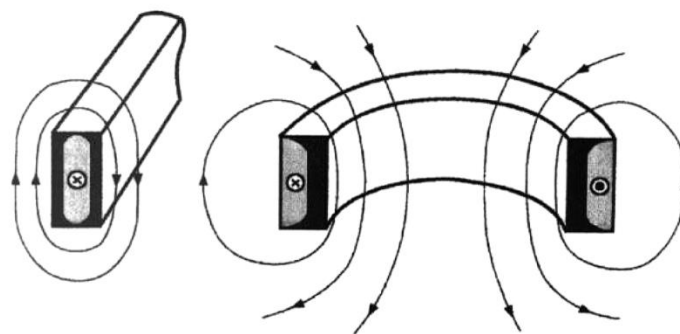


Figure 2-13: Electromagnetic ring effect (Rudnev et al., 2002)

Figure 2-14 (b) further illustrates the characteristic nature of electromagnetic fields lines

generated by the movement of electric charges in a continuous conductor wound as a solenoid coil; in accordance with the “right hand rule”, the field lines must concentrate inside the coil.

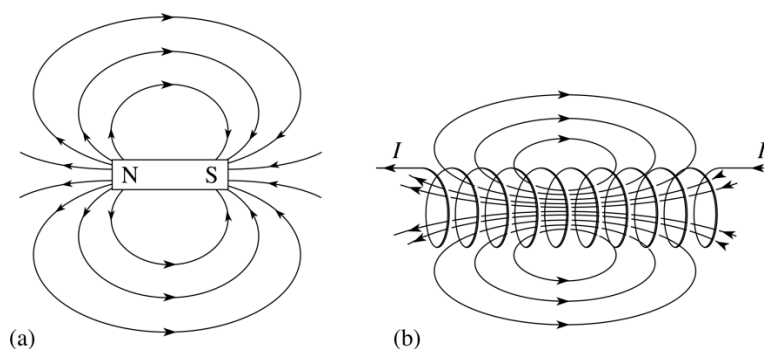


Figure 2-14: Magnetic field lines surrounding (a), a bar magnet; (b), a continuous conductor wound as a solenoid (PPLATO, 1996)

3. Framework for Development

This chapter documents the most important findings and considerations made during and prior to development to outline a basic requirement specification, as well as preliminary guidelines for decisions during and following this master project. Due emphasis is put on the research done with respect to implementation of induction heating technology in the proposed EMPIG subsea module embodiment.

As with the pre-master project, EMPIG is the thesis client. To ensure the usefulness of the master work and thesis, their opinions were made defining for the direction of the project in terms of decisions and priorities for the developed concept, as well as general shape of the report and subjects treated therein. The master work was carried out at the facilities of Inventas, enabling close and frequent communication with Fredrik Lund, founder and CTO of EMPIG and contact person at EMPIG/Inventas. This means exchange of and feedback on ideas and sketches were readily available, and this is reflected in the report to a large degree.

Again similar to the pre-master project, existing patents and development efforts had to be considered closely. Suggested concepts should adhere to selected claims and general core competency of EMPIG, and this was overseen by EMPIG through Fredrik Lund throughout the course of the master work.

Since the assignment is so directly industry related, the previous and anticipated future market response to different elements and concepts was also made defining for the direction of the development. This entails a focus on proven reliability and in most cases a generally conservative approach. It is understood that development should be based on market feedback and trends, and EMPIG was given the authority to make decisions on these matters from experience and insight. In particular, the pre-master results had to be assessed in order to shape the continuation.

3.1. Background and pre-master

The core of the master work and report is based largely on the work done in the pre-master project, but also on efforts and research from previous theses and collaborators and their partners. In particular, SINTEF has previously contributed both in terms of technology and business development. An assumed collaboration combines the EMPIG system with the SINTEF Saturn cold flow concept described in chapter 2.2 to enable the system as a whole to process both wax and hydrates. A preferred embodiment resulting from this master thesis

should still comprise the back feed loop as presented in the pre-master report without diminishing the value added by the advantageous re-structuring of the overall layout.

Serving as a continuation of the pre-master work, selected design elements treated therein should be reconsidered in the master thesis work. Revisiting key features is necessary in order to secure the coherence of the concept, and interdependence will consequently remain an important focus in the thesis.

The aspect of the system concept resulting from the pre-master project considered most valuable by EMPIG was the complete restructuring from a fragile kilometer long pipe stretch into a recognizable subsea module, and this is naturally assumed as foundation for the continued development. As such, a favorable outcome of the master thesis work would address a concept for the implementation of an induction heating solution accommodating an equal or similar structure.

3.1.1. Changed Premises

Much has happened since delivery of the pre-master report with respect to business and company vision, both leading up to and during the master thesis work. This has also impacted the project and report in several ways. As business development is an integral part of EMPIG activities at this point, it is natural for this to also be reflected in the thesis.

In the pre-master project report, considerations were made on the implementation of the proposed module in realistic subsea developments, and opportunities of in-field combinations beyond cold flow pre-transport cooling were indicated. Recognizing that a pure cold flow vision might be aiming towards a too distant future, the project is considered likely to benefit from realizing a proposition that is value adding for existing infrastructure and technology rather than paradigm changing. Considering the present trends and development, a system implementation within basic subsea processing schemes such as SSBI, i.e. subsea separation, boosting and injection, may prove the most realistic, and possibly give the quickest return on investment. A generic arrangement for a subsea processing system is illustrated in figure 3-1. An EMPIG system serving general subsea cooling needs may be advantageously implemented in combination with both separation and pumping and compression.

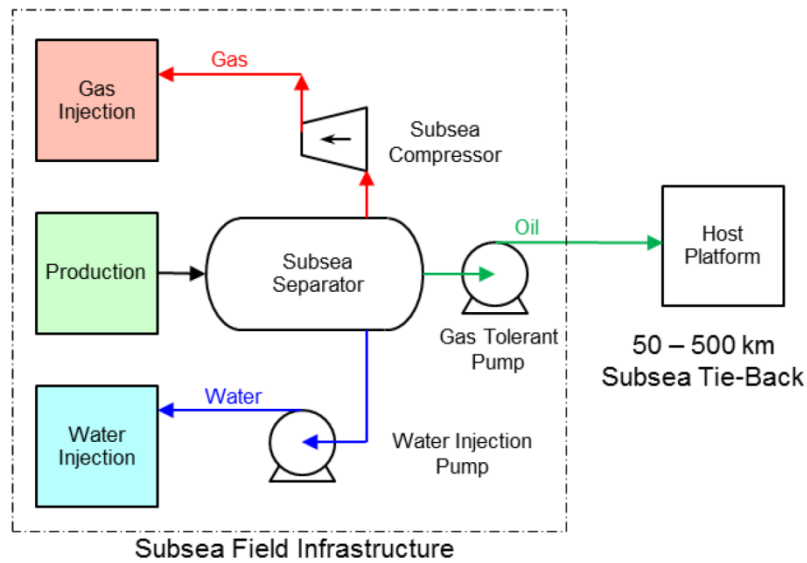


Figure 3-1: Generic subsea processing scheme (Lindland, 2014)

Extensive simulations on the passive cooling of a petroleum stream in seawater through relevant pipe material and diameter range have been carried out and documented at SINTEF by Larsen (2011a). Based on these, a requirement of an 800 m continuous cooling length was set in the pre-master report. This was, however, intended for the case of cold flow facilitation, in which the petroleum stream must be brought nearly, if not completely, to ambient temperatures. In passive convective cooling, the temperature reduction towards ambient is asymptotic in nature, and it is consequently concluded in the pre-master report that an increased allowable output temperature could entail substantial initial reductions in required cooling length.

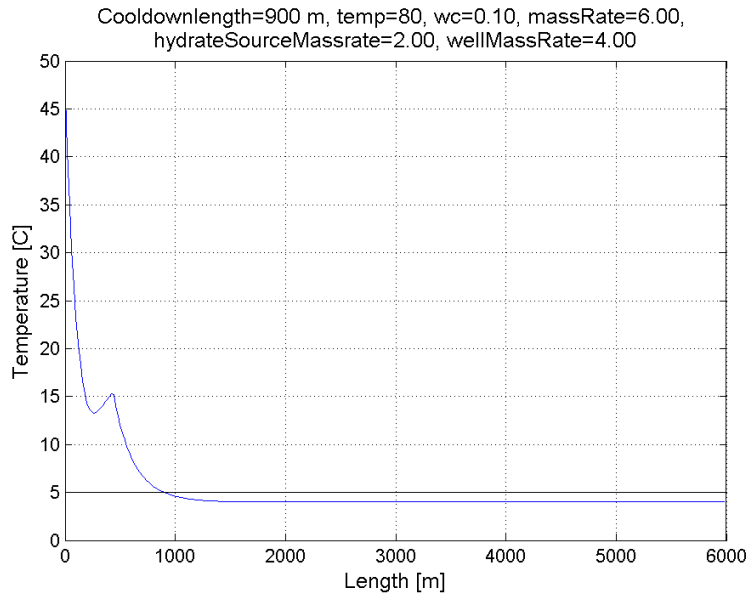


Figure 3-2: Typical asymptotic temperature profile for passive cooling of a bare pipeline exposed to seawater from thermal simulations carried out by SINTEF (Larsen, 2011a)

Further, an approach aimed towards general subsea cooling and in-field combinations such as discussed in the pre-master report is unlikely to pose as strict requirements in terms of cooling. Conclusively, moving away from the vision of cold flow may enable a more liberal pipe design, potentially increasing the solution space for the cleaning problem. No particular requirement was set with respect to cooling length, but in order to still be able to serve a wide range of well streams, a general solution accommodating a conservative 600-750 m cooling length should still be sought as starting point.

To facilitate the envisioned expansion of the value proposition, and in line with principles of modularity in design, a preferred embodiment of the induction heating solution should be scalable within reasonable limits, given a specified general operation-governing structure.

3.2. Induction Heating Technology

The main focus of this master thesis is the implementation of induction heating technology in the proposed EMPIG subsea cooling module, and key to the realistic consideration of this matter is knowledge of the technical workings of the induction heating technology itself. The theoretical background is presented in chapter 2, and the implications are considered in the following, with a focus on limitations imposed on development.

3.2.1. EFD Induction

As Europe's largest supplier of industrial induction solutions and longtime cooperator for EMPIG, considerations on implementation assume the use of technology by EFD Induction, who has contributed extensively with feasibility discussion and input. From their product range and in accordance with previous work, the Minac®¹ model 18/25 mobile heat generator is assumed as the most likely candidate for the proposed adaptation. This includes a mobile power supply unit with all the necessary electronics to rectify and generate an AC current with frequencies reaching 25 kHz, and a cable transmitting power and cooling water through a transformer to the induction coil in a general setup as illustrated below:

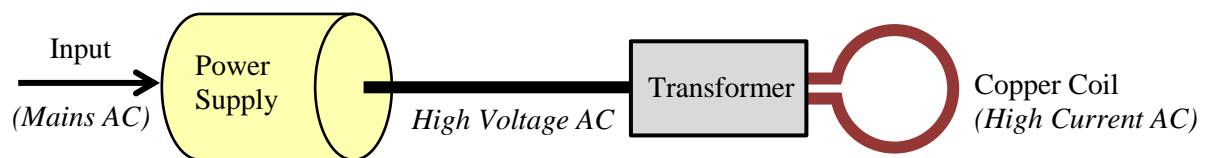


Figure 3-3: General Induction Heating Setup

The power unit has in fact already been marinated by EFD Induction for a project carried out by Statoil, where the power supply and electronics were encapsulated in cylindrical canister constructed to withstand pressures of water depths exceeding 1000 m. The canister had the approximate dimensions 300 mm by 1000 mm in diameter and length respectively, and the same is assumed in this thesis for the case of the EMPIG system. For the relevant power ratings, the transformers can be made “the size of a beer can” (Asperheim, 2014); in the mock-ups subject to this thesis, cylindrical dimensions of 85 mm and 140 mm are assumed for diameter and height respectively.

¹ A [brochure](#) is provided in appendix C.

The setup as shown in figure 3-3 is also considered necessary for the EMPIG application for reasons discussed in the following.

3.2.2. Managing losses

For induction heating to be efficient, the Joule heating in the workpiece must be maximized. As this is proportional to the square of the current I , as shown in equation 1, the current must consequently be maximized. Seeing as the strength of the magnetic field generated by an electric current varies with the magnitude of the current (Semiatin, 1988), the current carried by the induction coil itself must also be maximized to realize the highest heating efficiency. This can be seen from figure 3-4.

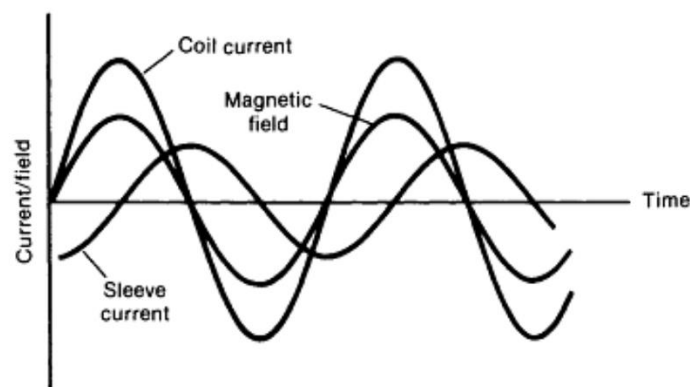


Figure 3-4: Typical variation of alternative electric current and the associated magnetic field strength (Semiatin, 1988)

The induction coil, thus carrying a low voltage, high current AC, however is also subject to the effects of Joule heating, and this high current transportation in fact causes the biggest electrical losses suffered in the process – for general wound components, these losses are typically referred to as “copper loss” (Clarke, 2008a). This means that in order to keep the overall efficiency high, the high current conduction must be limited to the coil only, and in close proximity of the workpiece to be heated. While this minimizes the overall losses system wise, the significant copper loss experienced by the coil must be consciously dealt with.

Seeing as the dimensions of the power supply (cf. chapter 3.2.1) are such that the coil in all likelihood must be separated from it by a cable to reach all required points of the pipe matrix, the power must travel across some distance. To limit the copper loss, the current in the cable must consequently be minimized. This is achieved by the power supply instead outputting high voltage AC in combination with an external transformer closely preceding the

coil, through which the current is drastically increased. As such, the transformer remains an invariant element of the setup, and must be accommodated in the concept design.

3.2.3. High frequency operation

The most significant obstacles to the implementation of induction heating in the EMPIG system concept as identified in this thesis work are those incurred by the high frequencies at which the induction equipment operates. As was described in chapter 2, the frequency of the alternating current has a direct impact on the penetration depth of the generated eddy currents in the workpiece (cf. skin effect), but the same is also true for the induction coil itself, as well as for the cable that transmits the electric current from the Minac power unit out to the coil.

The rated operating range of the Minac 18/25 in terms of frequency is 10-25 kHz, and evaluating equation 2-3 for this, assuming a copper resistivity of $1.678 \cdot 10^{-8} \Omega m$ (Matula, 1979) and relative magnetic permeability of 1.0 (Clark, 2008) suggests a minimum skin depth ρ in the area of 0.4 mm. This means that for a larger conductor, as would be required for the considerable power ratings in question, the majority of the cross section and hence bulk of conductor material would be left unused, and this will have variable impact depending on location in the general setup.

For the coil, this will be a matter of dealing with the consequences. The efficiency of the induction heating is dependent on several factors, including the gap between coil and workpiece as well as frequency and coil design (Semiatin, 1988). The copper loss, which is inversely proportional to the efficiency of the heating, inevitably will be dispersed as heat in the coil material. For a power range of 10-20 kW of high current AC through the coil, the generated heat may be significant.

Overheating of the coil is in fact a common failure mode, and the typical solution is to simply run cooling water through the hollow core of the coil to continuously remove the generated heat. While providing excellent cooling in an intuitive fashion, this also requires additional hardware in the form of a water pump and radiator at the very least. For a subsea implementation, the entailing increase in complexity and risk of failure may prove unacceptable for a concept already challenging conservative perceptions of feasibility. In coil and system design, alternative means of cooling should be investigated, as also requested by EMPIG. It was stated specifically that a passive solution was preferred, understood as one relying on natural convection with respect to cooling.

The power cable, transmitting high voltage AC from the power supply to the external transformer, will experience a similar current distribution behavior due to the skin effect, as the high AC frequency is already imposed upon leaving the power supply. For the potentially long cable, an inefficient conductor design is not tolerated, and measures must be taken to eliminate the detrimental consequences of the skin effect. For this case, a solution is readily available through the use of what is called litz wire.

The term litz wire is derived from “Litzendraht”, meaning braided or woven wire in German, and this is also the key to the solution. The litz wire comprises numerous strands of individually insulated wire that are woven together in a specific manner such that every strand of the bundle throughout the length of the cable tends to occupy all possible positions in the cross section. This effectively circumvents the unfortunate current distribution effects by ensuring a much larger conductor surface area as well as keeping all strand currents equal for the case of well woven wires. Figure 3-5 displays some simple litz wire configurations.



Figure 3-5: Examples of different litz wire configurations (SYNFLEX, 2013)

Still, the resulting dimensions of the flexible cable in the case of EMPIG impose certain limitations on its application through minimum bending radii that are significant relative to the overall system dimensions. As a rough estimate, Terje Solgård at EFD Induction conservatively recommends a bending radius of 400 mm. With respect to torsion, it is further stated that given a 180 degree twist at the cable end point, one should allow for approximately 1.5-2 m for the torsion to disperse.

Similar considerations are due for the transformer and power supply with respect to their adhering cable connections, which are to be considered equally rigid. This means that

the orientation of the power cable is fixed relative to the transformer and power supply respectively. For off-the-shelf equipment, the cable is tangentially aligned with the cylindrical transformer in the point of contact. This connection orientation may however be altered to specifications, granted that EMPIG or an industry partner will bear the associated alternative- and development costs. It should be noted that while expanding the solution space somewhat, similar flexibility constraints as previously set will still be present in any alternative configuration based on the same technology. Specifically, and greatly inconvenient, these aspects of the system structure are strictly prohibitive for the use of slip rings, which would otherwise simplify electric power transmission in a device with any rotational degrees of freedom by enabling a far more compact design.

The same cable as employed by EFD Induction also carries the tubing for the cooling water, and this must be considered contributory to the aforementioned geometric constraints. As such, removing the need for an internal cooling circuit may reveal additional opportunities for simplification by making the cable more manageable. Nevertheless, concept assessment and detailing was done with these conservative values in mind.

3.2.4. Efficiencies

The overall efficiency of the system depends on many factors. Most relevant to this thesis is the efficiency related to the electromagnetic coupling of the work piece and induction coil, and this is largely governed by the geometry of the coil in relation to the workpiece. Predominantly, the magnitude of the eddy currents induced in the workpiece will decrease with distance from the coil (Semiatin, 1988), and other form factors can be largely influencing, as indicated in table 3-1; Helical coils completely surrounding symmetrical workpieces generally have the highest efficiencies.

<i>Coupling efficiency at frequency of</i>	<i>10 Hz</i>		<i>450 kHz</i>	
Type of coil	Magnetic steel	Other metals	Magnetic steel	Other metals
Helical around workpiece	0.75	0.50	0.80	0.60
Pancake	0.35	0.25	0.50	0.30
Hairpin	0.45	0.30	0.60	0.40
One turn around workpiece	0.60	0.40	0.70	0.50
Channel	0.65	0.45	0.70	0.50
Internal	0.40	0.20	0.50	0.25

Table 3-1: Typical coupling efficiencies for different induction coil geometries and frequencies (Zinn & Semiatin, 1988)

In the case of the EMPIG implementation, retrievability becomes an obvious concern. For the updated system concept, the induction coil must allow operation in confined spaces, be able to traverse intermediate pipe supports, and satisfy some retrievability requirement – a rigid coil design may naturally not completely envelop the pipe. However, while efficiencies are important, a drop to well below the range of non-retrievable coils could be tolerated given sufficient cooling, cf. chapter 3.2.3. The final coil design will be a tradeoff between coupling and heating efficiency, mobility and reliability.

While successfully solving the cleaning function and giving proof of concept, it was recommended by Kjerschow (2014) that the induction coil should be developed further due to efficiency issues related to the retrievable coil design. Figure 3-6 shows the retrievable coil that was used for testing, featuring a typical ‘horseshoe’ design.



Figure 3-6: Retrievable coil design used in testing by Kjerschow (2014)

As discussed in chapter 4.3, it was further stated that a concept featuring two separate coils should be explored, an example of which shown in figure 4-16, as this would solve both efficiency and heat distribution issues. In addition to the lower efficiency, experiments with the retrievable coil showed an unfortunate cross-sectional temperature difference arising along the pipe circumference during heating, also pointing towards further efficiency reductions with respect to the specific application. However, the continued experiments with the retrievable coil still proved it successful in clearing the pipes of all wax deposition in spite of reduced efficiency, thus giving proof of concept and suggesting a relatively wide solution space with respect to coil design.

3.3. General concerns

It is well known that the oil and gas industry is characterized by widespread conservatism. As regularly discussed in media, e.g. Teknisk ukeblad (Qvale, 2014, 2015), this fact has time and again impeded the progress of entrepreneurs and smaller businesses in bringing innovative solutions into the industry. These tendencies have also proved strongly limiting in the case of the EMPIG system, and must naturally be taken into account in the continued development.

As emphasized in the pre-master report, maintainability through modularity and retrievability are important characteristics of a believable concept, and this remains valid also for this thesis. It is understood that intervention missions should be limited, though possible. This entails maximizing the service life through robust design, while also limiting size and weight, as the system downtime resulting from a malfunction is largely dependent on the time

it takes to find an appropriate service vessel (Gyllenhammar, 2012). Common industry practice is to store an identical spare of all components onshore, and in line with principles of modularity in design, see e.g. (Baldwin & Clark, 2004), a subdivided system consisting of interchangeable components is preferred. Further, the aforementioned modularity should ideally still be realized through vertical retrievability, such as illustrated in figure 3-7.

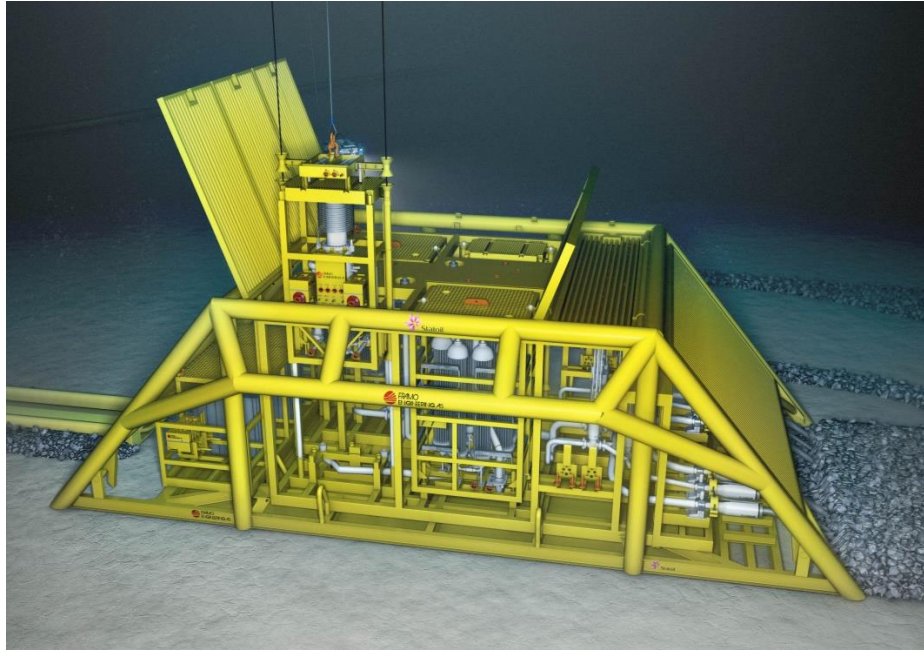


Figure 3-7: Vertical component retrieval from Gullfaks wet gas compressor (Statoil, 2012)

Particularly influencing for the market entry of the EMPIG system concept is the strong general reluctance towards moving parts that resides in the subsea industry. The majority of objection towards the EMPIG system typically trend around the apparent vulnerability of depending on a mobile sled for all flow assurance matters. The compact redesign introduced in the pre-master report is certainly extenuating in this regard, but the actual technical implementation of the InFlow concept in such a structure will likely incur an increase in complexity, making the system prone to the same criticism. As such, an important goal for the development must be to limit the number of degrees of freedom (DOF) in the mechanism relative to its functionality in the system, as well as the overall number of parts.

3.4. Potential hazards

Some of the most challenging operating conditions are those found in subsea environments. Factors that must be considered for a final InFlow system design include

- Corrosion
- Biofouling
- Elevated temperatures in working environment
- Exposed functional surfaces
- Magnetic effects on materials and electronics

Many of the associated requirements are fulfilled through proper material selection and protective measures, but several should be treated consciously already in conceptual design. This applies particularly to moving parts and surfaces or interfaces that are required to maintain properties related to tribology or heat transfer.

3.5. All electric

A clear trend that is currently emerging in the oil and gas industry is a shift towards electrically powered functional components as opposed to hydraulic and, encouraged by EMPIG, this is also to be reflected in development.

Advantages of an electric system as opposed to hydraulic are both functional and environmental, as it typically realizes significant system simplifications as well as removing the risk of hydraulic fluid discharge – an increasingly critical consideration. Accompanied by numerous valves, filters, sensors, accumulators and other moving parts that are inexpedient on their own, all hydraulic systems require a hydraulic power unit to deliver pressure through a series of hoses and couplings, and these are main sources of leaking and maintenance issues (Cavalieri & Wood, 2014). In contrast, electric systems are generally lighter, simpler, and less maintenance intensive, all important features for limiting cost and risk.

Winther-Larssen (2007) claims robustness, fault tolerance, scalability, reliability and flexibility to be main reasons for ‘going all electric’, as well as the ability to increase step-out distances with minimal modification of hardware – of increasing interest, especially considering the original EMPIG vision of cold flow facilitation. Naturally, the increased reliability of an all-electric EMPIG system is of particular importance with respect to credibility and should be duly emphasized.

4. Preliminary Concept Exploration

This chapter outlines fundamental features and decisions that were defining for the direction of the project, and their background, as well as discussion on concepts that for different reasons were not pursued any further. As this thesis constitutes both the current and foundation for the continued development, cf. chapter 3, this should also serve as reference in future decision making.

4.1. Layout and motion

In accordance with outlines of the EMPIG patents, to which any concept proposed in this thesis should adhere, the feature of linear motion along the length of the pipe sections are to be kept, and realized through some corresponding sled-based device.

It was early envisioned for the concept to take a more flexible embodiment than assumed in the pre-master, comprising one or several independent and redundant heater units. These would in turn comprise the induction heating apparatus, the general setup of which described in chapter 3.2.1, carried by an actuated mechanism to realize the range of motion necessary for reaching all required points of the operating volume. For the meandering pipe matrix, such a mechanism would at least require the three translational DOFs, i.e. vertical, longitudinal and transverse relative to the linear pipe stretches, and a number of additional distributed DOFs depending on principle solutions chosen for the induction coil and pipe interface and mode of operation.

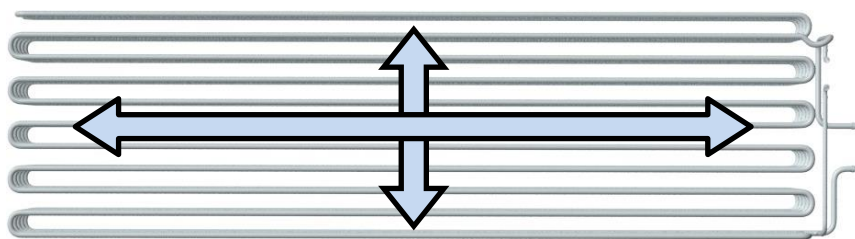


Figure 4-1: In-plane translational DOFs across general pipe layout

Given a sled-based design as previously indicated, this implies for the main translations to be planar – the fundamental motion is Cartesian, i.e. intuitively defined through main axes pertaining to said longitudinal and transverse directions. The sled as described in the pre-master report featured only the longitudinal DOF, and this is hence extended by an additional translation in the same or a close parallel plane, as shown in figure 4-1. For the subsequent

development, this is assumed realized through a second subordinate sled traversing the length of the primary sled, similar to what is commonly found in 3d-printers or general Cartesian industry robots.

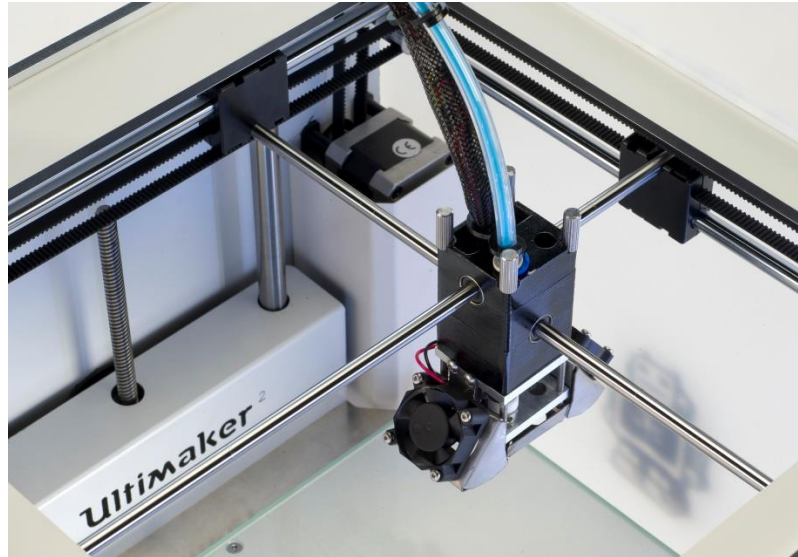


Figure 4-2: Cartesian motion in Ultimaker 3d-printer (Makerwise, 2013)

The overall layout of the pipe structure from the pre-master project is kept, meaning a continuous bare pipeline horizontally meandering through five vertically separated layers, each sequentially connected by further vertical pipe bends. As was assumed in the pre-master report, illustrated in figure 2-8, the pipe layout still accommodates the SINTEF Saturn recirculation loop, the position of which is indicated in figure 4-3 (a). The hot inlet directs the flow into the lowermost layer which it completely circulates before continuing upwards and sequentially through the layers in the same fashion. This seemingly counterintuitive flow sequence as set in the pre-master report was largely inferred from thermofluid considerations, for which the relevant theory is provided in appendix B through a pre-master excerpt, presenting investigations of turbulence effects in the buoyant plume downstream of heated cylinders.

Referring to chapter 3.1.1, as starting point for development, a slight reduction in length was assumed. This allowed for a subtle rearrangement of said vertical pipe bends, positioning all at the same end of the unit and making for a tidier layout, thus facilitating a flexible solution. Correspondingly, the opposite bends form a completely uniform array, likely increasing the solution space with respect to implementation of the chosen induction heating principle.

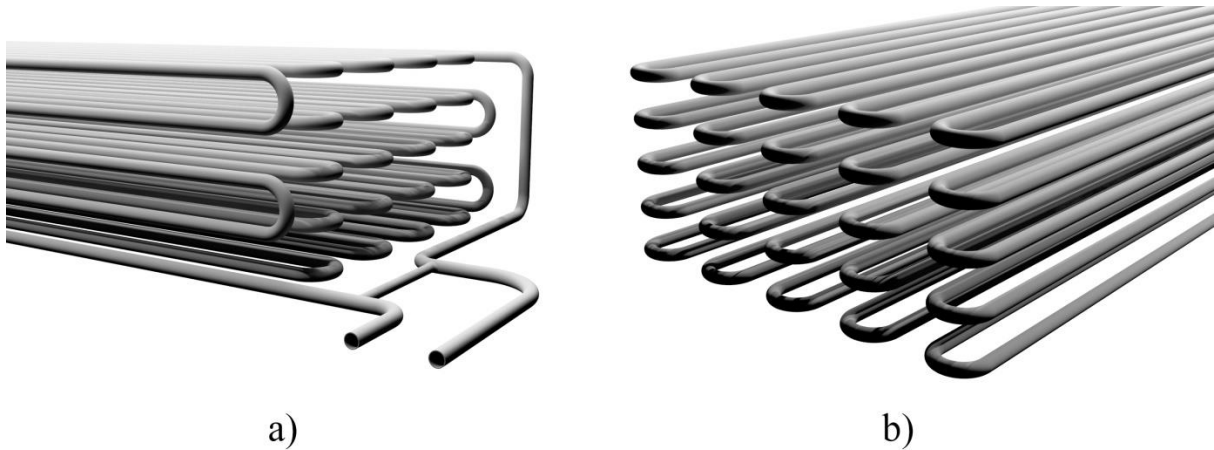


Figure 4-3: Pipe bend arrangement, (a) and (b) showing front and back respectively. Also indicated in (a) by the bridged pipes is the SINTEF Saturn recirculation loop

In fact, the pipe bends in general brought significant uncertainty to the concept, as they were not reasonably accessible by means of the assumed rigid sled. For the outer ends of the linear pipe stretches, simple pinned supports were assumed, largely industry customary. These provide the highest stiffness and stability, but require prominent transverse beams throughout the height of the pipe matrix. This is illustrated in figure 4-4 (a), where the inherent accessibility issues for bulky induction heating equipment with respect to the protruding pipe bends should be readily imaginable. Due to their inherent strength however, they can be made slim with respect to the length of the linear pipe sections, and it is assumed that indirect heating should provide sufficient fouling mitigation, given a flexible heater concept able to reach both sides.

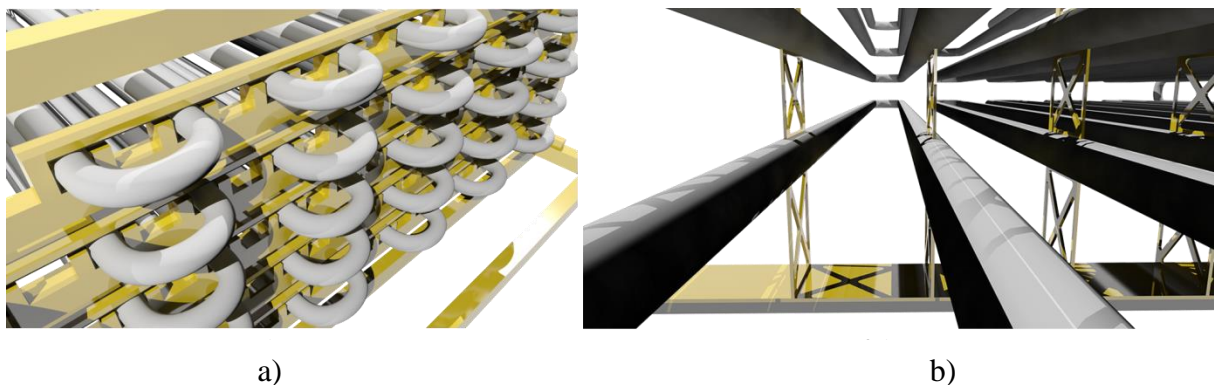


Figure 4-4: Pipe supports as proposed in the pre-master report (Bjørvik, 2014)

The dynamic response with respect to oscillations and vortex induced vibrations of an equivalent steel pipeline was studied by Radman (2012) to investigate the achievable free

span, and a conservative 15 m was set as maximum for a free bearing support regime, and 23 m for the case of fixed clamping support. It is preferred for the bending moments at the supports to be limited, and in the pre-master report, the length of the linear pipe stretches was assumed to be 14 m, and this is kept for this thesis.

While unproblematic with respect to static stress analysis, finite element analysis still indicated for the 14 m stretches to produce midpoint deflections in the area of 25 mm, and this was considered unacceptable for the presumably fine tolerances associated with operation of the rigid induction heating concept. As mitigation, a series of additional slender profiled supports were proposed, illustrated in figure 4-4 (b) (Bjørvik, 2014).

Given a more robust and flexible system, treating only a single pipe at a time and possibly comprising mechanical guides to secure operational precision underway, it is not unlikely that the deflections could be neglected to a larger degree. This was however not emphasized or specifically pursued in development. Instead, though eventually discontinued, initial development explored a regime of further pinned supports similar to those of the original end points. This effectively compartmentalized the pipe matrix volume, as the solid support racks still would block the path of any mechanism longitudinally traversing the same inner volume. This is illustrated below, based on the original core unit design:

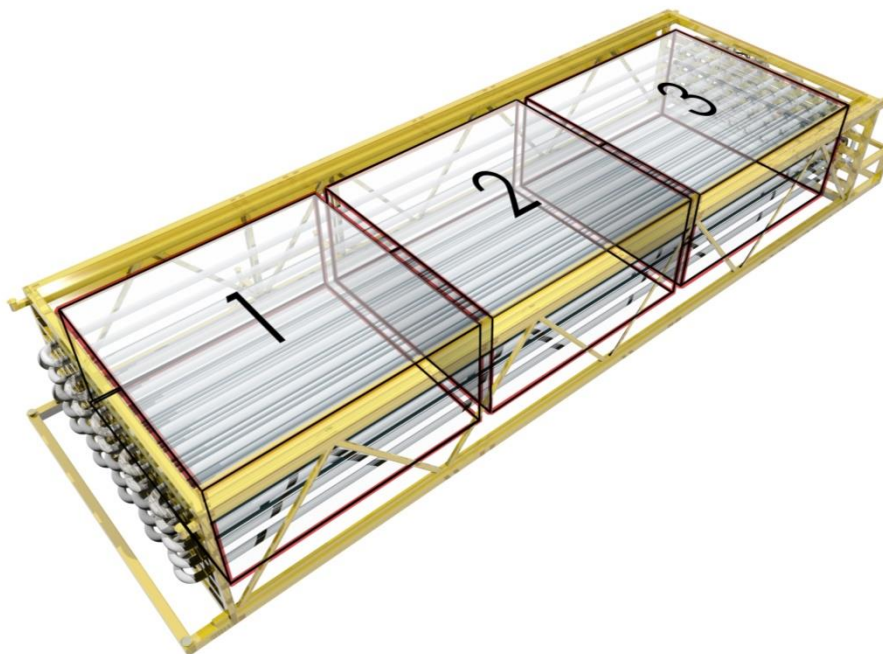


Figure 4-5: Core unit showing annotated compartmentalized operational space, sections divided by vertically planar pipe support racks

This was envisioned in conjunction with a highly flexible solution for the implementation of the induction heating concept, i.e. one that could reach all points in the pipe matrix regardless of direction – as would be necessary in order to accommodate such a partitioned operational space, as the induction heating coil must follow the pipe section until completely flush with the supports from both sides, so as to not leave cold spots. As mentioned, the supports themselves could be made slender, presumably allowing for indirect heating of the areas that would be inaccessible due to the pipe supports.

Figure 4-8 illustrates the outlined structure of a concept intended to operate in such conditions. The assumed cylindrical power supply is illustrated atop a sled carrying an actuated mechanism with DOFs sufficient to position some induction heating assembly at any point inside each pipe region from both front- and backside of the sled. The heater unit sled would traverse the primary sled, which would in turn carry it longitudinally with respect to the overall unit.

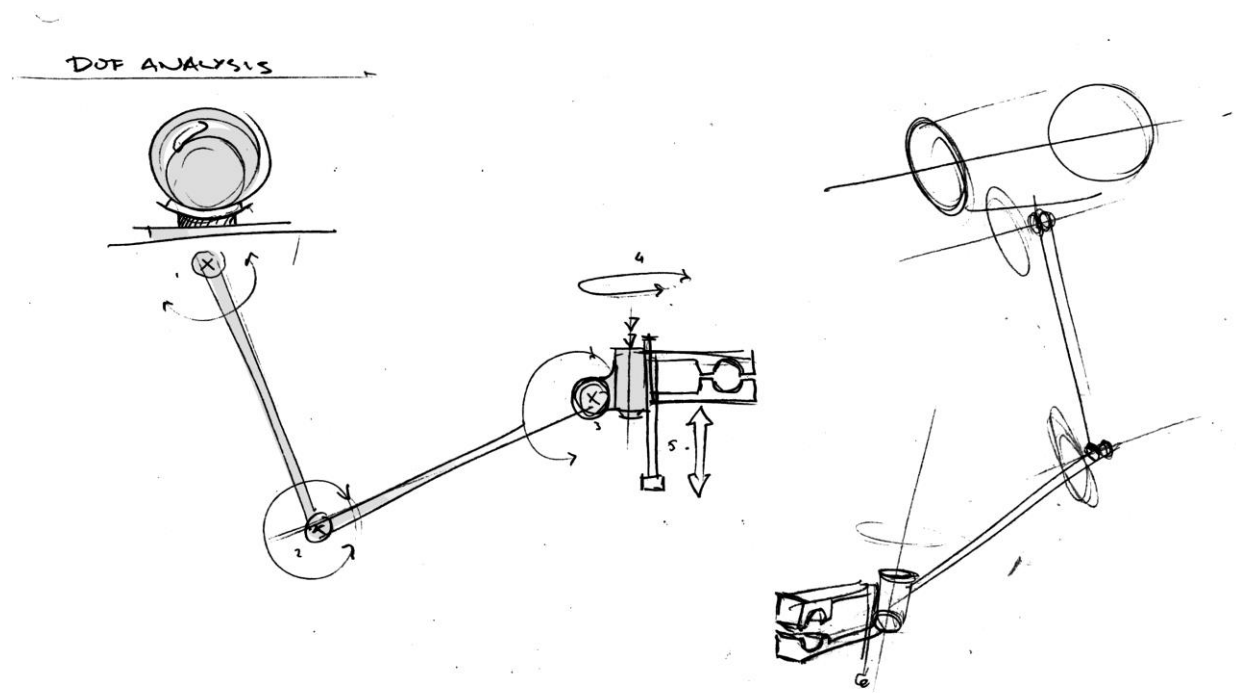


Figure 4-6: Sketch indicating DOFs for flexible multidirectional concept

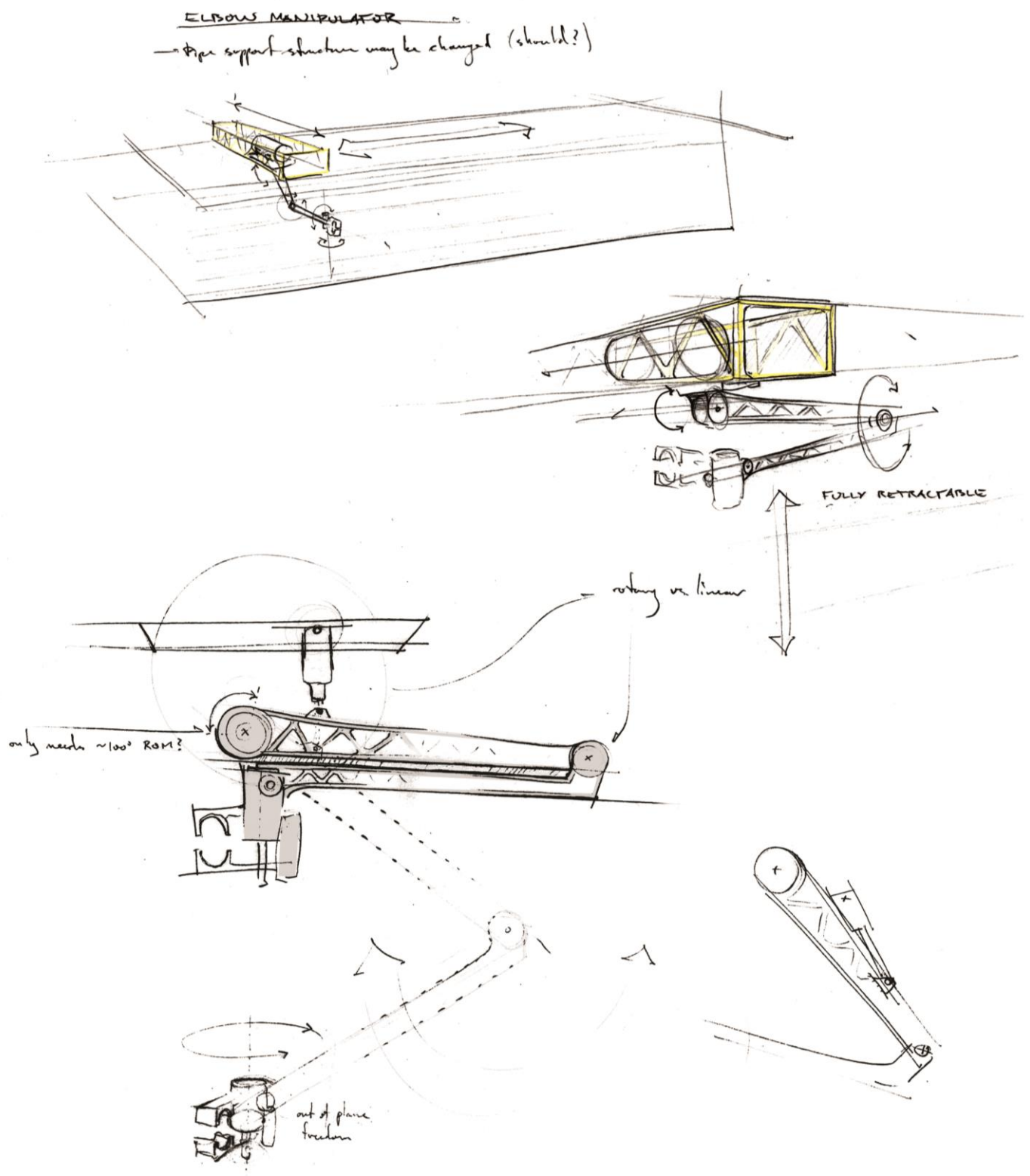


Figure 4-7: Exploratory sketches of multidirectional arm concept

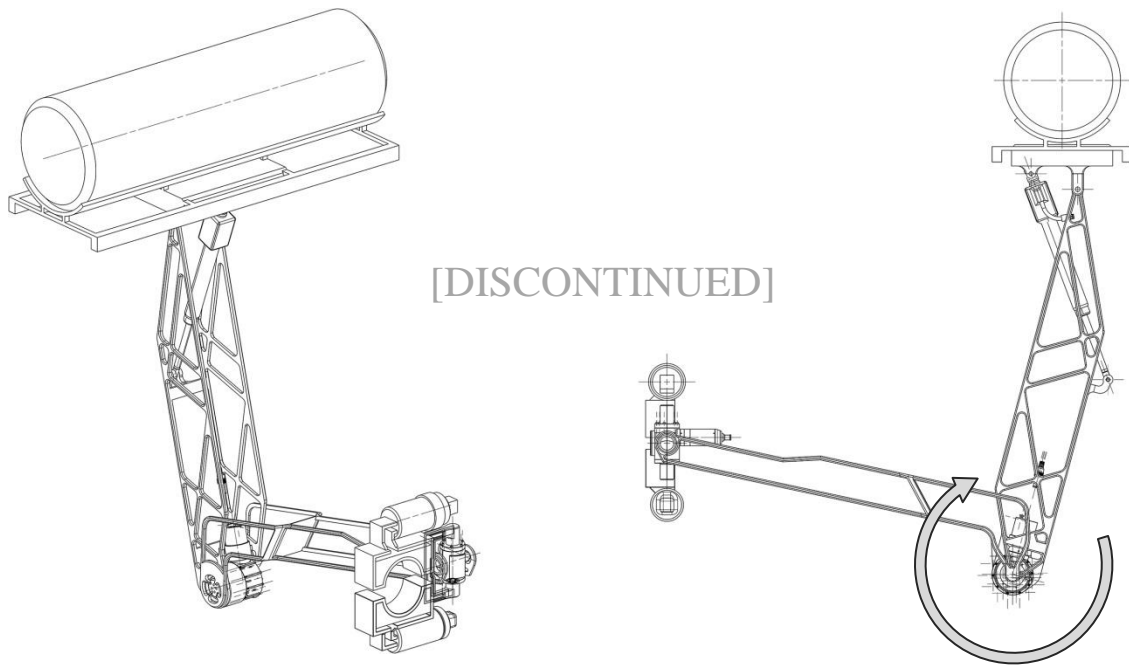


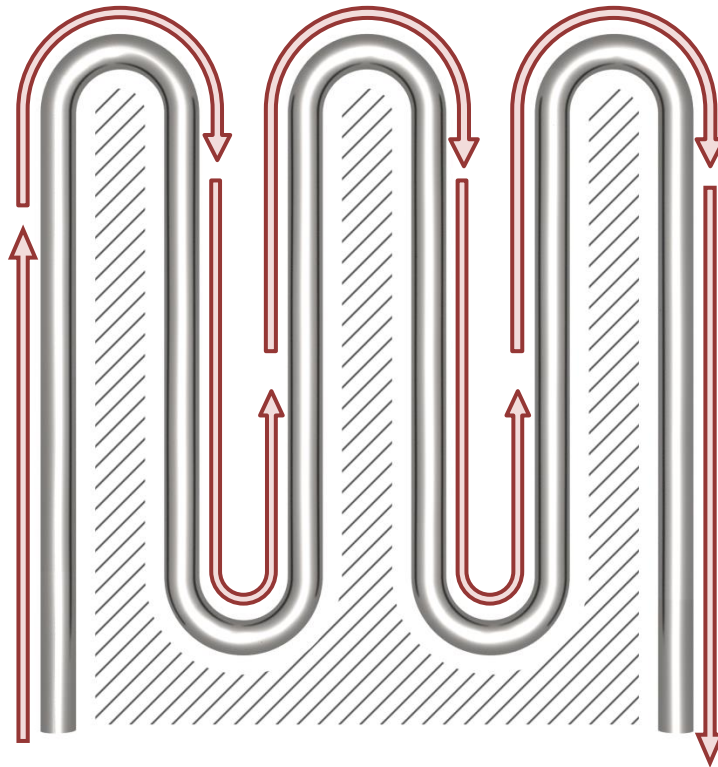
Figure 4-8: Multidirectional concept

This arrangement was motivated by the possibility of redundancy through the use of multiple units operating simultaneously. Having multiple units each capable of relatively complex maneuvers could also enable a physical interaction in between units in the case of malfunctions, given a clever design. A malfunctioning unit could thus be shut down and removed from the cooling zone by the remaining undamaged units, whereupon it is stored out of the way, so as to not interfere with the continued flow assurance operation, and to be readily available for retrieval upon the next intervention mission.

The obvious objection to such an embodiment is the large number of DOFs, and accompanying functional and moving parts; this also became decisive for the discontinued development of the concept in this embodiment. Considerations on operation in a compartmentalized regime also indicated intensive coupling and de-coupling requirements, as the heater would only operate continuously on relatively short pipe segments. This also implies for the servo operation to be almost continuous at several locations and thus inefficient.

While some elements of this initial concept were considered valuable and were carried over in further development, such as the inherent redundancy, the complex movements and geometry had to be simplified. The main focus and first measure in this regard was directed at the work path of the heater unit. In order to alleviate servos and allow for a wider range of

induction heater coupling principles, a concept allowing for a greater extent of continuous operation was sought.



With this realization, a corresponding support structure design may be inferred in the same fashion, i.e. one that allows uninterrupted operation of a retrievable induction coil engaged on the opposite side. Hence, an embodiment is assumed in which numerous distributed brackets engage the pipeline sideways by fixed clamping support. The crosshatched area in figure 4-9 indicates the placement of the supports opposite the heater work path. For a similar diameter range, inspiration may be drawn e.g. from common principles of handrail mounting, such as for use in swimming pools, shown in figure 4-10. A generic support structure is proposed based on the same principle, shown in figure 4-11 and 4-12.



Figure 4-10: Pool handrail mounting bracket (M-TC Sport, 2013)

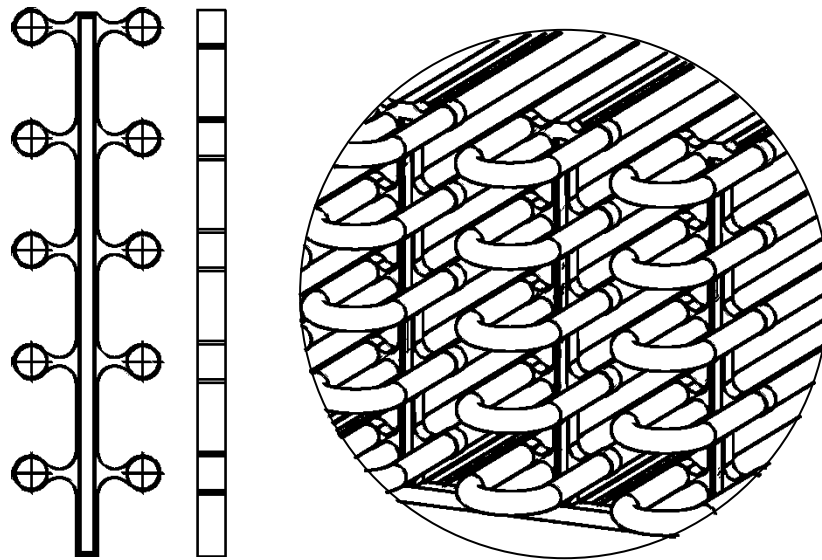


Figure 4-11: Generic pipe support structure with horizontal mounting brackets

This alternative means of support was envisioned early on, but was initially not preferred due to the increased structural complexity it would entail. However, the following concept exploration revealed that any customary solution would likely inflict a corresponding and relatively larger complexity increase in structure as well as operation of the sled assembly itself.

Assuming 4 inch STD/40 steel pipeline with weight per meter of 16.07 kg/m (Rolf Lycke, 2012) and cooling stretch of approximately 740 m gives a total weight of 11 891.8 kg for the complete pipe structure. In this report, 5 rows of bracketed pillars are assumed along the length of the 14 m linear pipe stretches. As each pillar may interact with directly neighboring pipes on both sides, the pillar rows further comprise 5 pillars across their width respectively. This makes a total of 25 pillars, comprising 10 brackets each. Consequently, the load carried by a single bracket would be just below 50 kg. Assuming a steel material for the

pillars, this is to be considered a minor loading – preliminary finite element analyses (FEA) indicate deformations in the range of thousandths of a millimeter, and associated stresses are equally negligible. It should also be noted that all considerations on mechanical strength are based on densities relative to air; due to buoyancy, the relative weight of all components will naturally be lower in submerged condition – i.e. for the majority of the unit's lifetime.

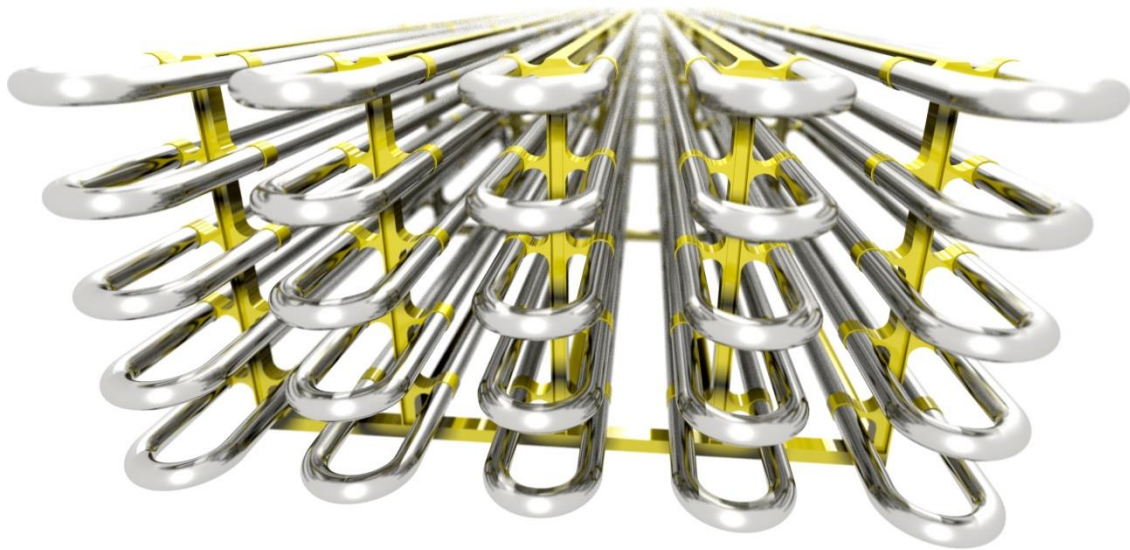


Figure 4-12: Rendering of proposed pipe support structure, the layout of which accommodates a continuous work path for the induction heating apparatus

No specific off-the-shelf components have been identified for this principle solution, but it is considered feasible, preferred by EMPIG, and substantiated by the above. Furthermore, the number and density of support pillars and adhering brackets may be increased freely, given proper design, thus reducing all respective loadings. Specifically, the clamps or sleeves enclosing the pipe must have a minimal diametrical profile in order to allow for an induction heating coil to pass unobstructed.

4.2. Primary sled

Figure 4-1 illustrates how the initially linear range of motion is expanded by an additional DOF in the transverse direction. The primary sled however still remains, and further motion is in fact reliant on it, as lower levels of the system are to be carried underneath. A common trussed structure is assumed, spanning the width of the cooling volume and supported on linear rails, in turn secured to the template structure. An embodiment is illustrated in figure 4-13.

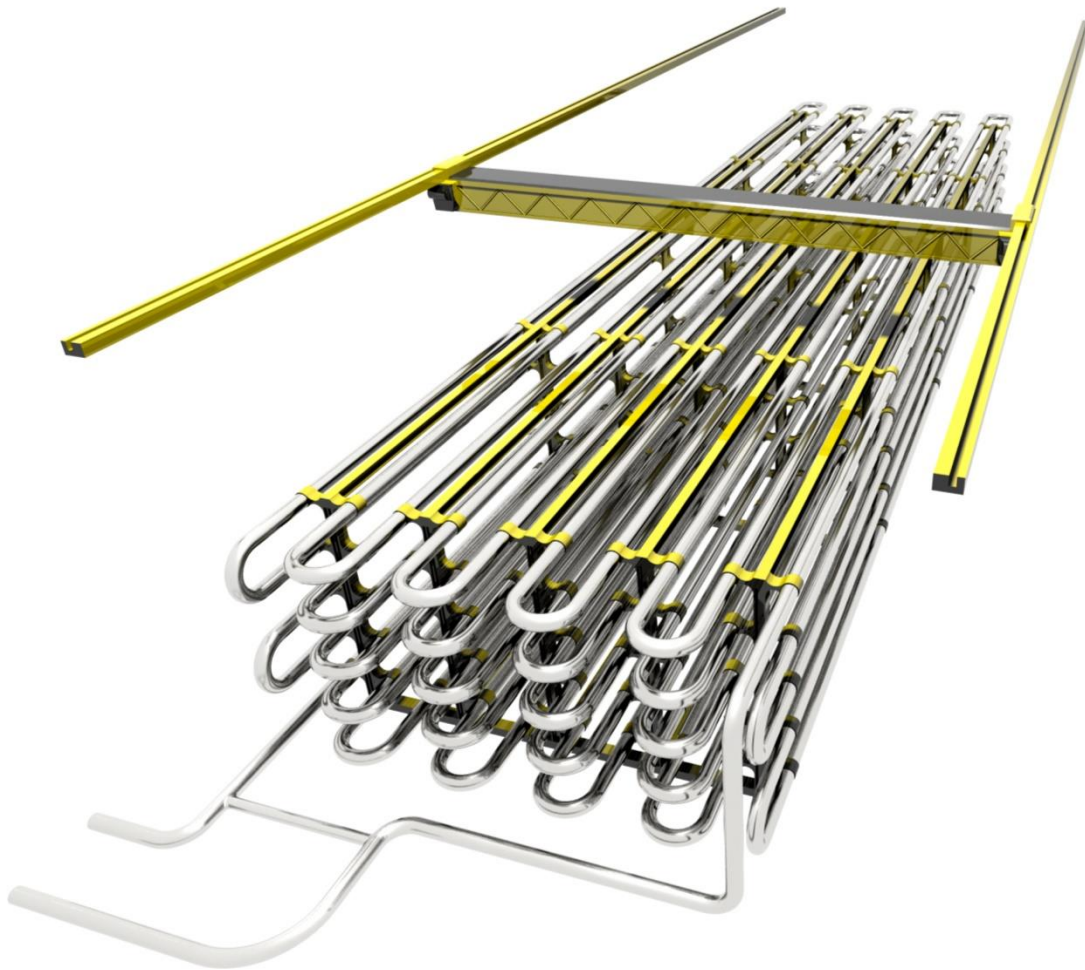


Figure 4-13: Rendering of primary sled suspended on linear rails above the pipe matrix

As shown in figure 4-14, the bottom face of the primary sled is open, except for the next set of linear rails to carry the heater unit. This allows for an intuitive means of access to the cooling matrix for the subsequent mechanism, hence increasing the solution space, but the structure is also motivated by shielding concerns. Referring to chapter 3.4, specifically

biofouling and exposed functional surfaces, the inclination of subsea equipment for general accumulation of unwanted organic and/or inorganic substances must be addressed in design. As there at any time will be such particles present in the surrounding seawater, the effect of gravity alone will tend to cause material to accumulate on any upwards facing surface. The general shape of the proposed sled is such that falling debris should be less prone to accumulate in critical regions suspended below.

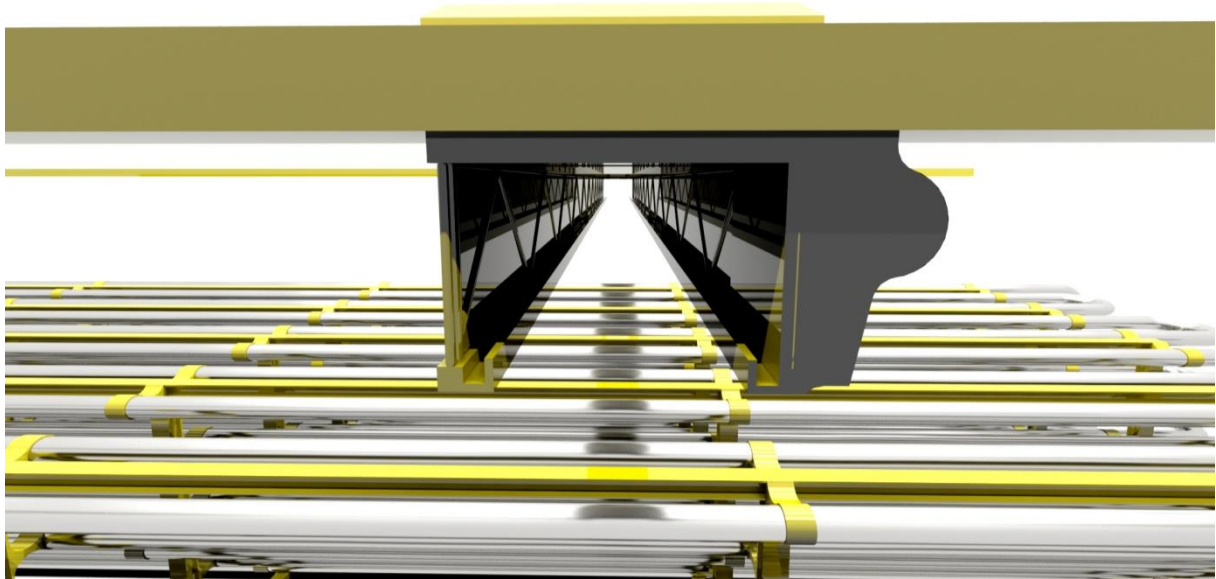


Figure 4-14: Side view of proposed primary sled structure

The term “functional surface” in this regard is understood as a surface interacting with some form of contact force, and this is of particular importance for the propulsion system. Though this feature has still not been dealt with in any detail, it is addressed and updated through general considerations, mostly with respect to redundancy and reliability. Redundancy issues and technological solutions in particular are discussed in the brief technology analysis given in chapter 6.1.

Nevertheless, all propulsion functionality is still assumed realized through rotary motion from a servo motor converted into linear by use of toothed rails. The physical interface through which the forces are transferred when driving the linear motion operates with certain dimensional tolerances, and tribological properties such as surface roughness play an additional role in both durability and efficiency. The contact forces are in fact integral to the inherent vulnerability of the interface with respect to these properties, as any impurity or foreign object risk entrapment between rail and pinion, potentially throwing off tolerances,

causing damage through grinding frictional wear, as well as a cumulative deterioration by ‘packing’, as the debris and fouling is repeatedly compacted. A fragile and improperly designed system could well face derailing due to these issues given sufficient time and adverse operating conditions.

As previously suggested, an important mitigation measure for debris related problems is component geometry and orientation – to avoid many issues e.g. related to packing, the rails and functional interfaces must be protected by covers, and it is further assumed for all such components to feature an inverted installation. I.e., the toothed rails are mounted upside down underneath the protruding body of the rails. Ideally, this will mitigate debris accumulation and lessen the packing tendencies of macroscopic fouling.

Considerations on the technical implementation assume similar improvements by adopting a robust regime of so-called roller pinions to realize the rack and pinion functionality. This is further necessitated by the increased precision requirements incurred by the complexity of the updated motion pattern; it can be seen from figure 4-9 how the precisely controlled work path in all likelihood will demand a significant positional accuracy in the general motion.

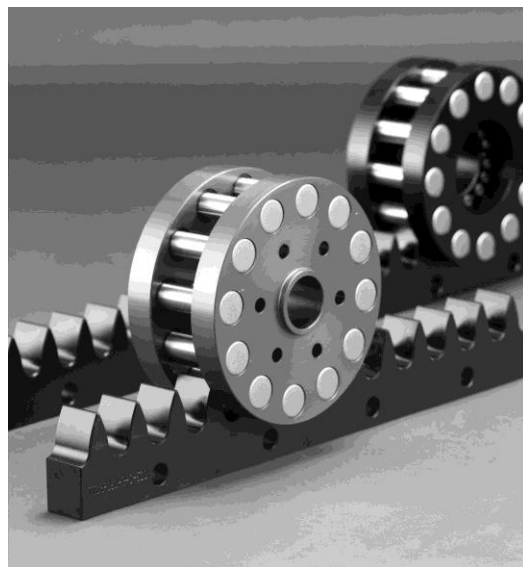


Figure 4-15: Example of typical roller pinions engaged on toothed linear racks
(DirectIndustry, 2013)

Roller pinions have a characteristic and seemingly coarse appearance, but are in fact integral to many high accuracy applications due to the same features that make them advantageous with respect to durability and reliability. While sharing the same basic operation principle as

ordinary rack and pinion setups, they differ by having bearing-supported rollers instead of a typical tooth profile. This modification essentially changes the mode of contact force interaction from that of a spur gear into something more resembling a cam and follower. Traditional rack and pinion systems are prone to jams and wear if the teeth are not designed with sufficient clearance, and the clearance is also strongly influenced by environmental factors. Such conventional systems will in any case experience backlash and continuously decreasing precision, and typically require frequent maintenance – an insurmountable barrier to subsea implementation. Roller pinion systems do not require clearance, and maintain a minimum of two engaged pinions at all times, thus eliminating backlash and inaccuracy. Furthermore, the rolling motion of the pinions drastically reduce friction and related issues, and may in fact operate lubrication-free for low speeds even in air (Kliber, 2012).

The racks and general functional surfaces are however still likely to experience biofouling of different sorts, though this may and should be mitigated by material selection and/or the implementation of occasional active cleaning measures, such as water jetting. These do however increase complexity by again requiring moving parts such as pumps and valves, so a passive solution would be much preferred, e.g. by considering coatings or inherently resistant materials.

No inquiries or further detailing of these solutions has been carried out, though the space allocated for a motor assembly is indicated in the rendering in figure 4-14. There should be at least two servo motors sharing the load at any time, located at opposite ends of the primary sled. For redundancy purposes, additional sets of motors may be placed alongside, given some release mechanism to disengage the original motor and transmission in case of malfunction.

4.3. Coil interface

In the updated system concept as presented in the pre-master report, an adaptation of an induction heating concept explored by Kjerschow was proposed. As mentioned, it was recommended by Kjerschow for a concept comprising two separate coils enclosing the pipe to be explored further, and this was also chosen as starting point for the concept exploration subject to this master thesis. Figure 4-16 shows a twin coil setup as manufactured by EFD Induction.

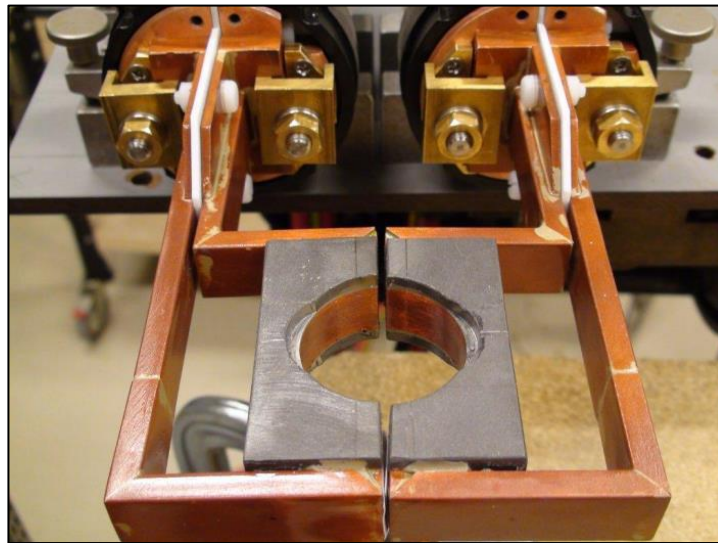


Figure 4-16: EFD Induction twin coil design

As the coil itself must be retrievable with respect to the pipe, and allow clearance for pipe supports to pass at different points, it must either have some clamping functionality or be retractable as is. For a single static coil, this entails leaving the back side of the pipe to be heated indirectly, as there may be no part of a solid coil surrounding it, as such decreasing the coupling efficiency, and the twin coil concept was preferred due to the inherent efficiency issues of such coil designs.

The advantageous working principle behind the twin coil concept comprises EFD Induction company secrets and is not disclosed herein. The effect however, is a dramatic increase in coupling efficiency, approaching that of helical non-retrievable coils, and the resulting heating pattern is naturally evened out correspondingly. For the twin coil concept to realize its full range of benefits, it also requires two transformers and precise control from the power supply, as well as accurate positioning with respect to both pipe and the respective

coils. A sturdy actuated mechanism comprising mechanical guides would also be required at the heater end of the unit.

In proceeding with the shaping of a realistic implementation, substantial practical difficulties were uncovered. These were largely due to range of motion problems in the confined space available in the unit and pipe matrix in general. Referring to the geometric constraints with respect to the cable motion as discussed in chapter 3.2.3, combined with the required implementation of an external transformer directly ahead of the coil, no embodiment has yet been identified which believably allows for two separate coils acting together to traverse the pipe matrix. The double set of transformers would correspondingly require separate power cables, further exacerbating difficulties, especially considering the additional DOF necessary for the clamping functionality. Further consideration of e.g. durability of such an embodiment is expected to be equally unpromising. The illustration below indicates the limited operation space in which the solution would be implemented.

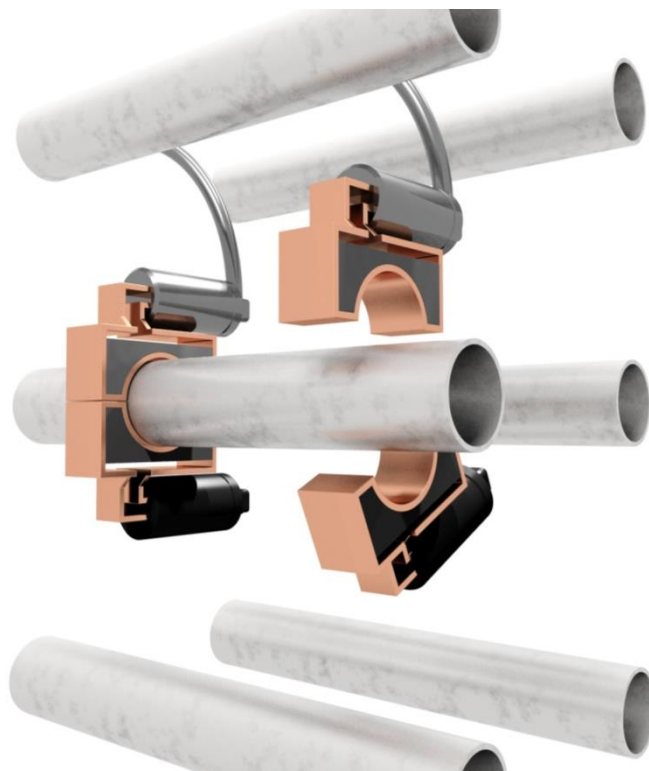


Figure 4-17: Illustration of relative dimensions in a 'twin coil' embodiment, showing both an open and closed (active) configuration

Realizing that the twin coil concept was too challenging to implement for the system in its current shape, development reverted back to retrievable coil designs, and the starting point was again based on previous work by Kjerschow, specifically the retrievable coil design

shown in figure 3-6, a slight adaptation of which shown in figure 4-18.

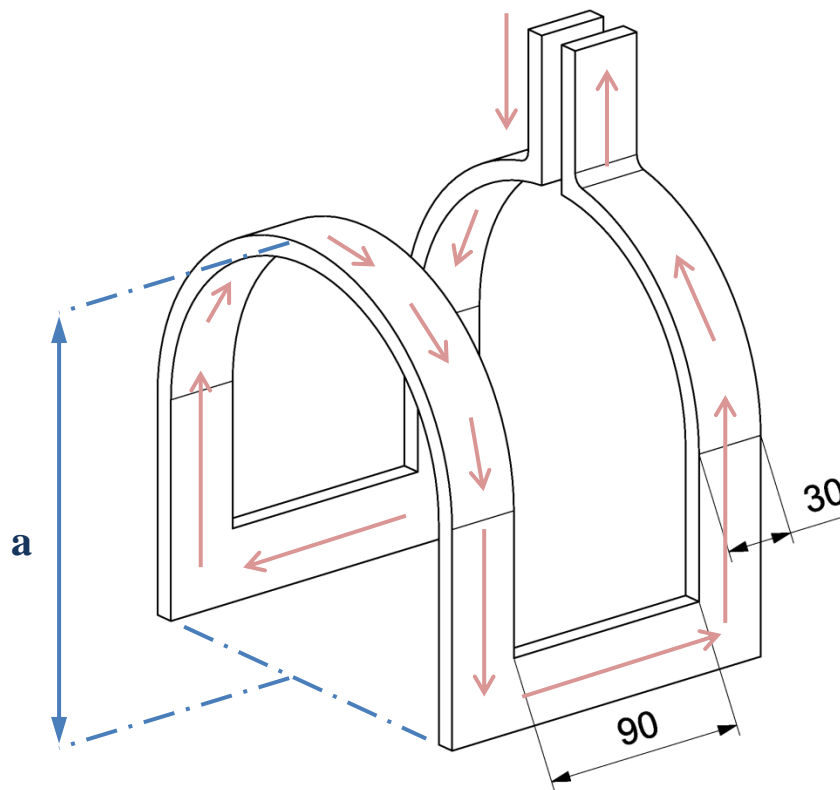


Figure 4-18: Adaptation of the retrievable 'horseshoe' coil design, arrows indicate direction of electric current flow, critical dimensions are annotated [mm]

The relative dimensions annotated in figure 4-18 must be calibrated consciously, due to the flow direction of the current and corresponding electromagnetic effects, c.f. chapter 2.5. Specifically, the separation distance of the two tangentially directed coil sections must be sufficient to avoid interaction and cancellation of the respective magnetic fields. The design of the coil used for testing by Kjerschow was performed in collaboration with EFD Induction, and conservative estimates state for the separation distance to equal three times the width of the coil section – 90 mm and 30 mm respectively (Kjerschow, 2014). These were also kept as starting point for the development subject to this thesis.

Further, the distance between the axially aligned coil sections and the pipe must also be such that the induced eddy currents in the pipe are not affected. For the 3 inch pipes used in testing, the dimension marked as a in figure 4-18 was initially assumed to be 130 mm, but eventually increased to 160 mm to improve the temperature distribution (Kjerschow, 2014). As stated in chapter 3.2.4, the coupling efficiency is inversely proportional to the separation distance between the coil and workpiece, so the coil radius and the distance between the

axially directed coil elements should be minimized within reasonable limits set by mode of operation, dimensions of pipe, and tolerances with respect to operational accuracy. But again, a looser coupling is acceptable given sufficient means of dealing with copper losses.

Optimization or exact detailing of the coil itself has not been subject to this thesis, as the main goal was rather to identify relevant and/or dependent parameters to serve as guidelines for continued development.

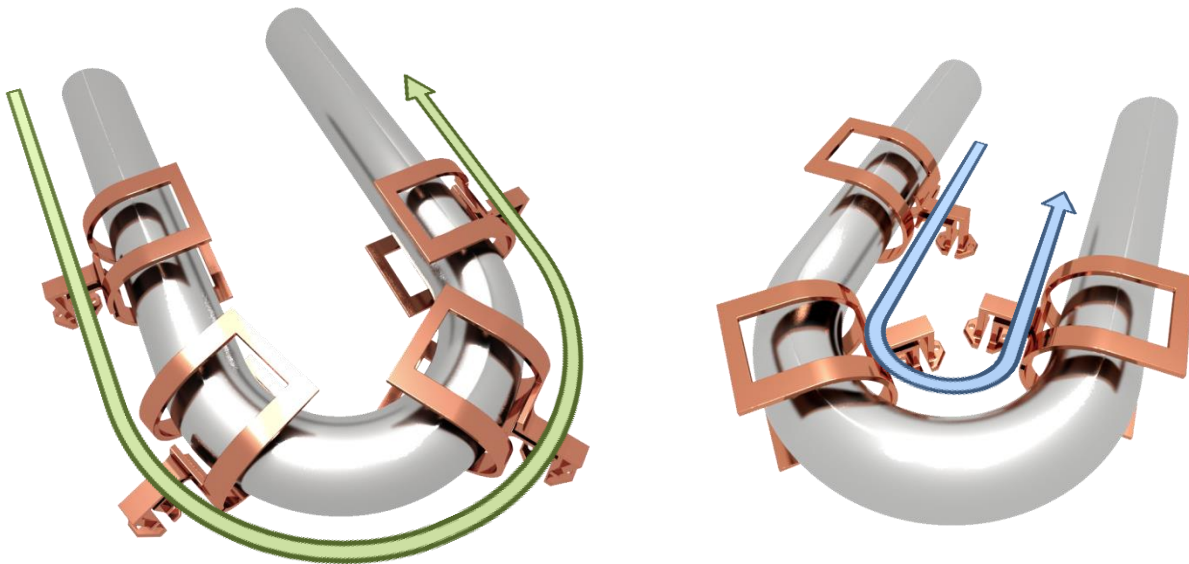


Figure 4-19: Visualization of work path through 180° pipe bends in horizontal plane for retrievable coil, showing outside path and inside path on the left and right respectively

Figure 4-19 illustrates how the coil geometry and the aforementioned dimensions in particular play a role with respect to accessibility during a continuous operation regime in the horizontal plane of meandering pipeline. In order to retain coupling efficiency and a somewhat predictable current distribution and associated heating pattern in coil and pipe while traversing pipe bends with small radii, it is advantageous for the spacing between the tangentially directed coil elements to be minimized. The distance a should similarly be increased for optimal performance through the bends, but it is also subject to a tradeoff with respect to the pipe support brackets – increasing the size of a entails a corresponding increase in length of the bracket ‘arms’, thus increasing stresses and deformations as well as the overall weight of the structure.

The coil work path and orientation indicated in figure 4-19 is assumed for the horizontal pipe bends, and should ideally be implemented correspondingly for the vertical

pipe bends. However, this would pose significant demands for the heater unit mechanism with respect to maneuverability and general DOFs, and may not be feasible. A possibly more realistic embodiment comprises a mechanism in which the coil traverses the vertical pipe bends still engaged sideways, as illustrated in figure 4-20.

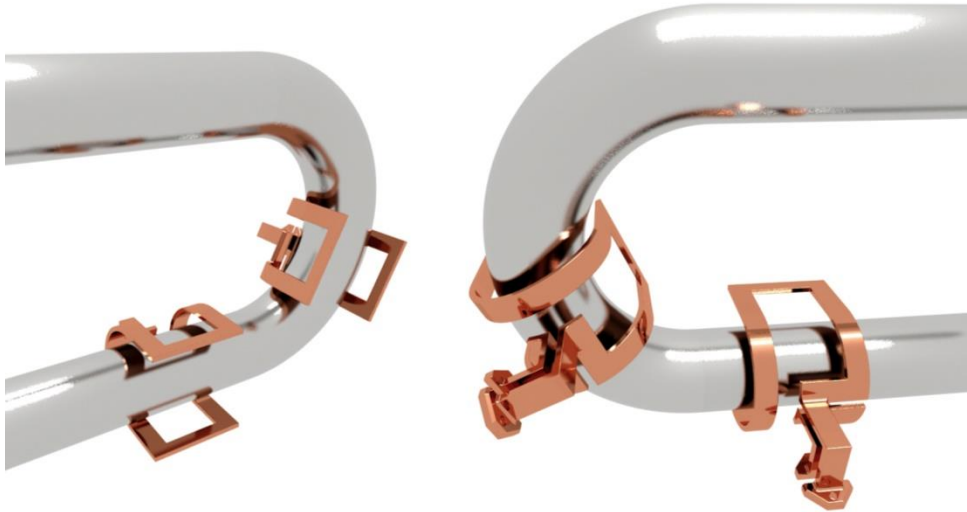


Figure 4-20: Retrievable coil traversing vertical pipe bend engaged from the side

As can be imagined examining figure 4-20, completing said maneuver with a rigid retrievable coil is more challenging, as the distance between the tangentially directed coil elements tends to cause collisions with the pipe. This can be mitigated by increasing the coil radius, which is arguably tolerable, and may prove a necessary measure either way, due to tolerances, proper protection of the coil, and allowing for the implementation of other features, such as mechanical cleaning of the pipe outer surface. An embodiment is illustrated in figure 4-21 in which said modifications of the coil are indicated. It should be noted that while increasing the radius as such does reduce the electromagnetic coupling, it also allows for a subtle change of shape, e.g. enabling more enclosing coil geometry, while retaining the inherent retrievability. This should in turn counter the cross-sectional temperature differences arising in the pipe during use of the typical horseshoe-design coil, given sufficient accuracy in the positioning of the pipe in the center; the proximity effect has a severe impact on current distribution in both coil and pipe, and must be taken into account. Should the pipe stray too close to one region of the coil, this will cause potentially damaging localized overheating in the pipe and in fact also in the coil itself, thus emphasizing the importance of precise control of the motion across the structure, which should likely be facilitated by use of mechanical guides of some sort.

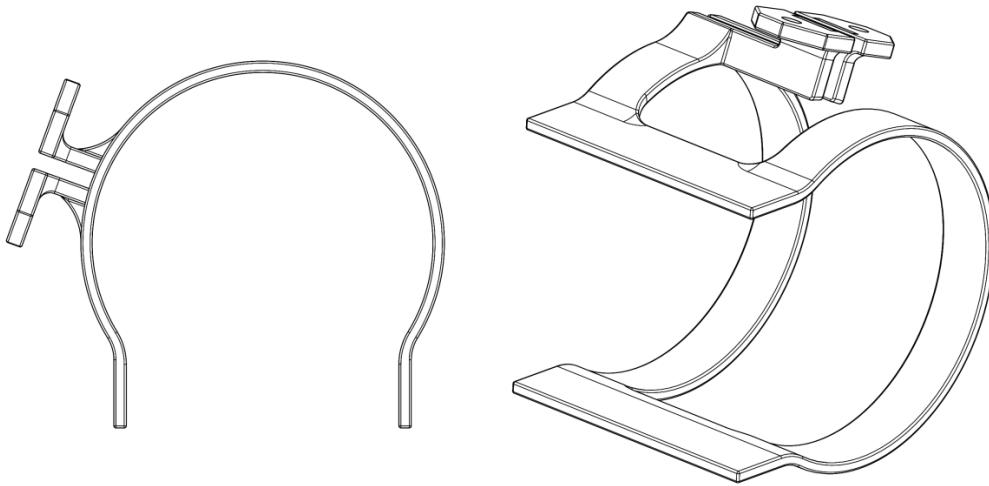


Figure 4-21: Modified retrievable coil design, showing increased radii

Still, while dedicated attempts were made, no embodiment has yet been identified in which this functionality is believably implemented, largely due to the previously described issues of the power cable. However, seeing as there are only 4 vertical pipe bends, the most pragmatic solution may well be to service these through a separate heating system. Any robust principle of heat generation with possibility of redundancy may be used, e.g. direct or indirect electric heating or some adapted induction heating concept of a more stationary nature. A simple principle of indirect heating is shown in figure 4-22, in the form of clamp-on band heaters.



Figure 4-22: Mineral insulated band heaters by Watlow (2015)

4.4. Realizing accessibility

In order to fulfill the flow assurance functionality, the heating equipment must be able to reach all points in the cooling pipe matrix. A main priority in development of the corresponding heater carrying mechanism was to limit the number of DOFs and adhering active components, such as servos. As the pipe and support structure, work path, induction coil design, and required maneuverability of the heater unit are so closely related, neither could be meaningfully considered separately. The concept embodiment described previously and illustrated in figure 4-8 is an example of this, in that the traditional support regime incurred complexity in both structure and operation of an otherwise reasonable concept.

A multitude of concepts were considered, some of which are illustrated in figure 4-23, the third being subject for significant evaluation as previously suggested. Concepts 1 and 2 were abandoned due to fragility, pinch hazard and exposed functional surfaces – variations on concept 2 featured vertical rack and pinion setups similar to that proposed for the linear translational motion in chapter 4.2, but were deemed unsuitable as a solution by EMPIG. Given the pipe support structure and simplified work path as shown in figure 4-9, these may however still prove satisfactory if a reasonable embodiment is identified at any point.

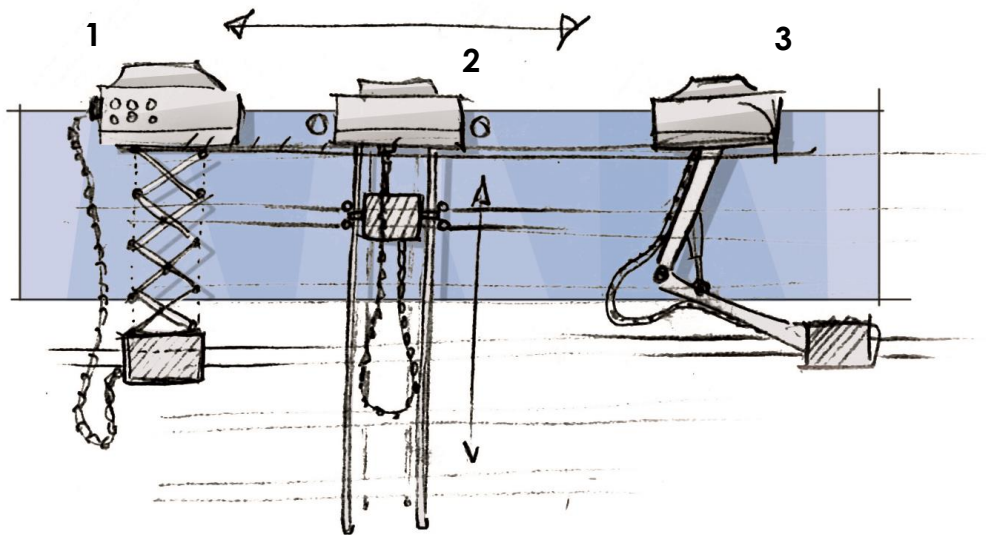


Figure 4-23: Early concept sketches

The previously described objections associated with concept 3 were also seen in conjunction with the assumed application of the two-coil concept mentioned in chapter 3 and further addressed in chapter 4.3. Reconsidering all elements resulted in a simplified concept for the

heater unit, in which the elevation of the coil assembly may be controlled by a rigid single section arm, like shown in the sketch in figure 4-24.

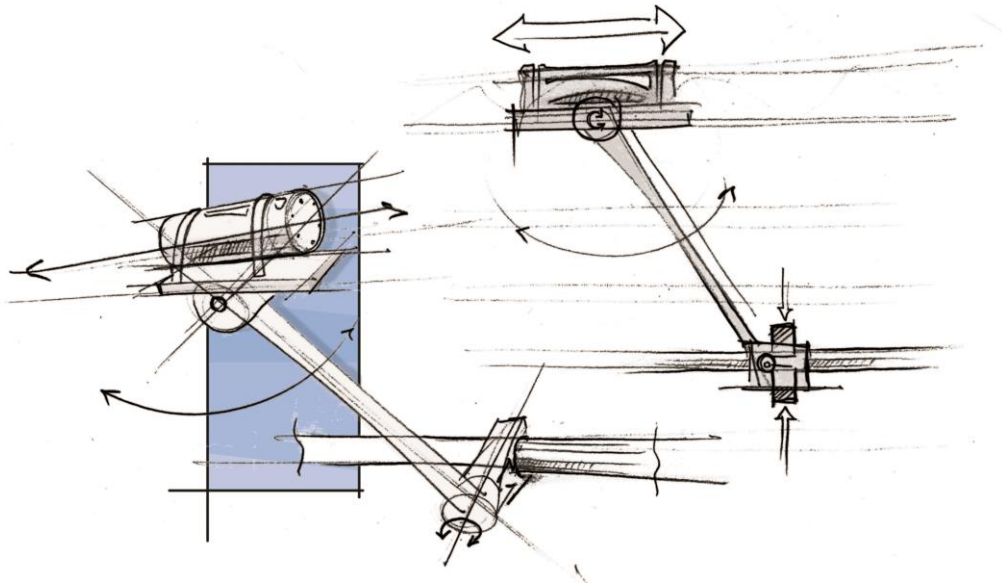


Figure 4-24: Rigid single section arm

The final concept for the heater unit mechanism was largely dependent on the principal solution of the induction coil. In the end, a coil design as shown in figure 4-21 was assumed, but lacking the possibility of serving the vertical pipe bends. As shown in figure 4-9 however, it should still traverse the entire horizontal planes of meandering pipeline without decoupling.

Based on this, a preferred embodiment is further detailed in chapter 6, so as to indicate the structure of a possible technical implementation.

5. Induction coil marinization

Concluding from considerations documented in chapter 4.3, a retrievable induction coil design as previously described is to be assumed for the subsequent development. This chapter will address some of the concerns raised in chapter 3 with respect to an actual subsea implementation, the most important of which being the presumably severe copper loss and associated cooling requirements.

Current trends in the oil and gas industry indicate a continuing shift of focus towards subsea and offshore development, see e.g. Kennedy (2013), and this is of course defining for present and future technological development. As increasing functionality is required for subsea applications, suppliers become accustomed to the accompanying challenges, including the marinization of different kinds of electrical equipment. While much has been done in the past, also by EFD Induction, little can be found in literature on the subject of continuously submerged application of induction coils, especially over time. Nor has EFD Induction much relevant practical experience. As mentioned in chapter 3.2.1, a complete induction heating unit has in fact been marinized in a Statoil commissioned project, in which it was used for pre-welding heat treatment. An illustrational video of the operation is available at Statoil's webpage ("Statoil med fjernstyrt verdensrekord på Åsgard²," 2013). However, the actual heat treatment however took place in an artificial atmosphere that was created in a housing enclosing the induction coils and transformers, and the rig as a whole was only intended for single missions, i.e. no extended submersion.

Many challenges are to be expected in such an application, including, but not limited to, those arising from subjects raised in chapter 3.4. The typical copper material is nevertheless inherently resistant in several ways, showing excellent properties in marine environments. Copper is well known for its corrosion resistance, but it also exhibits an inherently high resistance to biofouling, and macrofouling in particular – this often completely eliminates the need for coatings or treatment. Common applications for copper materials on-shore and off-shore already include different kinds of heat exchangers and condensers, as well as piping, tubing, components for pumps and valves, etc., implying unparalleled properties in several regards, and that the properties are retained over time, even in hostile environments (Powell & Webster, 2012).

² http://www.statoil.com/no/NewsAndMedia/News/2012/Pages/13Sep_hottap.aspx

Copper is the natural choice for induction coils due to its high electrical conductivity and low resistivity, but as implied by the above, its excellent thermal properties should also be of particular interest. High thermal conductivity, about thirty times that of stainless steels, means heat will be quickly dissipated from the coil, and high melting points further add to the confidence. Copper alloys do not undergo a ductile-brittle transition either, and are in fact ductile into cryogenic temperatures – suggesting compatibility with arctic environments, increasingly important for future developments. Further, and unlike stainless steels, copper alloys are not sensitive to chloride stress corrosion cracking or chloride induced pitting and crevice corrosion and they do not display the typical related temperature dependence either. They are however prone to erosion corrosion, also known as impingement attack, and this must be considered in case of high flow rates (Powell & Webster, 2012), but as can be seen from figure 5-1, this is unlikely to cause problems for the general application, as the critical velocity at which impingement attack occurs, the breakaway velocity, far exceeds velocities expected due to natural and induced convection currents, as will be shown later.

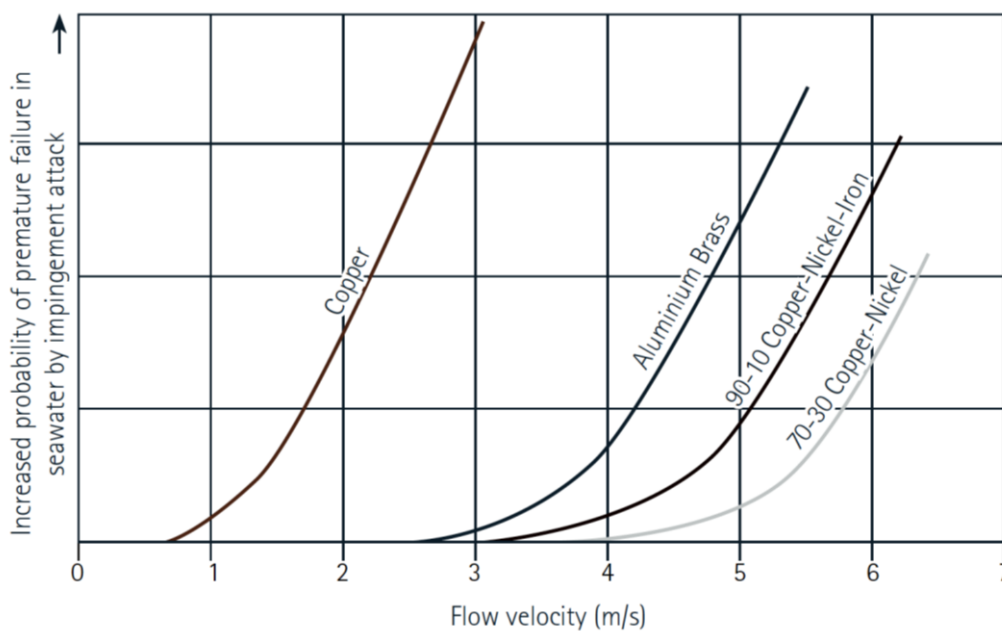


Figure 5-1: Relative velocities at which impingement attack may occur in copper alloys in seawater (Powell & Webster, 2012)

On the other hand, considering a forced convection cooling regime as currently used by EFD Induction, internal flow rates are significant; cooling water is run through the coil at rates of more than 7 liters per minute (“Minac® 18/25 SM,” 2014a), and given a subsea application in which the coolant is drawn from the surrounding seawater, as would be reasonable to assume,

erosion effects must be taken into account. A filtering system should be included in any case, as solid matter in the stream such as sand and biological substances also play a role in this regard. As stated in chapter 3.2.3, the possibilities of a passive cooling scheme should be investigated for reasons related to reliability and simplicity, and this is naturally further motivated by the above.

The case of an EMPIG implementation, however, poses additional challenges. Wan et al. (2012) studied the corrosion behavior of copper at elevated temperatures, and an exponential relation between temperature and corrosion rates was identified – examining samples subject to one hour exposure, the amount of corrosion at 800°C was 33920 times that at 100°C. While not insurmountable, this underlines the importance of proper heat and temperature management. As is common in the industry however, several of these effects may be mitigated through coating, as will be addressed later.

5.1. Electrical conductivity effects

Intuition does not advocate the combination of high power electricity and water. However, the relatively low voltage applications of induction coils are not observed to be affected by the submersion as such; a demonstration was in fact carried out at the facilities of EFD Induction in Skien, in which a Minac unit was, without problems, used to heat a steel bolt under water, a video screenshot shown below. See also “Heating Of Tube Under Water” (Sic) (2009)³ for additional footage from EFD Induction.



Figure 5-2: Screen capture from video of underwater induction heating demonstration at the facilities of EFD Induction in Skien

³ <https://www.youtube.com/watch?v=iEJ-2mlhuCw>

While promising with respect to the general principle, the relevance of these observations must be subject for discussion, as none of the aforementioned experiments have actually been conducted in seawater. It is well known that electrical conductivity is greatly affected by salinity, and seawater must therefore be expected to support a much larger current. The SI unit for electrical conductivity is Siemens per meter (S/m), and seawater is typically measured in the range of 5-6 S/m (CWT, 2004). While higher than typical fresh water (0.005-0.800 S/m), compared to copper, at around 58.5 MS/m (Tibtech Innovations, 2011), the difference seems negligible.

Liquids are in fact often used as electrical insulators, and for electric fields of relatively low strength, current magnitude is as suggested dominated by impurities. Nevertheless, similar to air and other gases, liquids experience so-called dielectric breakdown, through a sudden and dramatic reduction in resistance. This becomes possible upon exceeding a voltage potential threshold, as electron emission then may initiate at the impurity interfaces and be multiplied by ionization processes (Tommasini, 2009). This would in turn effectively short-circuit and potentially damage the coil. The Minac power supply itself does in fact comprise built in safety features to prevent damage during such events, e.g. in case the coil makes physical contact with the workpiece, and while unfortunate with respect to the coil, the situation is resolved through a simple reset (Sølgård, 2015).

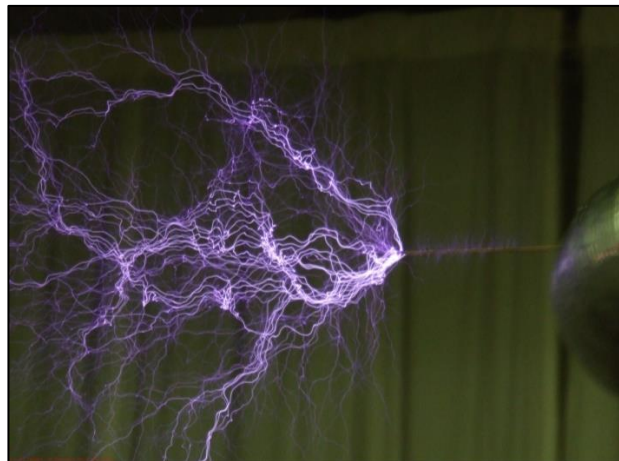


Figure 5-3: Dielectric breakdown of air from a charged Tesla-coil (Tresman, 2005)

As the assumed induction setup features relatively low voltages and may be further equipped with different precautionary measures, significant current leakage or short circuiting due to dielectric breakdown is not believed to pose insurmountable obstacles for the concept at this stage, though experiments have not been carried out for the relevant setup, nor have any

detailed calculations. While undeniably introducing some degree of uncertainty to the concept, it is assumed that any problems may be mitigated through a dielectric barrier of some sort, i.e. an electrically insulating substance to separate the conductor regions that are problematically close together with respect to aforementioned concerns. This may be realized e.g. through ceramics, polymers or composite materials partially or completely enveloping the exposed coil.

5.2. Aluminum oxide coating

A common solution for short circuiting issues and general protection of induction coils is the application of a thermal sprayed coating of aluminum oxide, Al_2O_3 , a ceramic material otherwise known as “Alumina”. Alumina features some remarkable properties in several of the areas previously discussed; typical uses include high temperature and high voltage insulation, wear pads, furnace liner tubes, ballistic armor and grinding media, and high purity alumina may be used in oxidizing as well as reducing atmospheres reaching 1925°C (“Aluminum Oxide,” 2013). The most common and stable crystalline structure of alumina, α , in fact forms the mineral corundum, of which the gem-stone sapphire is a variety. Sapphire features remarkable hardness, and is therefore often exploited in non-ornamental applications, such as in wristwatch crystals.



Figure 5-4: Wristwatch featuring aluminum oxide crystal, metal housing showing visible wear from daily use, whereas the alumina is 'crystal clear'

Illustrative for the excellent dielectric properties of alumina, an alumina coated induction coil may safely make full contact with the workpiece such that conductive metal effectively bridges the input and output of the transformer without any electric repercussions (Solgård,

2015). Furthermore, the alumina material is considered bioinert (Lindo et al., 2015), i.e. it does not interact with biological material. Samélor et al. (2011) concluded that amorphous alumina coatings could serve as oxidation and corrosion barriers and, nanostructured with platinum or silver nanoparticles, could exhibit anti-fouling as well as catalytic surface properties. Huang, Liu, Jianhui and Hua (2014) specifically studied potential marine applications of aluminum-alumina composite coatings fabricated by flame spraying against both corrosion and wear with promising results.

Other key factors for its relevance in a potential EMPIG implementation are thermal properties, and neither in this regard has anything definitively prohibitive been identified. AZO Materials (“Alumina,” 2014) also claim alumina to have good resistance against thermal shock as well as ‘high’ thermal conductivity, though this must be seen relative to other ceramics.

All of the above point towards an aluminum oxide coating being a viable starting point for further investigation, and it may well be preferred for reasons discussed in the following.

5.3. Thermal considerations

As suggested in chapter 3.2.3, the retrievable induction coil must be expected to generate significant heat due to the copper losses associated with reduced coupling efficiency. The resulting rise in temperature should be monitored precisely, and regulated by appropriate means in accordance with requirements established by thorough investigation of all related phenomena, including but not limited to the aforementioned effects of corrosion and fouling and structural integrity.

It is assumed that the implementation of a forced convection cooling regime as currently employed in typical induction heating applications of similar power ratings is feasible, though certainly unfavorable. Hence, efforts herein are focused around natural convection cooling processes.

5.3.1. Solid coil profile

As mentioned, common practice for cooling of induction heating coils is to run water through a closed loop inside of the coil throughout its length, and this naturally calls for a hollow and relatively unobstructed cross section. General coil design and construction is largely governed by recommended practices and experience, and the accommodation of proper internal water flow is part of this process. Removing the need for an internal cooling circuit should thus

facilitate far simpler coil geometry, and if so, significantly reduce manufacturing time and related expenditures. Correspondingly, and perhaps of greater importance, the reduced complexity should entail a far more robust design in general – typical wall thicknesses of induction coils employed by EFD Induction are in the area of 1 mm, and their fragile structure makes them prone to mechanical damage. In fact, workpiece collisions and impact constitute main failure modes for induction coils in common applications (Solgård, 2015). The electromagnetic field itself also generates considerable forces relative to the coil structure, which may potentially cause failure as a result of mechanical fatigue. Due to concerns of both electrical and mechanical nature, the complex structures are typically carefully silver-soldered together by hand.

For a subsea implementation in particular, the value of simple geometry should thus be evident, and subsequent considerations assume a coil structure comprising a solid cross section, i.e. a single copper body. An embodiment comprising such copper sections is illustrated in figure 5-5.

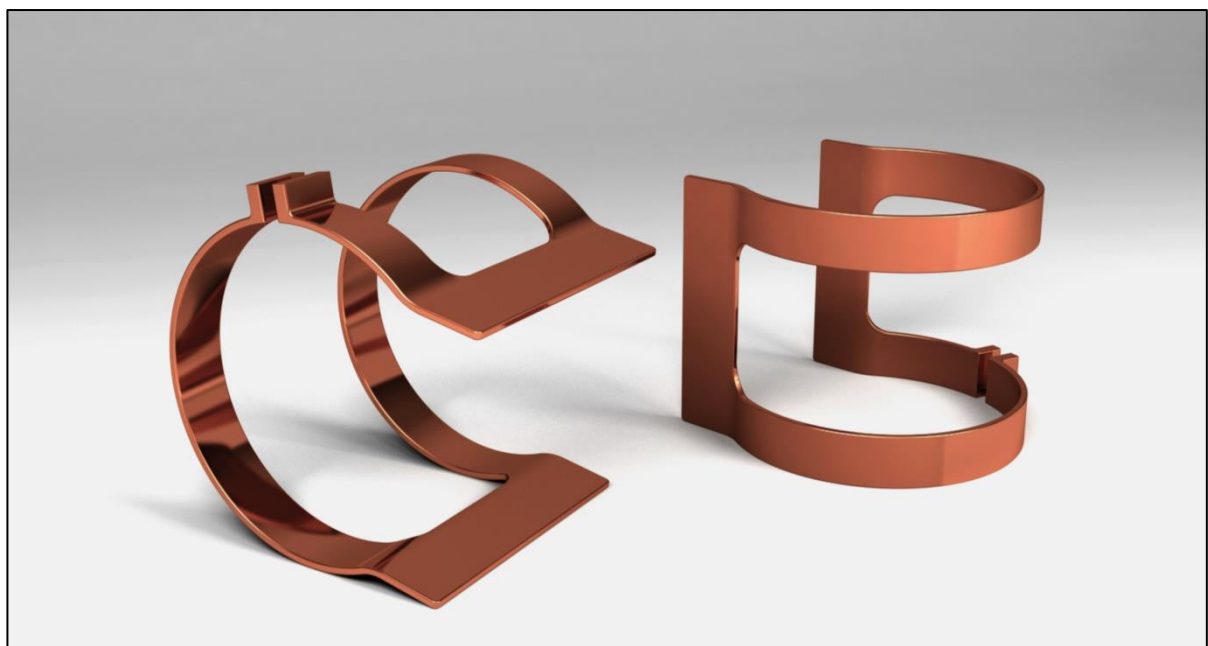


Figure 5-5: Solid copper coil embodiment

5.3.2. Thermal analyses of copper element

In order to take the first step towards validation of the solid coil concept, some understanding of the relative sizes in question should be obtained, though their realistic assessment on a theoretical basis is a difficult task. The following chapters will address the issue with respect to cooling through a preliminary computational investigation of the temperature rise resulting from joule heating in a copper metal element submerged in seawater and the associated convective heat dissipation.

5.3.2.1. Case

Parameters are set based on an assumed application of a solid coil as shown in figure 5-5 and confirmed by EFD Induction. The heat generated in the coil during use is assumed to equal the copper loss, which in turn is inversely proportional to the electromagnetic coupling efficiency. For such retrievable designs, efficiencies in the area of 40 % must be expected (Solgård, 2015). Assuming continuous application of 20 kW through the coil hence gives a considerable 12 kW of copper loss to be dissipated as heat.

It is reasonable to assume that the bulk of the heating will concentrate in the conductor region facing the pipe, as this is where the majority of the current will be traveling due to skin effect (skin depth of ~ 0.4 mm at 25 kHz), proximity effect and ring effect. Thermal conduction will then disperse the heat in the coil body, until presumably reaching some steady state in which all generated heat is dissipated from the surfaces of the coil. Based on this, and as foundation for calculations, a heating pattern is assumed as shown in figure 5-6.

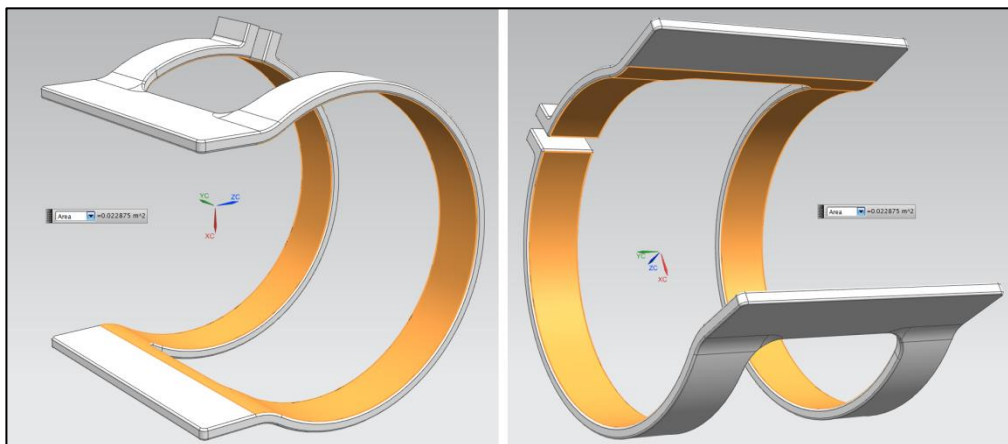


Figure 5-6: Assumed areas through which the bulk of the current will be traveling, and consequently where the heating will concentrate. Area is measured to 0.022875 m^2 .

Simplified and modeled as surface heat generation, this gives a generation rate of 524,590 W/m². Further, the ambient water temperature at the seabed is assumed to be 4°C, as for simulations by SINTEF (Larsen, 2011a), and a water pressure of 100 bar, corresponding to a physical depth of roughly 1000 m. These basic values are kept for the most part throughout simulations to facilitate comparison.

5.3.2.2. Simplified one-dimensional modeling

As starting point and basis for comparison of simulation results from computational fluid dynamics (CFD) software, a simplified manual approach is taken based on heat transfer literature. As analytical solution of the governing equations is difficult, and arguably beyond the scope of this thesis, the problem is simplified into one-dimensional relationships which may be evaluated iteratively in search of the steady state condition in which the heat generated in the copper element is dissipated through natural convection, such that the element is in thermal equilibrium with the surrounding seawater.

For initial calculations, a quadratic copper element with sides measuring 20 mm and thickness 6 mm is assumed. Further simplified, the heating is modeled as volumetrically uniform throughout the element body – the approximation becoming more accurate for decreasing element thicknesses; this of course substantiated by the excellent thermal conductivity of copper. Evaluating the heat generation rate for the assumed element geometry gives a ‘tangible’ volumetric heat load of approximately 210 W.

Further, the steady state form of Newton’s law of cooling is assumed as the basis for the convective heat transfer estimation, such that

$$q = \bar{h}(T_{element} - T_{\infty}) \quad \text{Equation 6}$$

where \bar{h} is the average heat transfer coefficient over the respective surface of the body, with units W/m²K, and T_{∞} is the ambient temperature of the surrounding seawater.

However, heat convection is a complicated process, and in the case of natural convection, the heat transfer coefficient will depend on the temperature difference between the element and the surroundings through a multitude of correlations (Lienhard IV & Lienhard V, 2011). Determining the heat transfer coefficient is integral to the calculation, and this is achieved through consideration of certain flow parameters in the so-called boundary layer adjacent to the respective surface. The relationships are derived from experimental

correlations, and are evaluated for thermophysical properties of the fluid and surface geometry and orientation, as well as temperatures.

The relationships used in the following are described by Bahrami (2014), and comprise the Rayleigh, Grashof, Prandtl and Nusselt numbers. For natural convection, the heat transfer coefficient h may be found from the Nusselt number Nu in that

$$Nu = \frac{h\delta}{k} \quad \text{Equation 7}$$

k being the thermal conductivity of the fluid, and δ the characteristic length. The Nusselt number is further dependent on the Rayleigh number Ra through the relation

$$Nu = CRa^n \quad \text{Equation 8}$$

in which the constants C and n are given from geometry and orientation of the surface, and the enveloping flow as follows: For a vertical plate,

$$Nu = \begin{cases} 0.59Ra^{\frac{1}{4}} & 10^4 < Ra < 10^9 \\ 0.1Ra^{\frac{1}{3}} & 10^9 < Ra < 10^{13} \end{cases} \quad \text{Equation 9}$$

For the upper and lower surfaces of the horizontal plates respectively, the following applies:

$$Nu = \begin{cases} 0.54Ra^{\frac{1}{4}} & 10^4 < Ra < 10^7 \\ 0.15Ra^{\frac{1}{3}} & 10^7 < Ra < 10^{11} \end{cases} \quad \text{Equation 10}$$

and

$$Nu = 0.27Ra^{\frac{1}{4}} \quad 10^5 < Ra < 10^{11} \quad \text{Equation 11}$$

The Rayleigh number is defined as the product of the Grashof and Prandtl numbers Gr and Pr such that

$$Ra = GrPr = \frac{g\beta(T_{element}-T_{\infty})\delta^3}{\nu^2} Pr \quad \text{Equation 12}$$

where:

g = acceleration of gravity

β = coefficient of volume expansion

δ = characteristic length

ν = kinematic viscosity of the fluid

(Bahrami, 2014)

These thermophysical fluid parameters for sea water, e.g. the Prandtl number, are dependent on temperature and salinity and must be retrieved or extrapolated from tables, such as by Sharqawy, Lienhard V and Zubair (2010)⁴. Fortunately, the library routines for these sea water properties are available in MATLAB format as well as EES and JACOBIAN from (“Thermophysical properties of seawater,” 2012)⁵. The thermal expansion coefficient in particular is calculated in *sw_alpha.m*, originating from Phil Morgan (1993)⁶

Based on above relationships and combined with the libraries of Sharqawy et al. and Morgan, MATLAB functions *Natural_convection.m* and *Grashof.m* were constructed, provided in appendix D and E respectively. *Natural_convection.m* takes in the following parameters:

Input parameter	Explanation
amb_temp	Ambient temperature of sea water [°C]
heat_load	Global copper loss in coil [W]
side_length	Side length of quadratic copper element [m]
thickness	Thickness of copper element [m]

⁴ http://web.mit.edu/seawater/Seawater_Property_Tables.pdf

⁵ http://web.mit.edu/seawater/SEAWATER_MATLAB_2012-07-17.zip

⁶ http://www.math.nyu.edu/caos_teaching/physical_oceanography/numerical_exercises/sea_water/sea_water.zip

pressure	Water pressure at assumed depth [decibar]
simulation_time	Total duration of simulation [s]
time_step	Duration of each iterative time step [s]

Table 5-1: Input parameters of MATLAB function *Natural_convection.m*

For *Grashof.m*, parameters are:

Input parameter	Explanation
beta	Coefficient of volume expansion [from table]
density	Density of sea water [from table]
L	Characteristic length [m]
coil_temp	Temperature of copper element [°C]
amb_temp	Ambient temperature of sea water [°C]
viscosity	Viscosity of sea water [from table]

Table 5-2: Input parameters of MATLAB function *Grashof.m*

As stated, the goal is to obtain a steady state solution with respect to $T_{element}$ from equation 6. In order to achieve this, *Natural_convection.m* employs an iterative scheme in which every thermophysical parameter is reevaluated each time step as if conditions were in fact steady. Any deviance from the assumed equilibrium is then carried over into the next iteration as basis for the next evaluation of said thermophysical parameters. The general algorithm for this approximated transient analysis is outlined in the following.

Based on the geometric input, the physical properties of copper are applied to the element, and the relative heat generation rate is set to incur a temperature increase evaluated as

$$\Delta T = \frac{Q}{cm} \quad \text{Equation 13}$$

where Q is the heat generation rate for the specified element area, c is the specific heat of copper and m is the mass of the specified copper element, both retrieved from Lienhard V and Lienhard IV (2011). Given said temperature increase, flow parameters are calculated and/or retrieved from aforementioned tables, and the heat transfer coefficients are determined for the

respective surfaces of the element. The heat transfer coefficients are in turn used to reevaluate equation 6 with respect to the heat dissipated during the same iteration, and thus the corresponding temperature drop according to equation 13. This is repeated with the specified time step resolution for the total duration of the simulation, in the course of which conditions ideally will have reached a steady state, i.e. when the element temperature is sufficient for the convective heat transfer to equal that of the generated heat due to copper loss. *Grashof.m* simply evaluates the Grashof number in the respective iteration when called by *Natral_convection.m*. It should further be noted that the temperature used to evaluate the majority of the flow parameters is the ‘film temperature’, which is simply the arithmetic mean of the surface temperature and that of the ambient fluid surrounding it, as this is the common and recommended practice for such problems.

5.3.2.3. Computational results

The computational model *Natural_convection.m* is run with parameters as follows:

Input parameter	Value
amb_temp	4
heat_load	12 000
side_length	0.02
thickness	0.006
pressure	1000
simulation_time	60
time_step	0.01

Table 5-3: Input values for computational model

The resulting element temperatures are plotted against physical simulation time in figure 5-7. As can be seen from the graph, a steady state condition is developed after approximately 10 seconds, with an element temperature converging at just above 100°C (~ 103°C).

The behavior for different input geometries was investigated. In particular, the thickness was reduced. The computational model was run again with the input as shown in table 5-4, and the resulting temperature plot is displayed in figure 5-8.

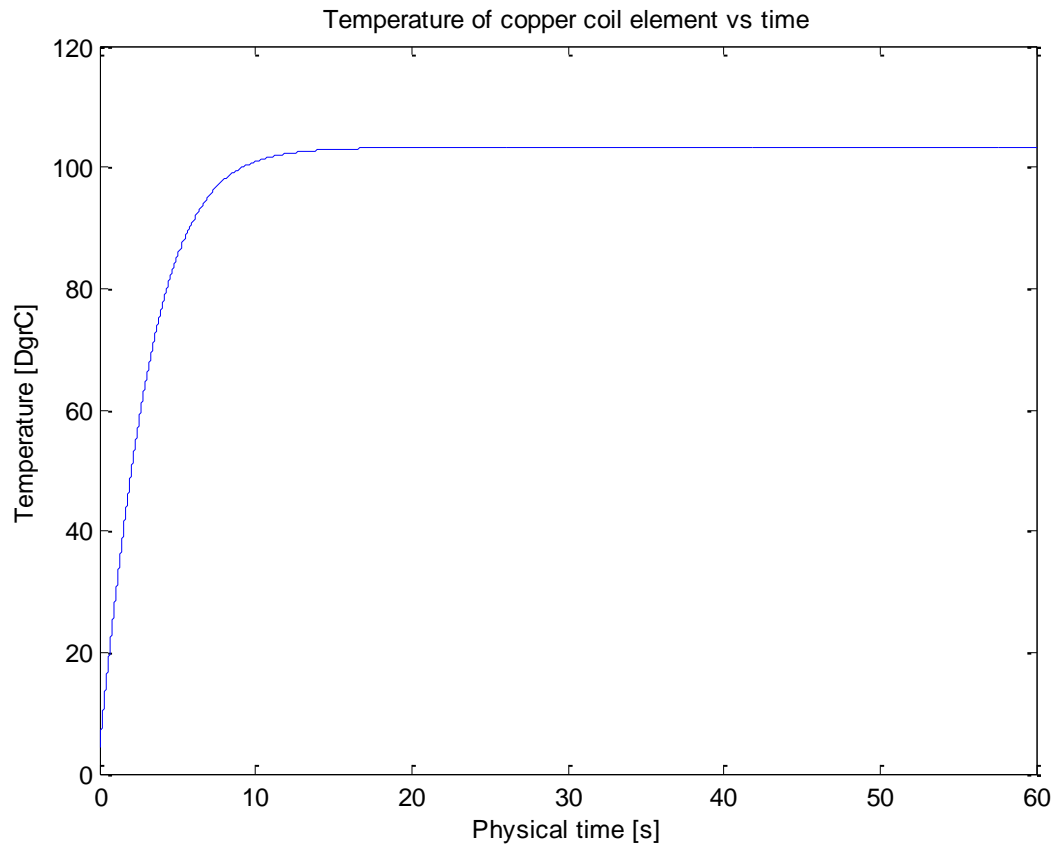


Figure 5-7: Temperature time plot given element side length 20 mm and thickness 6 mm

Input parameter	Value
amb_temp	4
heat_load	12 000
side_length	0.02
thickness	0.004
pressure	1000
simulation_time	60
time_step	0.01

Table 5-4: Input values for computational model

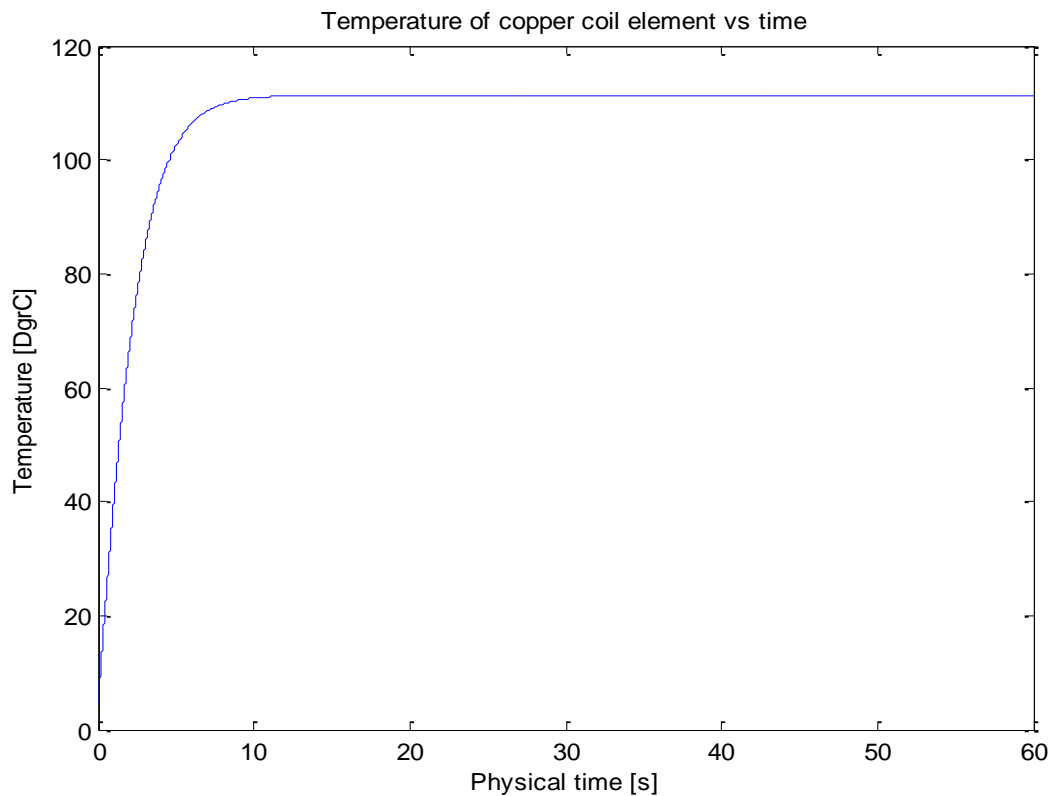


Figure 5-8: Temperature time plot given element side length 20 mm and thickness 4 mm

For the case of reduced thickness, the computational model indicates a slightly higher steady state temperature, $\sim 111^{\circ}\text{C}$. Further cases were also examined, including other geometries; trends are increasing temperatures for decreasing thicknesses and increasing side lengths. E.g. for the element dimensions $30 \times 30 \times 6$ mm, the steady state temperature is indicated to be in the area of 118°C .

5.3.2.4. CFD approach using Solidworks Flow Simulation

For comparison, a similar basic case is modeled using Solidworks and Solidworks Flow Simulation, i.e. comprising a quadratic copper element with side lengths 6 mm and thickness 6 mm submerged in water. The same heat load is applied, and again assumed to be volumetrically uniform, starting from initial conditions at 4°C ambient temperature in water and solid, and velocity field equal to zero – natural convection. Detailed setup for and additional results from simulations are provided in simulation reports in appendix H.

The simulation was run as a transient analysis, and figure 5-9 shows the resulting temperature time plot.

Transient natural convection analysis of 20*20*6 mm copper plate
in water, 210 W volumetric heat generation

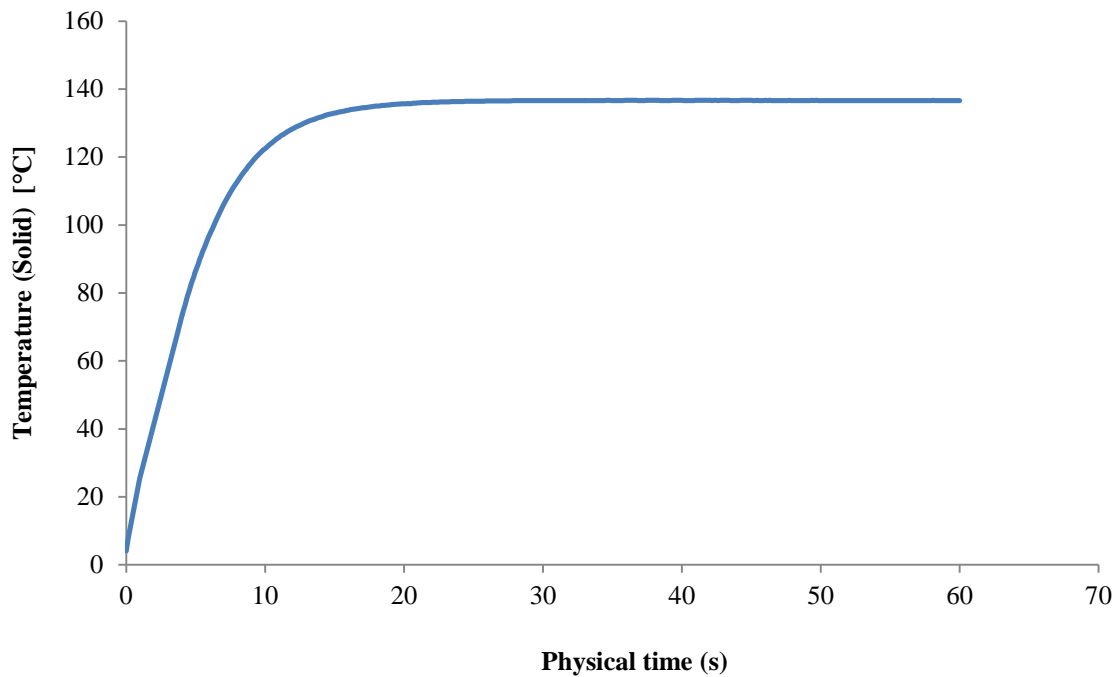


Figure 5-9: Temperature time plot from Solidworks Flow Simulation

The Solidworks simulation similarly reaches a steady state of heat generation in equilibrium with natural convection heat transfer to the surrounding water, though slightly slower, and indicating a higher steady state temperature, ~136°C. In order to produce physically meaningful results, Solidworks includes the effects of heat conduction in the solid element, and the temperature distribution arising inside the element at steady state conditions is displayed in the cut plot in figure 5-10.

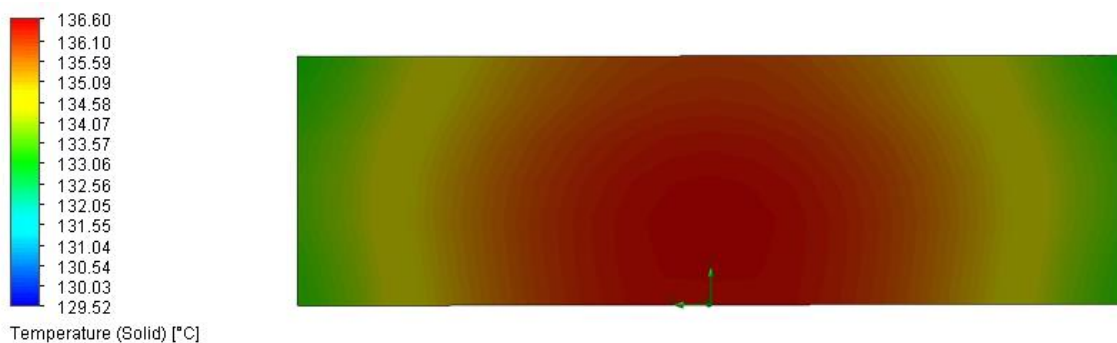


Figure 5-10: Cut plot showing temperature distribution through the thickness of the copper element

Further cases were also considered, as before including that of a copper plate with thickness 4 mm, resulting temperature time plot in figure 5-11, indicating steady state conditions at approximately 152°C – an increase of about 16°C.

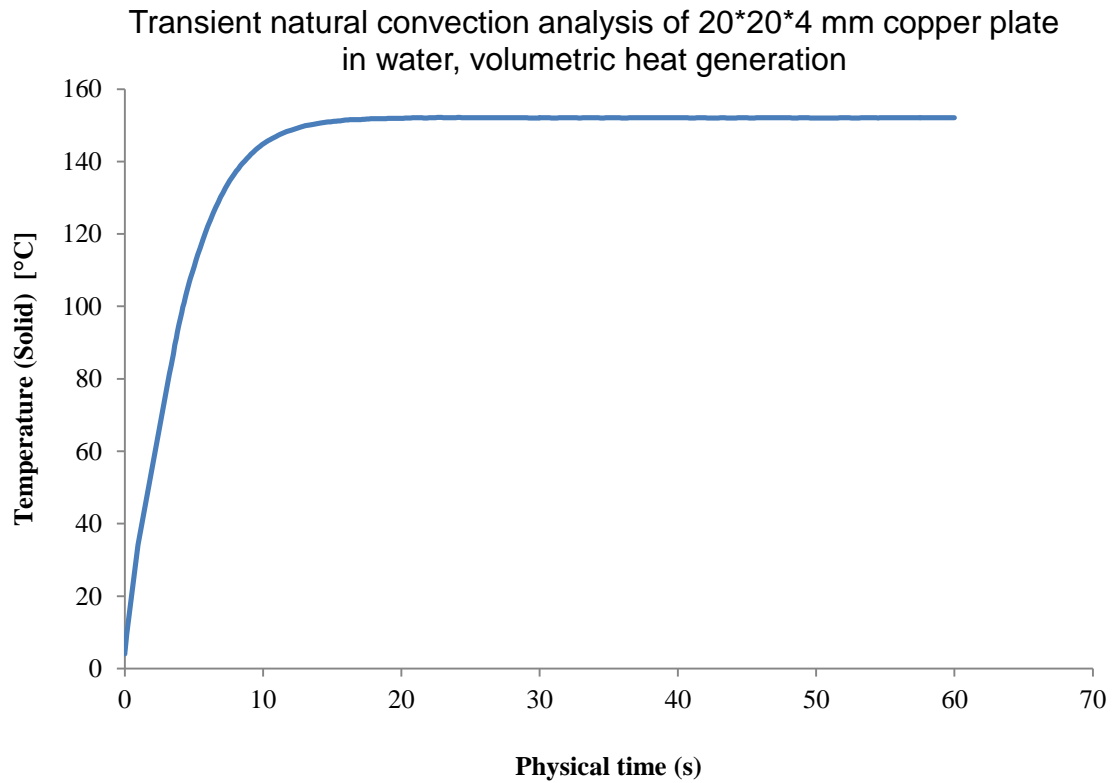


Figure 5-11: Temperature time plot for 4 mm element thickness

5.3.2.5. Thermal conduction effects

Considering the physical conditions during actual operation of such a copper coil, as suggested in chapter 5.3.2.1, the heat generation due to joule heating will occur in the skin layer of the conductor. As such, it is of interest to investigate the effect of the different heat generation definitions on the results with respect to maximum temperature in the solid at steady state conditions, as well as the temperature distribution within the element. A large gap between temperatures at respective surfaces would suggest for localized overheating to become problematic, as the heat would not be effectively dispersed, and the cooling process in general would likely be unpredictable.

As mentioned, the Solidworks CFD software includes thermal conduction through the solid body in the calculations, thus constituting a combined study of convective and conductive heat transfer – what is commonly referred to as a conjugate heat transfer. To consider this in a corresponding fashion, the computational model described in chapter 5.3.2.2 was modified to also include the effects of thermal conduction through the thickness of the element, by use of another simple numerical approximation.

Simple heat conduction is commonly described by Fourier's law, and as there is little difficulty associated with determining the direction of heat flow for the one-dimensional case of an element in which heat generation takes place solely in a 'skin layer' at one end, it may conveniently be written in scalar form (Lienhard IV & Lienhard V, 2011):

$$q = k \frac{\Delta T}{L} \quad \text{Equation 14}$$

where the heat flux q is proportional to the thermal conductivity k and the temperature difference ΔT , and L is the thickness in the direction of heat flow. By subdividing the quadratic body in further horizontal elements which are all assigned their corresponding physical properties, i.e. mass and heat capacity, and further iterating Fourier heat conduction from element to element for each time step, a heat diffusion approximation was obtained.

Combined with a corresponding iterative scheme as before, this was implemented in MATLAB functions *Conjugate_heat_simulation.m* and *Vertical_HTC.m*, provided in appendices F and G respectively. *Vertical_HTC.m* is called by *Conjugate_heat_simulation.m* for the calculation of heat transfer coefficients for the vertical surfaces.

Inputs for the function are the same as in table 5-1, except for the addition of the sub-element thickness z_step , i.e. the resolution of the subdivision. For efficient computation and

intuitive accommodation of the skin layer heat generation, z_{step} is set as 0.5 mm (0.0005), thus subdividing the thickness in 12 elements.

Running *Conjugate_heat_simulation.m* with the parameters in table 5-5 produced the results displayed in figure 5-12 and 5-13, in the form of a temperature time plot and a bar diagram showing the elemental temperature distribution through the thickness.

Input parameter	Value
amb_temp	4
heat_load	12 000
side_length	0.02
thickness	0.006
pressure	1000
simulation_time	60
time_step	0.0002
z_step	0.0005

Table 5-5: Input parameters for conjugate heat transfer computational model

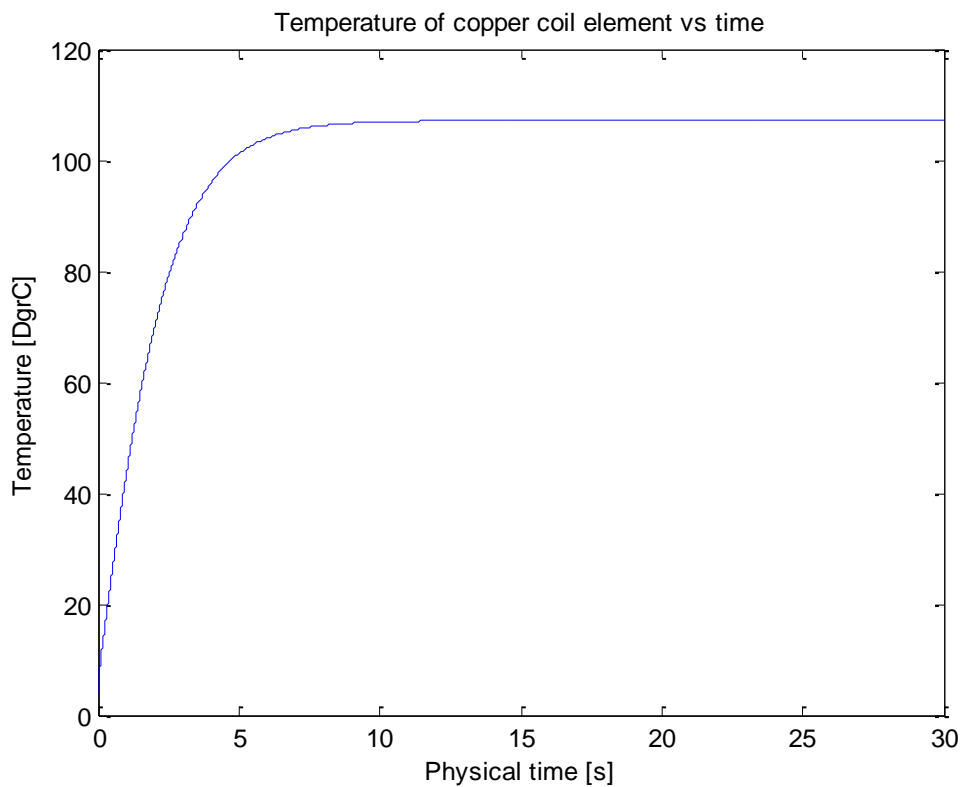


Figure 5-12: Temperature time plot of corresponding conjugate heat transfer simulation

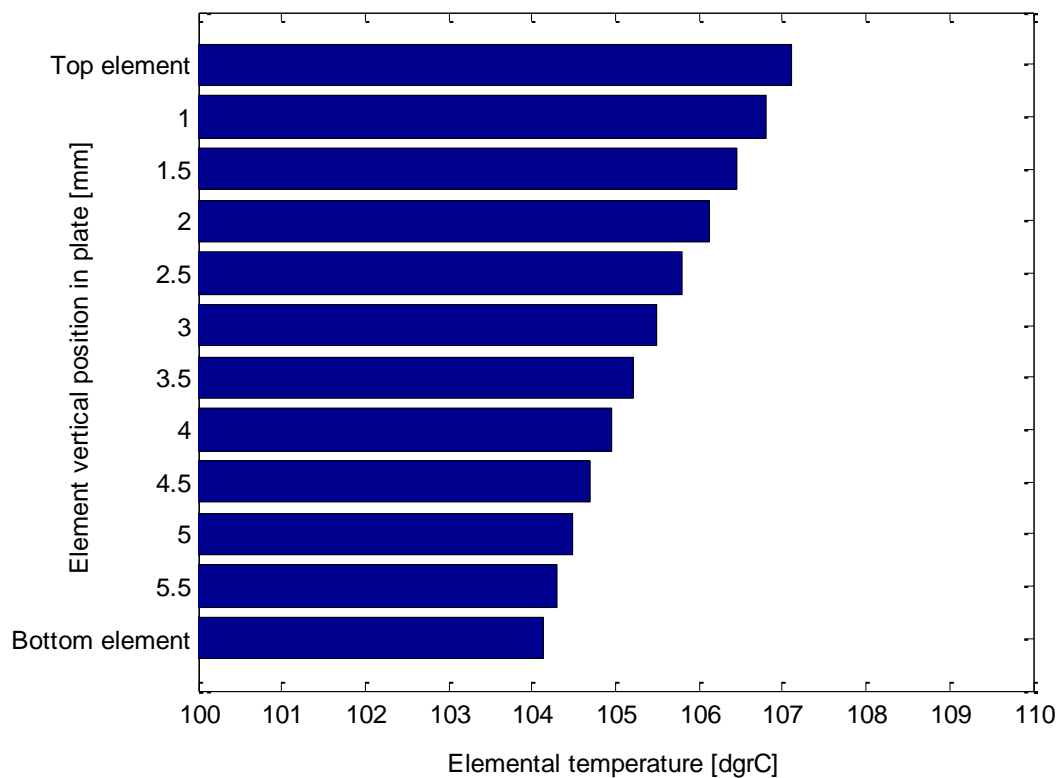


Figure 5-13: Elemental temperature distribution from conjugate heat simulation

For the appropriate time-step adaptation with respect to choice of ‘grid’, the simulator can be shown to generate corresponding results: the maximum element temperature converged to a steady state at around 107°C, and as displayed in figure 5-13, the temperature difference between the top and bottom of the copper plate is indicated to be in the area of 3°C. A similar temperature difference was to be expected and in fact sought, e.g. from simple evaluation of equation 14: Assuming less than half of the generated heat to traverse the plate thickness, as the convective heat transfer is less effective at the bottom, and a thermal conductivity of 390 W/mK, the required temperature difference becomes less than 4°C – this is of course useful in calibration of the computational model.

5.3.2.6. Solidworks surface heat load

Subsequent simulations approximate the thermal conductivity effects through surface heat loading as opposed to volumetric, though of equal magnitude. A similar transient Solidworks simulation was carried out, only substituting these boundary conditions, resulting temperature plot shown in figure 5-14.

Transient natural convection analysis of 20*20*6 mm copper plate
in water, 210 W top surface heat generation

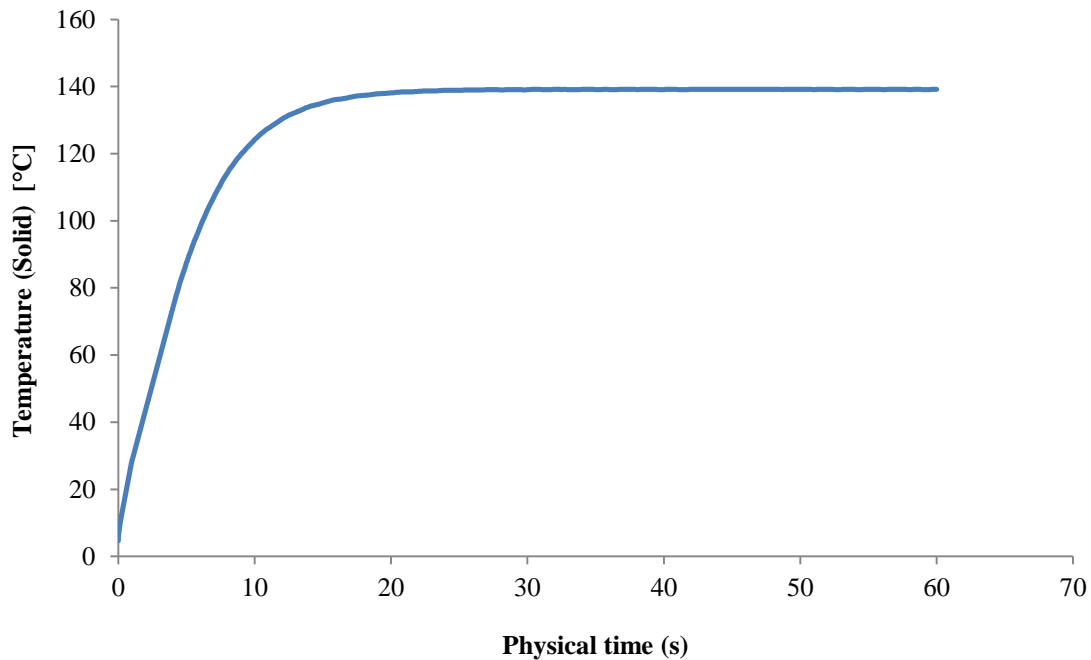


Figure 5-14: Temperature time plot from Solidworks Flow Simulation, top surface heat loading

The resulting steady state temperature from the Solidworks simulation at around 139°C does not differ much from the case of volumetric heat loading either, and similar results were shown in simulations where the heat loading was applied on the bottom surface. Surface temperature plots corresponding to this case are shown in figure 5-15, and a cut plot is shown in figure 5-16. As can be seen, the temperature difference is indicated to be in the area of 3°C.

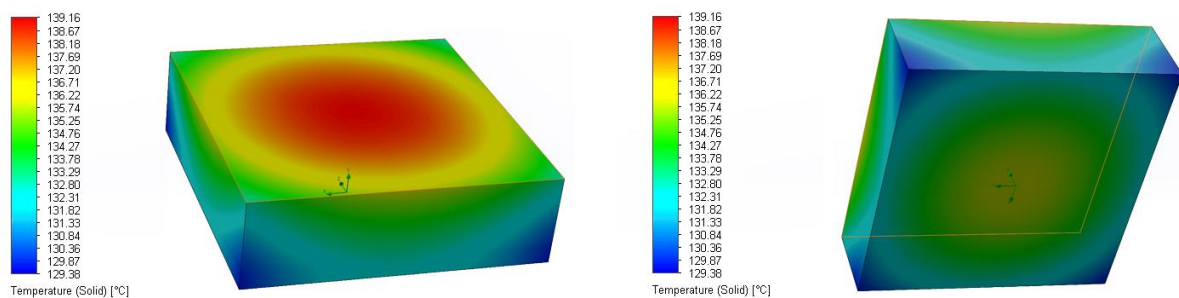


Figure 5-15: Surface temperature plots

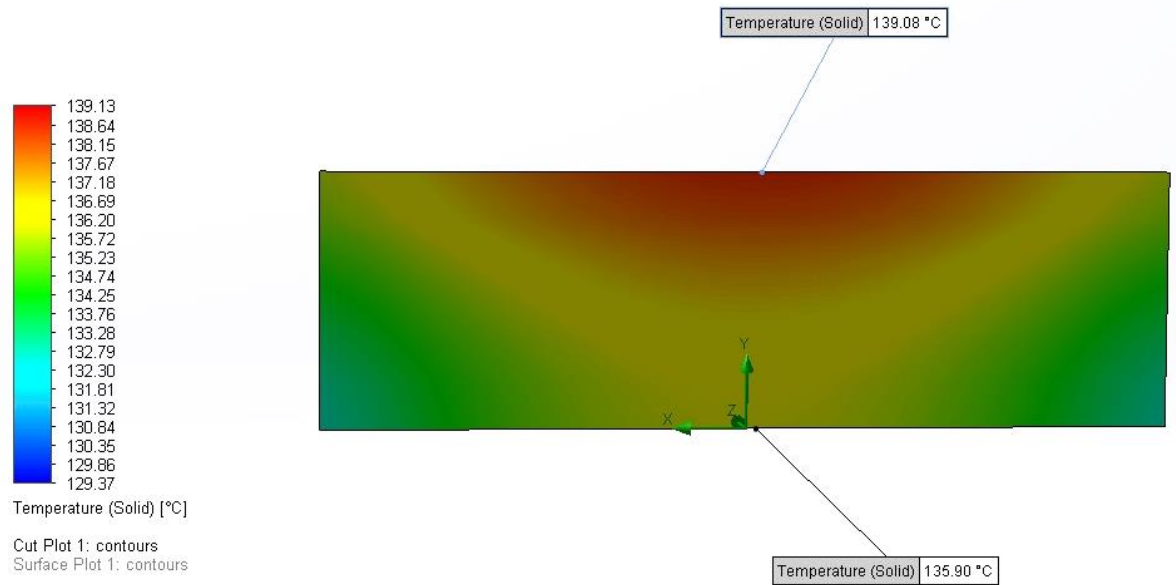


Figure 5-16: Cut-plot showing resulting temperature distribution in the copper plate for the case of top surface heat loading

5.3.2.7. Discussion of copper element analyses

The one-dimensional computation model for volumetric heat generation underestimates the steady state temperatures compared to the solidworks simulation, and this must be expected, considering the substantial simplifications it comprises. The model does not include heat conduction in the solid, and idealizes all surfaces as isothermal, even though the solid in reality will retain heat in the core, exhibiting radial temperature gradients in all planes, and as such generally overestimates heat transfer coefficients.

The somewhat faster convergence of the one-dimensional models, as for most other anomalies, could also likely be accounted for by the general unphysical nature of the approximation. The models do not e.g. consider the actual physical motion of the convection currents in vicinity of the element; there is no delay due to temperature-driven buoyancy effects having to initiate the fluid flow around the element, as illustrated in figure 5-17. This is also believed to influence the computational results for elements of increasing side lengths, as this is where the model deviations start to increase the most – Solidworks indicates an increase of about 40°C when going from 20 mm to 30 mm elements, whereas MATLAB suggests less than half of that.

As such, the computation models described herein must be treated carefully for the output to be meaningful, in accordance with the rule of thumb in the professional field:

“garbage in, garbage out”. The conjugate heat transfer model in particular is highly sensitive with respect to the time-step increment for different reasons, and requires calibration so as to not produce unphysical results, especially considering the inefficient computation – it becomes quickly bogged down upon increasing element resolution, and has consequently not been run with much precision exceeding the above pragmatic approach.

The results considered to be of highest value are the trends they indicate, e.g. increasing temperature for decreasing plate thickness and increasing side lengths, rather than absolute value of the temperatures. In these regards and in comparing results before and after including heat conduction effects, there is a reasonable match between models if deviations due to aforementioned concerns are compensated for. The estimated general temperature ranges are however considered encouraging at this point.

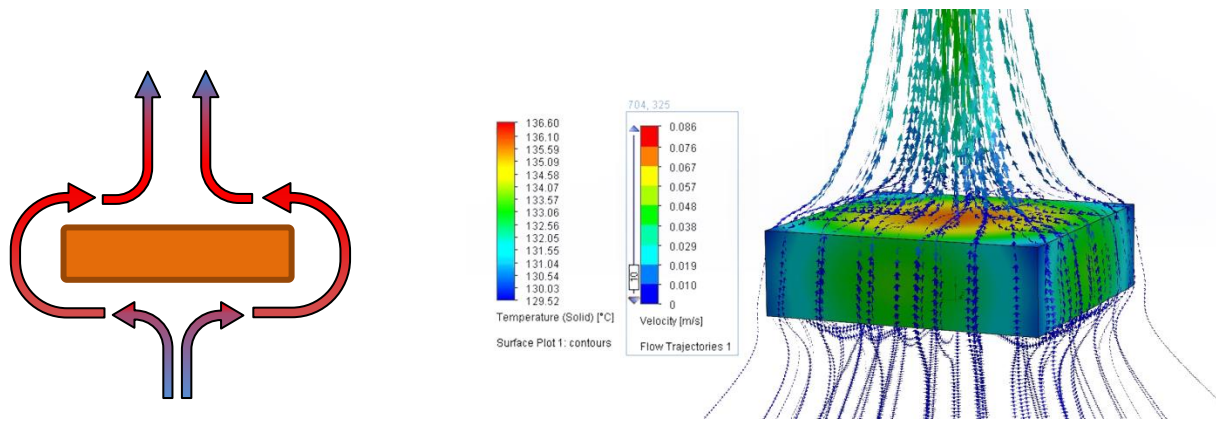


Figure 5-17: Convection currents in vicinity of copper element

Another source of error is the fact that only fresh water was available in the fluid database of the Solidworks Flow Simulation software. Many of the relevant thermophysical properties show similar behavior, but salt in solution does have three effects that will alter the cooling performance: i.e. lowered vapor pressure, reduced specific heat, and increased density. While the performance is generally decreased by the lowering of vapor pressure and specific heat, the increased density actually compensates for this to some degree, though not completely (Nelson, 1986). This suggests for the Solidworks simulations to be less conservative, though the effect is believed to be small for the relevant salinities (~ 35 psu); running the same MATLAB simulations for zero salinity only indicates a difference of about 1°C and 2°C for the volumetric and conjugate approximations respectively – and the temperature difference through the thickness remain constant within thousands of a degree.

For further assessment of the overall confidence level associated with the simulations, proper grid convergence studies should be carried out. While not documented herein, initial simple investigations have indicated for the models to be relatively independent of mesh, and furthermore that mesh refinement sees steady state temperatures converging in a decreasing fashion.

5.3.3. Thermal simulation of coil geometry

For the final thermal analyses, attempts were made at modeling the proper case in accordance with chapter 5.3.2.1. The solid coil geometry featuring copper sections of 6 mm thickness was imported and meshed, and the surface heat load was applied as shown in figure 5-18.

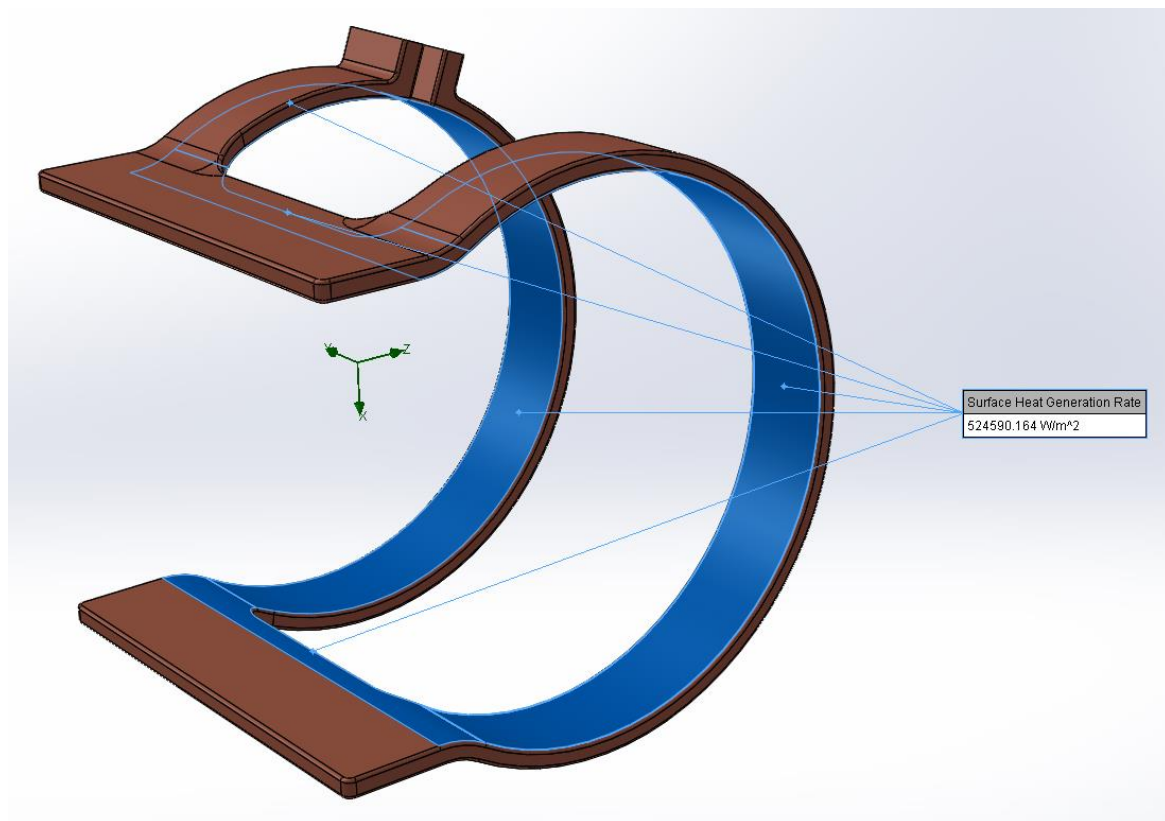


Figure 5-18: Surface heat load on solid copper coil for Solidworks Flow Simulation

The resulting time plot of the maximum solid temperature in the course of the transient natural convection thermal analysis is shown in figure 5-19, and surface plots of associated temperatures at steady state in figure 5-20.

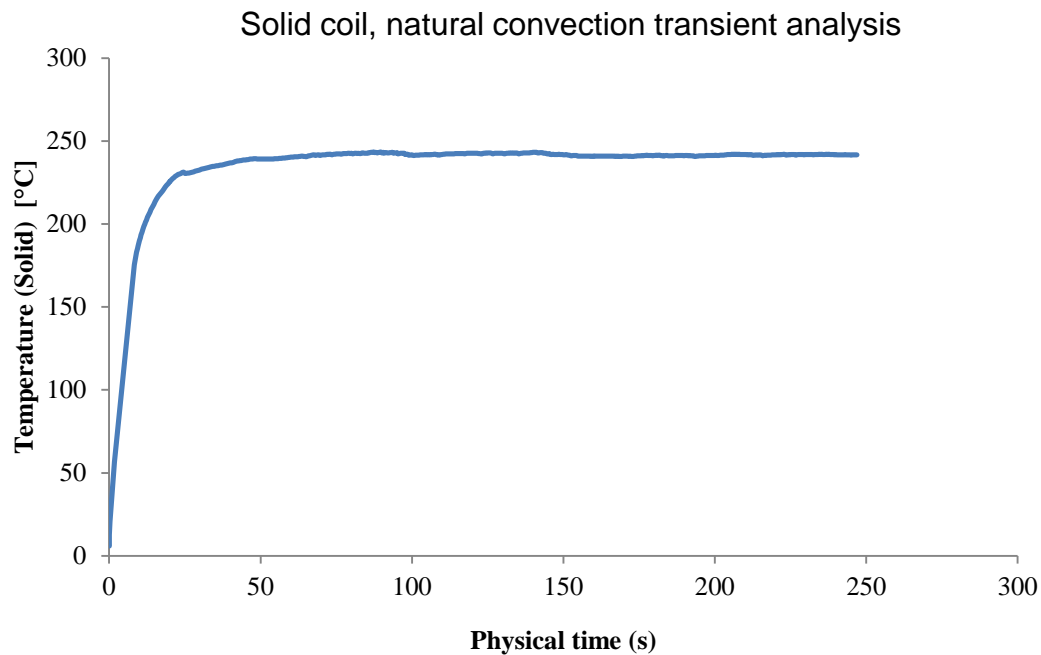


Figure 5-19: Temperature time plot for transient analysis of solid coil

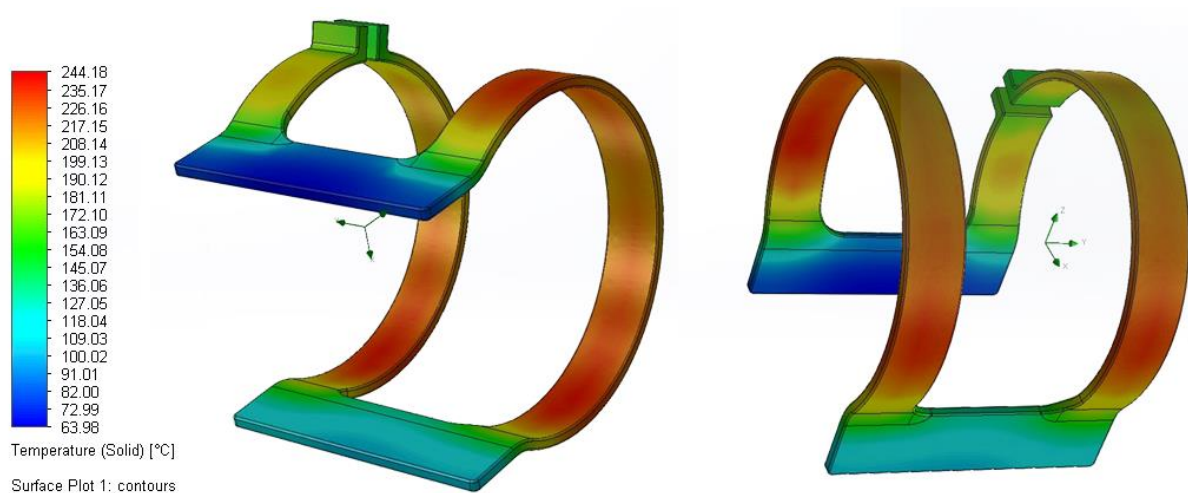


Figure 5-20: Surface temperature plot at steady state conditions

As can be seen from the figures, Solidworks indicates steady state copper temperatures exceeding 240°C , though it is uncertain how much of this can be accounted for by the far more complex geometry e.g. through improper meshing, as both project time and hardware were limiting factors in the thermal investigation. The temperature plot is also visibly unsteady, but the full 12 kW is certainly dissipated in the copper. Assuming for now the estimation of convective heat transfer to be conservative, this serves as basis for comparison for the following.

5.3.3.1. Coil geometry for increased convective heat dissipation

These initial thermal considerations have shown significant temperatures to be generated in the coil material, but also substantiated the excellent thermal conductivity of copper. Further, it is well known in any industry concerned with convective cooling that it is beneficial to maximize the surface area of the heated component. Combining this knowledge intuitively suggests for fins to be added to the coil design, as illustrated below:

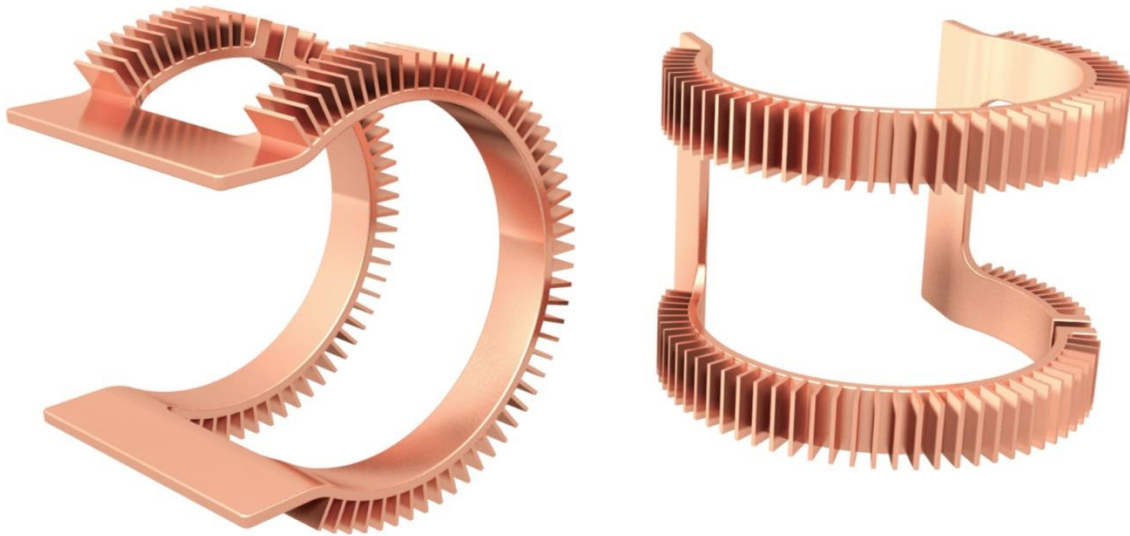


Figure 5-21: Solid coil embodiment comprising cooling fins for increased convective cooling

For comparison, this design was subject to same simulation, with results shown correspondingly in figure 5-22 and 5-23.

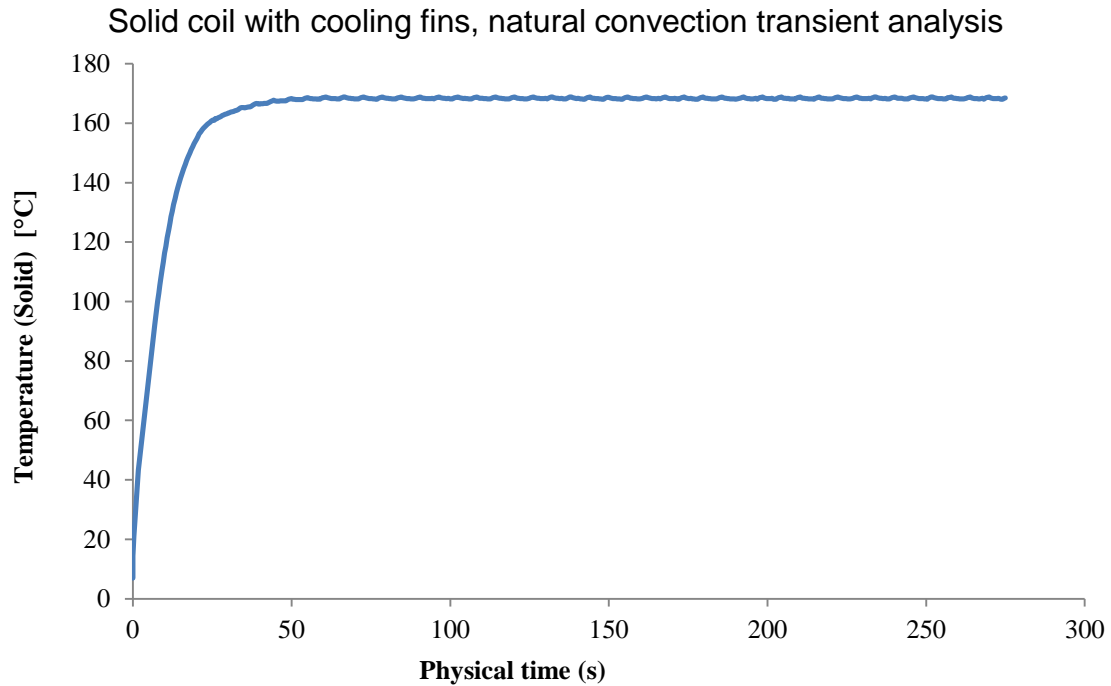


Figure 5-22: Temperature time plot for transient analysis of ribbed coil

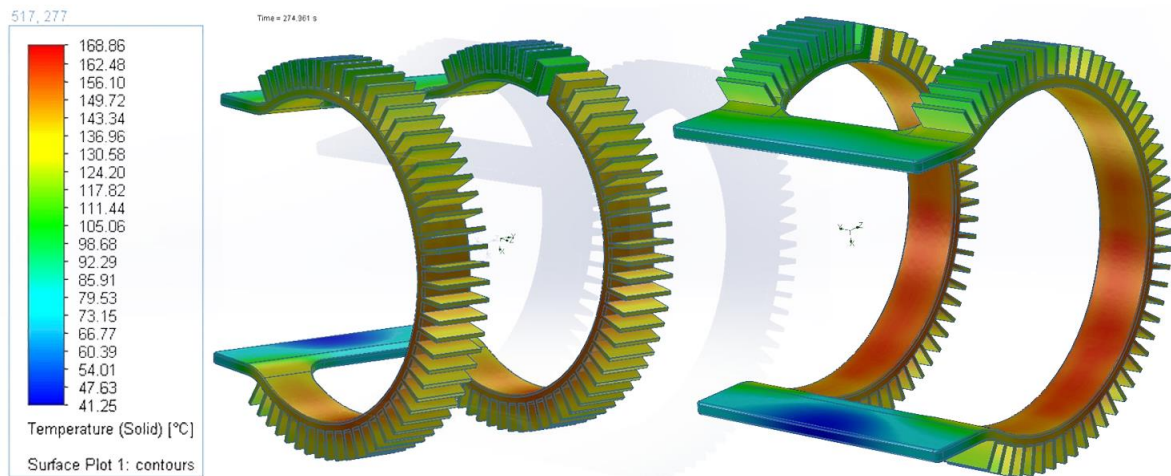


Figure 5-23: Surface temperature plot of ribbed coil at steady state, approximately ranging from 40°C to 170°C

With maximum temperatures now in the range of 170°C, the simulations show dramatically improved cooling, as was not unreasonable to expect. The thermal properties of copper have indeed long been exploited in similar fashion, and the considerations documented herein, while associated with a great deal of uncertainty with respect to absolute temperatures, certainly serve to substantiate the belief that a passive cooling regime should be achievable

through optimization of a similar design.

The temperature plot shows signs of oscillation, and again mesh refinement indicates decreasing temperatures, as is not unexpected for such complex geometry, as the grid likely becomes increasingly suited for approximating the flow conditions governing heat transfer in direct vicinity of the solid, and this of course particularly reasonable considering the multitude of narrow channels which undeniably has critical impact on the cooling performance, see e.g. figure 5-24.

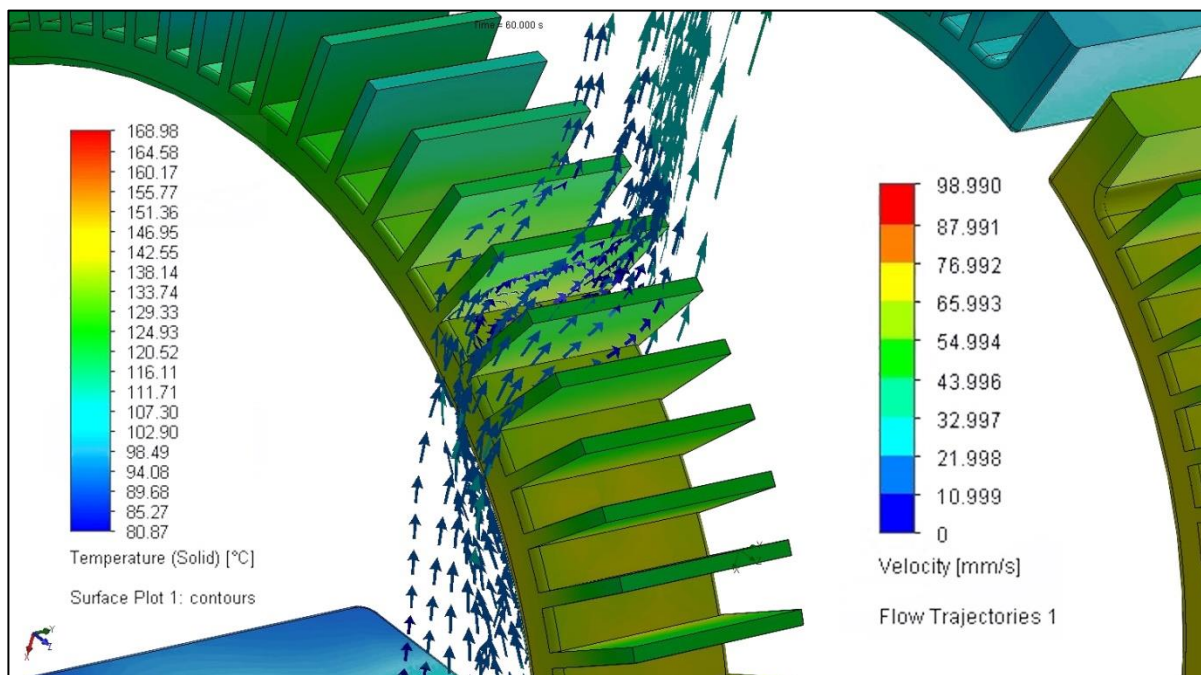


Figure 5-24: Flow trajectories illustrating convective currents around two of the cooling fins

Figure 5-25 further illustrates the flow conditions surrounding the complex coil geometry. The simulations imply significant convective buoyancy flows to be initiated, during operation, and it is further indicated how this in fact contributes to the cooling of the uppermost region of the coil, visible in figure 5-26. The generated flow causes improved convective heat transfer upon impinging on the geometry above, as is also exploited in the cooling regime of the general pipe structure, see also appendix B for relevant literature.

Figure 5-26 also suggests that there should be opportunities of further improvement with a more reasonable fin design, e.g. one that causes less entrapment of the rising convective currents.

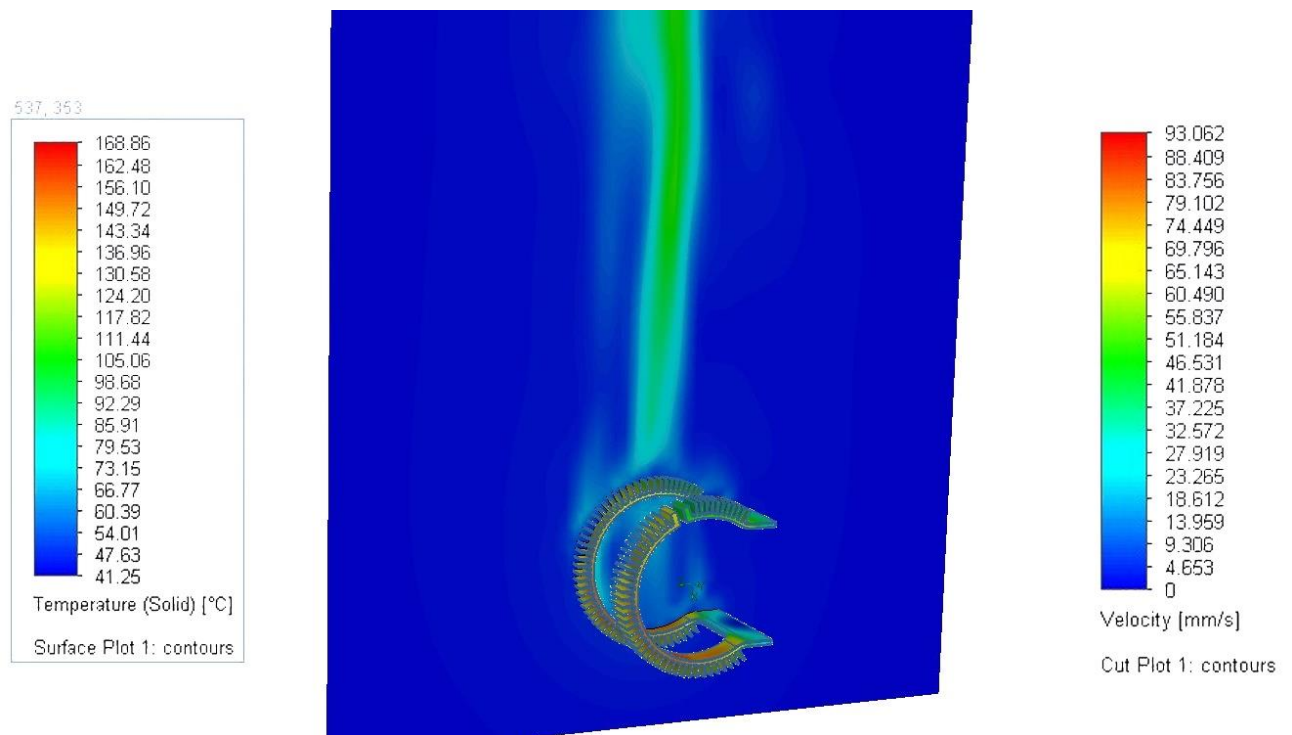


Figure 5-25: Cut plot of flow velocities in vicinity of the coil structure

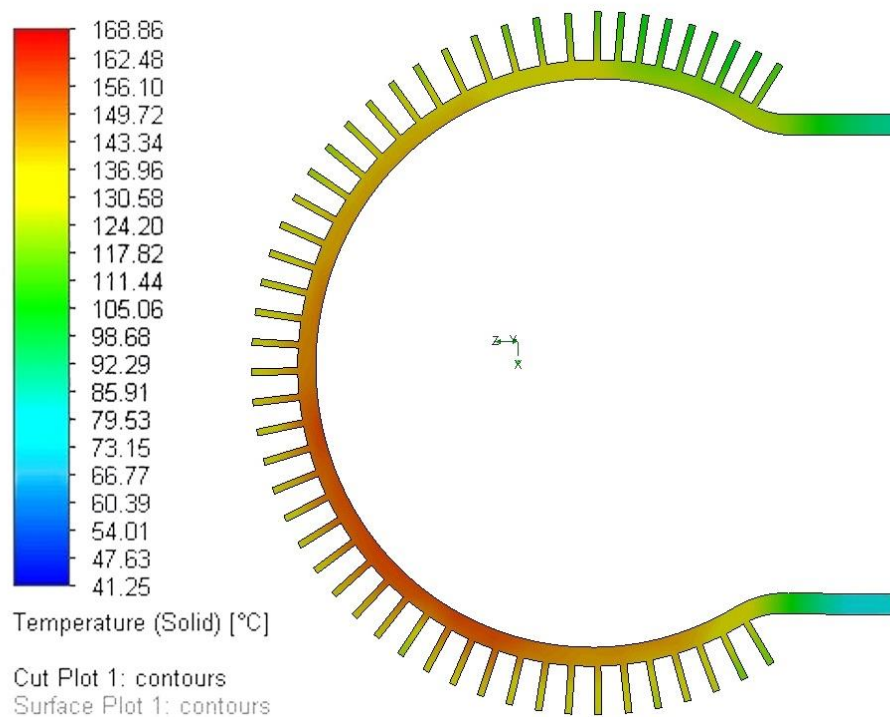


Figure 5-26: Cut plot of typical internal temperature distribution in a cross section of the ribbed coil

5.3.4. Conclusions

Through the initial considerations documented above, the relative sizes of effects and governing parameters have been explored, and the results are considered uplifting and substantiating for the belief that a passive cooling regime is also achievable for an induction coil exhibiting massive copper loss.

The cases that have been explored conservatively assume initial velocity fields to be zero, i.e. absolute worst case scenarios with respect to cooling. Considering typical ambient flow conditions at the seabed, based on measurements from the Barents Sea (Faltinsen, 1990), one might expect currents in the area of 80 mm/s, and this might have substantial impact on cooling performance of both pipes and coil. A simulation case, report again provided in appendix H, assuming 20 mm/s vertical flow due to convective currents from the pipe impinging on a copper element indicates an incurred temperature reduction in the area of 20°C, and this is further assuming laminar flow – it is well known that turbulence and mixing is key to convective heat transfer, as also described in appendix B, and operation within the cooling pipe matrix except for the lowermost pipes is believed to further improve the coil cooling. As such, it should be beneficial for the coil to be implemented so that rising buoyancy currents are not obstructed in passing the coil.

The temperature ranges in question may be considered with respect to aforementioned corrosion concerns, but this is likely mitigated through coating, such as aluminum oxide. Otherwise, as stated by EFD Induction, it is not expected to see real damage to the copper material itself for temperatures below 600-700°C, when material changes may start to occur e.g. due to grain growth (Solgård, 2015).

Too high operational temperatures may nevertheless cause localized boiling at small depths, and vaporous cavitation is identified as causative for considerable damage to copper metal given the right conditions, see e.g. Hihara et al. (2013), but assuming relatively deep water applications, this should not be a problem either, as implied by figure 5-27. For simplification in above considerations, ambient conditions were as mentioned assumed corresponding to 1000 m water depth, entailing a boiling point exceeding 300°C.

The effects of any coating on cooling performance have not been considered in particular, though it is not believed to have significant impact.

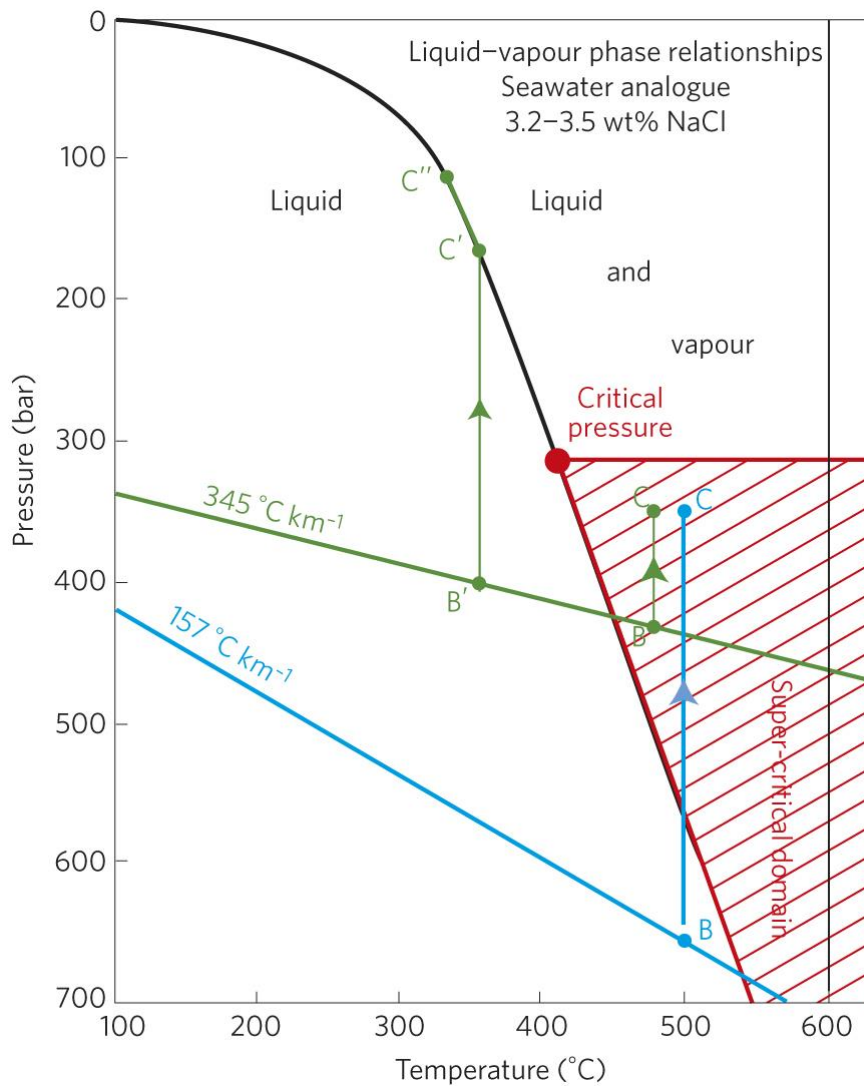


Figure 5-27: Phase diagram for seawater, showing the significant increase in boiling point at depths

Another previously mentioned concern with respect to operation and proper cooling was biofouling, but the heat itself may actually serve to mitigate this issue. Heating is in fact a common means of countering fouling at many facilities in which seawater is used for cooling purposes, see e.g. Graham et al. (1975).

6. Further concept detailing

In this chapter, the chosen concept is explored further and elaborated upon in a successive fashion with respect to design elements, emphasizing the interdependence of the various components. Some preliminary assessment of solutions with respect to feasibility, potential hazards, and general concerns of safe and reliable operation are documented as appropriate.

6.1. Preliminary technology analysis

The concept as described in chapter 4 still comprises several degrees of freedom, and these must be accommodated in accordance with principles of redundancy and safe operation. This chapter outlines the research carried out with respect to relevant technology that is available, and preferably off-the-shelf.

6.1.1. Inherent redundancy

As stated in chapter 3.5, Winther-Larssen (2007) claims robustness among other things to be an advantage of an all-electric development, and in fact, a transition into electrically actuated solutions enables what is referred to by suppliers as ‘full redundancy’ inherent to the component. This is achieved by equipping e.g. servo motors with multiple sets of independent electrical windings as well as for any adhering electronics, so that in case of a malfunction in one set, the other may automatically take over.

6.1.2. BLDC motors and general considerations

The EMPIG system concept as described herein will feature several degrees of freedom which must be accommodated safely, and also precisely; accurate control of the actuated mechanisms is integral to the reliable flow assurance operation. While mechanical guides should aid in the critical positioning, real-time position feedback and control is likely important features in an EMPIG implementation. Further, typical actuator solutions will often feature stepper motors, but brushless direct current (BLDC) motors controlled in a closed loop scheme are considered more appropriate due to increased performance in dynamic and real time control situations. The closed loop feedback scheme is inherently more robust, as it will protect against the phenomenon of ‘stepper motor stall’, in which a stepper motor will lose synchronization with the commutation sequence due to disturbances such as excessive torque,

e.g. from obstructed motion in traversing the pipe matrix, whereas a BLDC motor running closed loop will remain oriented and may automatically compensate based on rotor position feedback, typically from built-in hall effect sensors (Quartararo, 2015).

Common practice for subsea actuation systems is for the functional components to be completely filled with an inert oil to protect electronics as well as for pressure compensation – the housing already holds higher pressure than the surroundings, thus preventing water from entering. The inert oil will further increase thermal dissipation due to convective heat transfer, and allow for the actuators to be slightly overdriven.

For linear actuators, the problem of biofouling becomes apparent, again due to exposed functional surfaces, but this is often mitigated by equipping the actuators with shaft scrapers for mechanical removal.

6.1.3. Wittenstein Motion Control

Wittenstein Motion Control has developed and deployed subsea actuation systems since 2001, mostly working on Statoil projects, and specifically aimed towards the replacement of hydraulic solution with electrical, for longer step-outs and deeper waters. Wittenstein components may be equipped with the aforementioned redundancy features, and all equipment may further be customized from modular building blocks, each pre-qualified and rated for use in extreme conditions, i.e. depths up to 3000 m. Designs are described as robust, durable and vibration resistant, with a submerged lifetime of 25 years. Furthermore, safe ambient operational temperatures range from -56°C to 250°C, potentially valuable for an EMPiG implementation (Perry, 2015).



Figure 6-1: Wittenstein Motion Control SSEAC subsea electric actuator: Dual Channel
(Perry, 2015)

The value proposition of Wittenstein as described in a company presentation is summarized in the following points (Perry, 2015):

- Installed base track record over 20 years
- Technical accountability
- Complete system responsibility
- Technical readiness level
- Mature development processes
- Manufacturing readiness

It is duly emphasized that track record is key for the oil and gas industry, and Wittenstein Motion Control should be considered a potential supplier for actuation solutions for an EMPIG implementation.

6.1.4. *Ultramotion*⁷

Further results of industry inquiries suggest subsea actuation supplier Ultramotion as a viable alternative, and potentially enabling for early submerged testing due to lower price range – starting at ~ 4,100 USD for their U-series. A datasheet for Ultramotion Series U2 is provided in appendix I. The Ultramotion actuators are capable of 100 % duty cycles, well suited for the relatively high maneuverability demands of the EMPIG system concept in realizing the flow assurance functionality.



Figure 6-2: Ultramotion U2 linear actuator (appendix I)

Pressure compensated and rated for depths up to 6000 m, Ultramotion may provide solutions

⁷ <http://www.ultramotion.com/industries/underwater-linear-actuator/>

both off-the-shelf and built to order. Regarding track record, Ultramotion has already delivered many subsea actuators that have been in the field in excess of 10 years with no malfunctions and “a lot of abuse” (Quartararo, 2015).

6.1.5. *Tecnadyne*⁸

Serving the worldwide robotics community for two decades, propulsion and motion control company Tecnadyne has been identified as a relevant supplier of BLDC rotary actuators.

Tecnadyne actuators are also pressure compensated and rated for full ocean depths. The actuators may be installed with electrical load holding brakes to avoid back drive under load without power, but the Model 20WD⁹ features a worm drive gear that securely locks the mechanism and cannot be back driven by the load on the shaft.

6.1.6. *Linear solenoid actuation*

A highly relevant actuation principle for certain functions, e.g. small linear loads, locks, pins, release mechanisms etc., see e.g. (“Solenoid Actuators,” 2014).



Figure 6-3: Hydracon Subsea solenoid linear actuator (“Solenoid Actuators,” 2014)

The main advantage of the strictly electromagnetic operational principle of the solenoid type actuators is the completely seal-less magnetic coupling of the rod. This effectively eliminates the obvious source of leaks and failures common in subsea application of other solutions. Solenoids could well serve as enabling technology for the necessary safety mechanisms that undeniably must be included in a believable EMPIG implementation.

⁸ <http://www.tecnadyne.com/cms/index.php/products/products-overview/rotary-actuators>

⁹ Brochure: <http://www.tecnadyne.com/cms/images/products/pdf/Model%2020WD%20Brochure.pdf>

6.1.7. Joints and bearings

Entailing from the proposed DOFs and joints are bearing demands, and as always, subsea conditions are challenging, but a common means of subsea bearing lubrication is actually for the water itself to act as lubricating medium. Eliminating oils and greases is both environmentally friendly and robust, and such bearings can be made maintenance free, such as plain bearings from Schaeffler (“Corrosion-resistant and media lubricated bearings for water power applications,” 2014). Rolling solutions may comprise CRA-based rings in combination with ceramic rolling elements, further guided by special water resistant plastic bearing cages.

6.2. Rigid single section arm

The conceptual development and considerations as documented thus far state for the pipe accessibility to be realized through a rigid single section arm. Consideration of the characteristic dimensions of the assumed cooling pipe structure in which it will operate gives a minimum range of motion requirement of 1600 mm vertically, i.e. the distance between the top and bottom pipes. To reasonably accommodate this with said single section arm, the length requirement was increased to 2000 mm.

6.2.1. Reach and kinematics

Project inspiration has largely been drawn from industrial robots, and existing subsea manipulation technology, like used by ROVs, e.g. the ECA Group solution shown below:



Figure 6-4: Subsea manipulator arm (“ARM 7E,” 2015)

For a strong and self-supporting mechanism without backlash, the main actuation solution at this point assumes the use of a BLDC driven 8 inch stroke length version of the Ultramotion U2 series subsea actuator. Further, the single section mechanism is intuitively ‘borrowed’ from such designs as the ECA Group ARM 7E, in particular the upper arm, and with a similar mounting scheme in order to realize the $\sim 90^\circ$ range of motion. The kinematic interactions of actuator, mounting points and arm frame are illustrated in figure 6-5.

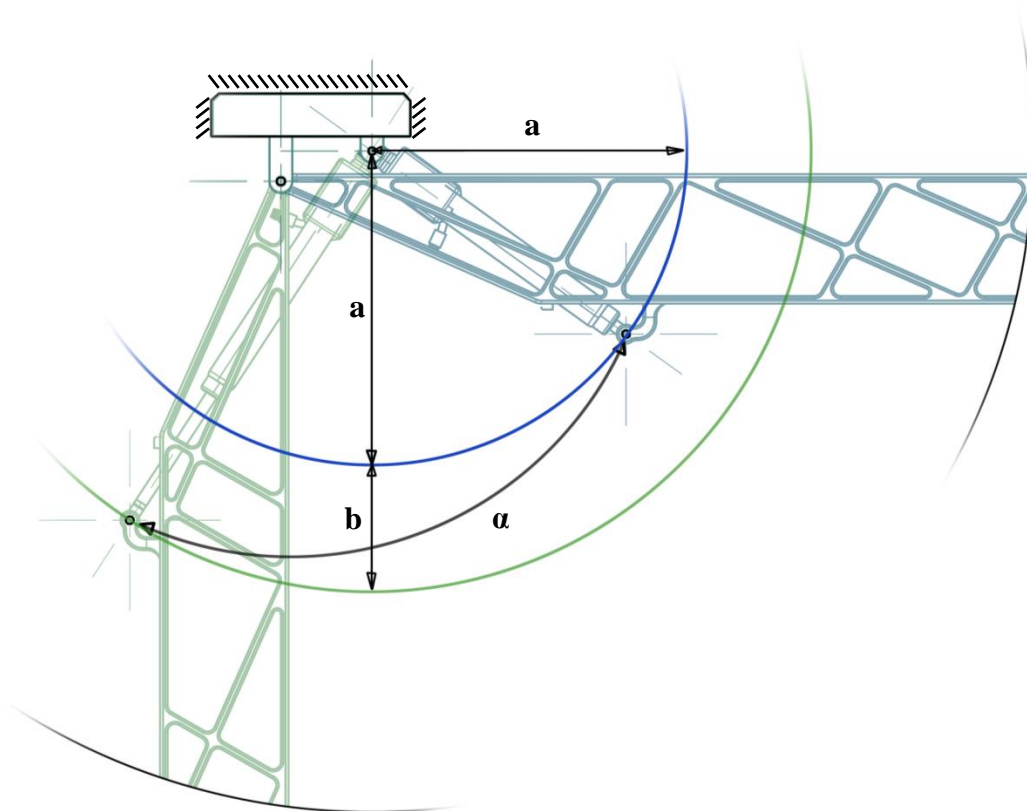


Figure 6-5: Kinematic scheme of actuated rigid arm. The blue circle with radius **a** traces the path of the retracted actuator, whereas the length **b** is the stroke of the actuator. The position of the arm frame mounting point traces the angle α

When driving the actuator rod outwards the length of the stroke **b**, the mechanism forces the rigid arm through the angular motion α . The actuator stroke **b** is 4 inches or approximately 200 mm.

6.2.2. Structure and materials

The weight of the general structure should be minimized for several reasons. As always, complexity and time frame of the already expensive intervention missions are largely dependent on the weight of the component. However, given the considerable ROM required in the mechanism, it also becomes a matter of safe and reliable operation, as the life of the actuator is also largely dependent on loading. There is in fact a cubic relationship between actuator life and load magnitude, and the weight of the arm should consequently be minimized.

Assuming a generic trussed metallic structure, this becomes a matter of material selection. For such complex geometry, efficient cathodic protection may be difficult to ensure, and seeing as it also will be permanently exposed to seawater, NORSOK standard M-001 demands for it to be fabricated in materials that are immune to corrosion in seawater. Relevant recommendations include alloy 625 and other nickel alloys with equal or higher PREN value, as well as titanium.

For a light weight structure, the obvious choice will fall on titanium, as it has a density almost half that of said nickel alloys. Furthermore, recommended practice in material selection is for the number of different materials to be limited. While advantageous with respect to hazards associated with general dissimilarity of metals in galvanic contact, keeping titanium as the structural material for subsequent components is beneficial also due to its magnetic properties – or rather lack thereof. As titanium is largely non-magnetic, it will be less affected by the alternating magnetic field in vicinity of the induction coil than e.g. ferrous materials and alloys.

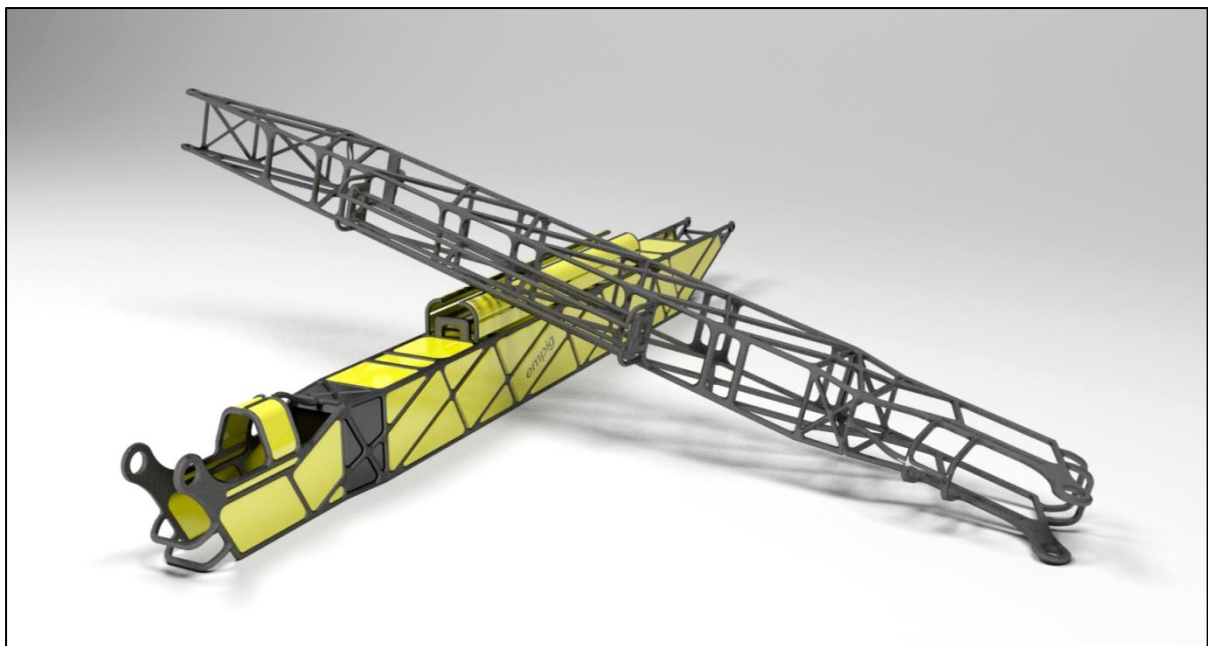


Figure 6-6: Visualization of rigid arm embodiment

Assuming a titanium material, the generic frame structure as illustrated in figure 6-6 has a weight of approximately 11 kg in air. Compensating for the density of seawater at 4°C and salinity of 35 g/kg, $\sim 1028 \text{ kg/m}^3$, the weight in water becomes about 8.3 kg. However, the weight of the frame as well as the coil carrying assembly may be fully or partially compensated for by the addition of floatation elements to the structure. Also indicated in one

of the structures in figure 6-6 are covers and such floatation elements, providing a net force upwards due to buoyancy. Illustrated more clearly in figure 6-7, the elements have a total volume of about 19 liters. Assuming the application of e.g. Premium Buoyancy Foam AM-24 by Forum Energy Technologies, rated for pressures in excess of 100 bars, and with density of 384 kg/m^3 (“Standard Buoyancy Foams,” 2014), this provides a net upwards force of around 12 kg when submerged.



Figure 6-7: Syntactic buoyancy foam elements

For the relative sizes in question, the syntactic foam thus enables at the very least a neutrally buoyant design. Considering the nature of the ‘elbow’ movement with respect to mass center and lever and angle of attack for the actuator, the added buoyancy in fact secures optimal loading conditions throughout the mechanism ROM, as the largest gravitational loading on the actuator coincides with that of buoyancy, i.e. when the rigid arm is in the horizontal position, maximizing the lever.

Ideally, the only force exerted by the linear actuator will be that required to initiate and sustain the motion, however slow, while displacing the body of water nearby. With no specific demands with respect to the speed of the movement, the actuator loading could thus be limited, and referring to the aforementioned cubic load/life dependency, this is of course highly beneficial for the operational reliability of the concept.

6.3. Coil carrying assembly

Still assuming a retrievable coil with general structure as previously described and comparing figures 4-19 and 4-24, it is clear that the mechanism to support the coil and transformer and accommodate the required motion needs DOFs as illustrated below:

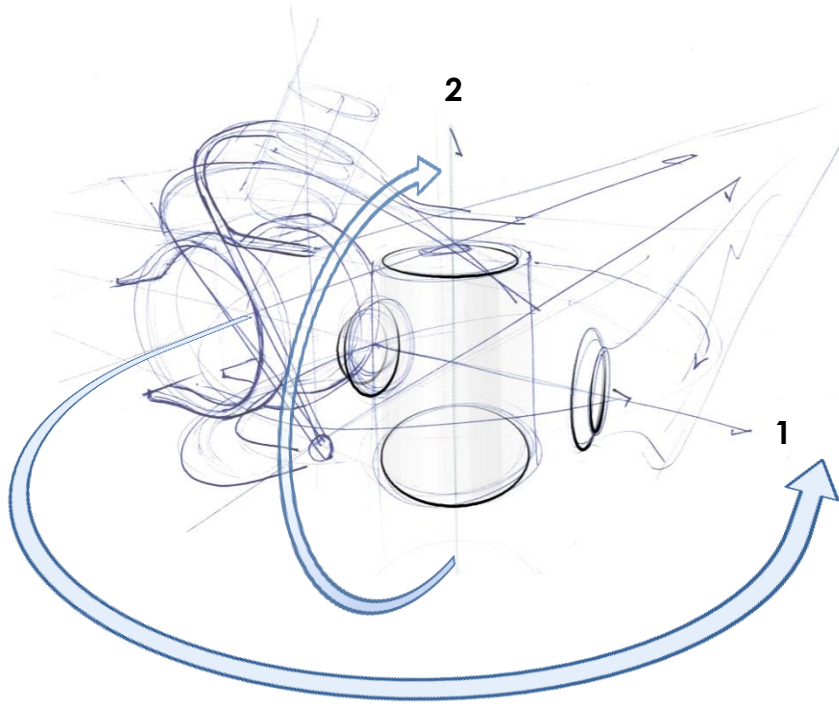


Figure 6-8: Coil assembly DOFs

Indexes 1 and 2 indicate the horizontal and vertical axes of rotation respectively. The first is required for leveling of the assembly, i.e. keeping the major axis of the coil aligned with the horizontal pipe, and the second is for accommodating the horizontal pipe bends through a rotational motion of the entire coil and transformer.

The combined structure of the joints must be sufficiently compact to not obstruct the motion through the cooling pipe matrix, nor interfere with the operation and work path of the induction coil. Ideally, the radial distance from axis 2 should be half the horizontal separation distance of the respective cooling pipes, so as to traverse the pipe bends by a simple rotation about said axis, not involving any other DOFs

To realize the rotational motion, the Tecnadyne BLDC rotary actuator Model 20WD is assumed. Featuring a self-locking worm gear drive, it will effectively secure the orientation of the coil throughout operation, even in the case of significant resistance. This is advantageous because it enables the use of mechanical guides to ensure the required tolerances for the

inductive coupling and for safe maneuvering of the coil itself, as well as mechanical cleaning of the pipe outer surface, which may be necessary to retain proper convective heat transfer in possibly fouling environments. The compact profile of the worm gear actuator configuration is also highly convenient, in that the body and power cable of the BLDC motor may protrude backwards into a volume which may be both shielded and kept free of other objects, so that the final stage of the gear, and thus the shaft, may be secured in a titanium saddle structure at the intersection point of the first and second axis in figure 6-8. As such, the rotary actuator drives the motion about the second axis, maneuvering the coil and transformer around the bend, and securing it perpendicularly with respect to the arm during the continuous operation across the linear pipe sections.

As mentioned, the only function of the first axis DOF is to keep the assembly level, i.e. parallel to the horizontal plane, and this is envisioned realized through a passive indirectly driven mechanical link, such as a hinged rod or series thereof. The orientation about the first axis is in fact a mere function of the orientation of the main arm, linear as such, and said passive coupling scheme is a commonly used solution in similar kinematic setups, but is not detailed herein.

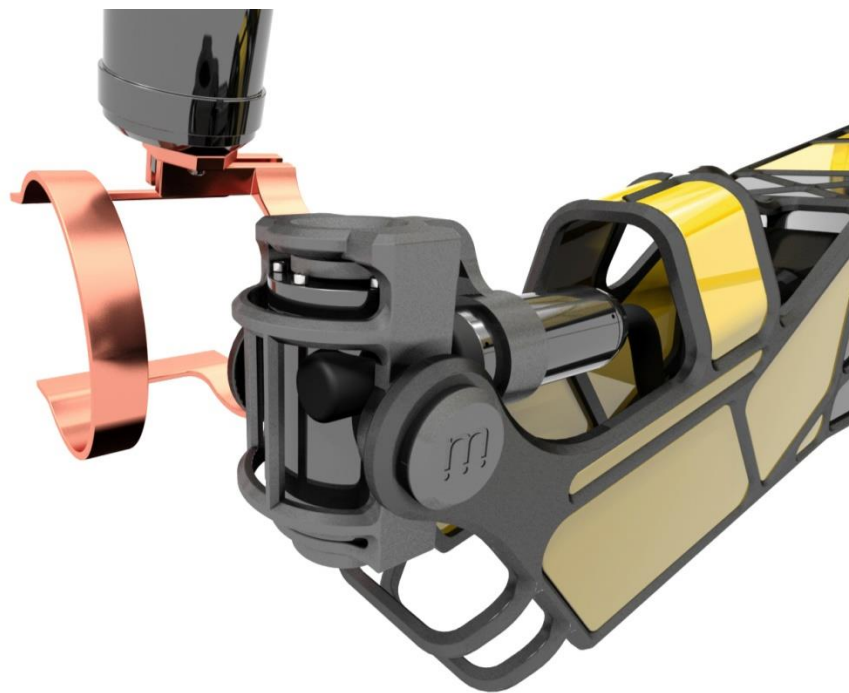


Figure 6-9: Hinged mounting of Tecnadyne Model 20WD

Plain bearings as mentioned in chapter 6.1.7 are assumed at both rotation points, though not detailed in particular either. The titanium saddle with the mounted rotary actuator is shown

positioned at the end of the rigid arm in figure 6-9, also indicating the relative position of the coil and transformer. In order to facilitate the movement of the stiff power cable so as to avoid collisions with pipes and supports, the transformer is slightly tilted relative to the rotation axis of the actuator. The power cable is considered further in chapter 6.4.

A potential concern of the design is the positioning of the electric actuator in close proximity of the induction coil. As suggested in chapter 2.5.3 on electromagnetic effects, and especially visible in figure 2-14, the bulk of the magnetic flux generated by the coil will concentrate around the pipe, but there will likely be some amount of stray flux present also at the opposite side, i.e. potentially impinging on and disturbing the servo motor assembly. Figure 6-10 shows the close spacing, as well as an indicated addition of simple copper shielding to absorb the unwanted flux.

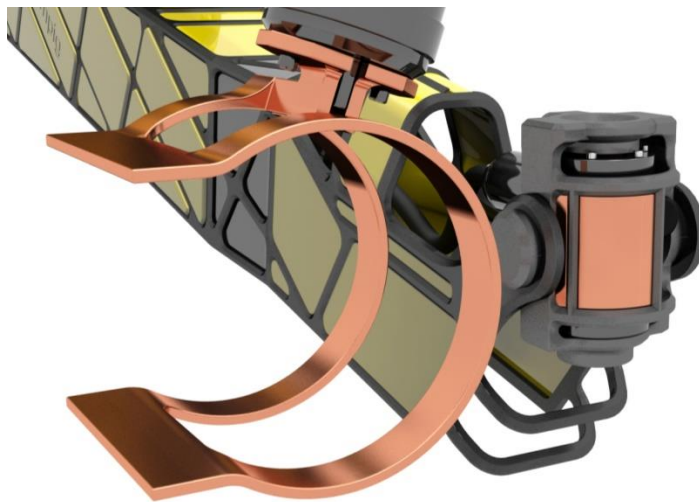


Figure 6-10: Coil and rotary actuator comprising copper shielding

Such magnetic shielding is being used to an increasing degree in applications in which electromagnetic interference may become problematic. The shielding could be passive, as illustrated above, or active – by having an additional and specifically adapted coil generate a second and opposite magnetic field in selected regions, said regions may be effectively protected from the effects of the first (“Magnetic shielding,” 2015). See also e.g. (“Practical Electromagnetic Shielding,” 2015).

Another means of controlling the path of the magnetic flux is the application of so-called flux concentrators. These are typically used for directing and intensifying the magnetic field for precise heating applications, but were not advised for the EMPIG implementation by EFD Induction, who instead recommended the copper shield.

For the support and shielding of the coil and transformer, another subordinate hinged titanium structure is assumed, supported by double bearings perpendicular to those of the actuator saddle, and connected to the shaft of the rotary actuator from the bottom. Typical practice for the mounting of the induction coil itself is for it to be simply bolted to the transformer body, and this is shown in illustrations. With a solid profile however, the massive copper coil has a weight of close to 2 kg in air, so additional support should possibly be considered. The subordinate transformer hinge is illustrated in figure 6-11.

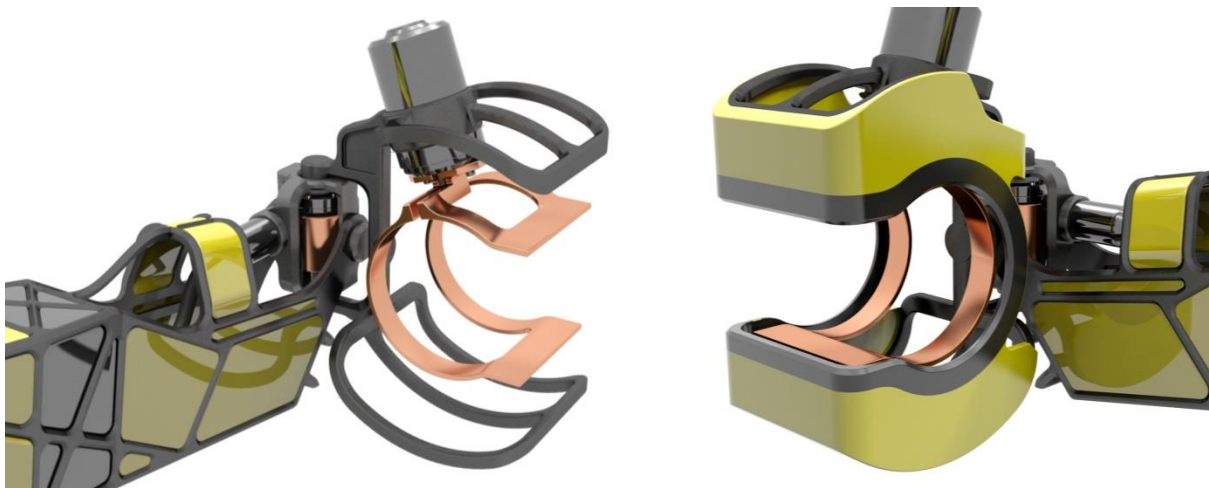


Figure 6-11: Transformer support and coil shielding

Also indicated in figure 6-11 is a generic cover structure for general shielding of the coil during operation. As illustrated on the right, the application of some lightweight composite material is assumed for this purpose, but the exact conditions in the presumably elevated operating temperatures in the vicinity of the coil has not been sufficiently considered, and this may prove prohibitive for such material options. Simple consideration of the high heat capacity of water does however suggest for the actual temperature increase associated with the absorption of heat from coil and pipes to be relatively small. In fact, EFD Induction do have positive experience with the use of composites, e.g. in the form of GPO3 glass fiber, even in direct contact with the coil (Solgård, 2015), but another set of requirements and standards altogether will naturally be governing for possibilities of any similar subsea implementation.

However, the idea of non-metallic material selection is again motivated by concerns of electromagnetic interference, as having metallic, and especially magnetic, structures too close to the coil will both lower the efficiency of the heating application and potentially damage the

respective structure. It was attempted in development for these separation distances to be maximized, though again naturally hampered by the generally confined spaces in question.

The aforementioned application of mechanical guides to support the precise motion of the coil assembly relative to the pipe is similarly assumed solved by use of plastic or composite materials, and the same applies for the external pipe cleaning functionality. This is further motivated by the EMPIG-requested implementation of some form of passive elastic ‘snap connection’ of the guides and pipe, so as to allow for more liberal motion control with respect to tolerances in the approach of the coil assembly onto the pipe. None of these elements, though shown in subsequent illustrations, have been considered in any detail.

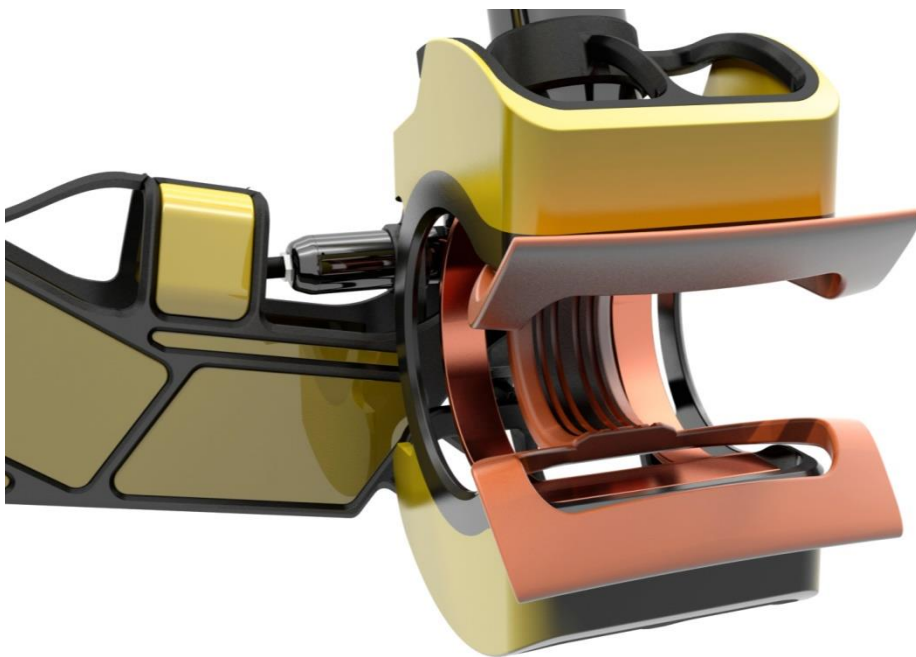


Figure 6-12: Combined pipe snap-connector and mechanical cleaning and guides

As can also be seen in the illustrations, the main covers have been shaped such that a largely unobstructed flow path vertically through the volume occupied by the coil remains, this of course to facilitate a passive cooling scheme for the solid induction coil as discussed in chapter 5, by allowing the rising buoyant convection currents to pass. Any snap-connector or similar must naturally also accommodate this in some way, and could well be attached further from the coil, depending on shielding requirements. As illustrated however, the combined scraper and snap-connector also serves the purpose of thermally insulating the heated portion of the pipe between the coil sections during the scanning motion, so as to protect from the same forced convection cooling effects otherwise experienced by the pipes and thus help retain the elevated temperatures.

6.4. Cable management and system

The issue of the seemingly unmanageable power cable remains. Due to geometric constraints as suggested in chapter 3.2.3, no elegant means of properly ‘hiding’ the cable has been identified. However, the key to the solution assumed thus far is again the restructured continuous work path, also combined with the acceptance of the inaccessibility of the vertical pipe bends. By limiting the DOFs, the behavior of the cable becomes increasingly predictable, and may as such be controlled to a large degree, thus ensuring snag-free operation amidst the cooling pipes and supports. Inspiration was also drawn from existing cable management schemes for industrial robots such as shown below:



Figure 6-13: Industrial robot cable management (“Adjustable Retraction System,” 2013, “Robotic Cable Management Made Easy,” 2013; thomasnet.com, 2012)

Comparing figures 6-5 and 6-8, the only DOFs required for the cable to accommodate are those associated with the angle of the rigid arm, i.e. in-plane bending down into the allocated operational space in the cooling pipe matrix to the end of the single section arm, and the rotational motion of the coil and transformer assembly. For the latter, the movement is significantly simplified by the combined aforementioned tilting of the transformer and the continuously horizontal orientation of the general joint – calibrating the tilt angle with respect to a specified cable bending radius effectively transforms the bulk of the horizontal plane bending when traversing the pipe bends into a torsional load which may disperse comfortably throughout the length of the cable. Further, said limitations on bending radius, while already confined by the physics of the cable, may be fixed to specification by use of bend restrictors, strapped around the circumference. This is a common solution, and is assumed part of the cable management in the EMPIG system concept proposed in this thesis.

Protruding from the transformer, adjoining to the vertical plane spanned by the ROM of the rigid arm and proceeding towards the power supply unit, the bend-restricted cable is fixed mid-way with respect to curvature and sideways displacement by a bracket, but allowed and indeed encouraged to slide longitudinally along the arm, the movement preferably governed by another passive kinematic linkage between said bracket and the relative motion of the rigid arm and subordinate sled under which it is suspended. A system overview is shown in figure 6-14, in which two heater units are illustrated acting together in a redundant scheme as previously described in combination with the flexible and multidirectional, though discontinued, concept described in chapter 4.1.

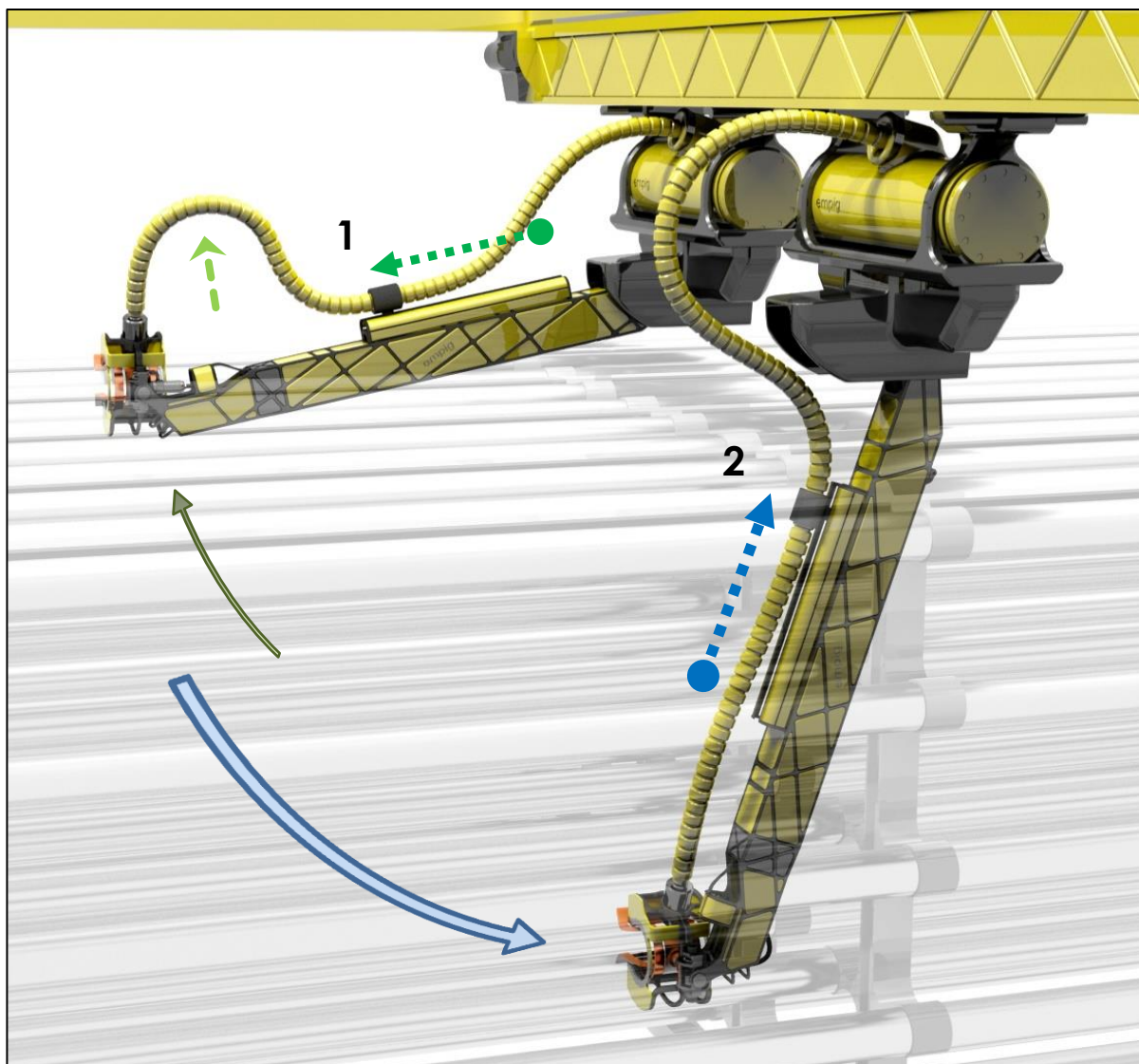


Figure 6-14: Two heater units suspended underneath subordinate sleds traversing the primary sled. The ROM of the cable and ‘cable sled’ atop the rigid arm also illustrated and annotated

The heater units are illustrated engaged on the upper- and lowermost horizontal layers of cooling pipes respectively, arrows indicating the relative motion of the rigid arm, cable and cable carrying sliding brackets, or ‘cable sleds’. The principle idea is for the cable slack itself, necessitated by the geometric constraints, to be displaced from front to back upon lowering the arm, so as to keep the cable curvature constant in the upper region in which it connects to the power supply unit.

In position 1, servicing the top pipe, the cable sled is fully extended forwards, thus bringing the slack closer to the now perpendicularly aligned transformer, to allow for the cable to bend sufficiently. As the arm is lowered into the pipe matrix, the continuous indirect leveling of the coil assembly causes the transformer, and hence cable, to align longitudinally with the arm. To accommodate the shift of orientation, the cable sled retracts towards the power supply unit to allow for the cable to retain its relaxed pose in the region in which it protrudes from the power supply body. In position 2, the cable sled is fully retracted, as is the slack in the cable, thus relaxing the path of the cable into the pipe matrix. As can be seen in figures 6-14 and 6-15, the leveling of the coil assembly and consequent alignment of cable and arm minimizes the profile of the cable section located inside the cooling matrix, thereby largely eliminating the snag hazards otherwise incurred through use of an external cable.

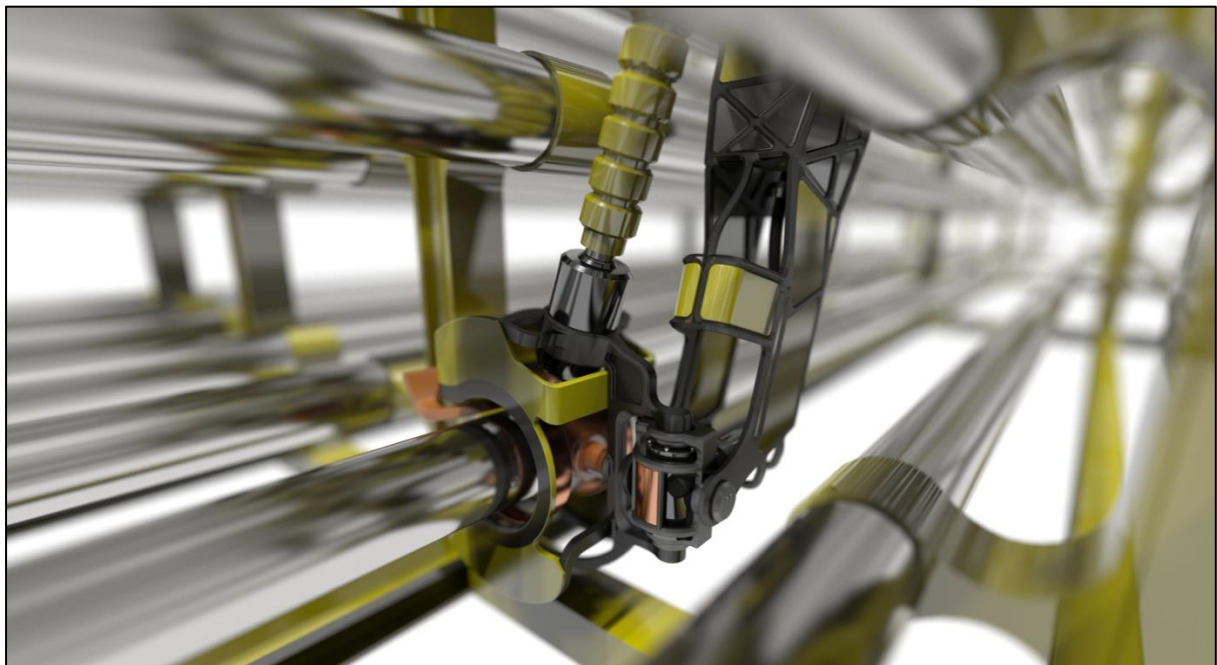


Figure 6-15: Heater unit engaged on a pipe in the lowermost region. The upright and tilted transformer orientation directs the cable safely away from the surrounding structure



Figure 6-16: Front view of heater units; arrows indicate the transversal DOF of the subordinate sleds

As mentioned, and indicated in figures 6-14 and 6-16, the power supply units are carried by bi-directional sleds traversing the primary sled structure as described in chapter 4.2. Specifically, the subordinate sled rails are shielded within the open-bottomed primary sled, as with the rotary actuators, and pertaining controls and electronics, which provide the motorization through an inverted roller pinion system. Few other features related to the equipment described herein have been detailed, but anything closely pertaining to the heater unit is also assumed shielded inside the primary sled within reasonable limits. The subordinate sleds should likely comprise some form of individual tether management system (TMS) for the initial distribution of power from a central power supply.

Additional renderings of the concept are provided in appendix J.

6.5. Operation

Several factors will be governing for the general operation of a system concept as proposed herein, largely related to the flow assurance functionality. Firstly, from basic observations by Kjerschow (2014), it is clear that the direction in which the fouling mitigation efforts should progress along the cooling pipeline is downstream. The energy requirements were measured in both directions, and observed to be significantly larger in the upstream case. This is accounted for by the interaction of the turbulent flow in the pipe, and the nature of the separation of wax and hydrates from the pipe walls – by melting only the thin adhesive layer closest to the wall, the wax will tend to separate in larger flakes which in turn will be essentially ‘torn’ from the wall by the turbulent flow in the pipe. For the pipe structure assumed herein, this entails a progression in which the starting point of the induction processing corresponds with that of the cooling section, i.e. the hot inlet. The heater will then traverse the complete horizontal layers successively, only interrupted by the separate heating solution addressing the vertical pipe bends.

The frequency at which the system will be activated should be determined from deposition rates and associated tolerances in the respective fields, and naturally from the scanning velocities required for complete deposit removal. Kjerschow concluded that a scanning velocity of 34 s/m was sufficient both with respect to proper cleaning and cleaning intervals considering deposition rates as described in chapter 2.1.3. For the case of two units working in parallel, the complete length of the cooling stretch will naturally be traversed in half the time.

However, the actual distribution of the deposits throughout the cooling section should also be considered before any real assessment of the actual operating scheme can be carried out. Given a high inlet temperature, the stream will travel some distance into the cooling matrix before actually reaching the wax appearance temperature. This may in fact prove enabling for a passive coil cooling scheme as described in chapter 5, in that the worst case operating conditions with respect to the critical convective heat transfer coincide with the lowermost plane of cooling pipes, as the advantageous turbulence effects (c.f. appendix B) arise only in the buoyant plume some distance above it. As such, and substantiated by preliminary analyses of forced convection heat transfer, limited operation in the lowermost layer will be beneficial. Should operation in adverse conditions with respect to convective cooling be required, heating issues may be mitigated simply by reduced duty cycles, e.g. by

allowing time for the coil to cool without current, or possibly by a general reduction of power and scanning velocity, though this must also be subject to more detailed consideration.

6.5.1. Redundancy and safe operation

As described in chapter 4.2, the primary sled may be equipped with any number of redundant servos for propulsion, and the same is true for the subordinate heater unit sleds. Furthermore, given a rotary actuator scheme also featuring full inherent redundancy as discussed in chapter 6.1, the overall reliability of the Cartesian motion system would become twofold. This is of particular interest given a redundancy scheme as suggested in chapter 4.1, in which the template comprises a pre-allocated heater unit storage compartment, intended for collecting malfunctioning units, and possibly interchangeable spare units, should the practicalities of proper tether management allow for it. This functionality would likely require the primary sled to retain mobility at all times in order to reach said location(s), as indicated in figure 6-17, and facilitate intervention missions – underlining the importance of its inherent redundancy, as further safety features are largely reliant on it. Of course, as for subsea equipment in general, it should also comprise manual ROV-operable mechanical overrides for worst case scenarios, and should in itself be vertically retrievable with or without suspended heater units.

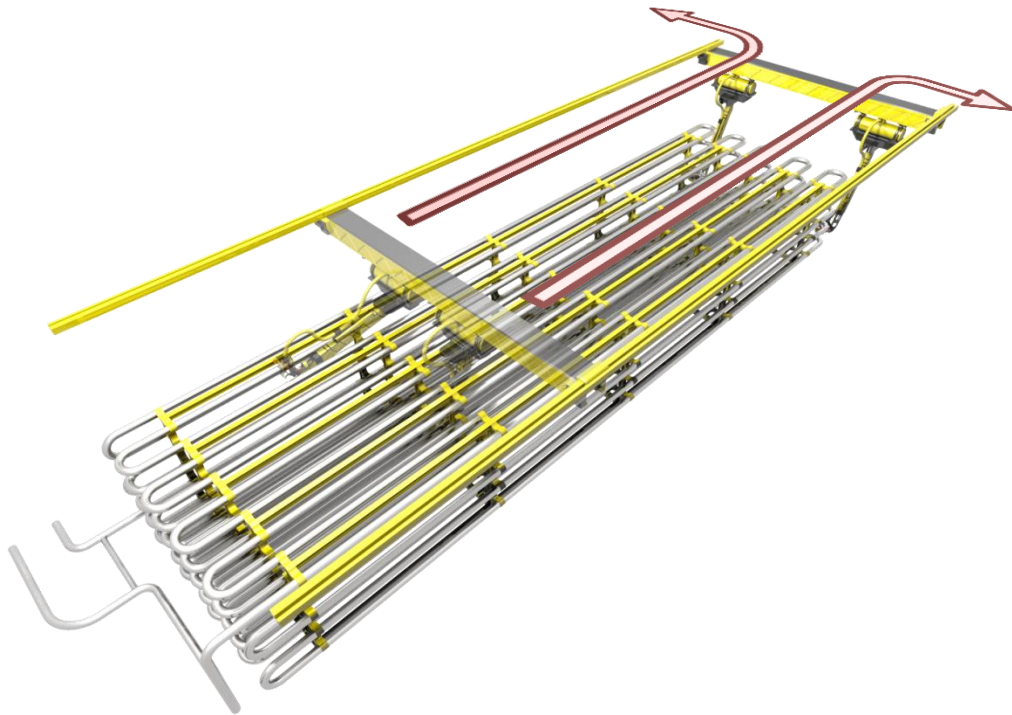


Figure 6-17: Separate retrieval of modular heater units

A final linear actuator design should feature similar redundancy features, in addition to allowing for mounting of multiple actuators in parallel. However, the gearing may and possibly should be made such that the actuator is self-locking, similar to the worm drive of the Model 20WD rotary actuator, meaning it will hold the load steady without power. This is typically achieved by use of an ACME screw, though less common for BLDC motor driven applications. Separate load holding breaks could also be applied, though this would introduce additional moving parts and risk of failure.

In any case, the coil assembly design is such that the heater unit may be completely retracted by the primary sled without decoupling, simply slipping off the end, so there should be no risk of flow assurance disruptions due to trapped malfunctioning units blocking the work path. Upon complete retraction of the primary sled, some redundant quick release mechanism, possibly solenoid actuated, should release the pin joining the linear actuator(s) to the arm frame, thus relaxing the pose and making retrieval independent of actuator position and state, i.e. the actuator may also fail at any point without affecting retrieval possibilities or process.

7. Summary and Conclusions

Based on research into the practicalities of a subsea implementation of the assumed electromagnetic induction heating principle and combined with a brief review of the pre-master results, a basic framework for development was defined. The goal was to realize the induction heating based flow assurance functionality within a general structure as described in the pre-master report through a flexible though robust heater unit. This was understood as a mechanism comprising the smallest possible number of DOFs still able to service the entire length of horizontally meandering pipeline.

Limiting factors for a practical implementation are largely related to the high frequencies at which the induction equipment operates, and the management of associated electrical losses. Specifically, an external separate transformer directly ahead of the induction coil remains an invariant element of the setup, and must be accommodated in conceptual design. Further, electromagnetic effects causing adverse cross-sectional redistribution of electric current in the conductor between power supply and coil pose additional requirements for the structure of the power cable. Current designs consequently exhibit reduced flexibility in bending and torsion and eliminate the possibility of slip rings, hence limiting the solution space for a heater carrying mechanism.

Nevertheless, an all-electric concept was proposed in which an inherently retrievable induction coil is carried by an actuated single section arm comprising a two DOF double hinged joint. Said joint is continuously and indirectly leveled by a kinematic linkage to the angular displacement between arm and base, thus ensuring constant horizontal orientation of the coil assembly, and further comprises a worm-driven rotary actuator to enable the coil to traverse the horizontal circular pipe bends through 180°. A continuous work path through the horizontal layers of meandering pipeline was enabled through a restructuring of pipes and supports, specifically through use of horizontally protruding brackets, allowing for a retrievable coil to pass unobstructed.

Though the initial goal of complete accessibility within the cooling pipe structure for the induction coil was abandoned due to complexity concerns with respect to the mechanism, only the four vertical pipe bends remain unserviceable by the main heater units. These were positioned at the same end of the unit through the pipe restructuring, and assumed easily accommodated by another redundant means of local direct or indirect heating.

The efficiency of electromagnetic induction heating depend mainly on induction coil geometry, and the retrievable design proposed herein is not considered optimal in this regard.

However, it is concluded that it may still prove the most reliable solution, given sufficient coil cooling, as any other concept will likely demand an unacceptable complexity in the associated mechanism. Given due consideration, the coil design may also be improved upon to a large extent, as such relieving the efficiency concerns.

Inversely proportional to said efficiency, the induction coil will generate significant amounts of heat in operation. The cooling requirements thus incurred could again increase the concept complexity e.g. by demanding pumps and filters, and a passive cooling scheme would be much preferred. Hence, to assess the possibility of such a simplification, the thermal properties of copper metal submerged in seawater at depths were investigated theoretically with respect to natural convection heat transfer. Though far from conclusive, the results of the preliminary analyses carried out thus far do substantiate the belief that such a passive cooling scheme is realizable. The credibility of the simulations documented herein has not been properly assessed, and they must as such be assigned considerable uncertainty on a professional scale. However, assuming trends, dependencies and relative sizes to be more credible than the absolutes, it is believed that the excellent thermal conductivity of copper should enable an induction coil of solid sections to be sufficiently cooled by natural convection only, given an appropriate and optimized design.

Other uncertainties related to the proposed concept mainly involve the moving parts and DOFs in general – the concept features a large degree of mobility, which it must also retain throughout its lifetime to satisfy the critical flow assurance functionality. While measures have been assumed to guarantee the reliable operation between intervention intervals, e.g. inherently redundant electric components, the related complaints may still prove too prohibitive for the concept to be successful in the market. Also, the considerations subject to this thesis generally suffer from the lack of physical experiments and data to support it, e.g. with respect to induction coil marinization and passive cooling, though this is a natural next step for development, cf. chapter 8.

In spite of the remaining uncertainties, further opportunities and improvements are evident in comparison with the concept as of the pre-master. While not strikingly robust in the typical subsea manner, redundancy has in fact been introduced into the concept, and the horizontal pipe bends no longer require separate and equally complex solutions to be serviced. Retrievalability is maintained, and further redundancy is made possible through simultaneous application of several identical units and the possible implementation of in-field storage of spare units as well as malfunctioning units awaiting intervention.

8. Recommendations for Further Work

Though substantiated by theoretical considerations, all assumptions and solutions need to be proven by physical experiments in increasingly realistic conditions in order for EMPIG to increase the adhering technology readiness level. This of course becomes intuitive subjects for continued research and development, as proper setups will likely require significant investments in time and resources.

Further work should include:

- Validation of the passive induction coil cooling solution by practical experiments and further analysis
- Realistic assessment of increased power consumption in cold subsea environments, and additional proof of concept for submerged application
- More detailed technology analysis and market research
- Exploration of alternative concepts for the induction heating solution based on the updated pipe support scheme

Specifically, the practical setup for an investigation of heating efficiencies in a submerged application should comprise realistic flow conditions both outside and inside the pipe, with respect to turbulence as well as temperature and composition. For a worst case scenario with respect to scan-heating of the pipe, this could entail internal and external turbulent flow at close to 4°C, meaning that the section to be heated will be simultaneously and efficiently cooled by both the petroleum stream and the surrounding seawater. Countermeasures for said cooling effects should also be investigated, e.g. combined with a scraper feature as mentioned in chapter 6.3.

9. References

- Adjustable Retraction System. (2013, April 11). Retrieved from <http://www.designworldonline.com/adjustable-retraction-system-for-cable-guidance-from-igus/>
- Alumina (Aluminium Oxide) - The Different Types of Commercially Available Grades. (2014, July 16). Retrieved May 27, 2015, from <http://www.azom.com/article.aspx?ArticleID=1389>
- Aluminum Oxide | Al₂O₃ Material Properties. (2013, December 6). Retrieved May 26, 2015, from <http://accuratus.com/alumox.html>
- ARM 7E. (2015). Retrieved June 2, 2015, from <http://eca-media.ecagroup.com/medias/thumb/228c6f213f5a90419a81e3c1bd52d89c.jpg&w=1500&h=1000>
- Aske, N. (2011, March). *Wax Control*. Retrieved from <http://www.ipt.ntnu.no/~jsg/undervisning/prosessering/gjester/LysarkAske2011.pdf>
- Asperheim, J. I. (2014). Conversation with EFD Induction.
- Bahrami, M. (2014, October 10). Natural Convection, ENSC 388 Engineering Thermodynamics and Heat Transfer. Simon Fraser University. Retrieved from <http://www.sfu.ca/~mbahrami/ENSC%20388/Notes/Natural%20Convection.pdf>
- Baldwin, C. Y., & Clark, K. B. (2004). *Modularity in the Design of Complex Engineering Systems*.
- Bjørvik, T. B. (2014, December 17). *Deposit Processing Subsea Cooler: Rethinking the EMPIG System* (Pre-master thesis). NTNU, IPM.
- Carroll, J. (2014). *Natural Gas Hydrates: A Guide for Engineers*. Gulf Professional Publishing. Retrieved from http://books.google.no/books?id=SORuAwAAQBAJ&pg=PA12&lpg=PA12&dq=conditions+necessary+for+hydrate+formation&source=bl&ots=5S7zNERPXY&sig=TXQfdfikckzzzW0mxqzzOrqU30Q&hl=no&sa=X&ei=BWxmVOPbCoK_ywP_rICACg&ved=0CHEQ6AEwCA#v=onepage&q=conditions%20necessary%20for%20hydrate%20formation&f=false
- Cavalieri, M., & Wood, T. S. (2014). *Oil Industry Moving from Hydraulic to Electrical Motor Systems* (White paper). KOLLMORGEN. Retrieved from http://www.kollmorgen.com/uploadedFiles/kollmorgencom/Service_and_Support/Knowledge_Center/White_Papers/OilIndustry_whitepaper_04_11B_FINAL.pdf

- Clarke, R. (2008a, February 8). Power losses in wound components. Retrieved April 23, 2015, from http://info.ee.surrey.ac.uk/Workshop/advice/coils/power_loss.html
- Clarke, R. (2008b, August 2). Magnetic properties of materials. Retrieved May 7, 2015, from <http://info.ee.surrey.ac.uk/Workshop/advice/coils/mu/index.html#mur>
- Clark, R. (2008, August 2). Magnetic properties of materials. Retrieved April 24, 2015, from <http://info.ee.surrey.ac.uk/Workshop/advice/coils/mu/#mur>
- Corrosion-resistant and media lubricated bearings for water power applications. (2014, January). Retrieved June 2, 2015, from <http://www.industrialtechnology.co.uk/search-corrosion-resistant-and-media-lubricated-bearings-for-water-power-applications.html>
- CWT. (2004). Electrical conductivity/salinity Fact Sheet, FS-3.1.3.0(EC). Clean Water Team (CWT). Retrieved from http://www.swrcb.ca.gov/water_issues/programs/swamp/docs/cwt/guidance/3130en.pdf
- DirectIndustry. (2013, July 14). linear-rack-roller-pinion-drive-27322-3041343.jpg. Retrieved May 19, 2015, from http://img.directindustry.com/images_di/photo-g/linear-rack-roller-pinion-drive-27322-3041343.jpg
- EMPIG AS. (2012). empig.no. Retrieved November 21, 2014, from <http://empig.no/wp-content/uploads/2014/06/System-overview.jpg>
- EMPIG AS. (2014, September 10). InFlow Whitepaper. Retrieved December 17, 2014, from http://empig.no/wp-content/uploads/2014/10/TechSpec-InFlow_03.pdf
- Faltinsen, O. M. (1990). *Sea Loads on Ships and Offshore Structures*. Cambridge University Press.
- Gate Inc. (2013). Paraffin Wax: Formation, Mitigation Methods & Remediation Techniques. Retrieved November 13, 2014, from <http://www.gateinc.com/gat2004-gkp-2013-04/>
- Grafsrønningen, S., & Jensen, A. (2012). Natural convection heat transfer from two horizontal cylinders at high Rayleigh numbers. *International Journal of Heat and Mass Transfer*, 55(21), 5552–5564.
- Grafsrønningen, S., & Jensen, A. (2013). Natural convection heat transfer from three vertically arranged horizontal cylinders with dissimilar separation distance at moderately high Rayleigh numbers. *International Journal of Heat and Mass Transfer*, 57(2), 519–527.
- Grafsrønningen, S., Jensen, A., & Anders Pettersson Reif, B. (2011). PIV investigation of buoyant plume from natural convection heat transfer above a horizontal heated

- cylinder. *International Journal of Heat and Mass Transfer*, 54(23–24), 4975–4987.
<http://doi.org/10.1016/j.ijheatmasstransfer.2011.07.011>
- Graham, J. W., Moncreiff, R. W., Benson, P. H., & Stock, J. N. (1975). Heat treatment for the control of marine fouling at coastal electric generating stations. In *OCEAN 75 Conference* (pp. 926–930). <http://doi.org/10.1109/OCEANS.1975.1154027>
- Guðmundsson, J. S. (2010, October). *Flow Assurance in Pipelines*. Retrieved from <http://www.ipt.ntnu.no/%7Ejsg/undervisning/naturgass/lysark/LysarkGudmundssonPipelineFlowAssurance2010.pdf>
- Gyllenhammar, S. E. (2012). *Evaluation of Process Cooling in Subsea Separation, Boosting and Injection Systems (SSBI)* (Master thesis). NTNU.
- Haimbaugh, R. E. (2001). *Practical Induction Heat Treating*. Materials Park, Ohio: ASM International.
- Heating Of Tube Under Water*. (2009). Retrieved from https://www.youtube.com/watch?v=UKY3scPIMd8&feature=youtube_gdata_player
- Hihara, L. H., Adler, R. P. I., & Latanision, R. M. (2013). *Environmental Degradation of Advanced and Traditional Engineering Materials*. CRC Press.
- Huang, J., Liu, Y., Jianhui, Y., & Hua, L. (2014). Al/Al₂O₃ Composite Coating Deposited by Flame Spraying for Marine Applications: Alumina Skeleton Enhances Anti-Corrosion and Wear Performances. *Journal of Thermal Spray Technology*, 23(4).
<http://doi.org/10.1007/s11666-014-0056-7>
- Kennedy, C. (2013, November 13). 5 Trends that are Set to Transform the Energy Sector. Retrieved May 25, 2015, from <http://oilprice.com/Energy/Energy-General/5-Trends-that-are-Set-to-Transform-the-Energy-Sector.html>
- Kjerschow, M. (2013). *Development of Heat System for Cleaning of Subsea Pipelines* (Pre-master thesis). NTNU.
- Kjerschow, M. (2014). *Development of Heat System for Cleaning of Subsea Pipelines* (Master thesis). NTNU.
- Kliber, T. (2012, October 31). Rolling On Down The Line. Retrieved from <http://www.designworldonline.com/rolling-on-down-the-line/>
- Larsen, R. (2011a). *EMPIG Thermal Simulations*. SINTEF.
- Larsen, R. (2011b). *Memo: EMPIG cost, implementation and market* (No. 275771.00). SINTEF Petroleum Research.

- Larsen, R., & Lund, A. (n.d.). *Improving Flow Assurance with Cold Flow Technology for both oil- and gas-dominated systems*.
- Lienhard IV, J. H., & Lienhard V, J. H. (2011). *A Heat Transfer Textbook* (Fourth Edition). Cambridge Massachusetts: Phlogiston Press.
- Lindland, H. J. (2014). *Russian - Norwegian Oil & Gas industry cooperation in the High North: Pipelines and Subsea Installations*. INTSOK Norwegian Oil and Gas Partners.
- Lindo, A. M., Pellicer, E., Zeeshan, M. A., Grisch, R., Qiu, F., Sort, J., ... Pané, S. (2015). The biocompatibility and anti-biofouling properties of magnetic core–multishell Fe@C NWs–AAO nanocomposites. *Phys. Chem. Chem. Phys.*, 17(20), 13274–13279. <http://doi.org/10.1039/C5CP01019E>
- Lundberg, N. H. (2014, September 29). råolje. In *Store norske leksikon*. Retrieved from <http://snl.no/r%C3%A5olje>
- Lund, H. (1998). *Investigation of Paraffin Deposition during Single-Phase Flow* (Master thesis). The University of Tulsa.
- Magnetic Permeability. (2015). Retrieved May 7, 2015, from <http://global.britannica.com/EBchecked/topic/357237/magnetic-permeability>
- Magnetic shielding. (2015). [Page]. Retrieved June 3, 2015, from <https://www.ugent.be/ea/eesa/en/research/areas/lfe/shielding.htm>
- Makerwise. (2013, October 2). ultimaker-ultimaker-2-02.jpg. Retrieved May 18, 2015, from <http://static.makerwise.com/static/img/3d-printer/orig/543/ultimaker-ultimaker-2-02.jpg>
- Marsters, G. F. (1972). Arrays of heated horizontal cylinders in natural convection. *International Journal of Heat and Mass Transfer*, 15(5), 921–933. [http://doi.org/10.1016/0017-9310\(72\)90231-1](http://doi.org/10.1016/0017-9310(72)90231-1)
- Maslin, M., Owen, M., Betts, R., Day, S., Jones, T. D., & Ridgwell, A. (2010). Gas hydrates: past and future geohazard? *Philosophical Transactions of the Royal Society A: Mathematical, Physical and Engineering Sciences*, 368(1919), 2369–2393. <http://doi.org/10.1098/rsta.2010.0065>
- Matula, R. A. (1979). Electrical Resistivity of Copper, Gold, Palladium and Silver. *J. Phys. Chem. Ref. Data*, 8(4). Retrieved from <http://www.nist.gov/data/PDFfiles/jpcrd155.pdf>
- Minac® 18/25 SM. (2014a, September 16). EFD Induction. Retrieved from <http://www.efd-induction.com/~media/0BA71BB4E68F4A20AF80BDFB38971CA1.ashx>

- Minac® 18/25 SM. (2014b, September 16). EFD Induction. Retrieved from <http://www.efd-induction.com/~media/0BA71BB4E68F4A20AF80BDFB38971CA1.ashx>
- Morgan, P. (1993). *SEAWATER*. CSIRO. Retrieved from http://www.math.nyu.edu/caos_teaching/physical_oceanography/numerical_exercises/sea_water/sea_water.zip
- M-TC Sport. (2013, July 30). Equipment for sports and communal (public) swimming pools: MTC “Sport.” Retrieved May 18, 2015, from <http://eng.sport-spb.ru/krepl-poruch.htm>
- Nelson, J. A. (1986, November 5). Cooling Towers & Salt Water. The Marley Cooling Tower Company. Retrieved from spxcooling.com/pdf/CTs-and-Salt-Water.pdf
- NIST. (2011). CODATA Value: magnetic constant. In *The NIST Reference on Constants, Units, and Uncertainty*. Retrieved from <http://physics.nist.gov/cgi-bin/cuu/Value?mu0>
- Perry, M. (2015). Correspondance with WITTENSTEIN Motion Control.
- Powell, C., & Webster, P. (2012, December). Copper Alloys for Marine Environments. Copper Development Association. Retrieved from <http://www.copper.org/applications/marine/cuni/pdf/pub206.pdf>
- PPLATO. (1996). PPLATO | FLAP | PHYS 4.4: Electromagnetic induction. Retrieved May 7, 2015, from http://www.met.reading.ac.uk/pplato2/h-flap/phys4_4.html
- Practical Electromagnetic Shielding. (2015, April 25). Retrieved June 3, 2015, from http://www.learnemc.com/tutorials/Shielding02/Practical_Shielding.html
- Quartararo, T. (2015). Correspondance with Ultramotion.
- Radman, A. (2012). *EMPIG* (Master thesis). NTNU.
- Robotic Cable Management Made Easy. (2013, November 5). Retrieved from <http://www.designworldonline.com/robotic-cable-management-made-easy/>
- Rolf Lycke. (2012). Present Stock Program API 5L X 52 PSL 2 / L360 N/Q. Retrieved November 21, 2014, from <http://www.rolflycke.com/stock-program-api5l-x52-l360/>
- Rosvold, K. (2008). *Wax Deposition Models* (Master thesis). NTNU.
- Rudnev, V., Loveless, D., Cook, R. L., & Black, M. (2002). *Handbook of Induction Heating*. CRC Press.
- Samélor, D., Lazar, A.-M., Aufray, M., Tendero, C., Lacroix, L., Béguin, J.-D., ... Vahlas, C. (2011). Amorphous alumina coatings: processing, structure and remarkable barrier properties. *Journal of Nanoscience and Nanotechnology*, 11(9), 8387–8391.
- Semiatin, S. L. (1988). *Elements of Induction Heating: Design, Control, and Applications*. ASM International.

- Sharqawy, M. H., Lienhard, J. H., & Zubair, S. M. (2010). Thermophysical properties of seawater: a review of existing correlations and data. *Desalination and Water Treatment*, 16(1-3), 354–380. <http://doi.org/10.5004/dwt.2010.1079>
- Sloan, E. D. (1998). *Clathrate Hydrates of Natural Gases*. 2nd ed.
- Solenoid Actuators. (2014). Retrieved from <http://www.hydracon.com/submersible-solenoid-actuator/>
- Solgård, T. (2015). Conversation with EFD Induction.
- Standard Buoyancy Foams. (2014). Retrieved June 2, 2015, from http://www.f-e-t.com/our_products_technologies/subsea-solutions/bouyancy/standard-buoyancy-foams/
- Statoil. (2012, May 16). GFcompressor.jpg. Retrieved May 15, 2015, from <http://www.statoil.com/no/NewsAndMedia/PressRoom/Downloads/GFcompressor.jpg>
- Statoil med fjernstyrt verdensrekord på Åsgard. (2013, November 19). Retrieved May 25, 2015, from http://www.statoil.com/no/NewsAndMedia/News/2012/Pages/13Sep_hottap.aspx
- SYNFLEX. (2013, June 19). org_49a6ab6a32679f5b17ed06a63967bed5.jpeg (JPEG-bilde, 1298 × 865 piksler). Retrieved April 27, 2015, from http://www.synflex.com/system/cache/bilder/org_49a6ab6a32679f5b17ed06a63967bed5.jpeg
- Thermophysical properties of seawater. (2012, August 4). Retrieved April 20, 2015, from <http://web.mit.edu/seawater/>
- thomasnet.com. (2012, March 29). 24449.jpg. Retrieved June 3, 2015, from <http://cfnewsads.thomasnet.com/images/large/024/24449.jpg>
- Tibtech Innovations. (2011). Properties table of Stainless steel, Metals and other Conductive materials. Retrieved May 26, 2015, from <http://www.tibtech.com/conductivity.php>
- Tokura, I., Saito, H., Kishinami, K., & Muramoto, K. (1983). An Experimental Study of Free Convection Heat Transfer From a Horizontal Cylinder in a Vertical Array Set in Free Space Between Parallel Walls. *Journal of Heat Transfer*, 105(1), 102–107. <http://doi.org/10.1115/1.3245526>
- Tommasini, D. (2009, June). *Dielectric Insulation & High Voltage Issues*. CERN.
- Tresman, I. (2005, May 27). Plasma-filaments.jpg. Retrieved May 26, 2015, from <http://upload.wikimedia.org/wikipedia/commons/0/03/Plasma-filaments.jpg>

- Valencia, K., Ashrafiyan, A., & Krogstad, M. K. (2013). *Cold Flow - Economic Feasibility Study*. Weatherford Petroleum Consultants AS.
- Wan, Y., Wang, X., Sun, H., Li, Y., Zhang, K., & Wu, Y. (2012). Corrosion behavior of copper at elevated temperature. *Int. J. Electrochem. Sci*, 7, 7902–7914.
- Watlow. (2015, April 23). Watlow Heater Catalogue. Retrieved from <https://www.watlow.com/downloads/en/catalogs/heaters.pdf>
- Winther-Larssen, E. H. (2007, June). *Design of an Electric X-mas Tree Gate Valve Actuator* (Master thesis). NTNU, Department of Engineering Cybernetics.
- Zinn, S., & Semiatin, S. L. (1988, June). Induction Coil Design and Fabrication. *HEAT TREATING*. Retrieved from <http://www.stanleyzinn.com/induction-heating/coil-design-1.html>

10. Appendix

- A. InFlow whitepaper***
- B. Thermofluids***
- C. Brochure: EFD Induction Minac 18/25***
- D. MATLAB function Natural_convection.m***
- E. MATLAB function Grashof.m***
- F. MATLAB function Conjugate_heat_simulation.m***
- G. MATLAB function Vertical_HTC.m***
- H. Solidworks flow simulation reports***
- I. Brochure: Ultramotion Series U2 Datasheet***
- J. Additional renderings***
- K. Signed risk assessment***

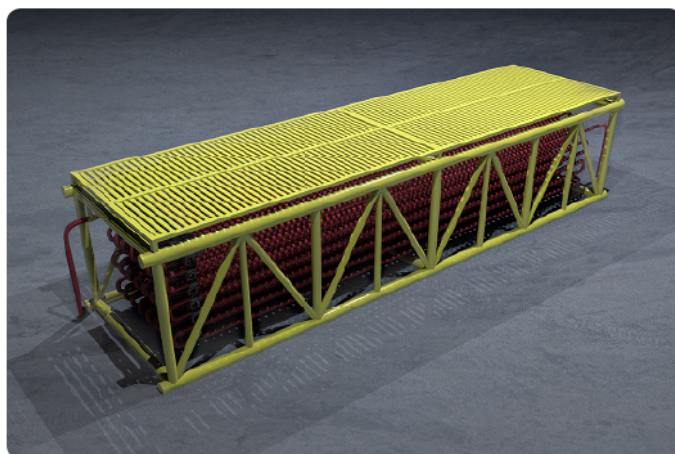
A. EMPIG InFlow Whitepaper

A whitepaper by EMPIG describing the status of the InFlow concept (EMPIG AS, 2014)

InFlow



EMPIG AS currently holds two complementary technologies for removal of pipe wall depositions in flow systems - PMFlow and InFlow. The Permanent Magnet Flow System (PMFlow) removes depositions mechanically by scraping the inner wall of the pipe with a non-intrusive hollow cleaning PIG. The Inductive Flow System (InFlow) removes pipe wall depositions by the means of heating the pipe using an induction coil. This document includes the work done, and current status for the InFlow System.



The concept sketch above illustrates how the compact cooling unit for the InFlow system may be used in a subsea application. The area of which the debris deposit on the pipe wall is limited to a predetermined area. The cooler system is modular and redundant with industry standard vertical tie in interfaces.

EMPIG's ambition has been to increase the maturity level of the InFlow technology. The activities performed are executed with the intention to achieve knowledge and experience relevant to the further development of the system.

Debris removal by induction heating

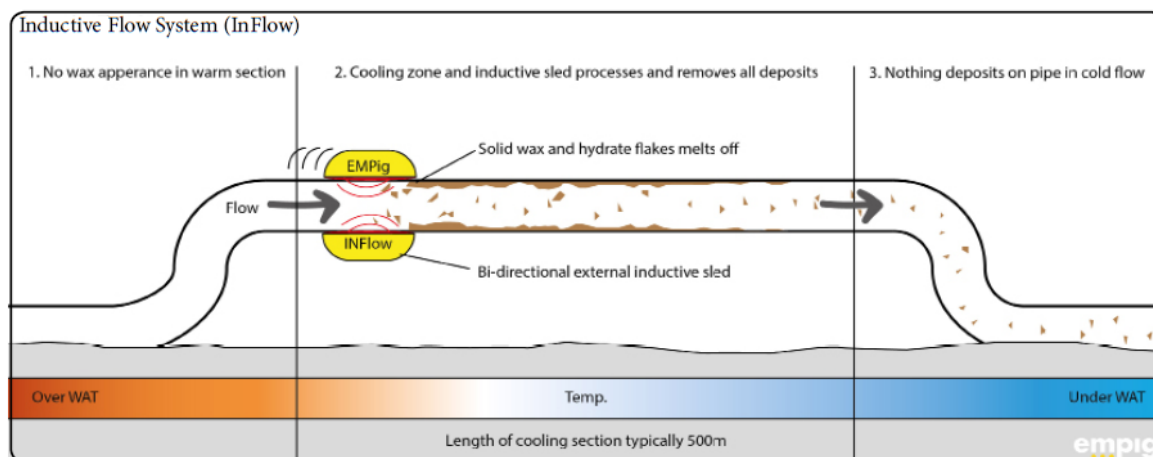
EMPIG AS has in the period of 2011-2014 carried out extensive feasibility studies and tests for the two flow assurance technologies. The activities performed have proven the technical concept feasible by the use of analytical tools, laboratory testing and simulations. The extensive studies have been done in collaboration with SINTEF, Smart Motor AS, Inventas AS, HiST and NTNU.

The two technologies may be used in any pipe processing plant application. Both systems will run continuously without requiring the plant to be

shut down during debris removal, which most traditional methods require.

Laboratory flow loop functional testing

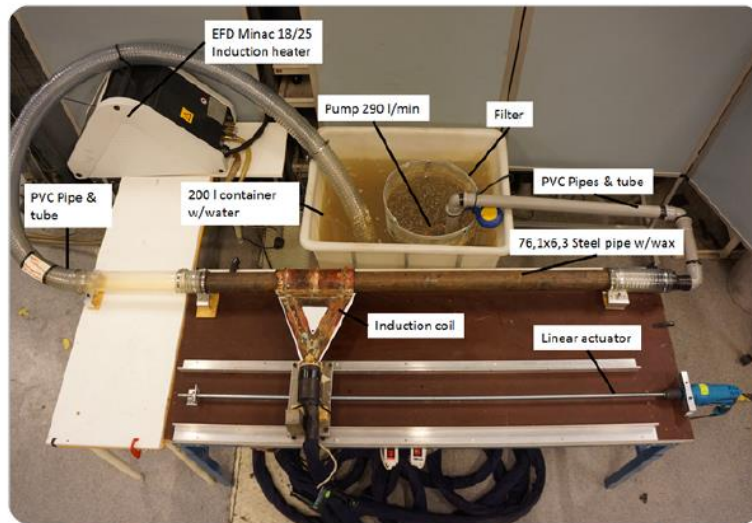
The feasibility of the InFlow system has been thoroughly investigated through laboratory functional testing. A flow loop was prepared, and water was used to simulate the liquid flow of a production pipeline. A wax mixture of 30 wt% paraffin wax, and 70 wt% semi synthetic oil was used for the 2 mm test pipe wax layer. The representability of this mixture was confirmed by our SINTEF collaborators. A high capacity adjustable induction



The InFlow system use a bi-directional external inductive sled, which removes deposit on the inner pipe using inductive heating. The flow is cooled down to ambient temperature in a specially designed cooling section. Cold flow is achieved and the flow may be transported over long distances without any issues related to deposits on the inner wall of the pipe.

coil system was included in the test to investigate the efficiency of debris removal by induction heating of the pipe. The main observations done in the

laboratory testing is included in the following.

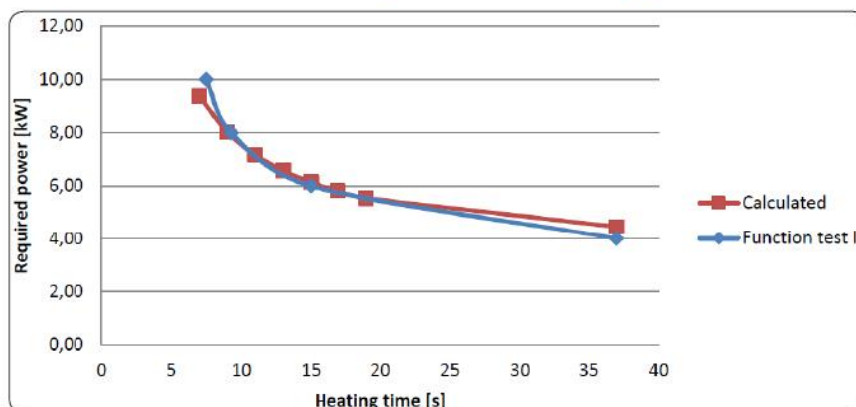


The laboratory function test setup is shown in the overview picture above. The induction coil power unit was adjustable, and numerous input power levels were investigated. Water was used in the flow loop. The preliminary testing has shown that the minimum input power should be in the area of 10 kW - 16 kW.



EMPIG has acquired valuable knowledge and experience about the InFlow system through laboratory function testing. The wax was removed by the retrievable induction coil in one section of the pipe and manually moved from one section to the next. As shown in the pictures above, the wax came off in a different shapes, such as flakes

and smaller particles. The shape of the removed wax depended on the input power, which was 16 kW for this particular photo. The laboratory testing activities has proven the InFlow system feasible. The energy requirement is in the area of 120 Wh/m when removing deposits by scanning the pipe line.



The correlation between the laboratory testing and the calculation results is shown in the graph above. The required power [kW] is shown as a function of heating time. In practice it illustrates the time needed for the wax layer to be removed at a given induction power input. The results of the function tests together with the preliminary calculations performed have proven the InFlow system feasible.

Visiting address
Otto Nielsens vei 12,
7052 Trondheim
post@empig.no

Morten Frøseth
morten.froseth@empig.no
Managing Director
+47 40 22 65 51

Fredrik Lund
fredrik.lund@empig.no
Technical Director
+47 99 24 98 89

Lars S. Strømmegjerde
lars.strommegjerde@empig.no
Mechanical Engineer, M.Sc.
+47 92 26 97 08

B. Thermofluids

The following is a direct excerpt from the pre-master thesis (Bjørvik, 2014):

Thermofluids is the study of heat transfer, fluid dynamics, thermodynamics and combustion combined. In the following, circumstances regarding the heat exchange from uniformly heated horizontal cylinders are presented.

The most prominent heat transfer mechanism for fluids, and also the main heat transfer mechanism for the passive cooling principle of the EMPIG system, is convection. The term convection in turn comprises the processes of simple heat conduction as well as advection – the heat transfer due to movement of fluid masses.

Grafsrønningen, Jensen and Reif (2011) studied the effects of heat transfer from a horizontal cylinder on the velocity field above it in water. Figure 2-6 shows the test setup and examples of instantaneous velocity fields above the heated cylinder.

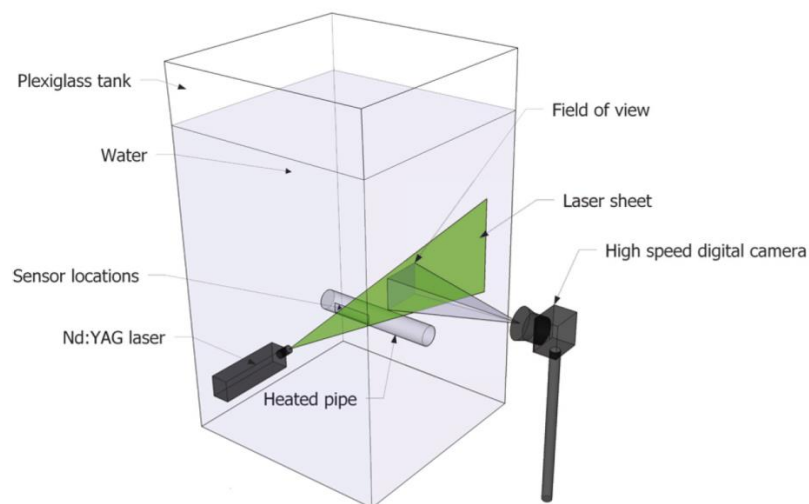


Figure 2-6: Test setup for investigating the flow characteristics above a heated cylinder
(Grafsrønningen et al., 2011)

A main conclusion was that the flow in immediate vicinity of the cylinder due to the buoyancy effects of heating the water was laminar, but that it at some point upstream underwent a transition into a turbulent flow regime. Examples of the velocity field above, i.e. downstream of the heated cylinder are shown in figure 2-7, in which indexes (a) through (f) indicates time ranging from 0 s to 2.5 s respectively with steps of 0.5 s. Axes are marked in the figure [mm], and colors indicate flow velocity [mm/s].

As turbulence in fluids is characterized by chaotic velocity fluctuations and thus large degrees of mixing, conditions for convective heat transfer from bodies surrounded by such flows are greatly enhanced, due to the increased driving forces. This suggests that advantageous heat transfer effects could be achieved for another heat exchanger element by placing it directly in the path of the turbulent flow downstream of a heated cylinder.

This effect was further studied in experiments on two horizontal cylinders (Grafsrønningen & Jensen, 2012), confirming improved heat transfer properties for the upper cylinder given certain boundary conditions, the most important of which being the distance between the respective cylinders. Furthermore, comparison of the buoyant plume above the second cylinder with that of the single cylinder uncovered pronounced differences in flow characteristics. In the case of the second cylinder, the plume was wider, and velocity fluctuations were twice the magnitude of those for the single cylinder.

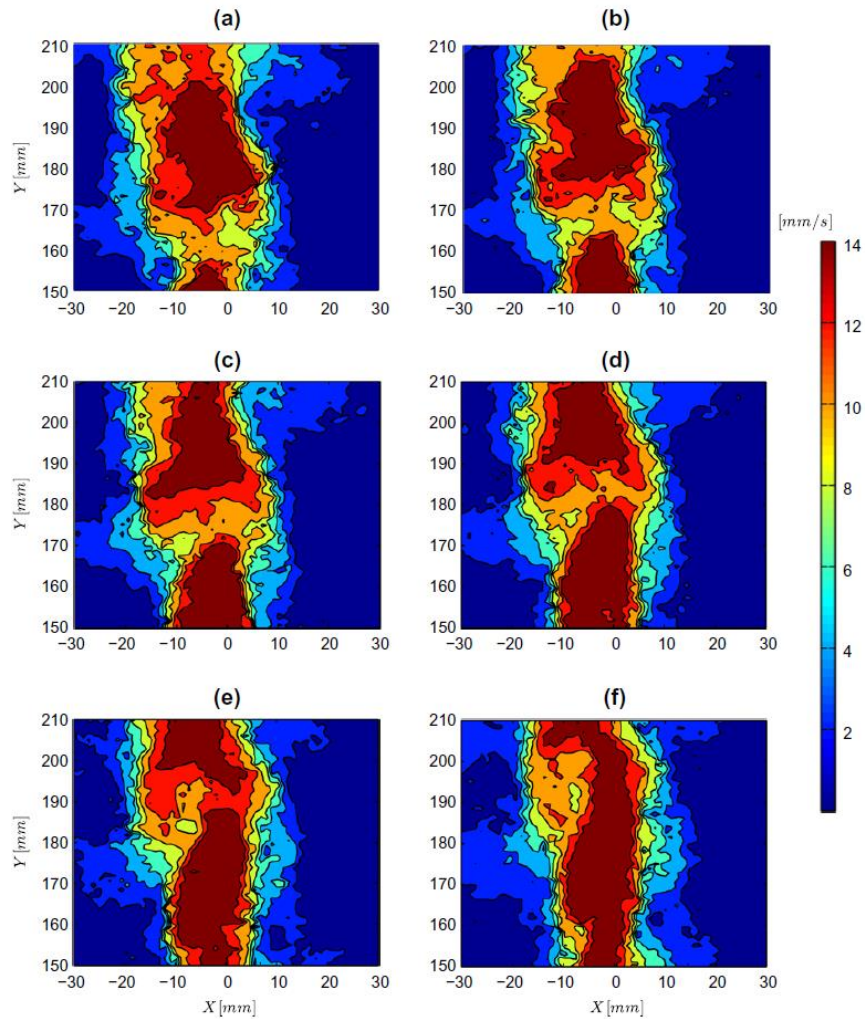


Figure 2-7: Examples of velocity fields downstream of the heated cylinder in the test setup shown in figure 2-3 (Grafsrønningen et al., 2011)

Similar investigations have also been carried out by others, and these have generally shown corresponding results. Arrays of more than two cylinders have been investigated in the past as well, and the same effect of improved heat transfer for cylinders positioned downstream of other heated cylinders has been documented, see e.g. Marsters (1972) and Tokura et al. (1983).

Further research by Grafsrønningen and Jensen (2013) considered the special case of three vertically arranged horizontal cylinders in which the middle and the uppermost cylinder were spaced closer together than the lowest to the second. It was shown that the heat transfer properties of both the upper cylinders had improved compared to the bottom cylinder, and furthermore that the separation distance of the upper cylinders did not have effect on the heat transfer properties of the uppermost cylinder. In conclusion, the advantageous turbulent flow effects on heat transfer properties for cylinders downstream of the first heated cylinder were present as long as the separation distance of the first and second cylinder was sufficient for a fully turbulent flow to develop.

End of excerpt.

C. Brochure: EFD Induction Minac 18/25

("Minac® 18/25 SM," 2014b)

Minac® 18/25 SM



A product within the Minac family

Mobile, flexible and easy-to-use. The Minac brings the benefits of induction to tough-to-access workpieces

Minac increases throughput.

Fast, easy, accurate and repeatable heat delivery improves productivity.

Minac improves quality.

Minac's microcontroller feature lets you pre-set temperatures and ramp-up and dwell times. Precise repeatability of heating cycles is assured.

Minac is environment friendly.

No flames, no gas and virtually no radiant heat mean a more comfortable, more productive working environment. Good news for the natural environment, too.

Minac lets you do more.

Minac's mobility and application versatility let you perform practically any heating task.

Minac reduces costs.

Precise heat delivery means you get things right the first time. Scrap, re-working and energy costs are minimized.

* The system shown is for illustrative purposes only. Coils and coil fixtures are optional extras.



Minac®18/25 SM

PRODUCT FEATURES

Mobile induction

Minac is light enough to be carried in a normal car. You no longer have to transport workpieces to the induction system—often a costly and time-consuming process.

Range of coils

Minac systems can be fitted with a practically limitless range of coil designs. EFD Induction are specialists at designing, testing and delivering customized, long-life coils.

Advanced MMI

Minac features advanced Man/Machine Interface (MMI) control panels. Minac's clear, menu-based and multi-language control panel maximize ease-of-use. Functionality is based on our specially designed microcontroller. The coil can either be fixed in position, or operated manually when attached to a handheld transformer (HHT).

Remote control

A remote control unit lets you control heating cycles via feedback to the microcontroller. Minac is available with field buses and is compatible with Profibus-DP, Devicenet, Ethernet. etc.

Robot compatible

Minac can be adapted to any robot, allowing quick, no-fuss intergration into automated production lines. The HHT can easily be mounted on a robot arm.

Maximum output power

With Minac's maximum power feature you can, for limited periods of time, operate with an output power far in excess of the continuous output power.

APPLICATIONS AREAS

Minac is ideal for a wide range of applications: brazing, shrink fitting, hardening, curing, straightening, heat treatment, etc. Minac is suitable for heating all kinds of electrical conductive materials like copper, aluminum, steel, stainless steel, brass, titanium, etc.

TECHNICAL DATA

Model	Minac 18/25 SM
Output	
Continuous output power	18 kW
Max. output power	25 kW
Duty factor / cycle time	50%/10 min
Output power regulation range	2-100%
Frequency range	10-25 kHz
HHT 240 power cable length	5 m / 10 m
Supply	
Supply voltage range	3 x 400-480 V \pm 10%
Frequency	50/60 Hz
Nominal voltage	400 V
Nominal line current	32A (RMS)
Max. line current intermittent	42A (RMS)
Nominal apparent power	23 kVA
Maximum apparent power	29 kVA
Recommended fuse	63 Amp
Mains cable length	5 m

Cooling

Water consumption, min.	7 l/min*
Water inlet temperature	max. 35°C
Water pressure min./max.	4/6 bar*
Cooling water quality - ph	between 7.0 and 9.0

Enclosure

Ambient operating temp.	+5°C - +50°C
Outer dimensions (WxDxH)	345 x 708 x 453 mm
Weight with HHT 240 / 5 m	54 kg (approx.)
Enclosure protection	IP 54
Color	RAL 7035 Grey
HHT 240 outer dimension (LxOD)	132 x 77 mm
HHT 240 weight without handle	3.5 kg

Subject to modification

* Dependent of coil

D. MATLAB function *Natural_convection.m*

```
function [ ] =
Natural_convection(amb_temp,heat_load,side_length,thickness,pressure,simulation_time,time_step)
% Natural_convection: Iterative numerical transient simulation of
% convective heat transfer from quadratic horizontal heated copper
% element submerged in seawater.

% The function takes in the ambient temperature, assumed heat loading due
% to copper loss, element geometry, water pressure and simulation
% conditions and calculates flow parameters alongside convective heat
% transfer according to Newton's law of cooling iteratively to reach
% a steady state in which the natural convective heat transfer from all
% surfaces are in equilibrium with the generated heat, which is assumed
% as volumetrically uniform

salinity = 35; %35 PSU typical salinity of deep ocean water
S_L = side_length;
coil_temp = amb_temp;
fT = amb_temp;

m_Cu = 8954*S_L*S_L*thickness; %mass of copper coil element
Cp_element = 384*m_Cu; %specific heat for copper element
heat = (heat_load/0.022875)*(S_L*S_L); %evaluating the surface heat
generation rate for the input geometry

coil_TEMP = [];
time_STEP = [];
RA = [];
L = (S_L*S_L)/(S_L*4); %characteristic length = Area/perimeter

for i = 0:time_step:simulation_time

    fT = (coil_temp - amb_temp)/2; %calculating film temperature
    density = SW_Density(fT,'C',salinity,'ppt');
    viscosity = SW_Viscosity(fT,'C',salinity,'ppt');

    %temperature rise from added power
    coil_temp = coil_temp + (heat*time_step)/Cp_element;

    %calculating boundary layer flow parameters
    Pr = SW_Prandtl(fT,'C',salinity,'ppt');
    Gr =
Grashof(sw_alpha(salinity,fT,pressure,'temp'),density,L,coil_temp,amb_temp,
viscosity);
    Gr_V =
Grashof(sw_alpha(salinity,fT,pressure,'temp'),density,thickness,coil_temp,amb_temp,viscosity);
    Ra = Gr*Pr;
    Ra_V = Gr_V*Pr;

    % Calculating Nusselt number for upper surface
    if Ra < 10^7 && Ra > 10^4
        Nu_U = 0.54*Ra^(1/4);
    elseif Ra < 10^11 && Ra > 10^7
        Nu_U = 0.15*Ra^(1/3);
```



```

elseif Ra < 10^4
    Nu_U = 0.54*Ra^(1/4);
end

% Calculating Nusselt number for lower surface
%if Ra < 10^11 && Ra > 10^5
    Nu_L = 0.27*Ra^(1/4);
%else
    % Nu_L = 0.01;
%end

% Calculating Nusselt number for vertical surface
if Ra_V < 10^9 && Ra_V > 10^4
    Nu_V = 0.59*Ra_V^(1/4);
elseif Ra_V < 10^13 && Ra_V > 10^9
    Nu_V = 0.1*Ra_V^(1/3);
elseif Ra_V < 10^4
    Nu_V = 0.59*Ra_V^(1/4);
end

k = SW_Conductivity(fT, 'C', salinity, 'ppt');

%heat transfer coefficients
h_U = (Nu_U*k)/L;
h_L = (Nu_L*k)/L;
h_V = (Nu_V*k)/thickness;

%heat transfer from Newton's law of cooling
Q_U = h_U*S_L*S_L*(coil_temp - amb_temp);
Q_L = h_L*S_L*S_L*(coil_temp - amb_temp);
Q_V = h_V*S_L*thickness*(coil_temp - amb_temp);

coil_temp = coil_temp - ((Q_U*time_step + Q_L*time_step +
4*Q_V*time_step)/Cp_element);

if mod(i,1) == 0;
    clc;
    disp('Coil element temperature:');
    disp(coil_temp);
end

coil_TEMP = [coil_TEMP, coil_temp];
time_STEP = [time_STEP, i];
RA = [RA, Ra];

end

plot(time_STEP, coil_TEMP);
title('Temperature of copper coil element vs time');
xlabel('Physical time [s]');
ylabel('Temperature [DgrC]');
% plot(time_STEP, RA);
% title('Calculated Rayleigh number vs time');
% xlabel('Physical time [s]');
% ylabel('Rayleigh number');

end

```

E. MATLAB function *Grashof.m*

```
function [ Gr ] = Grashof(beta,density,L,coil_temp,amb_temp,viscosity)

%Grashof Number: Temperature dependent flow parameter
% The function calculates the Grashof number for the flow and heating
% conditions

theta = coil_temp - amb_temp;

Gr = (beta*9.81*density^2*L^3*theta)/(viscosity^2);

end
```

F. MATLAB function *Conjugate_heat_simulation.m*

```
function [ T ] =
Conjugate_heat_simulation(amb_temp,heat_load,side_length,thickness,pressure
,simulation_time,time_step,z_step)
%   Conjugate heat transfer: Simulation of the conjugate heat transfer
%   related to a copper element submerged in seawater

%   The function combines convective heat transfer from the outer surfaces
%   with the effects of heat conduction through the thickness of the solid
%   by numerically approximating heat diffusion based on Fourier's law,
%   with heat generation in the uppermost thickness element.

n = thickness/z_step; %number of elements
T = []; %container for element temperatures

%initial conditions; solid completely at ambient temperature
for i = 1:n
    T(i) = amb_temp;
end

salinity = 35; %35 PSU typical salinity of deep ocean water
S_L = side_length;

m_Cu = 8954*S_L*S_L*z_step; %mass of copper elements
Cp_element = 384*m_Cu; %specific heat for copper elements
heat = (heat_load/0.022875)*(S_L*S_L); %evaluating the surface heat
generation rate for the input geometry
k_Cu = 390; %thermal conductivity of copper [W/mK]
L = (S_L*S_L)/(S_L*4); %characteristic length = Area/perimeter

Top_temp = []; %logging maximum temperatures (top element / T(1))
time_STEP = [];

for i = 0:time_step:simulation_time

    %temperature rise in first element from heat generation
    T(1) = T(1) + (heat*time_step)/Cp_element;

    % top element boundary layer thermophysical properties
    fT_T = (T(1) - amb_temp)/2; %calculating film temperature
    density_T = SW_Density(fT_T,'C',salinity,'ppt');
    viscosity_T = SW_Viscosity(fT_T,'C',salinity,'ppt');
    Pr_T = SW_Prandtl(fT_T,'C',salinity,'ppt');
    Gr_T =
Grashof(sw_alpha(salinity,fT_T,pressure,'temp'),density_T,L,T(1),amb_temp,viscosity_T);
    Ra_T = Gr_T*Pr_T;

    % Calculating Nusselt number for upper surface
    if Ra_T < 10^7 && Ra_T > 10^4
        Nu_U = 0.54*Ra_T^(1/4);
    elseif Ra_T < 10^11 && Ra_T > 10^7
        Nu_U = 0.15*Ra_T^(1/3);
    elseif Ra_T < 10^4
        Nu_U = 0.54*Ra_T^(1/4);
    end
```

```

% Fourier approximated heat conduction through the thickness
for z = n:-1:2
    T(z) = T(z) ...
        + ((k_Cu*(T(z-1)-T(z))/z_step)*(S_L*S_L)*time_step)/Cp_element;
    T(z-1) = T(z-1) ...
        - ((k_Cu*(T(z-1)-T(z))/z_step)*(S_L*S_L)*time_step)/Cp_element;
end

% bottom element boundary layer thermophysical properties
fT_B = (T(n) - amb_temp)/2; %calculating film temperature
density_B = SW_Density(fT_B, 'C', salinity, 'ppt');
viscosity_B = SW_Viscosity(fT_B, 'C', salinity, 'ppt');
Pr_B = SW_Prandtl(fT_B, 'C', salinity, 'ppt');
Gr_B =
Grashof(sw_alpha(salinity, fT_B, pressure, 'temp'), density_B, L, T(n), amb_temp, viscosity_B);
Ra_B = Gr_B*Pr_B;

% Calculating Nusselt number for bottom surface
%if Ra < 10^11 && Ra > 10^5
    Nu_L = 0.27*Ra_B^(1/4);
%else
    % Nu_L = 0.01;
%end

k_T = SW_Conductivity(fT_T, 'C', salinity, 'ppt');
k_B = SW_Conductivity(fT_B, 'C', salinity, 'ppt');

%Calculating respective heat transfer coefficients
h_U = (Nu_U*k_T)/L;
h_L = (Nu_L*k_B)/L;
h_TV = Vertical_HTC(T(1), amb_temp, pressure, salinity, z_step);
h_BV = Vertical_HTC(T(n), amb_temp, pressure, salinity, z_step);

%Corresponding heat dissipation from Newton's law of cooling
Q_U = h_U*S_L*S_L*(T(1) - amb_temp);
Q_L = h_L*S_L*S_L*(T(n) - amb_temp);
Q_TV = h_TV*S_L*z_step*(T(1) - amb_temp);
Q_BV = h_BV*S_L*z_step*(T(n) - amb_temp);

%Temperature decrease in first and last elements (with horizontal
surfaces
%pointing outwards)
T(1) = T(1) - (Q_U*time_step + 4*Q_TV*time_step)/Cp_element;
T(n) = T(n) - (Q_L*time_step + 4*Q_BV*time_step)/Cp_element;

% Convective heat transfer from vertical walls through the thickness
for m = 2:(n-1)
    h_V = Vertical_HTC(T(m), amb_temp, pressure, salinity, z_step);
    Q_V = h_V*S_L*z_step*(T(m) - amb_temp);
    T(m) = T(m) ...
        - (4*Q_V*time_step)/Cp_element;
end

%plotting results
if mod(i*4,1) == 0;
    clc;
    disp('Physical time in simulation [s]:');
    disp([num2str(i) '/' num2str(simulation_time)]);
    disp('Coil element temperature [degrC]:');

```

```
disp(T(1));
disp('Temperature difference through thickness [degrC]:');
disp((T(1)-T(n)));
end

Top_temp = [Top_temp, T(1)];
time_STEP = [time_STEP, i];

end
plot(time_STEP,Top_temp);
title('Temperature of copper coil element vs time');
xlabel('Physical time [s]');
ylabel('Temperature [DgrC]');
end
```

G. MATLAB function *Vertical_HTC.m*

```
function [ h_V ] = Vertical_HTC(T,amb_temp,pressure,salinity,z_step)

% Vertical heat transfer coefficients: The function is called by
% Conjugate_heat_simulation.m to calculate the fluid thermophysical
% properties at the respective thickness elements.

fT = (T - amb_temp)/2; %calculating film temperature
density = SW_Density(fT,'C',salinity,'ppt');
viscosity = SW_Viscosity(fT,'C',salinity,'ppt');

Pr = SW_Prandtl(fT,'C',salinity,'ppt');
Gr_V =
Grashof(sw_alpha(salinity,fT,pressure,'temp'),density,z_step,T,amb_temp,vis
cosity);
Ra_V = Gr_V*Pr;

% Calculating Nusselt number for vertical surface
if Ra_V < 10^9 && Ra_V > 10^4
    Nu_V = 0.59*Ra_V^(1/4);
elseif Ra_V < 10^13 && Ra_V > 10^9
    Nu_V = 0.1*Ra_V^(1/3);
elseif Ra_V < 10^4
    Nu_V = 0.59*Ra_V^(1/4);
end

k = SW_Conductivity(fT,'C',salinity,'ppt');

h_V = (Nu_V*k)/z_step;

end
```

H. Solidworks Flow Simulation reports

Transient natural convection heat dissipation analysis, volumetric heat generation in 20*20*6 mm copper element

System Info

Product	Flow Simulation 2014 SP5.0. Build: 2878
Computer name	TRYM
User name	TrymBrox
Processors	Intel(R) Core(TM) i7-4700HQ CPU @ 2.40GHz
Memory	12171 MB / 134217727 MB
Operating system	(Build 9600)
CAD version	SolidWorks 2014 SP5.0
CPU speed	2401 MHz

General Info

Model	20mm_plate.SLDPRT
Project name	vol_nat_lvl8
Units system	SI (m-kg-s)
Analysis type	External (not exclude internal spaces)
Exclude cavities without flow conditions	Off
Coordinate system	Global coordinate system
Reference axis	X

INPUT DATA

Initial Mesh Settings

Automatic initial mesh: On

Result resolution level: 8

Advanced narrow channel refinement: Off

Refinement in solid region: Off

Geometry Resolution

Evaluation of minimum gap size: Automatic

Evaluation of minimum wall thickness: Automatic

Computational Domain

Size

X min	-0.060 m
X max	0.060 m
Y min	-0.050 m
Y max	0.056 m
Z min	-0.060 m
Z max	0.060 m

Boundary Conditions

2D plane flow	None
At X min	Default
At X max	Default
At Y min	Default
At Y max	Default
At Z min	Default
At Z max	Default

Physical Features

Heat conduction in solids: On

Heat conduction in solids only: Off

Radiation: Off

Time dependent: On

Gravitational effects: On

Flow type: Laminar and turbulent

Cavitation: Off

High Mach number flow: Off

Default roughness: 0 micrometer

Gravitational Settings

X component	0 m/s ²
Y component	-9.81 m/s ²
Z component	0 m/s ²

Ambient Conditions

Thermodynamic parameters	Static Pressure: 1.00e+007 Pa Temperature: 4.00 °C
Velocity parameters	Velocity vector Velocity in X direction: 0 m/s Velocity in Y direction: 0 m/s Velocity in Z direction: 0 m/s
Solid parameters	Default material: Copper Initial solid temperature: 4.00 °C
Turbulence parameters	Turbulence intensity and length Intensity: 0.10 % Length: 6.000e-005 m

Material Settings

Fluids

Water

Solids

Copper

Heat Volume Sources

VS Heat Generation Rate 1

Source type	Heat Generation Rate
Heat generation rate	210.000 W
Components	Boss-Extrude1
Coordinate system	Global coordinate system
Reference axis	X

Goals

Volume Goals

VG Max Temperature (Solid) 1

Type	Volume Goal
Goal type	Temperature (Solid)
Calculate	Maximum value
Components	Boss-Extrude1
Coordinate system	Global coordinate system
Use in convergence	On

Calculation Control Options

Finish Conditions

Finish conditions	If one is satisfied
Maximum physical time	60.000 s

Solver Refinement

Refinement level	2
Approximate maximum cells	1e+007
Refinement strategy	Tabular refinement
Units	Travels
Relaxation interval	2e-001
Refinements	2, 3

Results Saving

Save before refinement	On
Periodic saving	Units: Physical time Period: 10.000 s

Advanced Control Options

Flow Freezing

Flow freezing strategy	Disabled
------------------------	----------

Manual time step (Freezing): Off

Manual time step: Off

RESULTS

General Info

Iterations: 388

Physical time: 60.000 s

CPU time: 1603 s

Calculation Mesh

Basic Mesh Dimensions

Number of cells in X	66
Number of cells in Y	58
Number of cells in Z	66

Number Of Cells

Total cells	252648
Fluid cells	249448
Solid cells	1944
Partial cells	1256
Irregular cells	0
Trimmed cells	0

Maximum refinement level: 0

Goals

Name	Unit	Value	Progress	Use in convergence	Delta	Criteria
VG Max Temperature (Solid) 1	°C	136.60	100	On	0.031858509	3.97789628

Min/Max Table

Name	Minimum	Maximum
Pressure [Pa]	9999465.71	1.00e+007
Temperature [°C]	4.00	136.60
Density (Fluid) [kg/m^3]	977.96	1000.75
Velocity [m/s]	0	0.086
Velocity (X) [m/s]	-0.010	0.010
Velocity (Y) [m/s]	-0.004	0.086
Velocity (Z) [m/s]	-0.010	0.010
Temperature (Fluid) [°C]	4.00	136.44
Temperature (Solid) [°C]	129.52	136.60
Density (Solid) [kg/m^3]	8960.00	8960.00
Vorticity [1/s]	3.540e-007	16.727
Shear Stress [Pa]	0	0.11
Relative Pressure [Pa]	-534.29	475.38
Heat Transfer Coefficient [W/m^2/K]	287.706	2387.839

Surface Heat Flux [W/m ²]	0	307737.125
Heat Flux [W/m ²]	22267.370	475077.328
Overheat above Melting Temperature [K]	-953.526	-946.447

Screen captures at steady state condition

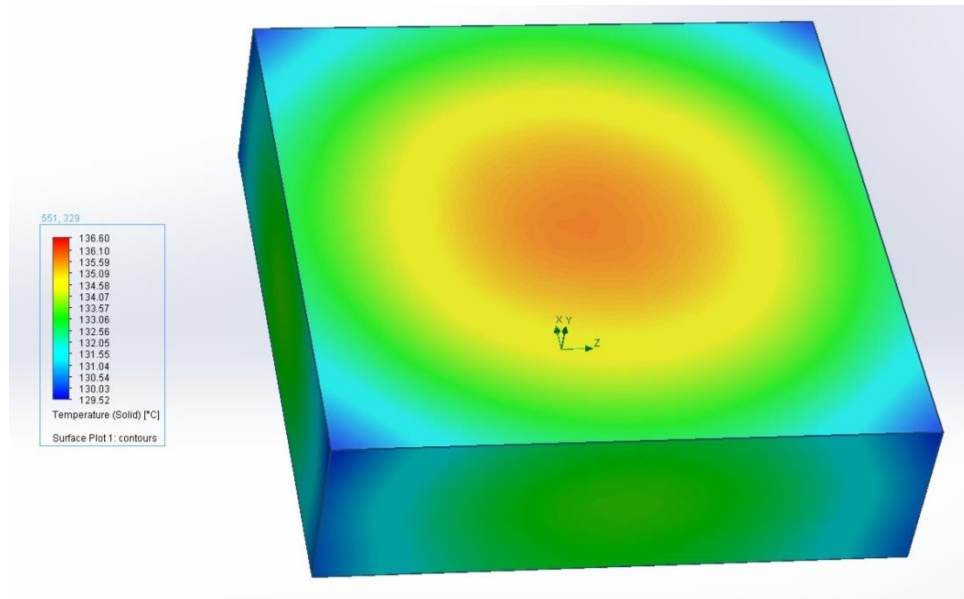


Figure 0-1: Top

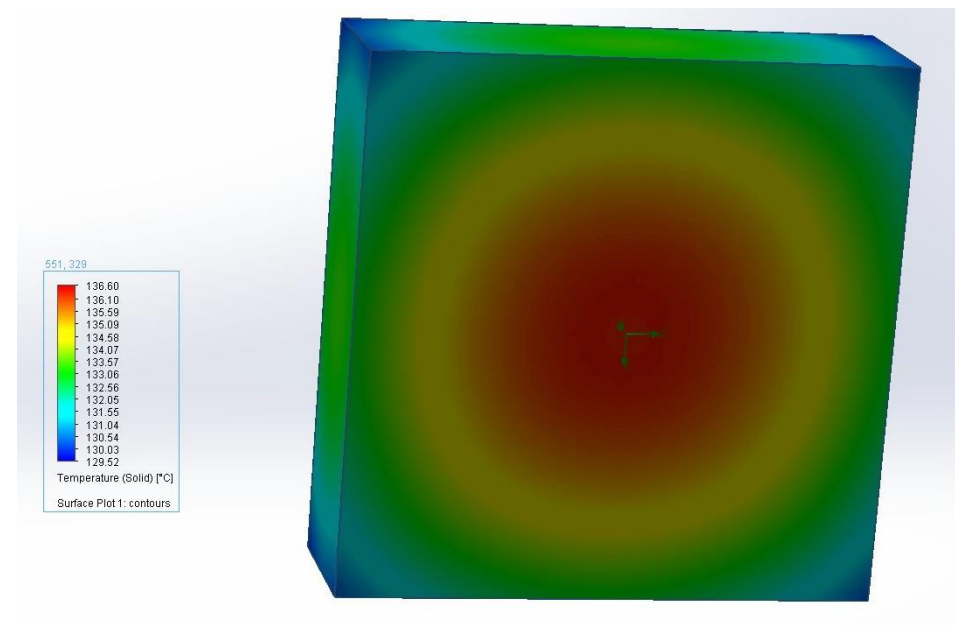


Figure 0-2: Bottom

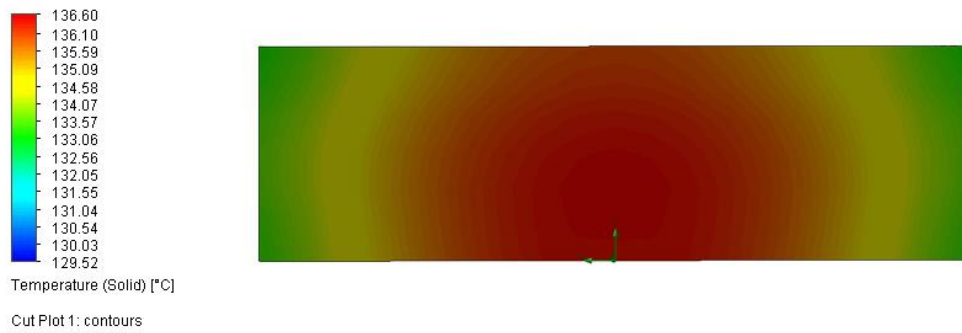


Figure 0-3: Cut plot, showing temperature distribution through the thickness of the element

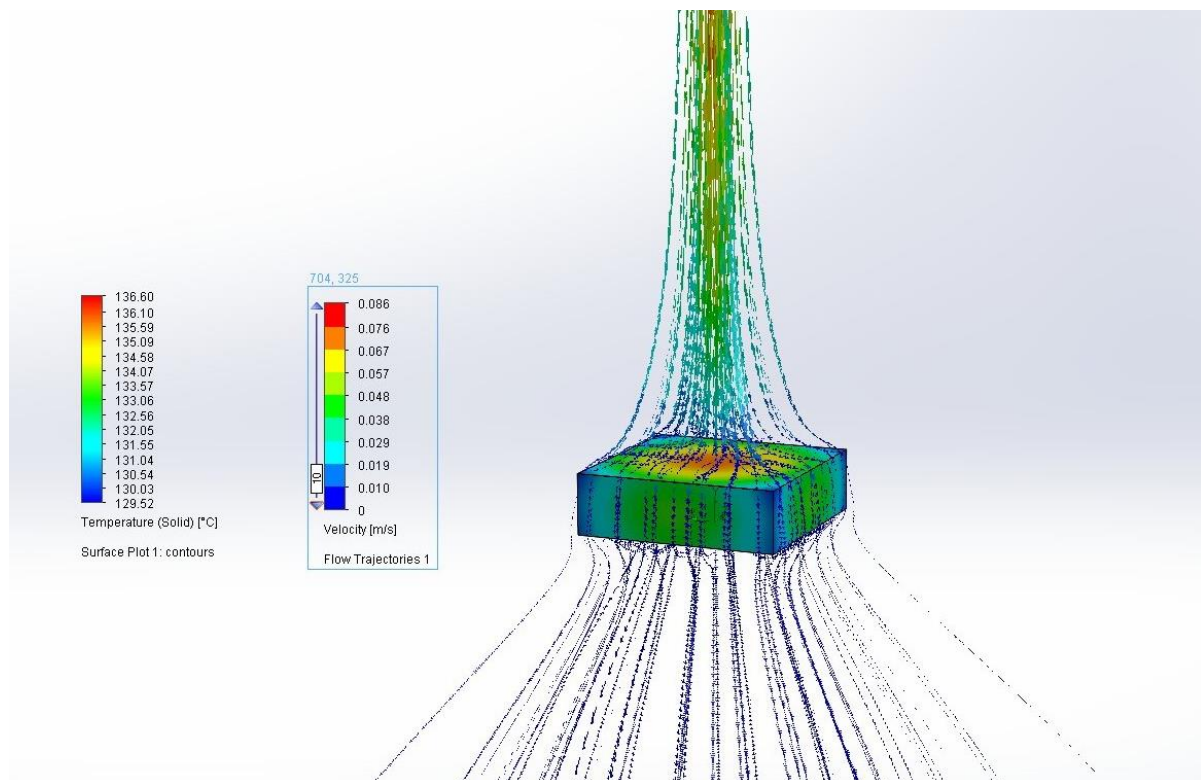


Figure 0-4: Flow trajectories around the element

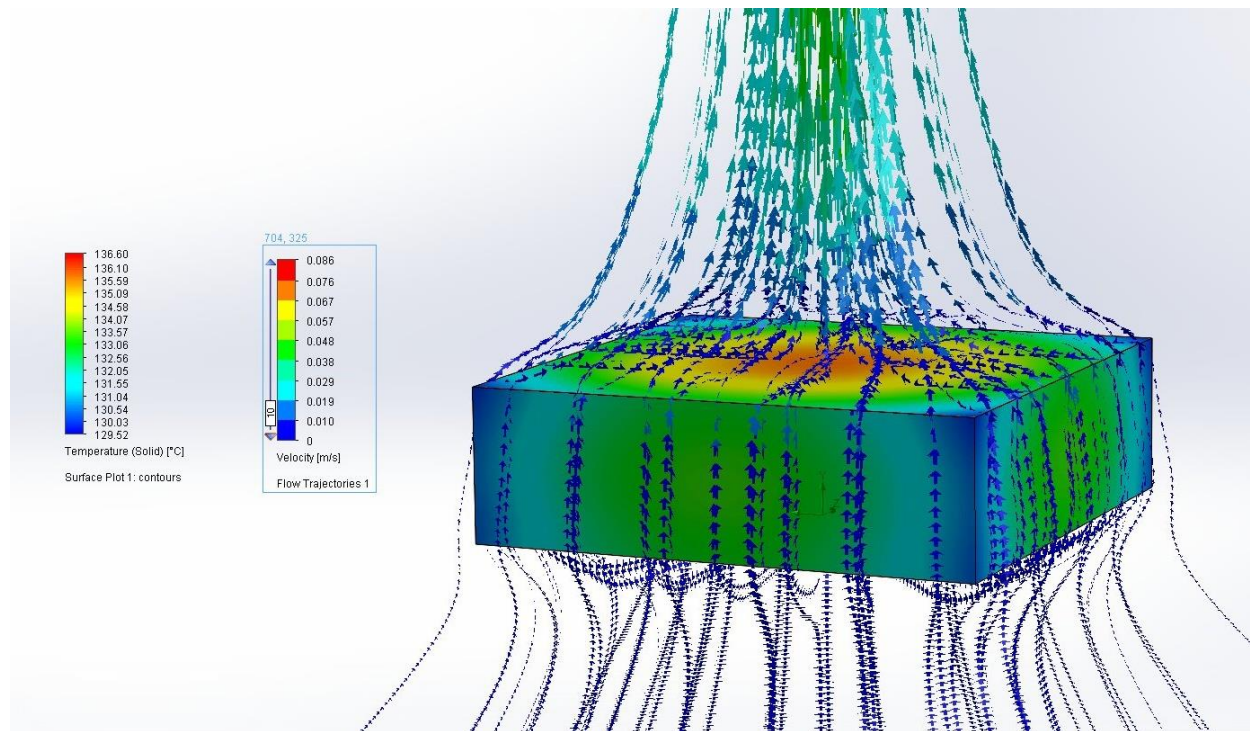


Figure 0-5: Flow trajectories around the element

Transient natural convection heat dissipation analysis, top surface heat generation in 20*20*6 mm copper element

System Info

Product	Flow Simulation 2014 SP5.0. Build: 2878
Computer name	TRYM
User name	TrymBrox
Processors	Intel(R) Core(TM) i7-4700HQ CPU @ 2.40GHz
Memory	12171 MB / 134217727 MB
Operating system	(Build 9600)
CAD version	SolidWorks 2014 SP5.0
CPU speed	2401 MHz

General Info

Model	20mm_plate.SLDPRT
Project name	top_nat_lvl8
Units system	SI (m-kg-s)
Analysis type	External (not exclude internal spaces)
Exclude cavities without flow conditions	Off
Coordinate system	Global coordinate system
Reference axis	X

INPUT DATA

Initial Mesh Settings

Automatic initial mesh: On

Result resolution level: 8

Advanced narrow channel refinement: Off

Refinement in solid region: Off

Geometry Resolution

Evaluation of minimum gap size: Automatic

Evaluation of minimum wall thickness: Automatic

Computational Domain

Size

X min	-0.060 m
X max	0.060 m
Y min	-0.050 m
Y max	0.056 m
Z min	-0.060 m
Z max	0.060 m

Boundary Conditions

2D plane flow	None
At X min	Default
At X max	Default
At Y min	Default
At Y max	Default
At Z min	Default
At Z max	Default

Physical Features

Heat conduction in solids: On

Heat conduction in solids only: Off

Radiation: Off

Time dependent: On

Gravitational effects: On

Flow type: Laminar and turbulent

Cavitation: Off

High Mach number flow: Off

Default roughness: 0 micrometer

Gravitational Settings

X component	0 m/s ²
Y component	-9.81 m/s ²
Z component	0 m/s ²

Ambient Conditions

Thermodynamic parameters	Static Pressure: 1.00e+007 Pa Temperature: 4.00 °C
Velocity parameters	Velocity vector Velocity in X direction: 0 m/s Velocity in Y direction: 0 m/s Velocity in Z direction: 0 m/s
Solid parameters	Default material: Copper Initial solid temperature: 4.00 °C
Turbulence parameters	Turbulence intensity and length Intensity: 0.10 % Length: 6.000e-005 m

Material Settings

Fluids

Water

Solids

Copper

Heat Surface Sources

SS Heat Generation Rate 1

Type	Heat generation rate
Faces	Face<1>
Coordinate system	Face Coordinate System
Reference axis	X
Toggle	On
Heat generation rate	210.000 W

Goals

Volume Goals

VG Max Temperature (Solid) 1

Type	Volume Goal
Goal type	Temperature (Solid)
Calculate	Maximum value
Components	Boss-Extrude1
Coordinate system	Global coordinate system
Use in convergence	On

Calculation Control Options

Finish Conditions

Finish conditions	If one is satisfied
Maximum physical time	60.000 s

Solver Refinement

Refinement level	2
Approximate maximum cells	1e+007
Refinement strategy	Tabular refinement
Units	Travels
Relaxation interval	2e-001
Refinements	2, 3

Results Saving

Save before refinement	On
Periodic saving	Units: Physical time Period: 10.000 s

Advanced Control Options

Flow Freezing

Flow freezing strategy	Disabled
------------------------	----------

Manual time step (Freezing): Off

Manual time step: Off

RESULTS

General Info

Iterations: 395

Physical time: 60.000 s

CPU time: 1642 s

Log

Mesh generation started	19:56:42 , May 30
Mesh generation normally finished	19:56:50 , May 30
Preparing data for calculation	19:56:50 , May 30
Calculation started 0	19:56:58 , May 30
Calculation finished 441	20:27:34 , May 30

Calculation Mesh

Basic Mesh Dimensions

Number of cells in X	66
Number of cells in Y	58
Number of cells in Z	66

Number Of Cells

Total cells	252648
Fluid cells	249448
Solid cells	1944
Partial cells	1256
Irregular cells	0
Trimmed cells	0

Maximum refinement level: 0

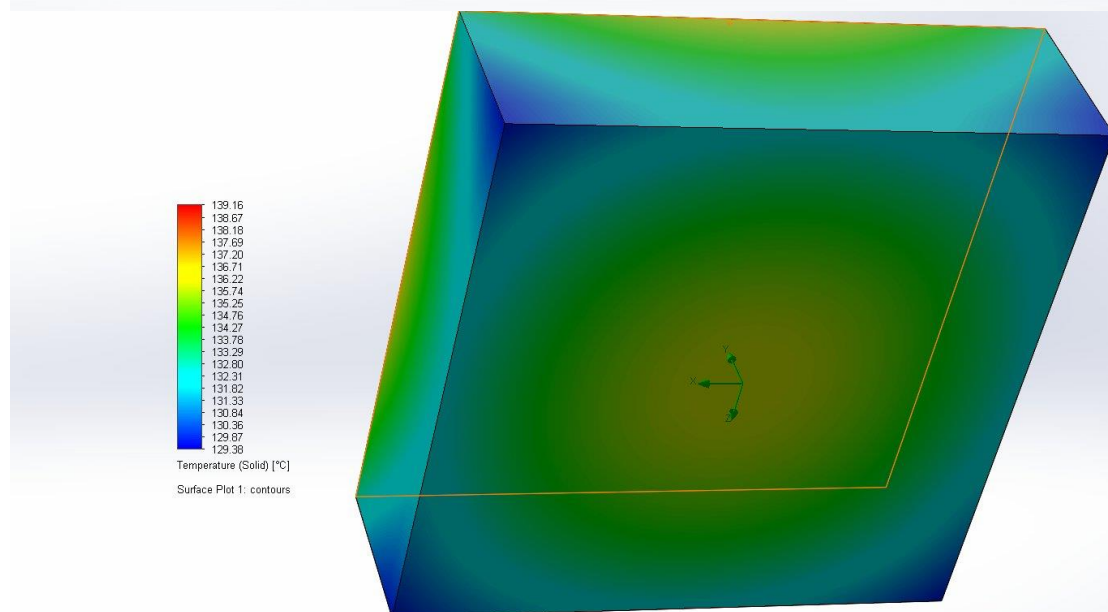
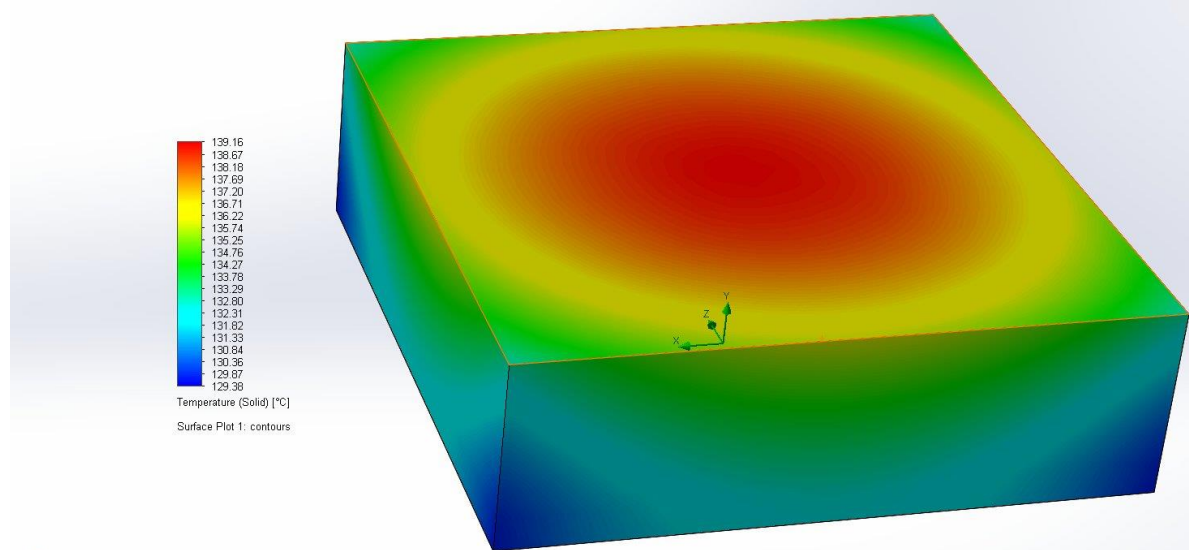
Goals

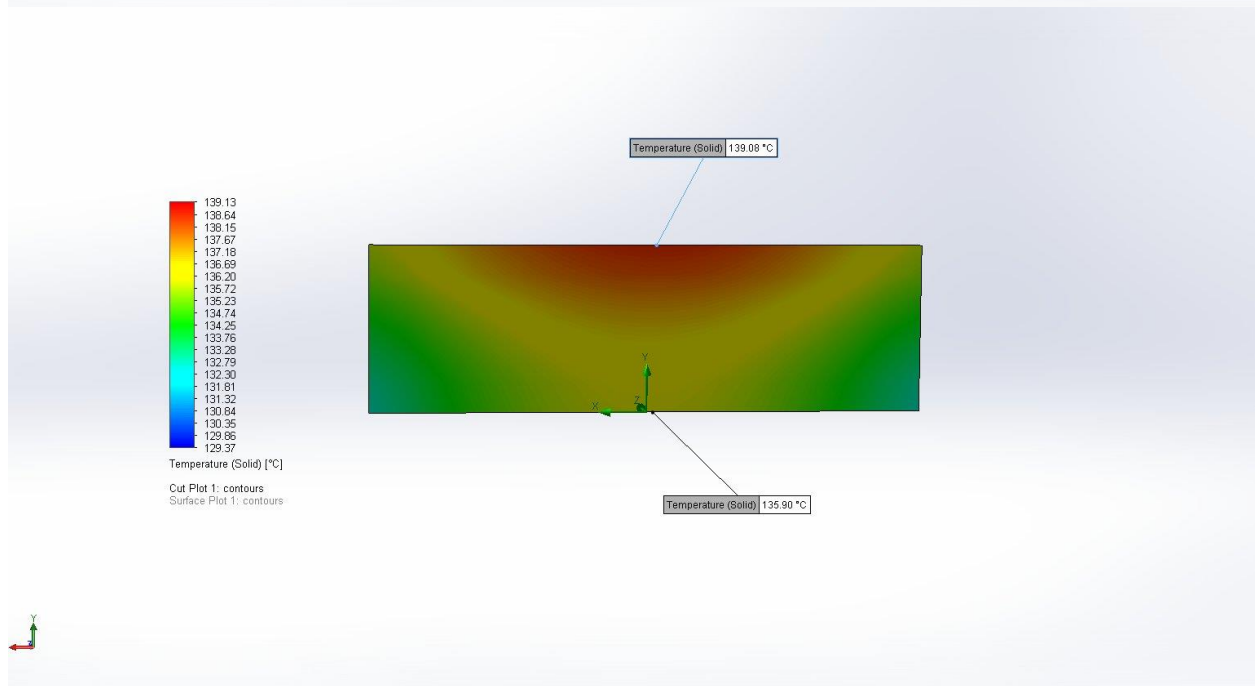
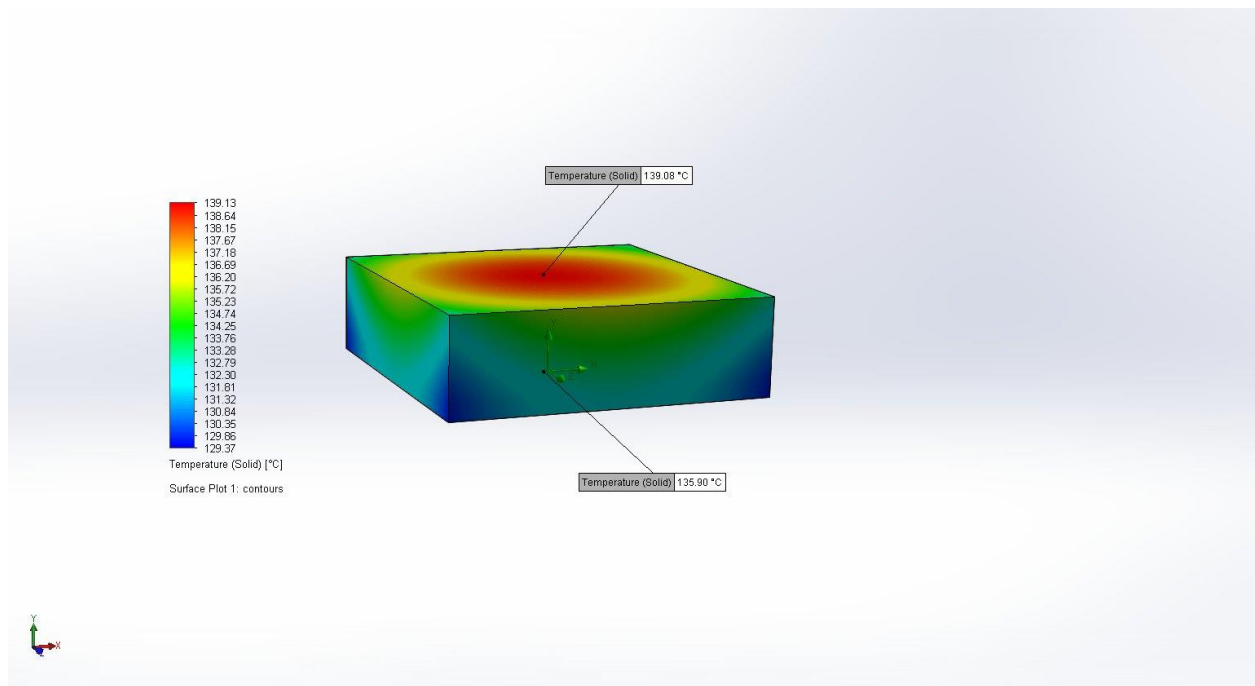
Name	Unit	Value	Progress	Use in convergence	Delta	Criteria
VG Max Temperature (Solid) 1	°C	139.13	100	On	0.129214016	4.02194196

Min/Max Table

Name	Minimum	Maximum
Pressure [Pa]	9999465.71	1.00e+007
Temperature [°C]	4.00	139.16
Density (Fluid) [kg/m^3]	977.65	1000.75
Velocity [m/s]	0	0.091
Velocity (X) [m/s]	-0.010	0.010
Velocity (Y) [m/s]	-0.004	0.091
Velocity (Z) [m/s]	-0.010	0.010

Temperature (Fluid) [°C]	4.00	139.16
Temperature (Solid) [°C]	129.38	139.16
Density (Solid) [kg/m^3]	8960.00	8960.00
Vorticity [1/s]	6.191e-007	17.826
Shear Stress [Pa]	0	0.11
Relative Pressure [Pa]	-534.29	475.38
Heat Transfer Coefficient [W/m^2/K]	196.300	2382.685
Surface Heat Flux [W/m^2]	0	305684.033
Heat Flux [W/m^2]	37168.018	528780.729
Overheat above Melting Temperature [K]	-953.673	-943.891





Transient natural convection heat dissipation analysis of solid coil, surface heat generation

System Info

Product	Flow Simulation 2014 SP5.0. Build: 2878
Computer name	TRYM
User name	TrymBrox
Processors	Intel(R) Core(TM) i7-4700HQ CPU @ 2.40GHz
Memory	12171 MB / 134217727 MB
Operating system	(Build 9600)
CAD version	SolidWorks 2014 SP5.0
CPU speed	2401 MHz

General Info

Model	std_solid.SLDPRT
Project name	coil_strd_nat_lvl8
Units system	SI (m-kg-s)
Analysis type	External (not exclude internal spaces)
Exclude cavities without flow conditions	Off
Coordinate system	Global coordinate system
Reference axis	X

INPUT DATA

Initial Mesh Settings

Automatic initial mesh: On

Result resolution level: 8

Advanced narrow channel refinement: Off

Refinement in solid region: Off

Geometry Resolution

Evaluation of minimum gap size: Automatic

Evaluation of minimum wall thickness: Automatic

Computational Domain

Size

X min	-0.613 m
X max	0.603 m
Y min	-0.635 m
Y max	0.545 m
Z min	-0.605 m

Z max	0.603 m
-------	---------

Boundary Conditions

2D plane flow	None
At X min	Default
At X max	Default
At Y min	Default
At Y max	Default
At Z min	Default
At Z max	Default

Physical Features

Heat conduction in solids: On
Heat conduction in solids only: Off
Radiation: Off
Time dependent: On
Gravitational effects: On
Flow type: Laminar and turbulent
Cavitation: Off
High Mach number flow: Off
Default roughness: 0 micrometer

Gravitational Settings

X component	9.81 m/s ²
Y component	0 m/s ²
Z component	0 m/s ²

Ambient Conditions

Thermodynamic parameters	Static Pressure: 1.00e+007 Pa Temperature: 4.00 °C
Velocity parameters	Velocity vector Velocity in X direction: 0 mm/s Velocity in Y direction: 0 mm/s Velocity in Z direction: 0 mm/s
Solid parameters	Default material: Copper Initial solid temperature: 4.00 °C
Turbulence parameters	Turbulence intensity and length Intensity: 0.10 % Length: 0.002 m

Material Settings

Fluids

Water

Solids

Copper

Heat Surface Sources

SS Surface Heat Generation Rate 1

Type	Surface heat generation rate
Faces	Face<3> Face<1> Face<4> Face<2> Face<5>
Coordinate system	Global coordinate system
Reference axis	X
Toggle	On
Surface heat generation rate	524590.000 W/m^2

Goals

Volume Goals

VG Max Temperature (Solid) 1

Type	Volume Goal
Goal type	Temperature (Solid)
Calculate	Maximum value
Components	Fillet3
Coordinate system	Global coordinate system
Use in convergence	On

Calculation Control Options

Finish Conditions

Finish conditions	If one is satisfied
Maximum physical time	120.000 s

Solver Refinement

Refinement level	2
Approximate maximum cells	1e+007
Refinement strategy	Tabular refinement
Units	Travels
Relaxation interval	2e-001
Refinements	2, 3

Results Saving

Save before refinement	On
Periodic saving	Units: Physical time Period: 10.000 s

Advanced Control Options

Flow Freezing

Flow freezing strategy	Disabled
------------------------	----------

Manual time step (Freezing): Off
Manual time step: Off

RESULTS

General Info

Iterations: 625
Physical time: 246.908 s
CPU time: 2508 s

Log

Mesh generation started	23:22:52 , May 30
Mesh generation normally finished	23:23:01 , May 30
Preparing data for calculation	23:23:01 , May 30
Calculation started 0	23:23:10 , May 30
Refinement 625	00:04:54 , May 31
Refinement 973	00:41:28 , May 31
Calculation has converged since the following criteria are satisfied: 973	00:42:59 , May 31
Max. phys. time is reached 973	
Calculation finished 974	00:44:13 , May 31

Calculation Mesh

Basic Mesh Dimensions

Number of cells in X	64
Number of cells in Y	60
Number of cells in Z	62

Number Of Cells

Total cells	243218
Fluid cells	241410
Solid cells	0
Partial cells	1808
Irregular cells	0
Trimmed cells	0

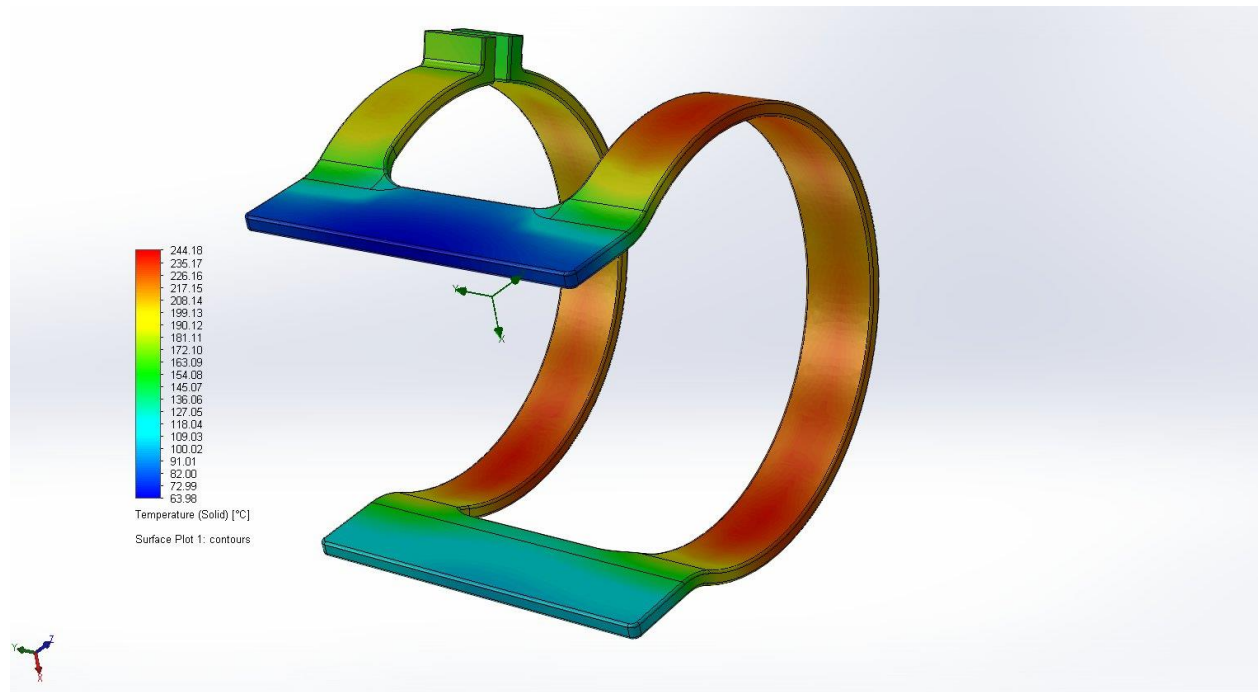
Maximum refinement level: 1

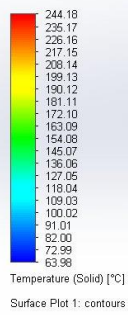
Goals

Name	Unit	Value	Progress	Use in convergence	Delta	Criteria
VG Max Temperature (Solid) 1	°C	241.69	100	On	0.47330111	7.04479997

Min/Max Table

Name	Minimum	Maximum
Pressure [Pa]	9994150.25	1.00e+007
Temperature [°C]	3.67	244.18
Density (Fluid) [kg/m^3]	915.24	1000.80
Velocity [mm/s]	0	87.477
Velocity (X) [mm/s]	-87.412	6.981
Velocity (Y) [mm/s]	-24.901	28.265
Velocity (Z) [mm/s]	-42.001	22.523
Temperature (Fluid) [°C]	3.67	244.18
Temperature (Solid) [°C]	63.98	244.18
Density (Solid) [kg/m^3]	8960.00	8960.00
Vorticity [1/s]	1.149e-008	4.633
Shear Stress [Pa]	0	2.93
Relative Pressure [Pa]	-5849.75	5750.96
Heat Transfer Coefficient [W/m^2/K]	52.053	7744.629
Surface Heat Flux [W/m^2]	0	1106644.531
Heat Flux [W/m^2]	34628.547	5238355.028
Overheat above Melting Temperature [K]	-1019.070	-838.865





Transient natural convection heat dissipation analysis of solid coil with cooling fins, surface heat generation

System Info

Product	Flow Simulation 2014 SP5.0. Build: 2878
Computer name	TRYM
User name	TrymBrox
Processors	Intel(R) Core(TM) i7-4700HQ CPU @ 2.40GHz
Memory	12171 MB / 134217727 MB
Operating system	(Build 9600)
CAD version	SolidWorks 2014 SP5.0
CPU speed	2401 MHz

General Info

Model	test_coil_ribbed_solid_more_ribs.SLDPRT
Project name	coil_ribbed_nat_lvl8
Units system	SI (m-kg-s)
Analysis type	External (not exclude internal spaces)
Exclude cavities without flow conditions	Off
Coordinate system	Global coordinate system
Reference axis	X

INPUT DATA

Initial Mesh Settings

Automatic initial mesh: On

Result resolution level: 8

Advanced narrow channel refinement: Off

Refinement in solid region: Off

Geometry Resolution

Evaluation of minimum gap size: Automatic

Evaluation of minimum wall thickness: Automatic

Computational Domain

Size

X min	-0.652 m
X max	0.652 m
Y min	-0.670 m
Y max	0.580 m
Z min	-0.639 m
Z max	0.652 m

Boundary Conditions

2D plane flow	None
At X min	Default
At X max	Default
At Y min	Default
At Y max	Default
At Z min	Default
At Z max	Default

Physical Features

Heat conduction in solids: On

Heat conduction in solids only: Off

Radiation: Off

Time dependent: On

Gravitational effects: On

Flow type: Laminar and turbulent

Cavitation: Off

High Mach number flow: Off

Default roughness: 0 micrometer

Gravitational Settings

X component	9.81 m/s ²
Y component	0 m/s ²
Z component	0 m/s ²

Ambient Conditions

Thermodynamic parameters	Static Pressure: 1.00e+007 Pa Temperature: 4.00 °C
Velocity parameters	Velocity vector Velocity in X direction: 0 mm/s Velocity in Y direction: 0 mm/s Velocity in Z direction: 0 mm/s
Solid parameters	Default material: Copper Initial solid temperature: 4.00 °C
Turbulence parameters	Turbulence intensity and length Intensity: 0.10 % Length: 0.002 m

Material Settings

Fluids

Water

Solids

Copper

Heat Surface Sources

SS Surface Heat Generation Rate 1

Type	Surface heat generation rate
Faces	Face<2> Face<5> Face<1> Face<3> Face<4>
Coordinate system	Global coordinate system
Reference axis	X
Toggle	On
Surface heat generation rate	524590.000 W/m ²

Goals

Volume Goals

VG Max Temperature (Solid) 1

Type	Volume Goal
Goal type	Temperature (Solid)
Calculate	Maximum value
Components	Imported1
Coordinate system	Global coordinate system
Use in convergence	On

Calculation Control Options

Finish Conditions

Finish conditions	If one is satisfied
Maximum physical time	60.000 s

Solver Refinement

Refinement level	2
Approximate maximum cells	1e+007
Refinement strategy	Tabular refinement
Units	Travels
Relaxation interval	2e-001
Refinements	2, 3

Results Saving

Save before refinement	On
Periodic saving	Units: Physical time Period: 10.000 s

Advanced Control Options

Flow Freezing

Flow freezing strategy	Disabled
------------------------	----------

Manual time step (Freezing): Off

Manual time step: Off

RESULTS

General Info

Iterations: 644

Physical time: 274.961 s

CPU time: 2884 s

Log

Mesh generation started	02:10:47 , May 31
Mesh generation normally finished	02:10:58 , May 31
Preparing data for calculation	02:10:58 , May 31
Calculation started 0	02:11:07 , May 31
Refinement 644	02:59:08 , May 31
Refinement 1011	03:50:20 , May 31
Calculation has converged since the following criteria are satisfied: 1011	03:52:25 , May 31
Max. phys. time is reached 1011	
Calculation finished 1012	03:53:41 , May 31

Calculation Mesh

Basic Mesh Dimensions

Number of cells in X	64
Number of cells in Y	62
Number of cells in Z	64

Number Of Cells

Total cells	265859
Fluid cells	261663
Solid cells	0
Partial cells	4196
Irregular cells	0
Trimmed cells	0

Maximum refinement level: 1

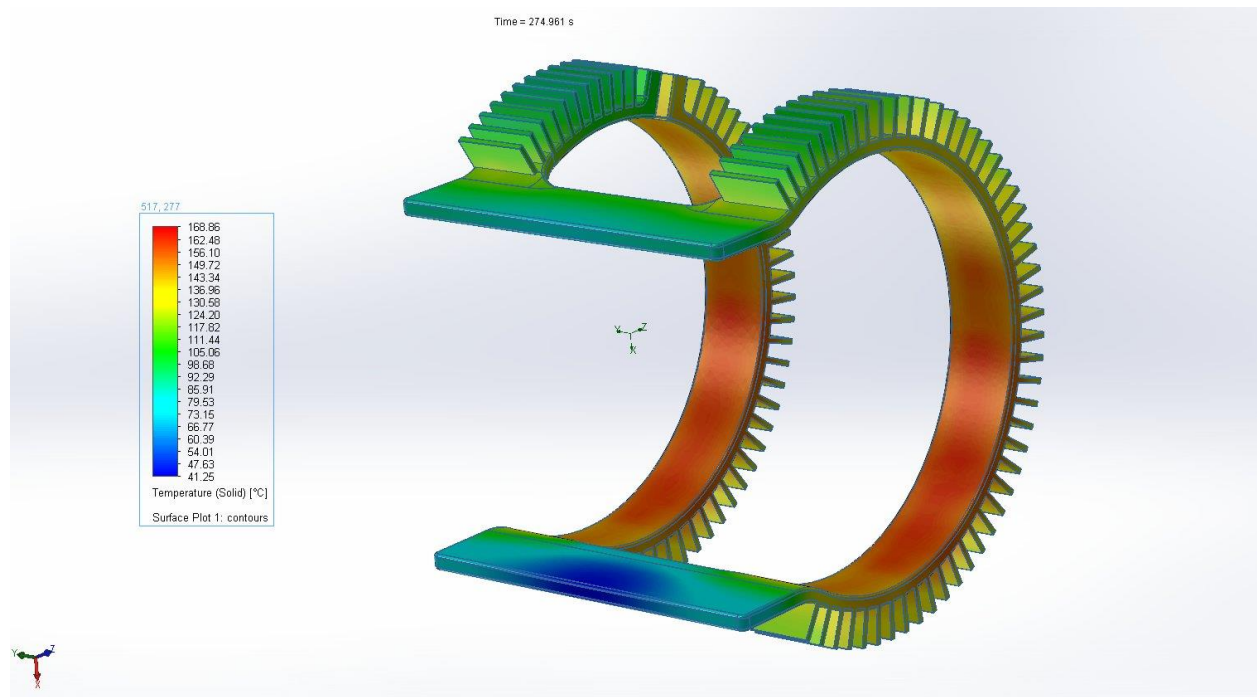
Goals

Name	Unit	Value	Progress	Use in convergence	Delta	Criteria
VG Max Temperature (Solid) 1	°C	168.53	100	On	0.0305672575	4.74705279

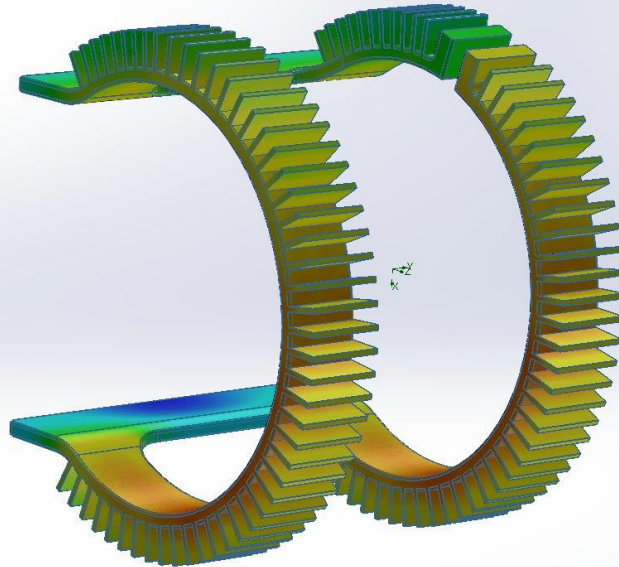
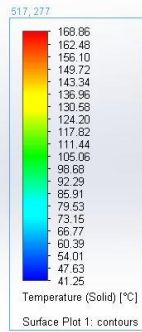
Min/Max Table

Name	Minimum	Maximum
------	---------	---------

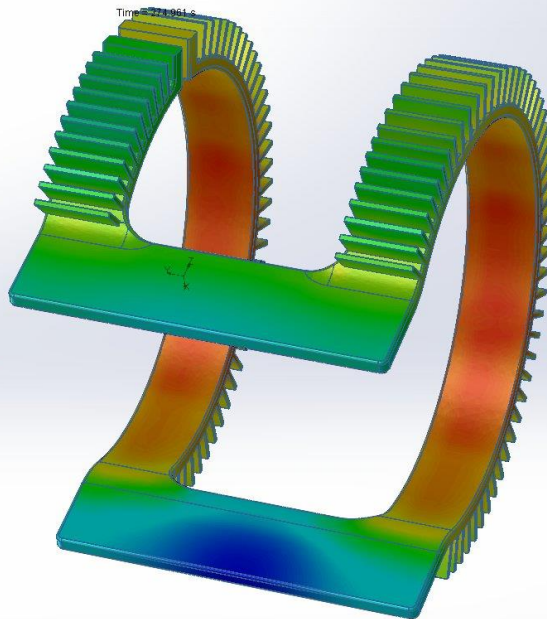
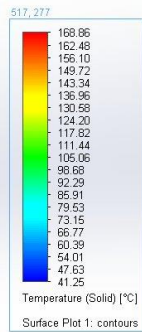
Pressure [Pa]	9993787.01	1.00e+007
Temperature [°C]	3.98	168.86
Density (Fluid) [kg/m^3]	935.81	1000.75
Velocity [mm/s]	0	93.062
Velocity (X) [mm/s]	-93.014	12.370
Velocity (Y) [mm/s]	-26.769	26.698
Velocity (Z) [mm/s]	-35.351	22.298
Temperature (Fluid) [°C]	3.98	168.86
Temperature (Solid) [°C]	41.25	168.86
Density (Solid) [kg/m^3]	8960.00	8960.00
Vorticity [1/s]	2.425e-008	8.976
Shear Stress [Pa]	0	2.85
Relative Pressure [Pa]	-6212.99	6212.79
Heat Transfer Coefficient [W/m^2/K]	76.961	13956.645
Surface Heat Flux [W/m^2]	0	1205958.021
Heat Flux [W/m^2]	25625.227	8833314.179
Overheat above Melting Temperature [K]	-1041.799	-914.190

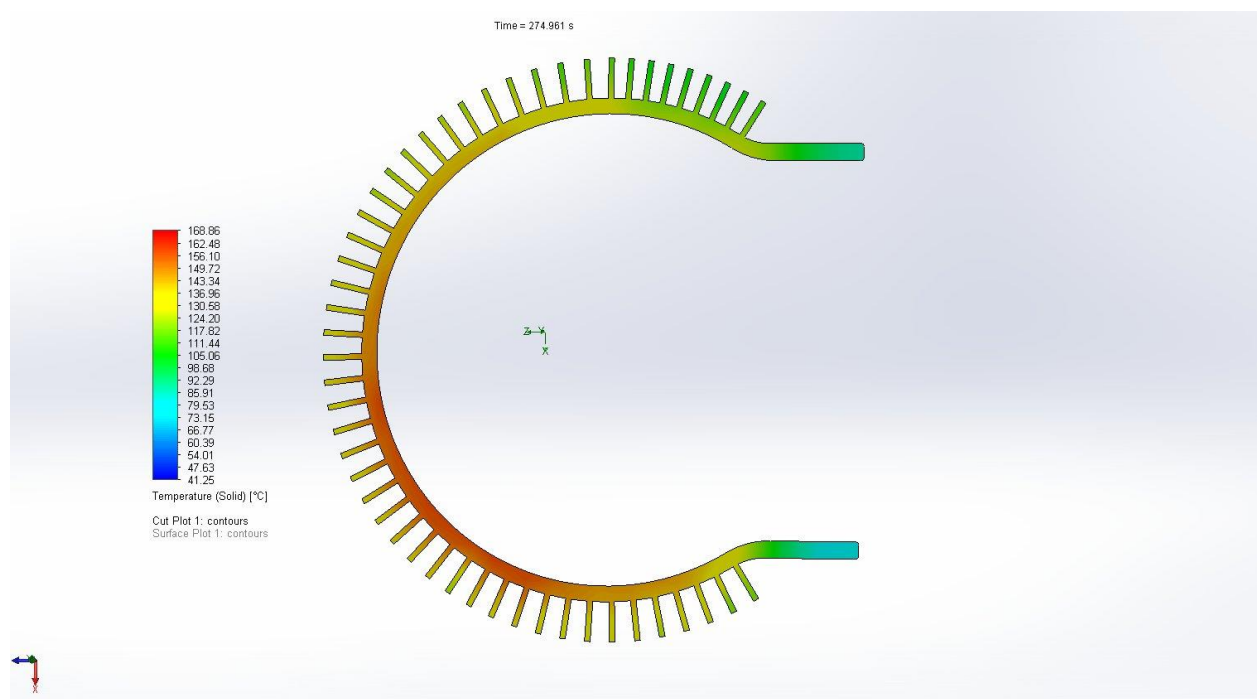
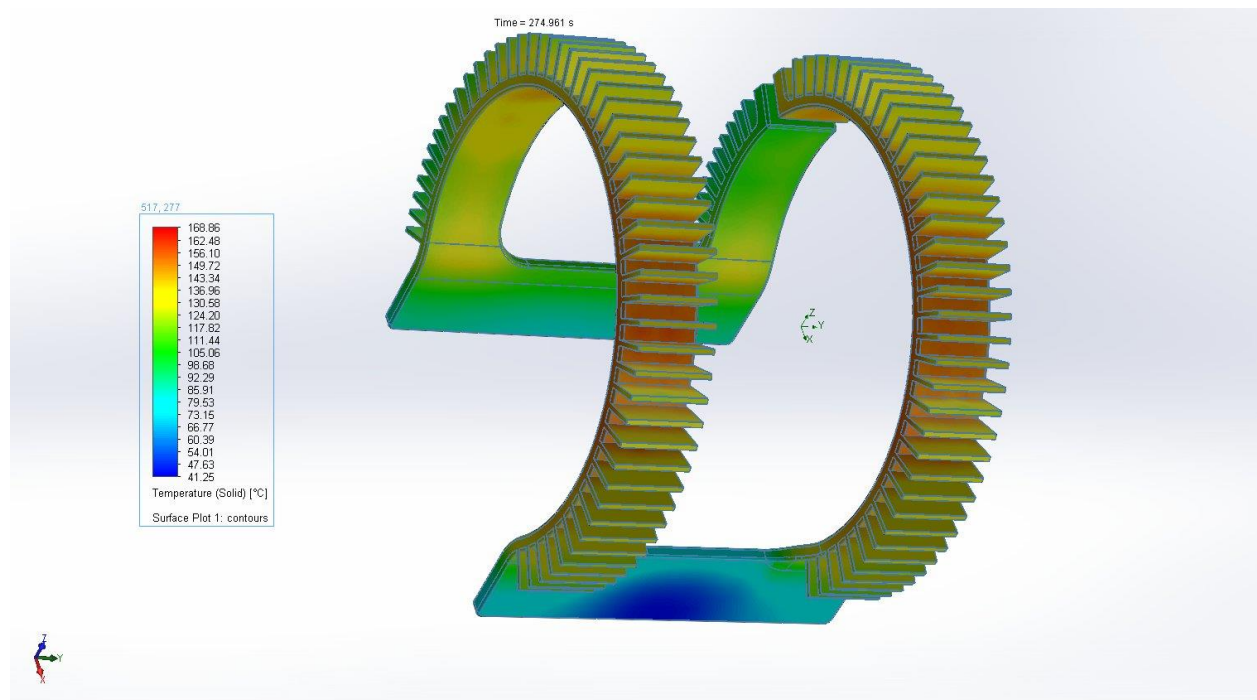


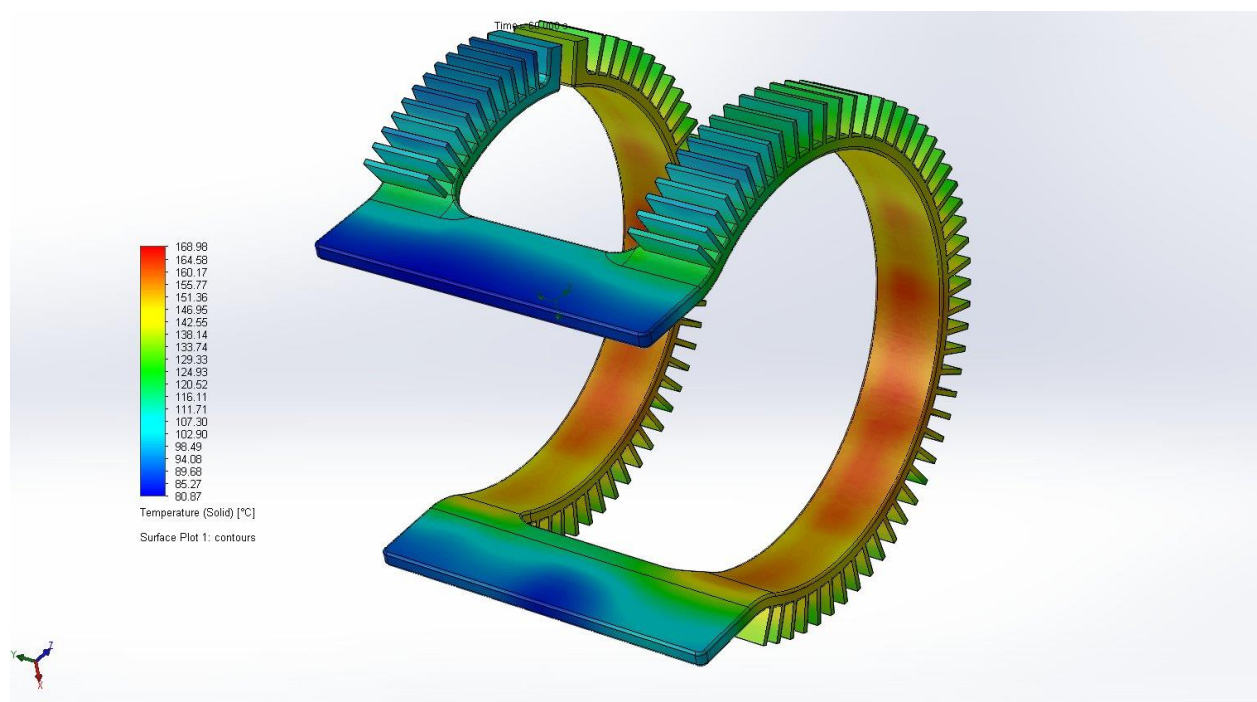
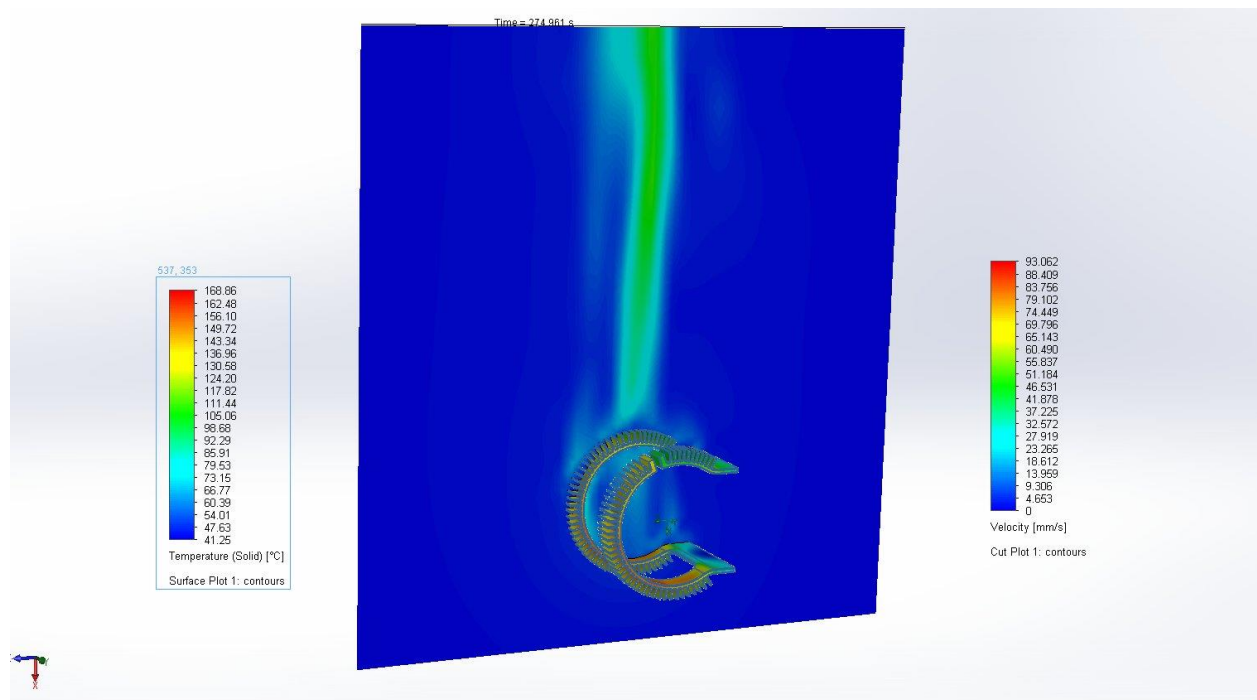
Time = 274.961 s

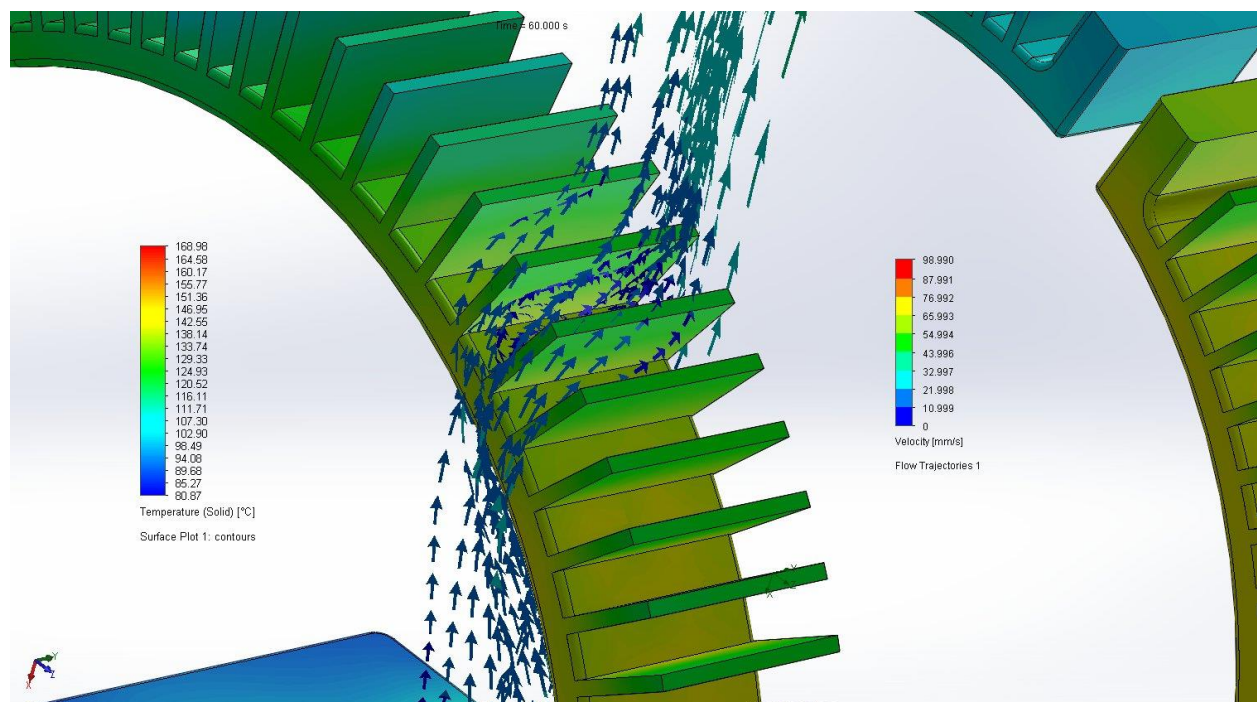
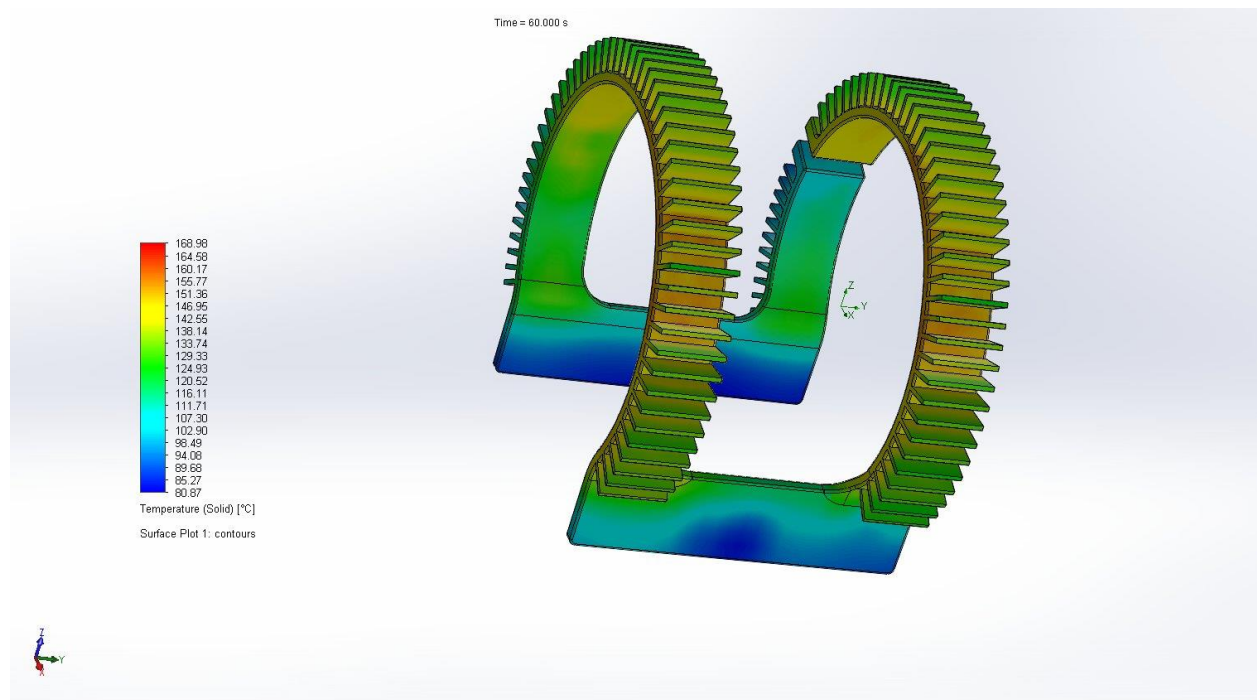


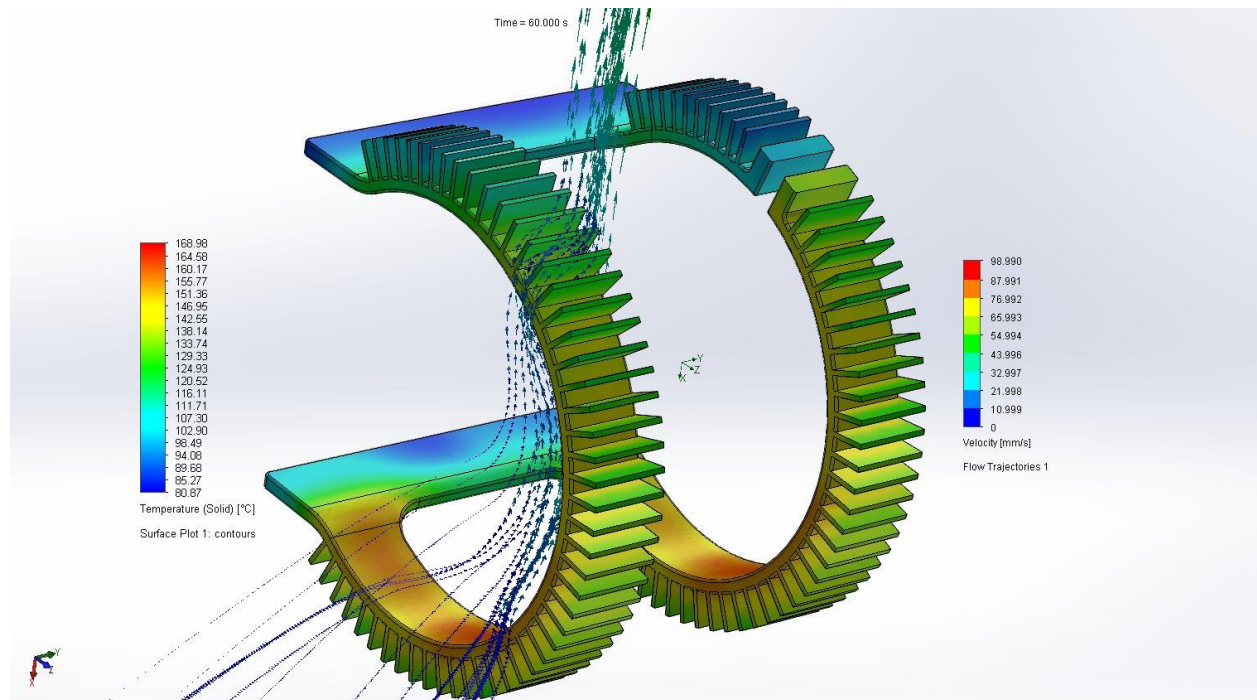
Time = 274.961 s











Transient forced convection heat dissipation analysis of 20*20*6 mm copper element

System Info

Product	Flow Simulation 2014 SP5.0. Build: 2878
Computer name	TRYM
User name	TrymBrox
Processors	Intel(R) Core(TM) i7-4700HQ CPU @ 2.40GHz
Memory	12171 MB / 134217727 MB
Operating system	(Build 9600)
CAD version	SolidWorks 2014 SP5.0
CPU speed	2401 MHz

General Info

Model	20mm_plate.SLDPRT
Project name	vol_forced_lvl8
Units system	SI (m-kg-s)
Analysis type	External (not exclude internal spaces)
Exclude cavities without flow conditions	Off
Coordinate system	Global coordinate system
Reference axis	X

INPUT DATA

Initial Mesh Settings

Automatic initial mesh: On

Result resolution level: 8

Advanced narrow channel refinement: Off

Refinement in solid region: Off

Geometry Resolution

Evaluation of minimum gap size: Automatic

Evaluation of minimum wall thickness: Automatic

Computational Domain

Size

X min	-0.070 m
X max	0.070 m
Y min	-0.060 m
Y max	0.106 m
Z min	-0.070 m
Z max	0.070 m

Boundary Conditions

2D plane flow	None
At X min	Default
At X max	Default
At Y min	Default
At Y max	Default
At Z min	Default
At Z max	Default

Physical Features

Heat conduction in solids: On

Heat conduction in solids only: Off

Radiation: Off

Time dependent: On

Gravitational effects: On

Flow type: Laminar and turbulent

Cavitation: Off

High Mach number flow: Off

Default roughness: 0 micrometer

Gravitational Settings

X component	0 m/s ²
Y component	-9.81 m/s ²
Z component	0 m/s ²

Ambient Conditions

Thermodynamic parameters	Static Pressure: 1.00e+007 Pa Temperature: 4.00 °C
Velocity parameters	Velocity vector Velocity in X direction: 0 mm/s Velocity in Y direction: 20.000 mm/s Velocity in Z direction: 0 mm/s
Solid parameters	Default material: Copper Initial solid temperature: 4.00 °C
Turbulence parameters	Turbulence intensity and length Intensity: 0.10 % Length: 6.000e-005 m

Material Settings

Fluids

Water

Solids

Copper

Heat Volume Sources

VS Heat Generation Rate 1

Source type	Heat Generation Rate
Heat generation rate	210.000 W
Components	Boss-Extrude1
Coordinate system	Global coordinate system
Reference axis	X

Goals

Volume Goals

VG Max Temperature (Solid) 1

Type	Volume Goal
Goal type	Temperature (Solid)
Calculate	Maximum value
Components	Boss-Extrude1
Coordinate system	Global coordinate system
Use in convergence	On

Calculation Control Options

Finish Conditions

Finish conditions	If one is satisfied
Maximum physical time	60.000 s

Solver Refinement

Refinement level	2
Approximate maximum cells	1e+007
Refinement strategy	Tabular refinement
Units	Travels
Relaxation interval	2e-001
Refinements	2, 3

Results Saving

Save before refinement	On
Periodic saving	Units: Physical time Period: 10.000 s

Advanced Control Options

Flow Freezing

Flow freezing strategy	Disabled
------------------------	----------

Manual time step (Freezing): Off

Manual time step: Off

Results

General Info

Iterations: 414

Physical time: 60.000 s

CPU time: 1914 s

Log

Mesh generation started	21:51:07 , May 30
Mesh generation normally finished	21:51:14 , May 30
Preparing data for calculation	21:51:15 , May 30
Calculation started 0	21:51:25 , May 30
Calculation finished 430	22:24:42 , May 30

Calculation Mesh

Basic Mesh Dimensions

Number of cells in X	62
Number of cells in Y	82
Number of cells in Z	62

Number Of Cells

Total cells	315208
Fluid cells	313672
Solid cells	784
Partial cells	752
Irregular cells	0
Trimmed cells	0

Maximum refinement level: 0

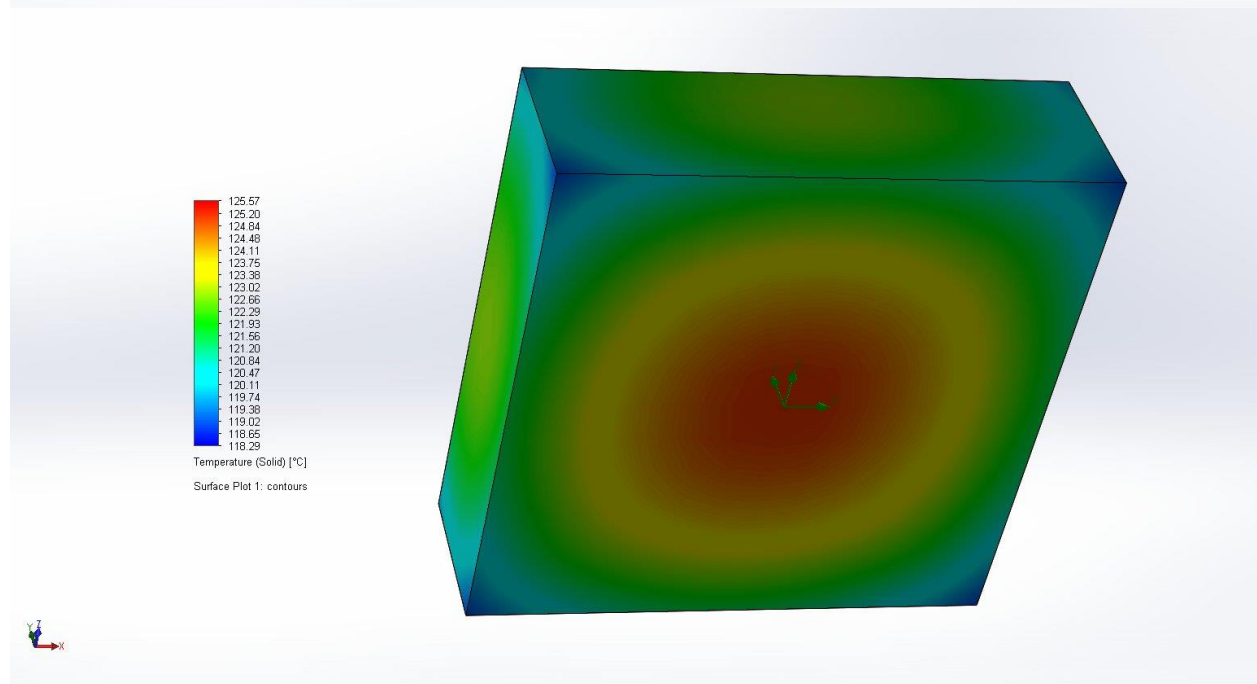
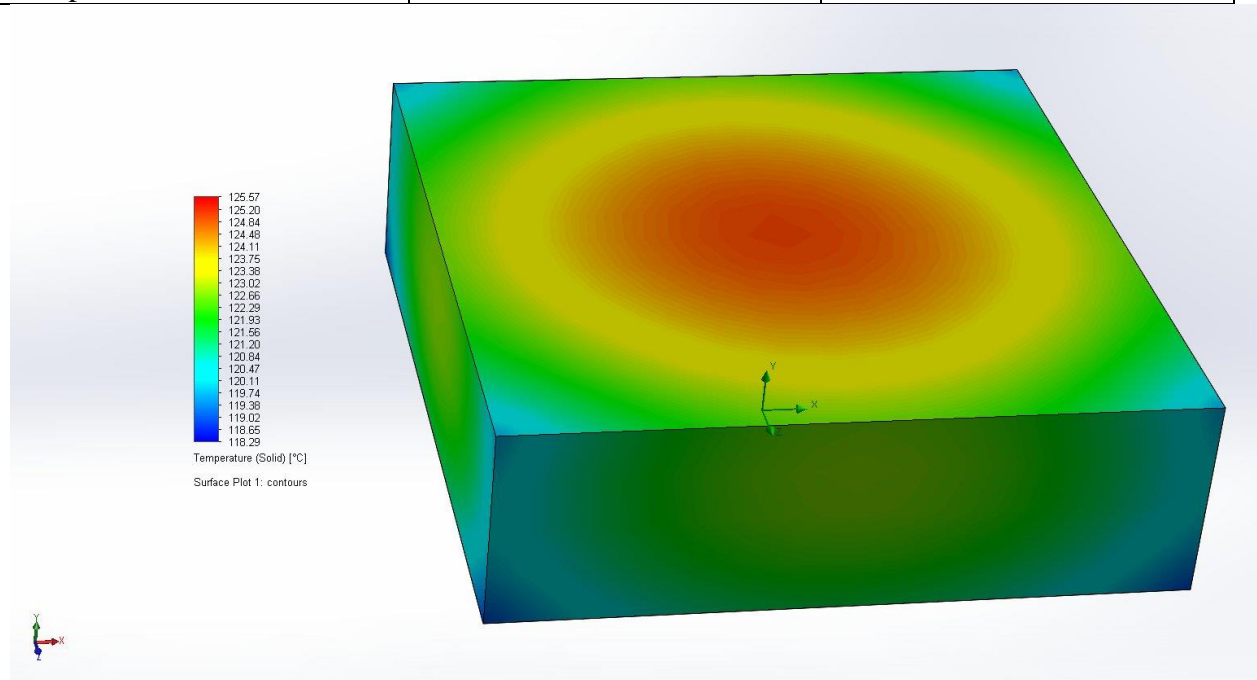
Goals

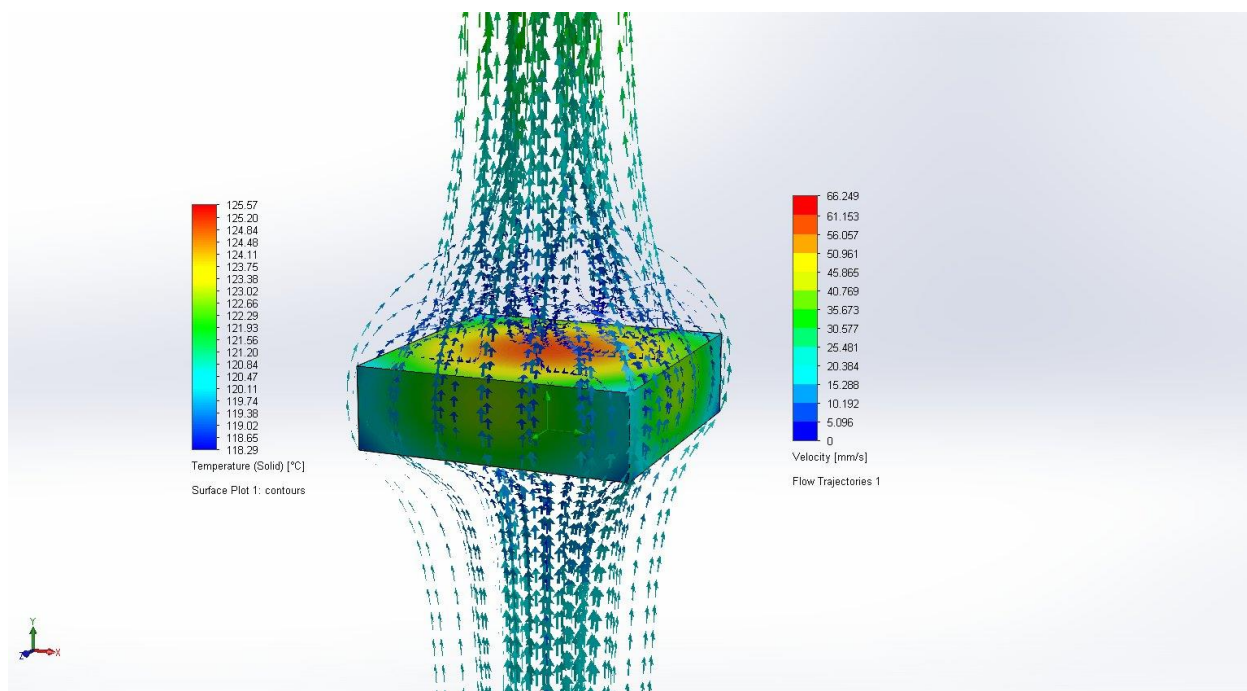
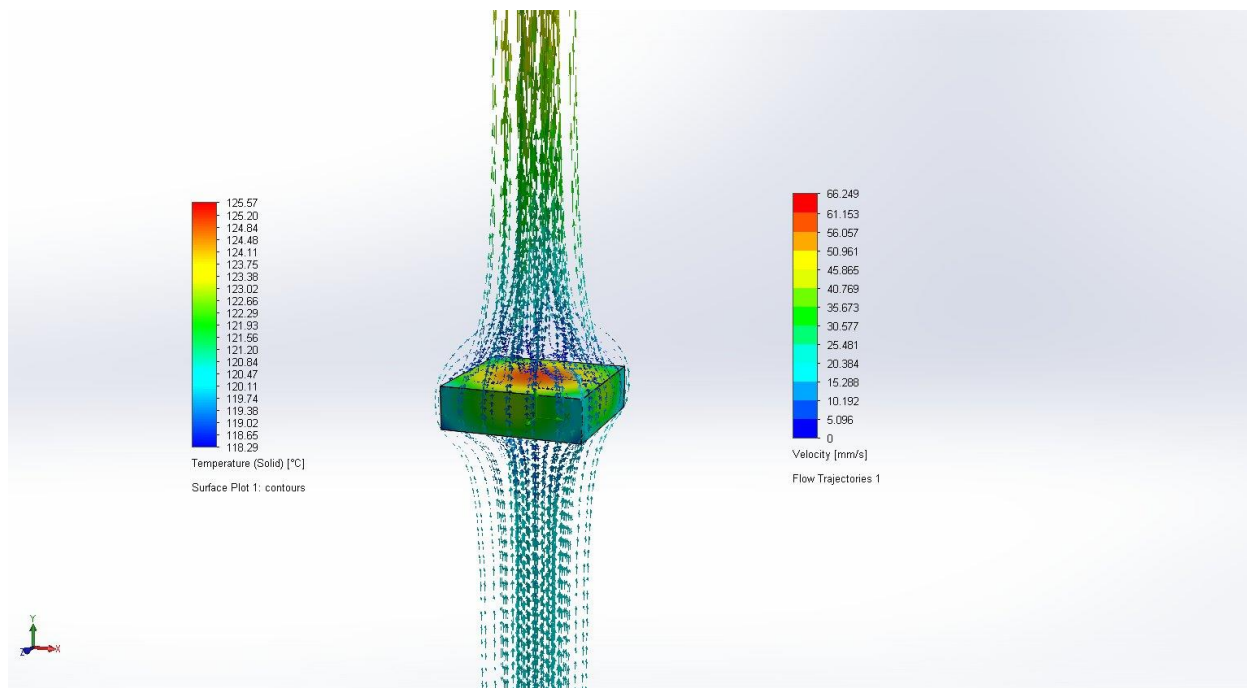
Name	Unit	Value	Progress	Use in convergence	Delta	Criteria
VG Max Temperature (Solid) 1	°C	125.57	100	On	0.0295384737	3.6169131

Min/Max Table

Name	Minimum	Maximum
Pressure [Pa]	9998978.98	1.00e+007
Temperature [°C]	4.00	125.57
Density (Fluid) [kg/m^3]	988.86	1000.75
Velocity [mm/s]	0	66.249
Velocity (X) [mm/s]	-18.331	18.380
Velocity (Y) [mm/s]	-6.472	66.249

Velocity (Z) [mm/s]	-18.340	18.337
Temperature (Fluid) [°C]	4.00	125.28
Temperature (Solid) [°C]	118.29	125.57
Density (Solid) [kg/m^3]	8960.00	8960.00
Vorticity [1/s]	1.546e-006	12.970
Shear Stress [Pa]	0	0.11
Relative Pressure [Pa]	-1021.02	569.65
Heat Transfer Coefficient [W/m^2/K]	423.284	4441.514
Surface Heat Flux [W/m^2]	0	520934.367
Heat Flux [W/m^2]	31742.424	735883.813
Overheat above Melting Temperature [K]	-964.762	-957.482





I. Brochure: Ultramotion Series U2 Datasheet

Brochure for the U2 series subsea actuator, courtesy of Ultramotion (Quartararo, 2015)

Ultra Motion Series U2 Linear Actuator

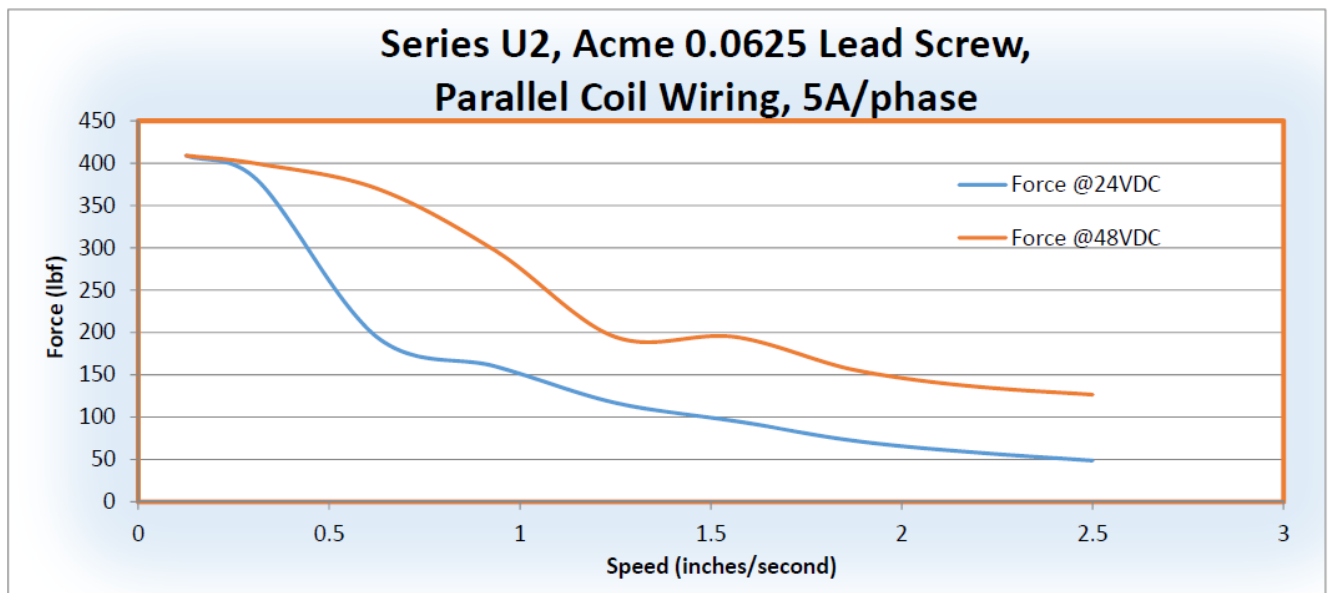
Product Features:

- Inline mounted motor
- NEMA 23 frame
- Standard high torque NEMA 23 stepper motor
- Available with potentiometer feedback
- Brushless DC motors available
- Standard stroke lengths: 2", 4" & 8"
- Custom stroke lengths to 16"
- Standard with 2-foot SeaCon underwater cable with 8-pin male connector & female locking sleeve
- 3D models available on request
- Rated to 20,000 feet below sea level or 10,000 psi.



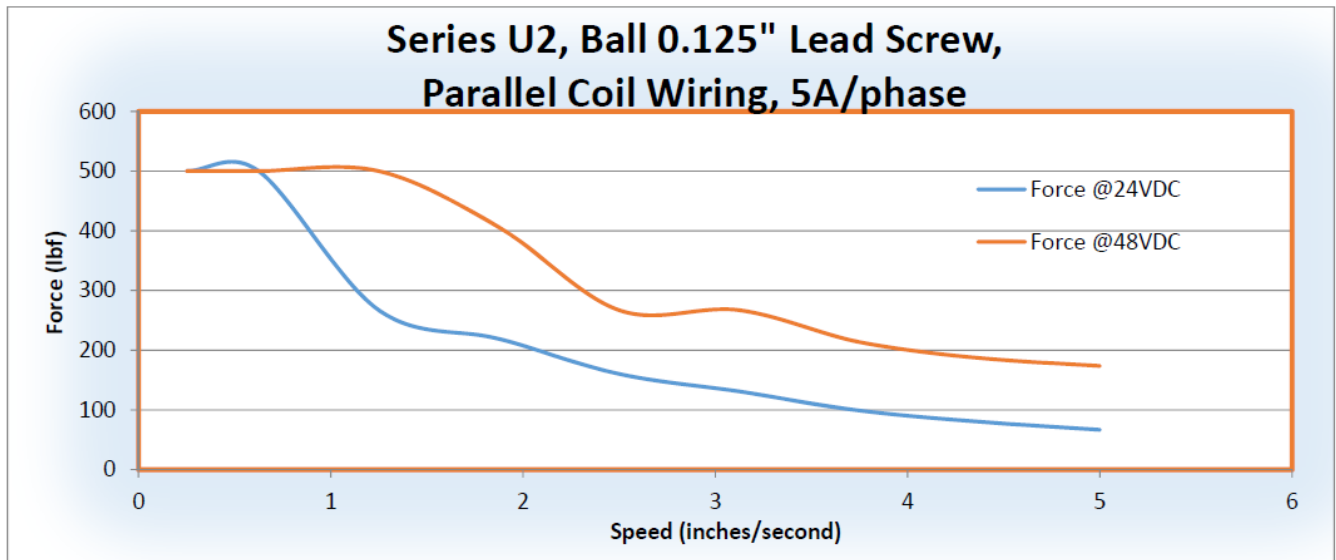
Speed/Force Graphs (with standard high torque NEMA 17 stepper motor):

With self-locking Acme 0.0625" lead screw:

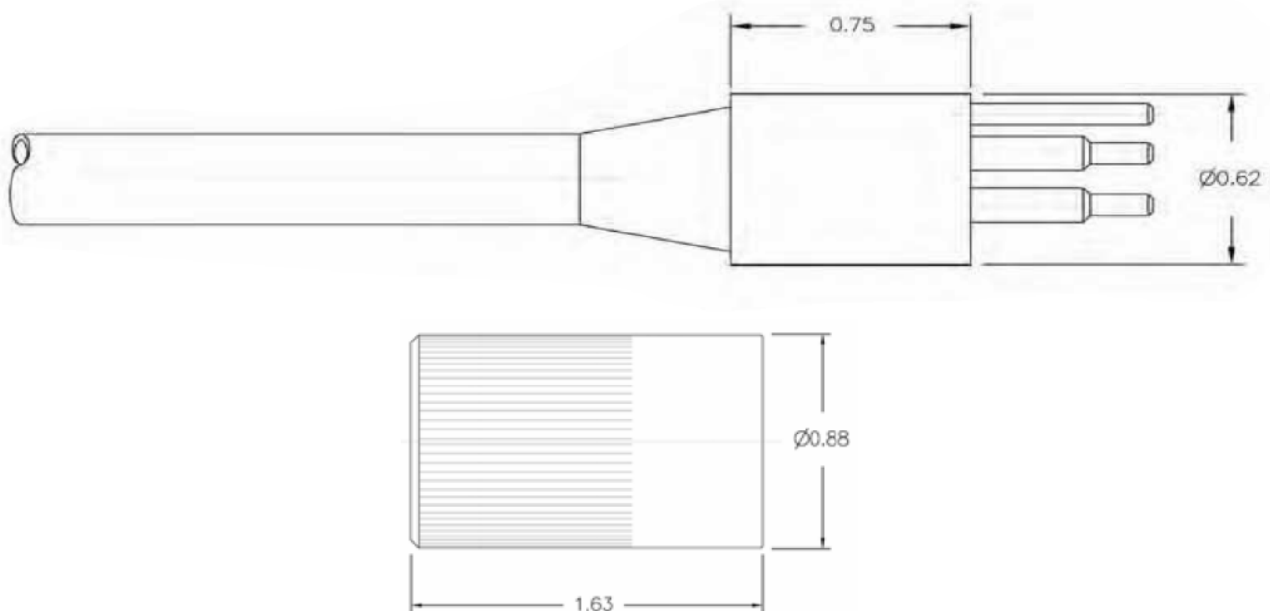


Ultra Motion Series U2 Linear Actuator

With high efficiency 0.125" ball screw option:



Connector & Locking Sleeve:



PROPRIETARY DATA		8	7	6	5	4	3	2	1
All information contained in this document is property of Ultra Motion LLC and shall not be released, performed, distributed, reproduced, used, or disclosed, in whole or in part, for any purpose other than to evaluate a product of Ultra Motion LLC, without the prior written consent of Ultra Motion LLC. This document is the property of Ultra Motion LLC and shall remain in any manner. All documents shall protect in this document as provided by 35 USC 4352-4352-1016. The information subject to this restriction is contained in every page of this document.									
MOTOR SIZE		RESISTANCE - PHASE TO PHASE							
NEMA17		~ 2.0 Ohm							
NEMA23		~ 0.8 Ohm							

CABLE END

Red w/ Black (Chassis Ground)

White w/ Black

Black (A+)

White (A-)

Red (B+)

Green (B-)

Blue

Orange

Black + Orange/White

Red + Yellow/White

Yellow + Red/White

POTENTIOMETER

MOTOR (PARALLEL WIRING)

NAME		DATE	
R. KOCH		11/10/2009	

FABRICATION INSTRUCTIONS	
UNLESS OTHERWISE SPECIFIED:	
- INTERPRET DIM IN INCHES	
- DIMENSIONS ARE IN INCHES	
- BREAK ALL SHARP EDGES	
- DRAWING TOLERANCES ARE:	
* ANGLES: 1°	
* 0.XX: 0.01	
* 0.XXX: 0.005	

THIRD ANGLE PROJECTION	
-	

MATERIAL	
-	

WEIGHT (lbs)	
-	

TITLE	
8-PIN PARALLEL WIRING	

SIZE		DWG No.		REV	
B		8PINPARALLEL		A.01	

DO NOT SCALE DRAWING WORK FROM DIMENSIONS	
SCALE: 1:1	

SHEET 1 OF 1	
SHEET 1 OF 1	

ULTRA MOTION

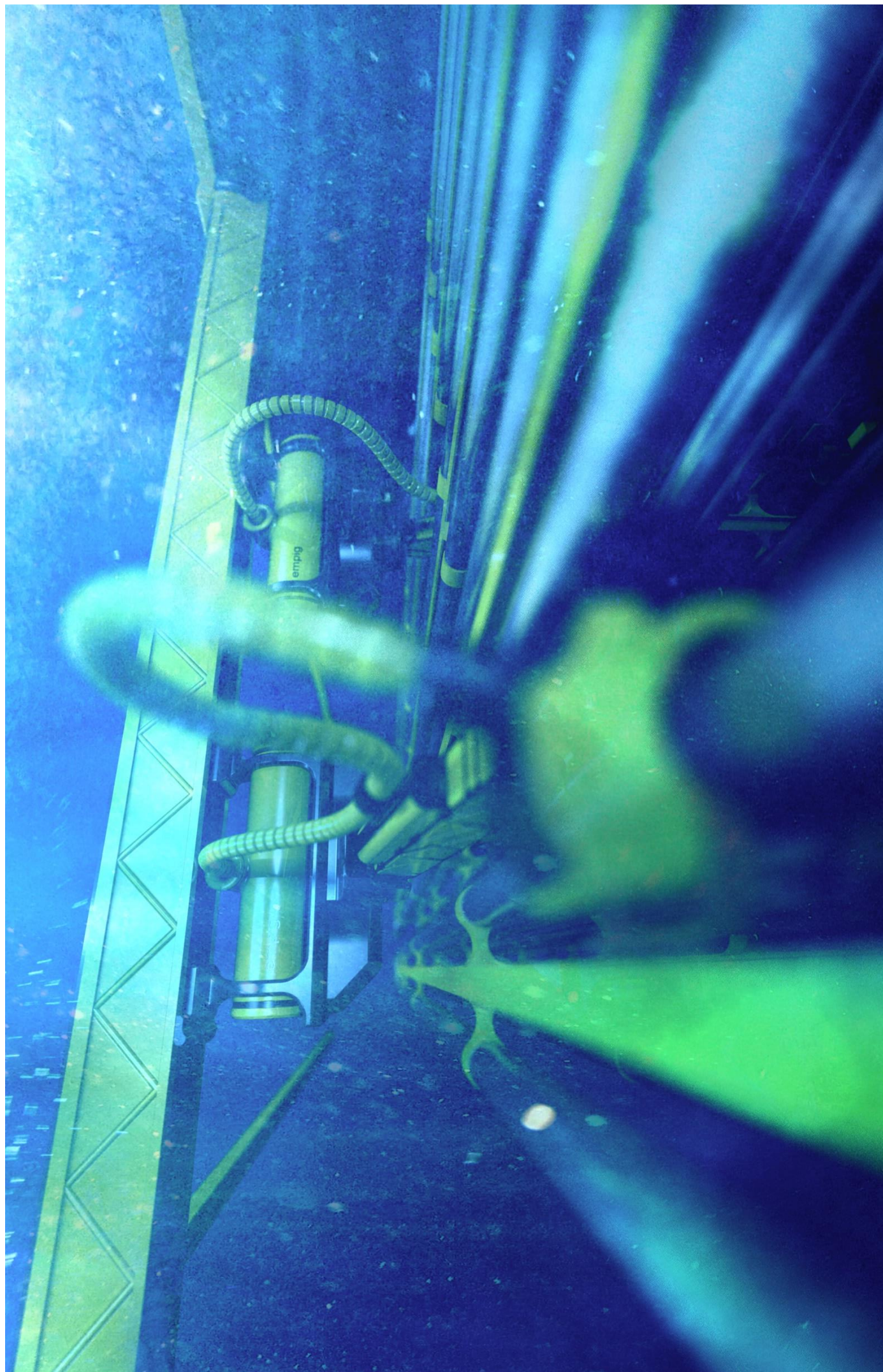
22355 COUNTY RD 48 UNIT 21 CUTCHOGUE NY 11935

Phone: 631 298 9179 Fax: 631 298 6693

WWW.ULTRAMOTION.COM INFO@ULTRAMOTION.COM

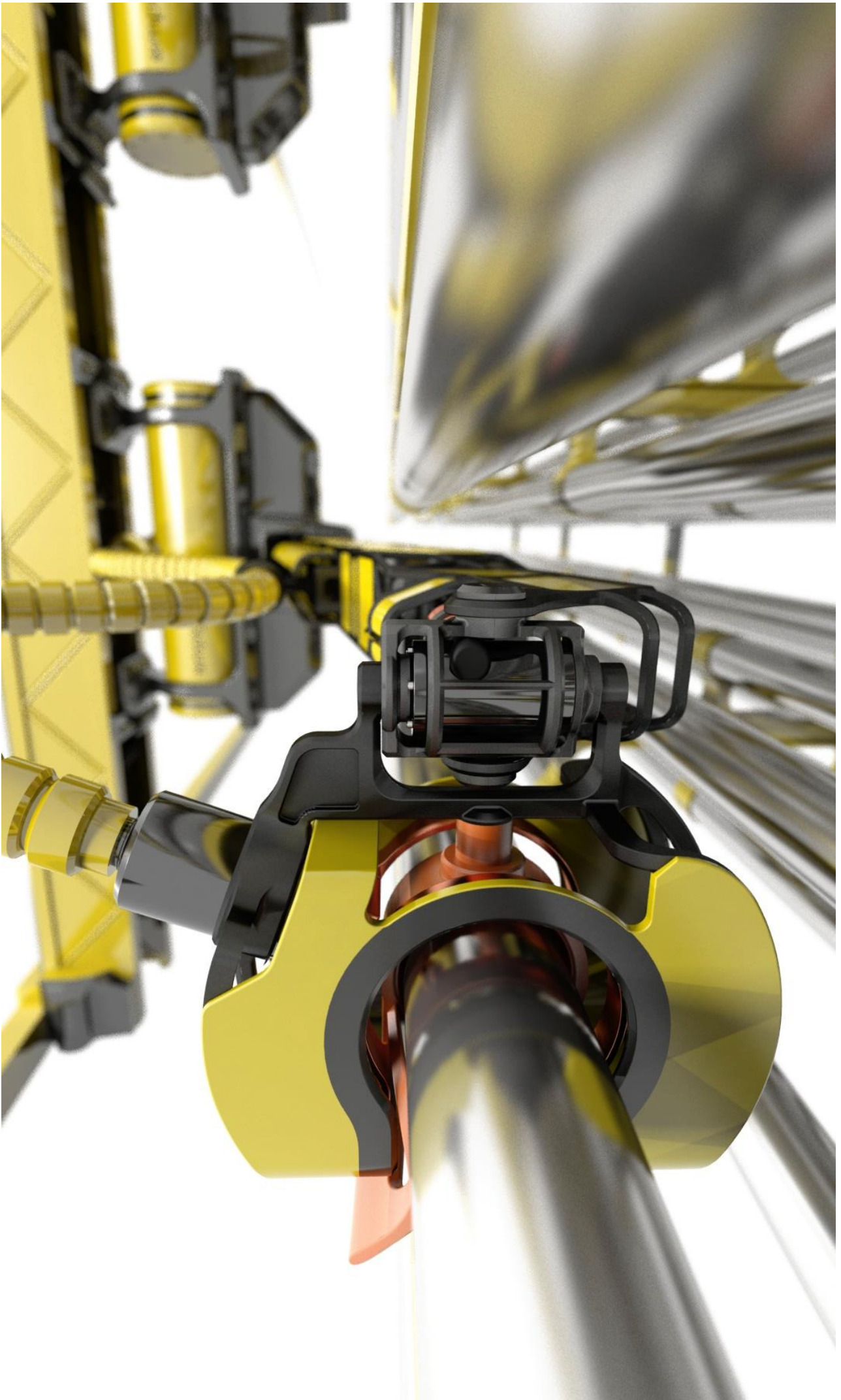
[illegible]

J. Additional renderings









K. Signed risk assessment

